

Non-Viral Delivery of Nucleic Acids and Image-Guided Assessment of *in vivo* Performance of Multifunctional Nanomedicines

Dissertation

zur Erlangung des Doktorgrades der Naturwissenschaften (Dr. rer. nat.)

dem

Fachbereich Pharmazie der Philipps-Universität Marburg

vorgelegt von

Olivia Monika Merkel

aus Villingen-Schwenningen

Marburg/Lahn 2009

Vom Fachbereich Pharmazie der Philipps-Universität Marburg als Dissertation am
24.08.2009 angenommen.

Erstgutachter: Prof. Dr. Thomas Kissel
Zweitgutachter: Prof. Dr. Carsten Culmsee
Drittgutachter: Prof. Dr. Werner Seeger

Tag der mündlichen Prüfung: 25.08.2009

Die vorliegende Arbeit entstand auf Anregung und unter Leitung von

Herrn Prof. Dr. Thomas Kissel

am Institut für Pharmazeutische Technologie und Biopharmazie
der Philipps-Universität Marburg.

Gewidmet meinen Eltern
in Liebe und Dankbarkeit

TABLE OF CONTENTS

1	INTRODUCTION	1
1.1	Nanomedicine	2
1.2	Non-Viral Delivery of Nucleic Acids.....	4
1.3	Targeted Gene Delivery Using Cell Specific Ligands.....	7
1.4	Dendrimers in Gene Delivery	8
1.5	Concepts of siRNA Mediated Post-Transcriptional Gene Silencing	11
1.6	Pulmonary siRNA Delivery.....	15
1.7	Nuclear Imaging of siRNA Delivery	17
1.8	Polymer Genomics and Nanotoxicology.....	20
1.9	Structure of the Thesis: Aims and Outline	22
1.10	References	24

PART I: NON-VIRAL *IN VITRO* DELIVERY OF pDNA

2	INTEGRIN ALPHA-v-BETA-3 TARGETED GENE DELIVERY USING RGD PEPTIDOMIMETIC CONJUGATES WITH COPOLYMERS OF PEGYLATED POLY(ETHYLENE IMINE)	44
2.1	Abstract	45
2.2	Introduction	45
2.3	Materials and Methods.....	46
2.4	Results and Discussion.....	52

2.5	Conclusion.....	70
2.6	Acknowledgements.....	70
2.7	References	71
3	POLYCATIONIC TRIAZINE-BASED DENDRIMERS: EFFECT OF PERIPHERAL GROUPS ON TRANSFECTION EFFICIENCY	77
3.1	Abstract	78
3.2	Introduction	78
3.3	Results and Discussion.....	80
3.4	Conclusion.....	87
3.5	Experimental.....	88
3.6	Acknowledgements.....	95
3.7	Notes and references	95
4	TRIAZINE DENDRIMERS AS NON-VIRAL GENE DELIVERY SYSTEMS: EFFECTS OF MOLECULAR STRUCTURE ON BIOLOGICAL ACTIVITY.....	99
4.1	Abstract	100
4.2	Introduction	100
4.3	Materials and Methods.....	101
4.4	Results and Discussion.....	105
4.5	Conclusion.....	118
4.6	Acknowledgements.....	119
4.7	References	119

PART II: NON-VIRAL *IN VITRO* AND *IN VIVO* DELIVERY OF siRNA

5	IN VIVO SPECT AND REAL-TIME GAMMA CAMERA IMAGING OF BIODISTRIBUTION AND PHARMACOKINETICS OF SIRNA DELIVERY USING AN OPTIMIZED RADIOLABELING AND PURIFICATION PROCEDURE.....	125
5.1	Abstract	126
5.2	Introduction	126
5.3	Materials and Methods.....	128
5.4	Results and Discussion.....	130
5.5	Conclusion	141
5.6	Acknowledgment	142
5.7	Supporting Information	142
5.8	References	142
6	STABILITY OF SIRNA POLYPLEXES FROM POLY(ETHYLENIMINE) AND POLY(ETHYLENIMINE)-G-POLY(ETHYLENE GLYCOL) UNDER IN VIVO CONDITIONS: EFFECTS ON PHARMACOKINETICS AND BIODISTRIBUTION MEASURED BY FLUORESCENCE FLUCTUATION SPECTROSCOPY AND SINGLE PHOTON EMISSION COMPUTED TOMOGRAPHY (SPECT) IMAGING	148
6.1	Abstract	149
6.2	Introduction	149
6.3	Materials and Methods.....	151
6.4	Results and Discussion.....	157
6.5	Conclusion	177

6.6	Acknowledgements.....	178
6.7	References	178
7	NON-VIRAL SIRNA DELIVERY TO THE LUNG – INVESTIGATION OF PEG-PEI POLYPLEXES AND THEIR IN VIVO PERFORMANCE	184
7.1	Abstract	185
7.2	Introduction	185
7.3	Experimental Section.....	187
7.4	Results and Discussion.....	192
7.5	Conclusion.....	212
7.6	Acknowledgements.....	213
7.7	References	213
8	OFF-TARGET EFFECTS IN NON-VIRAL SIRNA DELIVERY – A STUDY ON THE EFFECT OF POLYMER GENOMICS ON IN VITRO CELL CULTURE MODELS.....	220
8.1	Abstract	221
8.2	Introduction	221
8.3	Materials and Methods.....	222
8.4	Results and Discussion.....	226
8.5	Conclusion.....	238
8.6	Acknowledgements.....	238
8.7	References	239
9	SUMMARY AND PERSPECTIVES	245

9.1	Summary	246
9.2	Perspectives.....	249
9.3	Zusammenfassung.....	250
9.4	Ausblick	253
10	APPENDICES.....	255
10.1	Abbreviations.....	256
10.2	List of Publications.....	258
10.2.1	Articles	258
10.2.2	Patents	260
10.2.3	Poster Presentations	260
10.2.4	Lectures	262
10.2.5	Abstracts.....	263
10.2.6	Awards and Prizes.....	264
10.3	Curriculum Vitae	265
10.4	Danksagung.....	266

1 Introduction

1.1 Nanomedicine

The medical application of molecular nanotechnology, which is also referred to as “nanomedicine”, is believed to lead to progress in human therapeutics in terms of improving human health at the molecular scale (1), especially concerning so far “undruggable” targets (2) with new and smart medicines equipped with high bioavailability and little side effects. Nanomedicines are expected to have a variety of implications in treatment (3) and diagnosis (4), which is also expressed in the neologism “theragnostics” (5, 6). While nanotechnology enables diagnosis at the single-cell and molecular level, nanomedical therapeutics are expected to be specifically or even personally tailored. Especially concerning advanced drug delivery systems (7), the field of nanomedicine has increased and developed strongly in the last decade. In a multidisciplinary approach, drug delivery systems (DDS) can be generated that control the pharmacokinetics, toxicity, immunogenicity, biorecognition and efficacy of the drug (8). Drug carriers can be soluble or insoluble polymers which are formulated as nanoparticles using techniques such as the solvent displacement (9) or solvent evaporation/emulsion technique (10), biopolymers (11) or dendrimers (12). Other formulations include polymer complexes (13), “dendriplexes” (14), liposomes (15), micelles (16), and nanogels (17). Nanoscale particles that deliver insoluble small molecule drugs or macromolecules, such as proteins or nucleic acids, to their site of action are steadily being optimized while the total market for advanced DDS is expected to rise from \$64.1 billion in 2005 to \$153.5 billion in 2011, according to bcc Research (18). Smart and multimodal carriers do not only protect their load from degradation in physiologic fluids, but specifically target certain tissue or cell types, are decorated with imaging moieties that allow for non-invasive tracking in the body, or have controlled-release or stimuli-responsive properties, such as pH- or temperature-sensitivity. “Multifunctional” carriers that combine two or more of these favorable attributes are increasingly described in the literature (19-22). Targeting strategies can be divided into active and passive mechanisms. The best-known passive effect in tumor targeting is the so-called “enhanced permeability and retention” (EPR) effect, first described by Maeda et al. in 1986 (19). Due to the increased microvascular permeability and endothelial fenestration in tumor vasculature, compared to most healthy tissues, nanoparticles are passively targeted into the tumor where they show enhanced retention. Passive targeting requires long circulating nanomedicines that accumulate in the tumor by extravasation through the leaky

tumor vasculature over time. Active targeting, on the other hand, is based on ligand-receptor recognition between cell surface receptors and nanomedicines functionalized with the according ligands and facilitates intracellular uptake by receptor-mediated endocytosis.

In vitro and in vivo as well as real time imaging are other advantages of multifunctional nanomedicines. While nanoparticles that per se are most commonly used for molecular imaging are gold nanoparticles, quantum dots (QDs) and magnetic nanoparticles (4), some of them can as well be used for functionalization of nanomedicines (20). QDs are nanoparticles that emit specific wavelengths which can be tuned as a function of particle size (21). These inorganic particles are made of semiconductor cores, such as CdSe, CdTe or PbSe, which can be capped with a shell of ZnS. Due to their high toxicity they can not be used in vivo without modification. Because of their high sensitivity and bright and stable fluorescence, they can be applied for in vitro (22) and in vivo (20) fluorescence microscopy at cellular resolution. QD-based nanoparticles can both serve for immunofluorescence diagnostics (23) and for drug delivery (24). Magnetic nanoparticles are used for cell-tracking (25) and calcium sensing (26) by Magnetic Resonance Imaging (MRI). While clinical MRI is most commonly performed by aligning the nuclear magnetization of hydrogen atoms in water in the body, imaging quality and contrast can be enhanced by the use of paramagnetic contrast agents based on gadolinium or superparamagnetic iron oxide nanoparticles (SPIONs). Other applications for SPIONs than molecular imaging (27) and tumor diagnosis (28) are hyperthermia treatment after heating with radio frequency or laser light (29), and investigation of movement in an external magnetic field. Due to their relatively low intracellular labeling efficiency, new developments have arisen, such as 200 nm perfluorocarbon nanoparticles (30) that allow for medical imaging with elimination of background signals. Other imaging modalities include radioactive isotopes that emit gamma rays, such as ^{111}In (^{111}In) and $^{99\text{m}}\text{Tc}$ ($^{99\text{m}}\text{Tc}$), or positron emitting isotopes like ^{64}Cu (^{64}Cu) or ^{68}Gd (^{68}Gd). While ^{111}In and $^{99\text{m}}\text{Tc}$ can be used for Single Photon Emission Computed Tomography (SPECT) imaging, ^{64}Cu , ^{68}Gd , and ^{18}F are commonly used for Positron Emission Tomography (PET) imaging. SPECT and PET do not provide any morphological data but are routinely used for functional analysis. Both techniques can be used for assessment of pharmacokinetics and receptor binding of radiolabeled drugs by static and dynamic acquisition. Nuclear imaging can provide clinical data at an early stage of drug development and replace endpoint analysis. Non-invasive

longitudinal scans in pre-clinical research may even lead to for reduction of lab animals needed (31).

Taken together, multifunctional nanomedicines are favorable due to the many applications and detection methods that can be performed in the same experiment, animal or patient.

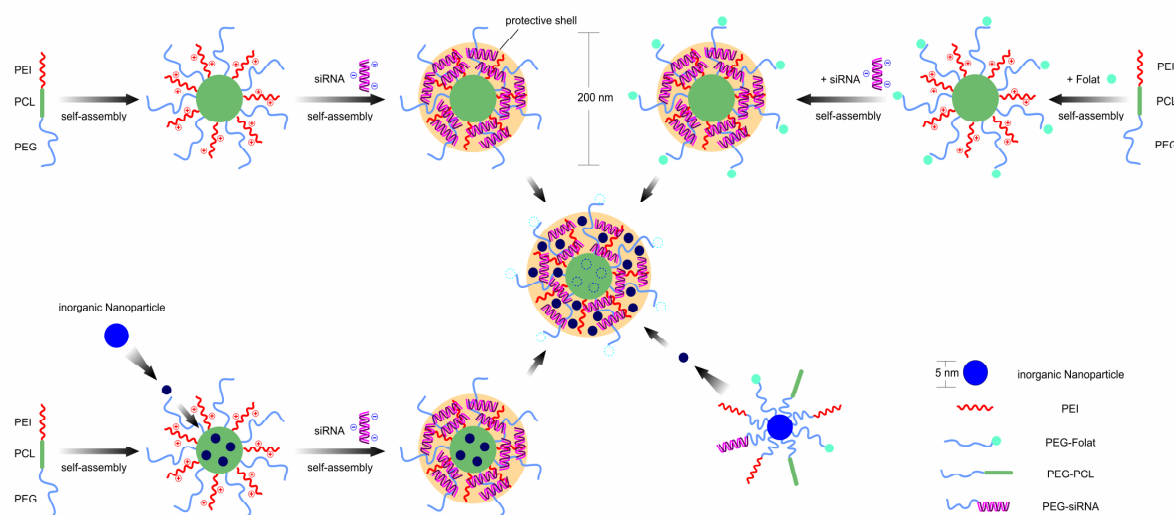


Figure 1: The design of potential multifunctional vectors for siRNA delivery. While the core of poly ethylene imine (PEI) complexes negatively charged nucleic acids and is known for its pH-sensitive “proton-sponge-effect” that triggers release of the complexes into the cytosol upon acidification (37), the second block in the block-copolymer-based delivery systems is poly caprolactone (PCL), a block that adds amphiphilicity. Poly ethylene glycol (PEG) is supposed to shield positive charges of siRNA/PEI complexes to reduce interaction with blood components and thereby increase circulation time in vivo (32). Addition of targeting moieties and inorganic particles for imaging further increases the multitude of possible applications.

1.2 Non-Viral Delivery of Nucleic Acids

One of the sectors of nanomedicine is delivery of nucleic acids, a sub-sector of drug delivery that this dissertation focuses on. In contrast to viral delivery vectors, which are highly efficient, non-viral counterparts bear less immunostimulatory, mutagenetic, and oncogenic complications, and some can approach viruses concerning their transfection efficiencies (33). Therapeutic nucleic acids of interest for nanomedicine can be DNA in plasmids (pDNA) (34), antisense oligonucleotides (AONs) (35), ribozymes (36), DNAzymes (37), and lately siRNA (38) and shRNA (39). While pDNA is used in gene

therapy to deliver missing or to replace dysfunctioning genes (40), all of the other therapeutic nucleic acids are utilized to down-regulate gene expression by post-transcriptional gene silencing (41). This also explains their different target compartments: pDNA as well as shRNA expression vectors need to be delivered into the nucleus for transcription, whereas the site of action of AONs, ribozymes, DNazymes, siRNA and shRNA is the cytosol. Unfortunately, cells lack an efficient uptake mechanism for nucleic acids, although there is evidence for a cell surface DNA-receptor (42) and for a putative transmembrane protein SID-1, which seems to be necessary for uptake of naked siRNA (43). Since all nucleic acids are labile, negatively charged biomacromolecules, spontaneous intracellular translocation that retains bioactivity of the macromolecules is unlikely. A sector of drug delivery research therefore focuses on protective formulation of nucleic acids into smart nanodevices that have high transfection efficiencies.

The primary prerequisites of delivery vehicles for nucleic acids that will finally make it from bench to bedside are biocompatibility and robust processes of assembly, conjugation and purification (7). Pre-formulation studies are commonly followed by the optimization of biophysicochemical parameters, and if successful, by scale-up for the manufacturing of therapeutic amounts. A broad variety of lipid based vectors, polymers, biopolymers, dendrimers, polypeptides, and inorganic nanoparticles have been investigated by groups all around the world (44). The most prominent polymeric vector is certainly poly (ethylene imine) (PEI), which is commercially available or can be polymerized as low or high molecular weight PEI (45). PEI was first introduced as non-viral gene delivery vector by Bousif et al. in 1995 (46) who described its outstanding property called the “proton-sponge-effect”. While liposomes escape the endo-/lysosomal compartment after endocytosis due to fusogenic properties, PEI is believed to attract an influx of chloride and subsequently an osmotic influx of water into the lysosome as it is protonated. This altogether leads to swelling and bursting of the lysosomes which release the polymer and nucleic acid into the cytosol.

Almost all polymeric vectors, unfortunately, have in common that they either form positively charged or amphiphilic complexes with nucleic acids that cause toxicity by interaction with negatively charged cell membranes (47) or cellular components and pathways after successful intracellular entry (48). There seems to be a correlation between transfection efficiency and toxicity up to the point where cells no longer survive. Since it has been reported that low molecular weight (LMW) PEI is significantly less toxic than

high molecular weight counterparts (34), a recent study investigated reversible disulfide-based cross-linking of LMW PEI (49) to achieve macromolecular vectors. A common principle for decreasing the surface charge of polycation-nucleic acids composites and their non-specific charge-dependent interactions was adopted from “stealth® liposomes” that are surface modified with poly (ethylene glycol) (PEG) or other hydrophilic compounds, such as carbohydrates (15). This steric stabilization decreased self-aggregation and interactions with proteins in biological fluids, and increased salt and serum stability (50). Also recognition and phagocytotic capture by cells of the reticulo endothelial system (RES) or aggregation within pulmonary capillary beds in vivo was prevented, and thereby their circulation half-lives were enhanced (51). Derivatives of PEI with PEG, saccharides and a monoclonal antibody (mAb) have been reported to yield stable complexes that partly retained their transfection efficiency (52). In a systematic study, different PEG grafting degrees and PEG chain lengths were investigated, suggesting that surface charge and toxicity decreased as a function of PEGylation. Transfection efficiency, on the other hand, decreased as well, at comparable polymer-to-DNA ratios, which could, because of the low toxicity, be readressed by increasing the polymer concentration (53). An even smarter system has recently been described where PEG chains are connected via a peptide sequence which is cleaved in presence of matrix metalloproteinases (MPPs) (54). Thus, the emerging multifunctional envelope-type nano devices (MENDs) are PEGylated extracellularly and lose the PEG block upon contact with an MPP that cleaves the peptide spacer. As non-specific endocytosis is triggered by interaction of cationic particles with heparin sulfate proteoglycans on the cell surface (55), a certain amount of positive surface charge of non-viral vectors is favorable. Other noteworthy modifications of PEI that were employed to enhance endosomal release, transfection efficiency, pharmacokinetic parameters, and biocompatibility, are full deacylation (56) and succinylation (57) of commercially available PEIs, crosslinking of branched HMW PEI (58, 59), synthesis of PEI-alginate composites (58), synthesis of amphiphilic (59) and cyclodextrin-threaded triblock copolymers (60), of 25kDa-PEI-cholesterol (61) and alkyl-oligoamine LMW-PEI derivatives (62), conjugation of melittin (63), grafting of chitosan (64), and immobilization on poly-L-lactide (PLLA) films for layer-by-layer assembly of polyelectrolytes (65) and, of course, conjugation of targeting ligands, as described below.

1.3 Targeted Gene Delivery Using Cell Specific Ligands

Targeted delivery systems are expected to selectively interact with internalizing receptors on certain cell types in a “lock and key” model that eventually triggers receptor-mediated uptake of the delivery system. Therefore, in this approach, non-specific, charge-related interactions that can also lead to non-specific toxicity are not necessary for efficient delivery. The dilemma that non-toxic, non-viral vectors which display neutral surface charge, are often less efficient than their non-shielded counterparts (53), can be overcome by attaching targeting ligands. As another advantage, selective delivery systems require much lower amounts of siRNA or DNA for the same effect as a result of specific transfection. Targeting approaches exploit the fact that certain receptors are overexpressed on a variety of tissues and especially malignant abnormal cells, due to their active proliferation and their demand for nourishment. Therefore, many targeted delivery systems are specific for growth factor receptors and are therefore suitable for tumor therapy (66). But one has to clearly differentiate between active and passive targeting. While tumor accumulation of nanoparticles is most likely due to the EPR effect (19) and has been reported to be not significantly different for targeted and non-targeted vectors, targeted intracellular uptake is mediated by cell-type and receptor-specific targeting moieties (67, 68). A variety of ligands have been used for modification of polymers to increase specificity, reduce the dose, and increase transfection efficiency. Conjugates of PEI are listed in Table 1.

Target Receptor	Ligand Used	Type of Cell or Tumor	Ref.
Asialoglycoprotein receptor	Lactose	Hepatocytes	(71)
	Galactose	Hepatocytes/ Airway Epithelial Cells	(69)
	Mannose	Dendritic Cells / Hepatocytes	(70)
Transferrin Receptor	Transferrin	Erythrocytes, Actively Proliferating Cells	(71)
Lactoferrin Receptor	Lactoferrin	Bronchial Epithelial Cells	(72)
Epidermal Growth Factor Receptor (EGFR)	Epidermal Growth Factor (EGF)	Variety of Cancer Cells	(73)
Human Epidermal Growth Factor Receptor 2 (HER2/neu)	Trastuzumab	Mamma Carcinoma	(74)

Target Receptor	Ligand Used	Type of Cell or Tumor	Ref.
Fibroblast Growth Factor Receptor	Fibroblast Growth Factor (FGF)	Fibroblasts	(75)
Nerve Growth Factor Receptor (NGFR)	Recombinant Peptide	Neuronal Cells	(76)
Folate Receptor	Folic Acid	Actively Proliferating Cells, Especially Nasopharyngeal KB Carcinoma Cells	(77)
Integrin Receptor ($\alpha_v\beta_3$)	RGD Peptides	Umbilical Cord Cells, Tumor Endothelial Cells	(78)
Hyaluronic Acid Receptor	Hyaluronic Acid	Liver and Kidney Cancer Cells	(79)
Platelet Endothelial Cell Adhesion Molecule (PECAM)	Anti-PECAM Antibody	Airway Endothelial Cells	(80)

Table 1: Conjugates of PEI for specific receptor interaction.

Even though successful targeting of liposomes was described in the literature almost 29 years ago (81), until today cell- or tissue-specific delivery has not been clinically exploited.

There are various further possible ligands such as aptamers (82), recombinant antibody fragments (83), affibodies (84), nanobodies (85) or synthetic peptidomimetics (86) which partly have been used to target other delivery systems than PEI. It is therefore obvious that a myriad of further multifunctional PEI-based vectors for known and to-be-determined targets are conceivable.

In this sense, Chapter 2 of this thesis describes specificity and activity of differently synthesized PEG-PEI-based gene delivery system coupled with a novel peptidomimetic small molecule targeting the integrin receptor alpha v beta 3.

1.4 Dendrimers in Gene Delivery

Dendrimers are highly branched monodisperse macromolecules with symmetrical architecture which can be synthesized by divergent or convergent routes (87). Their solubilizing properties are determined by the core and internal groups while their solubility and chemical behavior is mostly determined by their peripheral groups.

Because of their well-defined particle size and shape, dendrimers are of particular interest for gene transfer, but also for drug delivery and imaging applications (12, 94). Starburst polyamidoamine (PAMAM) is the most commonly used dendrimer in gene delivery and is commercially available as generation 4 “fractured” PAMAM (88) from Qiagen (SuperFect®) or in a variety of generations as cationic or half anionic dendrimers (96) from Dendritech. The heat-degraded structures are believed to feature higher chain flexibility which is drawn on for the increased transfection efficiency at low generation (88). PAMAM is also believed to interact with DNA like non-acetylated histones (89) in a way that initiation of transcription in the complexed DNA is inhibited. Due to their high buffer capacity, PAMAM dendrimers are thought to owe their transfection efficiency to the “proton sponge” effect first described for PEI (46). In an attempt to use poly (L-lysine) (PLL) modified PAMAM as transfection reagent, it was shown that PLL selectively condensed DNA, whereas PAMAM maintained endosomal release (90). While high transfection efficiencies of non-modified PAMAM are achieved only at relatively high generations of 5-10 (91), synthetic efforts were made to reduce the toxicity of PAMAM. This was successfully achieved by quarternization of the internal amines and by neutralizing the surface with a hydroxyl periphery, which on the other hand also reduced transfection efficiency (92). A year later, the same group reported another approach where they maintained high transfection efficiency in spite of low toxicity by synthesis of a PAMAM-PEG-PAMAM triblock copolymer (93). As already described for PEI, several modifications of PAMAM were synthesized to improve *in vitro* and *in vivo* parameters. Besides targeting strategies like the attachment of mannose (94) and galactose (95), further modifications include more amphiphilic vectors, such as alkyl chain- or phenylalanine-modified PAMAMs (96), other amino acid-modified PAMAMs (101), and cyclodextrin attachment to the surface (97).

Other dendrimers that have extensively been investigated and optimized for gene delivery are poly (propylenimine) (PPI) (98) and poly (L-lysine) (PLL) (99) based dendrimers. While PPI dendrimers exhibit their best transfection efficiencies at low generations of 2 and 3 (98), generations 5 and 6 of PLL dendrimers are most efficient (100). Several modifications of PPI, such as attachment of arginine (101) and quarternization (102) of the more acidic internal amines were achieved to improve transfection efficiency and DNA binding. Complexes of DNA and linear PLL are known to remain in the endo-/lysosomal compartment due to the lack of “protein sponge” effect of PLL (103). In line with the in

vitro results by Akinic et al., an in vivo study with PLL-based dendrimers was not successful concerning transgene expression although the dendriplexes accumulated in the tumor (104). PLL has also been modified in a number of synthetic approaches, for example by replacement of terminal lysine with arginine or histidine of which only the arginine modification enhanced transfection efficiency (105).

Additional groups of dendrimers that have been described as nucleic acid delivery systems are amino-functionalized dendritic polyglycerols (106), amine-modified polyaminophosphine dendrimers that show reduced aggregation behavior (107) and carbosilane dendrimers that have recently been employed for siRNA delivery to peripheral blood mononuclear cells and lymphocytic T-cells to reduce HIV replication (108).

In Chapter 3, structure-function relationships of a new class of dendrimers for delivery of nucleic acids are described, namely, differently substituted triazine dendrimers. Therefore, the impact of hydroxyl-, amine-, guanidinium-, or alkyl-periphery on physicochemical and biological parameters is evaluated.

Chapter 4 reports on the advancement of triazine dendrimers in terms of generation and core structure. As a result of further synthetic development, five different dendrimers of three different generations and 3 different core flexibilities were investigated concerning suitability as gene delivery vectors in a two-dimensional study design.

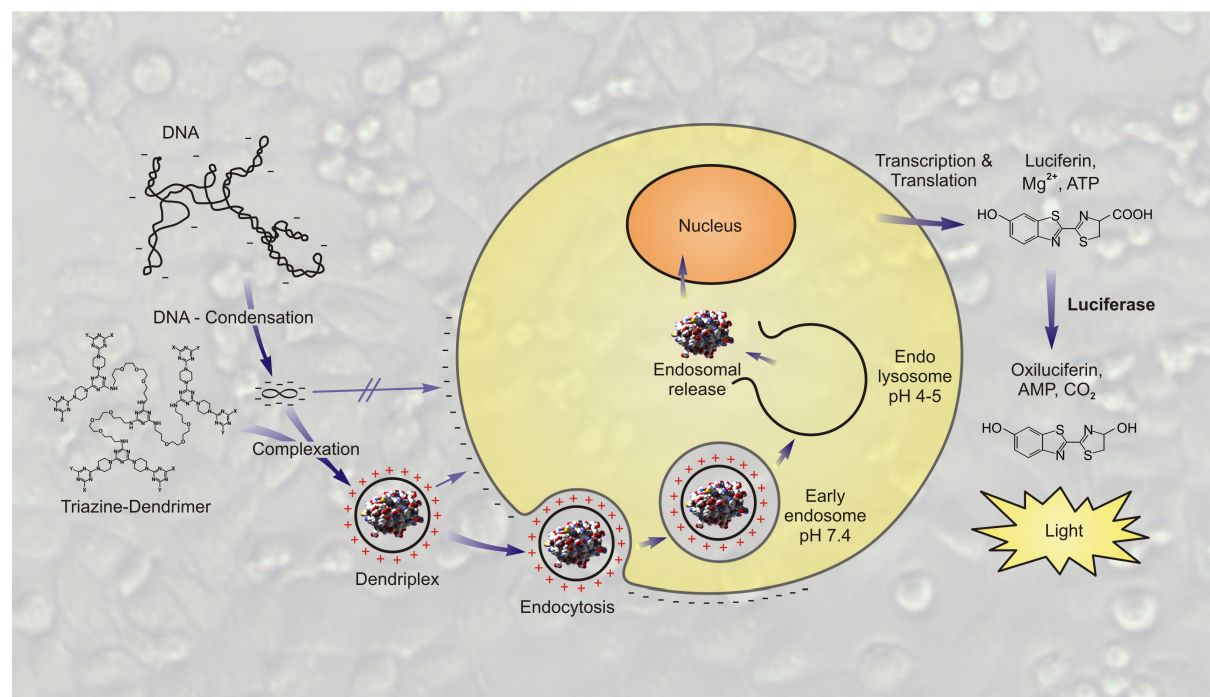


Figure 2: Triazine dendrimers are expected to condense pDNA, which is subsequently endocytosed. Efficient triazine dendrimer-mediated gene delivery of luciferase encoding

pDNA can be measured as bioluminescence in present of the substrate luciferin plus co-substrates. (Cover artwork for (109))

1.5 Concepts of siRNA Mediated Post-Transcriptional Gene Silencing

In 2006, Andrew Fire and Greg Mello were awarded the Nobel Prize in Physiology for their discovery of gene silencing by introduction of double-stranded RNA (dsRNA) (110). Their work lead to the identification of a catalytic mechanism of a multi-protein complex (111) which incorporates short RNAs that on their part are complementary in sequence to mRNA which is subsequently degraded (110). This mechanism which is an evolutionary conserved defense process for inactivation of foreign, e.g. transposable, viral or bacterial genetic information (112, 113), can also be exploited biotechnologically. Long dsRNA molecules which naturally or directedly reach the cytoplasm are degraded by “Dicer”, an RNase III-like enzyme, into small interfering RNAs (siRNAs) of 21 to 25 nucleotides in length (114). While long dsRNA can interact with Toll-like receptor 3 (TLR3) (115), synthetic short interfering RNA (siRNA) no longer than 19-21 base pairs with 2 nt 3’ overhangs is efficient (116, 117) and lacks interferon response (118). After being transferred into the cytosol, where it is incorporated into the RNA-induced silencing complex (RISC), double-stranded siRNA is cleaved upon activation of RISC, and complementary mRNA can bind to the antisense strand. Argonaute (Ago2), an endonuclease in the RISC, subsequently cleaves the mRNA leading to down-regulation of target gene expression.

Since the discovery of an RNA interference (RNAi) mechanism in mammalian cells, RNAi is routinely used in functional genomics and drug development (119, 120). RNA based therapeutics, on the other hand, are rather sparse. Due to their susceptibility to degradation by ubiquitous nucleases and their strongly negative surface charge, siRNA molecules require effective formulation and can not easily be compared with small molecule drugs (121). Besides interaction with plasma proteins and degradation by serum nucleases (122) and fast renal clearance in vivo (121), the bottlenecks in efficient RNAi are both translocation of siRNA across the plasma membrane, and its subsequent escape from the endosomal/lysosomal compartment. Despite of these drawbacks, successful reports on silencing efficacy of naked siRNA can be found in the literature where siRNA is instilled into the lung or the vagina (123-125) or delivered to the liver by high pressure tail vein injection (126, 127). Also most of the clinical trials involving siRNA based drugs rely on local administration to the eyes targeting age related macular degeneration (AMD) and

diabetic retinopathy (Acuity Pharmaceuticals, Alnylam Pharmaceuticals, Inc. and Sirna Therapeutics, Inc) or direct delivery to the brain or the lung (Alnylam Pharmaceuticals, Inc.). While SIRNA-Merck use chemically optimized siRNA in their clinical trial for the

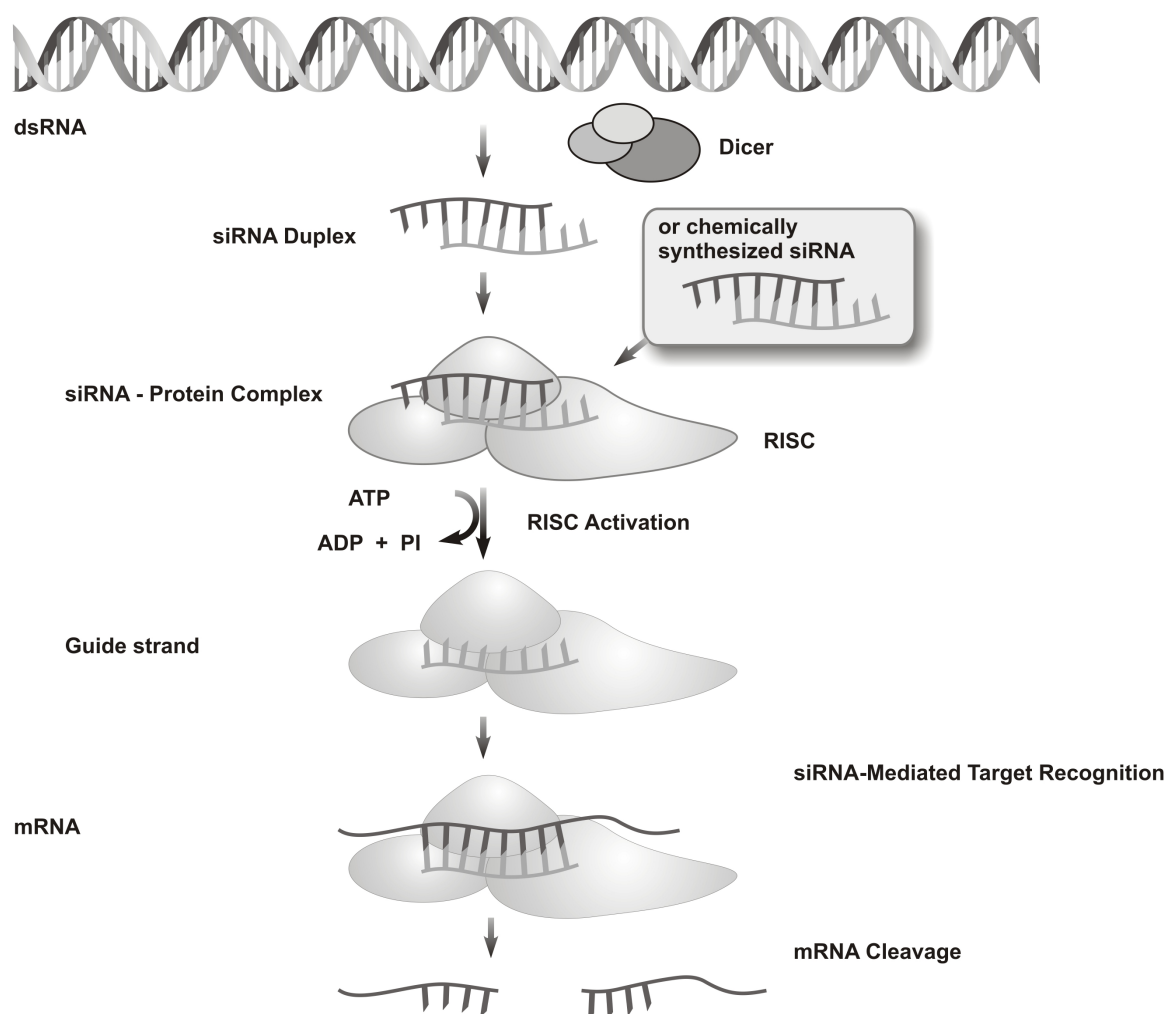


Figure 3: The mechanism of endogenous and induced RNA interference (RNAi). siRNA is eventually incorporated into the RISC where complementary mRNA binds before it is cleaved.

treatment of AMD, Alnylam apply cholesterol-attached siRNA targeting the nucleocapsid N gene of the respiratory syncytial virus (RSV), which was successful in their Phase II GEMINI study. Chemical modification of siRNA is not only a means to improve in vivo stability, which has been reported to be a result of modifications of backbone and/or ribose (128-130). The additional benefit of methylation of the ribose 2' hydroxyl group (2'-OMe) is the diminishing of immunostimulatory effects (131, 132) which have been described after liposomal delivery of siRNA (137). The knockdown kinetics of unmodified and nuclease-

stabilized siRNA was shown to be essentially the same (133). A promising systemic in vivo application of siRNA is gene silencing in the liver which can successfully be achieved with so called “SNALP” (stable nucleic acid lipid particles) formulations (134). Naked siRNA that is systemically applied is known to be excreted via the kidneys faster than it is degraded (135). Other formulations that have been investigated concerning their in vivo pharmacokinetics are post-PEGylated protamine-lipoplexes (68), adamantane-PEG-transferrin-bearing cyclodextrin-containing polyplexes (67), RNA–gold nanoparticle conjugates (136), chitosan, liposome and PEI formulated locked nucleic acids (LNAs) (137) and PEG-PEI polyplexes (138, 139). While post-PEGylation approaches (140) and cholesterol conjugation (135, 137) both extended the circulatory half-life, polyplexes made of pre-PEGylated PEI have often been presumed to disassemble in tissue (141) or circulation (139).

Even though RNAi-based knockdown of target mRNA or protein was frequently reported in the literature, none of the pharmaceutical companies have robust delivery systems that would lead to broad clinical translation into RNAi-based therapeutics. A highly interesting case is CALAA-01, the first experimental therapeutic that provides targeted delivery of siRNA in humans which has just completed phase I tolerability evaluation of intravenous application in adults with solid tumors refractory to standard-of-care therapies by Calando Pharmaceuticals (50). CALAA-01 refers to siRNA against the M2 subunit of ribonucleotide reductase (RRM2) formulated within the RONDEL™ delivery system, a transferrin-targeted cyclodextrin-containing polymer RNAi-nanotherapeutic.

Since the circulatory half-life and biodistribution of siRNA polyplexes has not been extensively conducted, in contrast to that of DNA polyplexes, Chapter 5 describes the optimization of a method for non-invasive determination of pharmacokinetics and biodistribution of siRNA polyplexes.

Chapter 6 makes use of the optimized method and correlates in vivo pharmacokinetics of various (PEG-)PEI/siRNA polyplexes with their in vivo stability, another parameter that is crucially important in the development of polymeric siRNA delivery systems.

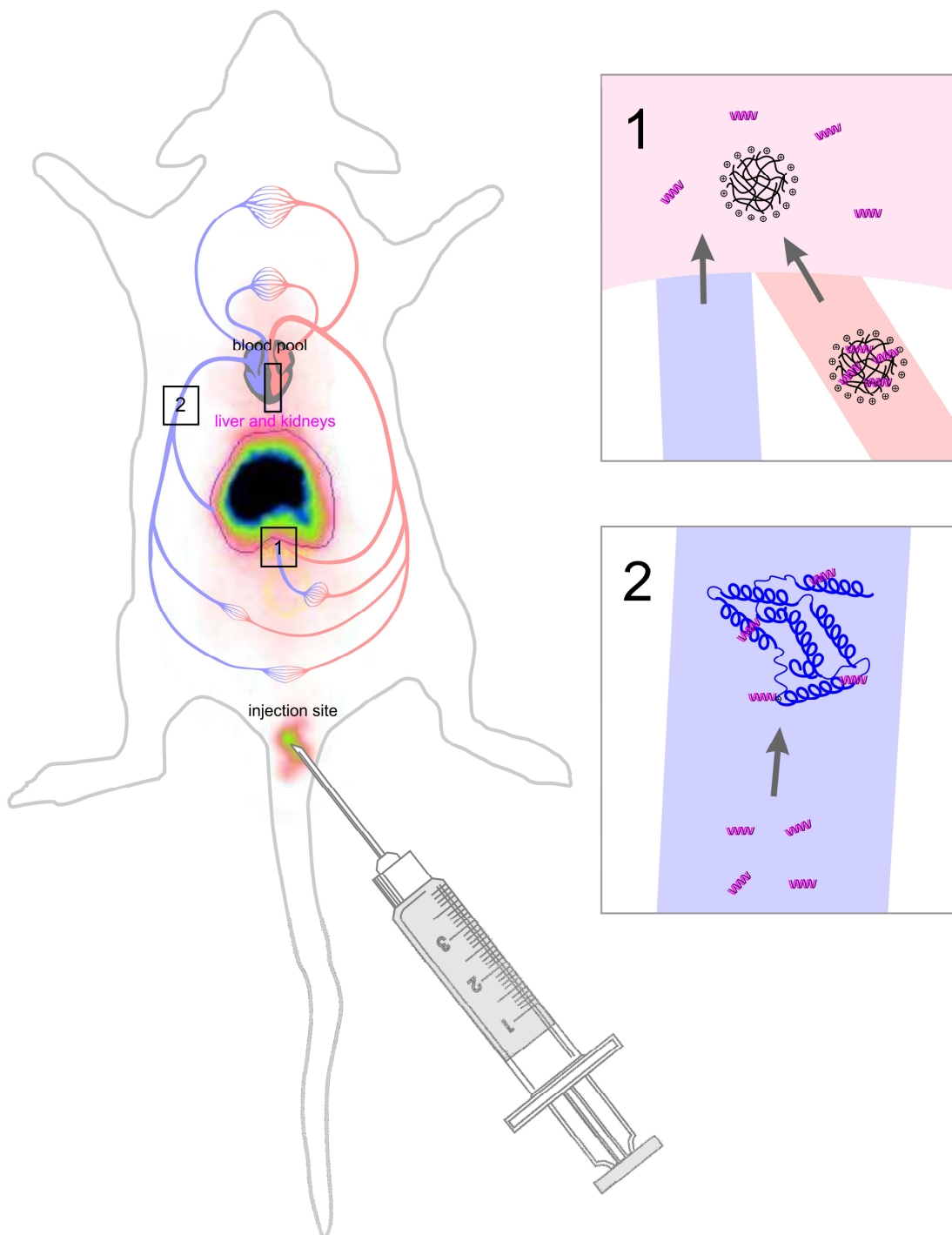


Figure 4: Intravenously applied complexes of nucleic acids and PEG-PEI have been suspected to disassemble either in the circulation or upon liver passage. If amphiphilic modifications of nucleic acids are used, binding to albumin is possible as well. (Table of Contents Graphic for (142))

1.6 Pulmonary siRNA Delivery

Delivery of siRNA to the lung has been studied as local administration of naked siRNA in 2004, already (124, 143, 144). As shown by Bitko et al. (143), knockdown efficiency could however be further enhanced by formulation with a delivery system. Major barriers that siRNA has to cross in the lung is the mucus secreted by goblet cells, the epithelium with tight junctions and the mucociliary and cellular clearance by macrophages. Despite of these hurdles, successful delivery of nucleic acids to the lung has been reported. While linear PEI (IPEI) of 22 kDa was described to be more efficient than branched PEI (bPEI) of 25 kDa molecular weight (145), coupling of the cell-penetrating-peptide TAT (146), derived from the HI virus, of transferrin (147), an RGD peptide (148) and galactose (149) via PEG increased transgene expression in the lung in non-viral gene delivery studies. Although gene delivery to the lung using PEI has been investigated by many groups, there are only little reports on pulmonary PEI-mediated siRNA delivery (56, 150, 151).

Local delivery of siRNA requires lower amounts, mostly avoids unwanted delivery to non-target organs and decreases elimination by renal filtration. Well described local applications of siRNA are intra-tumoral injections which have been reported to successfully down-regulate hypoxia inducible factor-1 α (HIF-1 α) in glioma xenografts (152) and direct application to the eye (153), but also intrathecal/intraventricular (154, 155) and intranasal (124, 143, 144) administration have been described. In an attempt to treat or prevent lung diseases, intranasal or intratracheal application of siRNA seems reasonable, while systemic delivery is not ideal for prevention of local infection. Since liposomal formulations that efficiently deliver siRNA (134, 156, 157) may be toxic to the mucosal epithelia and do not allow for controlled or sustained release (158), other effective, safe, non-irritating and preferentially smart delivery systems are needed. In a recent report by Robbins et al. that investigated off-target effects which had previously been misinterpreted as RNAi, activation of TLR7/8 or TLR3 was not observed when PEI complexes of 2'OMe siRNA were administered to the lung (151). PEI-mediated RNAi in the lung therefore seems to be possible and worthwhile to be further investigated.

In Chapter 7, pulmonary siRNA delivery with PEI and two PEGylated PEIs is described concerning biodistribution and systemic availability after intratracheal instillation as well as knockdown efficiency of EGFP in transgene mice. Referring to Robbins et al., in this study

2'OMe modified siRNA was used, and immune response was measured in the bronchioalveolar lavage fluid (BALF).

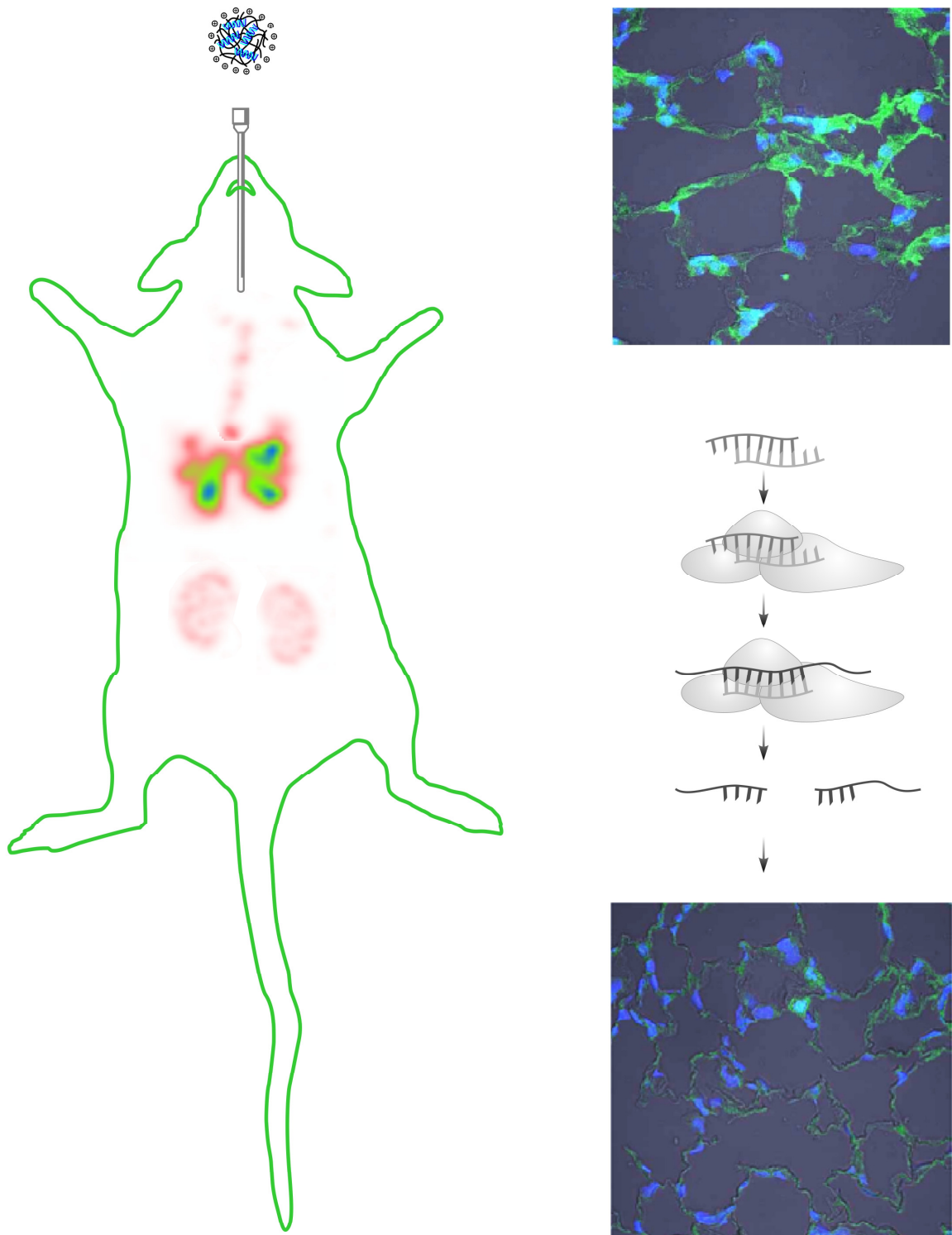


Figure 5: Investigation of biodistribution and bioactivity of intratracheally instilled siRNA by SPECT imaging and confocal laser scanning microscopy of lung tissue sections. (Table of Contents Graphic for (159))

1.7 Nuclear Imaging of siRNA Delivery

As recently described by Sanhai et al., one of the top priorities in nanomedicine is determination of nanoparticle biodistribution. Concerning kinetics of biodistributional changes, visualization over time or at certain timepoints in the same animal is crucial, and quantification of changes on a mass-balance basis is so far only provided by nuclear imaging (160). PET and SPECT are routinely used for diagnosis of cancer, inflammation, cardiac disease or neurological disorders (161). While the first small animal PET scans were of poor spatial resolution, today's small animal PET scanners with a resolution of 1 mm (162) even outrange pinhole-based small animal SPECT imaging. SPECT or gamma camera imaging detects gamma photons or X-rays of radionuclides that decay by electron capture or isomeric transition (163). A sodium iodide crystal in SPECT scanners detects the distribution of γ -ray emission, converts it into an electrical signal and eventually into an image. By (pinhole-)collimation between radioactive signal and detector, scattered radiation can be decreased. The γ -radiation energy of the radionuclide used needs to be high enough (80-250 keV) to penetrate the body in order to reach the detector, while energy can be decreased in small-animal imaging. The great advantage of SPECT is that various radionuclides with different photon energies can be acquired simultaneously in dual-isotope SPECT images. Sensitivity of SPECT is partly decreased due to the absorption of lead collimators, allowing only about 0.1 % of the γ -radiation to be detected. Therefore, high radiation doses and long acquisition times are needed for SPECT imaging (163). PET, on the other hand, uses radionuclides that emit positrons by β^+ decay which annihilate ubiquitous electrons, leading to conversion into two gamma photons of 511 keV. The detection of photons can either be instrumented with photon sensitive crystals or with detectors based on multi-wire gas chambers, where the photons are converted into electrons, which are multiplied in the gas and detected at the anode (164). The list of suitable positron emitters is not as broad as the one of gamma emitters. Additionally, PET imaging is more expensive, especially due to the high energy radionuclides, and can not be performed over several days because of their short half-lives.

Due to the possibility to acquire dynamic images and to non-invasively investigate biodistribution, nuclear imaging techniques are ideal methods to preclinically investigate pharmacokinetics and pharmacodynamics of new drugs, as has been reported for ^{18}F -fluoropaclitaxel (165). Nuclear imaging can even be seen as the bridging gap between basic, preclinical, clinical research, and clinical application (166). Since pharmacokinetic

parameters of siRNA delivery systems crucially affect their success and have to be evaluated for new delivery systems, PET and SPECT imaging are most helpful in preclinical investigations of delivery, binding and washout processes. Collection of kinetic data in small regions of interest (ROIs) even allows for calculation of pharmacokinetic parameters such as perfusion and clearance. Disadvantages of radiolabeling are surely instability issues and differences in biophysicochemical parameters of labeled and non-labeled particles. Both concerns have to be tested to obtain reliable results. Since no morphological data can be obtained from nuclear imaging, co-registration of MRI or computed tomography (CT) images in hybrid systems even enhances the significance of the images.

While tissue gamma counting and autoradiography have widely been performed with ^{32}P -labeled nucleic acids (*139, 167*), non-invasive detection of pharmacokinetics and biodistribution has only sparsely been reported (*67, 130, 168*), which can be understood as an issue in probe design.

Stability of self-assembled systems is an important issue under “working” conditions, especially if polycations are involved that are known to interact with cells and biological fluids, double labeling approaches are helpful in detecting biodistribution and kinetics of both the vector and the load (*139*).

Chapter 5 therefore challenges the probe design situation by optimizing a labeling and purification method for siRNA. In this chapter, pharmacokinetics and biodistribution of free siRNA versus PEI-complexed siRNA are described.

Chapter 6 investigates pharmacokinetics and biodistribution of multifunctional vectors made of pH-buffering PEI, sterical shielding PEG and an imaging moiety attached to either vector or load. In vivo stability is investigated utilizing fluorescently labeled siRNA for fluorescence fluctuation spectroscopy (FFS) and by radioactive double-labeling in order to correlate it with pharmacokinetics and biodistribution in a multicomponent approach.

In continuation of the results found in Chapter 6, Chapter 7 describes the suitability of local pulmonary application of siRNA/(PEI-)PEI polyplexes concerning biodistribution, assessed by imaging, and eventually in vivo knock down of target gene expression.

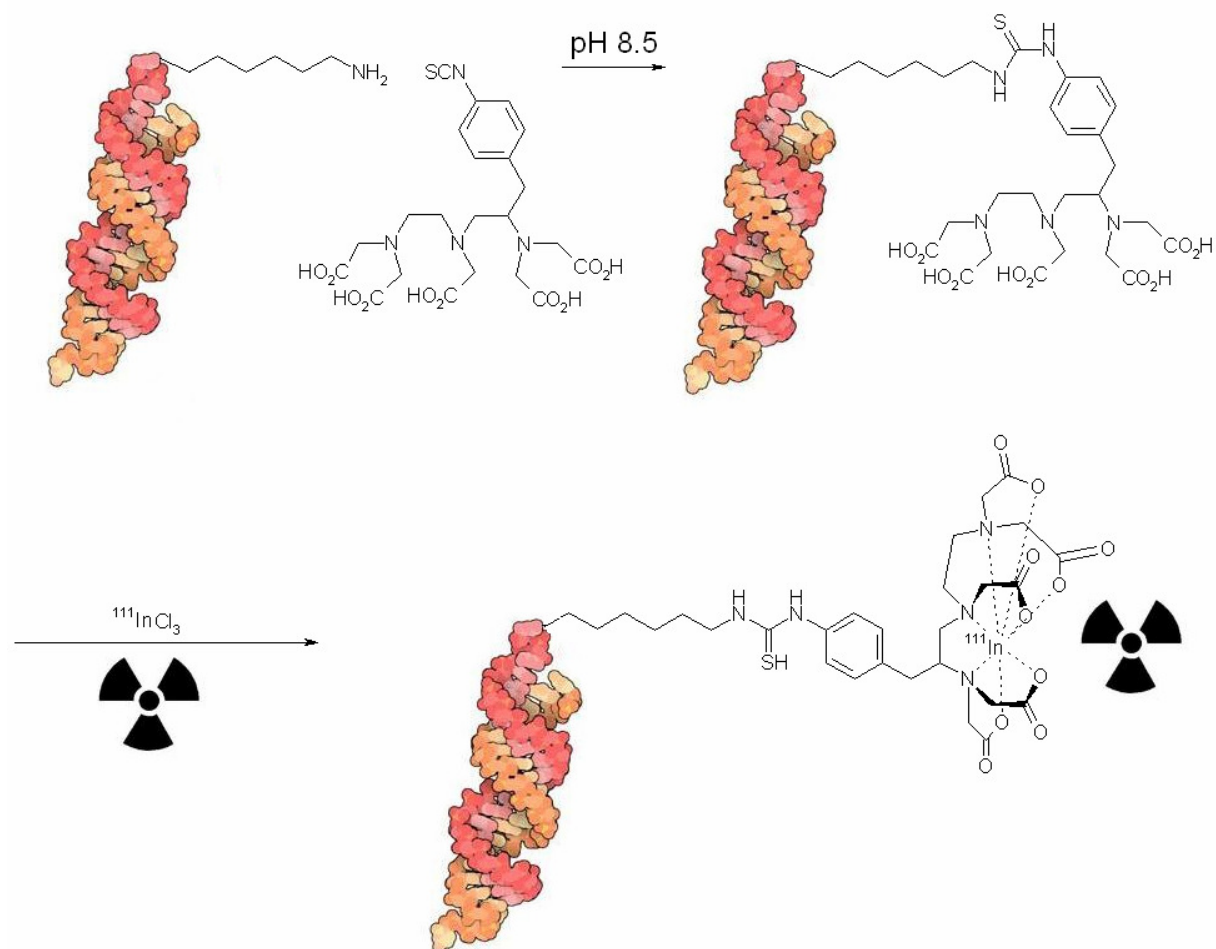


Figure 6: Amine-modified siRNA can easily be coupled with isothiocyanate derivatives of chelators for complexation of hot metal ions. Purification of the small RNA from excesses of chelator and metal ions has to be set great importance on to maintain valid data. (Similar as previously published (169))

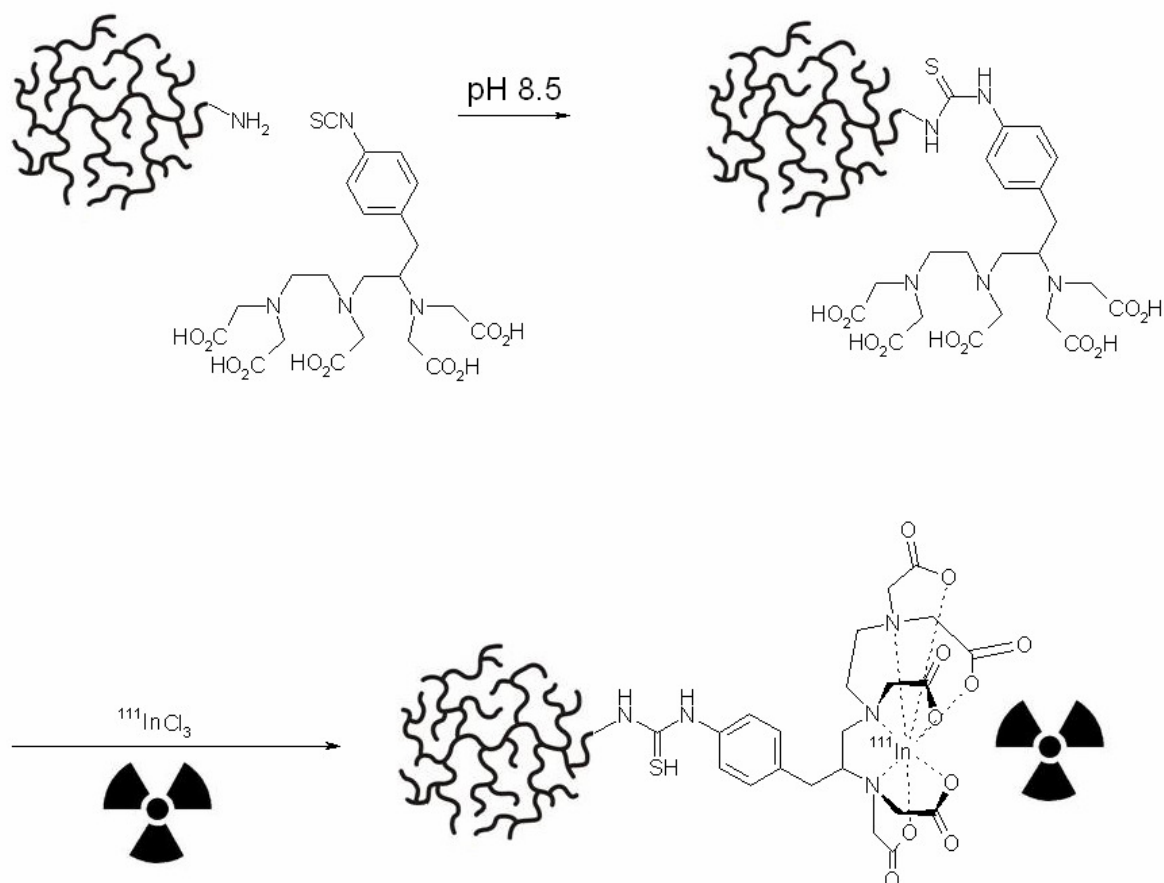


Figure 7: Polyamines like PEI can easily be radiolabeled and purified due to the large difference in molecular weights.

1.8 Polymer Genomics and Nanotoxicology

Potential safety issues that are a major concern for *in vivo* application of nano-sized particles can be neglected in certain *in vitro* diagnostics. As a difference is made between *in vitro* and *in vivo* applicability, QDs, for example, that are popularly used in cell culture, or even in animal models, do not have a good chance in becoming theragnostics for application in humans as a result of their material toxicity. Concerning nanotoxicity, the sort of material, the size, chemical composition at the surface, degradability, aspect ratio and soft- or hardness of matter are important parameters (170) with the main molecular mechanism for toxicity of nanomaterials being induction of oxidative stress (171).

While we are exposed to increasing concentrations of particulate matter (PM) in our daily lives (172), PM with a mean diameter of 2.5 μm (PM_{2.5}) can cause not only lung diseases but also cardio-vascular complications upon translocation of inhaled particles into other organs (173). The World Health Organization (WHO) has reported that life-expectancy can be decreased by up to ten months due to air pollution with PM (174), and the German Research Center for Environmental Health has proved that patients suffering from asthma exhibit augmented symptoms on days of high appearance of PM (175). Several American and European studies have shown a statistical correlation between air pollution and death rate, bronchitis, paranasal sinusitis and impairment of lung function (176). As it has been reported that environmental ultrafine particles (177) can have adverse effects on the respiratory tract, the potential of possible therapeutic nano devices is an important issue.

If it comes to toxicity of non-virally delivered siRNA, a less organ related level of toxicity but rather molecular toxicity can become an issue. Since endogenous small RNAs exist in perfect balance with their precursors and targets (178), cellular delivery of synthetic siRNA that is not optimally designed can cause saturation of the RNAi machinery and imbalance of the small RNA-mediated pathways, which leads to unwanted effects in the cell. Off-target effects such as activation of Toll-like receptors 3 (115) and 7/8 (179) have been reported, resulting in production of proinflammatory cytokines, and can be related to sequence-specific motifs in the sense or antisense strand (180). Other off-target effects can be caused by imperfect pairing between siRNA and mRNA (181), incorporation of the sense instead of the antisense strand into RISC (182), which can be avoided if the 5' phosphate group of the sense strand is modified (183). Without loss of specificity and bioactivity, immunostimulatory effects of siRNA have been reported to be diminished by chemical modification of the ribose, such as 2'OMe-, 2'F- or 2'deoxy-ribose (132, 156, 184, 185), while locked nucleic acids (LNAs) have been reported to cause hepatotoxicity in vivo (186). Another recent approach is synthesis of asymmetric shorter-duplex siRNA (asiRNA) that exhibit significantly decreased non-specific effects (187).

But unwanted and toxic effects in delivery of nucleic acids can as well be caused by the delivery vehicle or the emerging nanoscale particles. There are a number of reports in the literature explaining that drug delivery systems can not be considered as inert. Especially cationic polymers that are known to interact with membranes on the cellular level (47), but also subcellularly (188), can cause membrane toxicity and apoptosis. Additionally, a number of genes can be up- and down-regulated upon contact with polymers which is

investigated in “polymer genomics” or “toxicogenomics” (189, 190). Interestingly, polymers can have different effects than their polyplexes (189). Arising nanoparticulate devices therefore have to be well examined for their toxic potential (191), especially if applied to the lung, and nanomedicine unfortunately does not come without nanotoxicology (192).

Chapter 8 therefore investigates off-target effects related with nanotoxicity in a number of cell culture models and also factors in conditions given in artificial reporter gene expressing cell lines.

1.9 Structure of the Thesis: Aims and Outline

This thesis focuses on a number of issues in non-viral delivery of nucleic acids concerning biophysicochemical parameters and in vivo application. These factors are elucidated in this chapter and adopted in the following ones. Part I of the thesis describes new approaches in non-viral gene delivery vectors (Chapters 2-4), while Part II concentrates on in vitro and in vivo delivery of siRNA (Chapters 5-8).

In the context of targeted gene delivery, *Chapter 2* investigates bioconjugates of PEG-PEI and a novel peptidomimetic small molecule for integrin receptor targeting which are synthesized in two different routes. Hypothesizing that these conjugates would efficiently transfect integrin-overexpressing cells, their specificity, efficiency, biocompatibility and suitability are subject of that chapter. *Chapter 3* reports on a new class of dendritic non-viral vectors, namely triazine-based dendrimers. First of all, the impact of the peripheral groups of a generation 2 rigid dendrimer is observed by studies of complexation behavior, biocompatibility, and finally transfection efficiency. In continuation, *Chapter 4* describes the synthetic development of generation 1-3 rigid dendrimers, but also generation 2 bow-tie and flexible dendrimers, and their suitability as gene delivery vectors depending on structural parameters.

Chapter 5 emerged out of the lack of in vivo studies describing the pharmacokinetic parameters of naked or protected siRNA and establishes a method for fast and efficient radiolabeling and purification of siRNA for further non-invasive in vivo real-time imaging. This method is also applied in *Chapter 6* where pharmacokinetic parameters of siRNA complexed with differently PEGylated PEIs are compared. Additionally, that chapter accounts for instability issues of self-assembled complexes in a double-labeling approach and a specific investigation of stability in presence of serum using a sophisticated

fluorescence-based method. The same radiolabeled polyplexes are used for intratracheal application in *Chapter 7* which non-invasively observes residence times in the lung, but also bioavailability, biocompatibility and bioactivity in terms of target gene knock down. *Chapter 8* describes various reasons of off-target effects in non-viral siRNA delivery which can especially be observed in artificial cell lines that express reporter genes. Cytotoxic effects, gene regulation by polycations but also the impact of the promoter driving the reporter gene are investigated and new screening model cell lines are established.

All results are summarized in *Chapter 9*, where an outlook also provides information on further possible applications and developments.

1.10 References

- (1) Freitas, R. A., Jr. (2005) What is nanomedicine? *Nanomedicine 1*, 2-9.
- (2) Verdine, G. L., and Walensky, L. D. (2007) The Challenge of Drugging Undruggable Targets in Cancer: Lessons Learned from Targeting BCL-2 Family Members. *Clin Cancer Res 13*, 7264-7270.
- (3) Zhang, L., Gu, F. X., Chan, J. M., Wang, A. Z., Langer, R. S., and Farokhzad, O. C. (2007) Nanoparticles in Medicine: Therapeutic Applications and Developments. *Clin Pharmacol Ther 83*, 761-769.
- (4) Jain, K. K. (2007) Applications of Nanobiotechnology in Clinical Diagnostics. *Clin Chem 53*, 2002-2009.
- (5) Ozdemir, V., Williams-Jones, B., Glatt, S. J., Tsuang, M. T., Lohr, J. B., and Reist, C. (2006) Shifting emphasis from pharmacogenomics to theragnostics. *Nat Biotech 24*, 942-946.
- (6) Shubayev, V. I., Pisanic II, T. R., and Jin, S. (2009) Magnetic nanoparticles for theragnostics. *Advanced Drug Delivery Reviews 61*, 467-477.
- (7) Farokhzad, O. C., and Langer, R. (2009) Impact of Nanotechnology on Drug Delivery. *ACS Nano 3*, 16-20.
- (8) Charman, W. N., Chan, H.-K., Finnin, B. C., and Charman, S. A. (1999) Drug delivery: A key factor in realising the full therapeutic potential of drugs. *Drug Development Research 46*, 316-327.
- (9) Nguyen, J., Steele, T. W., Merkel, O., Reul, R., and Kissel, T. (2008) Fast degrading polyesters as siRNA nano-carriers for pulmonary gene therapy. *J Control Release*.
- (10) Yan, F., Zhang, C., Zheng, Y., Mei, L., Tang, L., Song, C., Sun, H., and Huang, L. The effect of poloxamer 188 on nanoparticle morphology, size, cancer cell uptake, and cytotoxicity. *Nanomedicine: Nanotechnology, Biology and Medicine In Press, Uncorrected Proof*.
- (11) Malafaya, P. B., Silva, G. A., and Reis, R. L. (2007) Natural-origin polymers as carriers and scaffolds for biomolecules and cell delivery in tissue engineering applications. *Advanced Drug Delivery Reviews 59*, 207-233.
- (12) Gao, Y., Gao, G., He, Y., Liu, T., and Qi, R. (2008) Recent advances of dendrimers in delivery of genes and drugs. *Mini Rev Med Chem 8*, 889-900.

-
- (13) Merdan, T., Kopecek, J., and Kissel, T. (2002) Prospects for cationic polymers in gene and oligonucleotide therapy against cancer. *Advanced Drug Delivery Reviews* 54, 715-758.
 - (14) Duncan, R., and Izzo, L. (2005) Dendrimer biocompatibility and toxicity. *Advanced Drug Delivery Reviews* 57, 2215-2237.
 - (15) Allen, T. M., Hansen, C. B., and de Menezes, D. E. L. (1995) Pharmacokinetics of long-circulating liposomes. *Advanced Drug Delivery Reviews* 16, 267-284.
 - (16) Kakizawa, Y., and Kataoka, K. (2002) Block copolymer micelles for delivery of gene and related compounds. *Advanced Drug Delivery Reviews* 54, 203-222.
 - (17) Van Thienen, T. G., Demeester, J., and De Smedt, S. C. (2008) Screening poly(ethyleneglycol) micro- and nanogels for drug delivery purposes. *Int J Pharm* 351, 174-85.
 - (18) bcc Research. (2006) in *Pharmaceuticals* (Shahani, S., Ed.) pp PHM006F, bcc Research.
 - (19) Matsumura, Y., and Maeda, H. (1986) A new concept for macromolecular therapeutics in cancer chemotherapy: mechanism of tumorotropic accumulation of proteins and the antitumor agent smancs. *Cancer Res* 46, 6387-92.
 - (20) Gao, X., Cui, Y., Levenson, R. M., Chung, L. W., and Nie, S. (2004) In vivo cancer targeting and imaging with semiconductor quantum dots. *Nat Biotechnol* 22, 969-76.
 - (21) Green, M. (2004) Semiconductor quantum dots as biological imaging agents. *Angew Chem Int Ed Engl* 43, 4129-31.
 - (22) Chen, A. A., Derfus, A. M., Khetani, S. R., and Bhatia, S. N. (2005) Quantum dots to monitor RNAi delivery and improve gene silencing. *Nucl. Acids Res.* 33, e190-.
 - (23) Chen, C., Peng, J., Xia, H. S., Yang, G. F., Wu, Q. S., Chen, L. D., Zeng, L. B., Zhang, Z. L., Pang, D. W., and Li, Y. (2009) Quantum dots-based immunofluorescence technology for the quantitative determination of HER2 expression in breast cancer. *Biomaterials* 30, 2912-8.
 - (24) Tan, W. B., Jiang, S., and Zhang, Y. (2007) Quantum-dot based nanoparticles for targeted silencing of HER2/neu gene via RNA interference. *Biomaterials* 28, 1565-71.
 - (25) de Vries, I. J., Lesterhuis, W. J., Barentsz, J. O., Verdijk, P., van Krieken, J. H., Boerman, O. C., Oyen, W. J., Bonenkamp, J. J., Boezeman, J. B., Adema, G. J., Bulte, J. W., Scheenen, T. W., Punt, C. J., Heerschap, A., and Figdor, C. G. (2005)

- Magnetic resonance tracking of dendritic cells in melanoma patients for monitoring of cellular therapy. *Nat Biotechnol* 23, 1407-13.
- (26) Atanasijevic, T., Shusteff, M., Fam, P., and Jasanoff, A. (2006) Calcium-sensitive MRI contrast agents based on superparamagnetic iron oxide nanoparticles and calmodulin. *Proceedings of the National Academy of Sciences* 103, 14707-14712.
- (27) Perez, J. M., Josephson, L., and Weissleder, R. (2004) Use of magnetic nanoparticles as nanosensors to probe for molecular interactions. *ChemBiochem* 5, 261-4.
- (28) Hartman, K. B., Wilson, L. J., and Rosenblum, M. G. (2008) Detecting and treating cancer with nanotechnology. *Mol Diagn Ther* 12, 1-14.
- (29) Kalambur, V. S., Longmire, E. K., and Bischof, J. C. (2007) Cellular level loading and heating of superparamagnetic iron oxide nanoparticles. *Langmuir* 23, 12329-36.
- (30) Partlow, K. C., Chen, J., Brant, J. A., Neubauer, A. M., Meyerrose, T. E., Creer, M. H., Nolta, J. A., Caruthers, S. D., Lanza, G. M., and Wickline, S. A. (2007) 19F magnetic resonance imaging for stem/progenitor cell tracking with multiple unique perfluorocarbon nanobeacons. *FASEB J* 21, 1647-54.
- (31) Rudin, M., and Weissleder, R. (2003) Molecular imaging in drug discovery and development. *Nat Rev Drug Discov* 2, 123-31.
- (32) Ogris, M., Brunner, S., Schuller, S., Kircheis, R., and Wagner, E. (1999) PEGylated DNA/transferrin-PEI complexes: reduced interaction with blood components, extended circulation in blood and potential for systemic gene delivery. *Gene Ther* 6, 595-605.
- (33) Li, S., and Huang, L. (2000) Nonviral gene therapy: promises and challenges. *Gene Ther* 7, 31-4.
- (34) Fischer, D., Bieber, T., Li, Y., Elsasser, H. P., and Kissel, T. (1999) A novel non-viral vector for DNA delivery based on low molecular weight, branched polyethylenimine: effect of molecular weight on transfection efficiency and cytotoxicity. *Pharm Res* 16, 1273-9.
- (35) Brus, C., Petersen, H., Aigner, A., Czubayko, F., and Kissel, T. (2004) Physicochemical and Biological Characterization of Polyethylenimine-graft-Poly(ethylene glycol) Block Copolymers as a Delivery System for Oligonucleotides and Ribozymes. *Bioconjugate Chem.* 15, 677-684.
- (36) Merdan, T., Kunath, K., Fischer, D., Kopecek, J., and Kissel, T. (2002) Intracellular processing of poly(ethylene imine)/ribozyme complexes can be observed in living

- cells by using confocal laser scanning microscopy and inhibitor experiments. *Pharm Res* 19, 140-6.
- (37) Dicke, T., Wegmann, M., Sel, S., Renz, H., and Garn, H. (2007) Gata-3-specific Dnazyme As An Approach For Asthma-therapy. *Journal of Allergy and Clinical Immunology* 119, S1-S1.
- (38) Mao, S., Neu, M., Germershaus, O., Merkel, O., Sitterberg, J., Bakowsky, U., and Kissel, T. (2006) Influence of Polyethylene Glycol Chain Length on the Physicochemical and Biological Properties of Poly(ethylene imine)-graft-Poly(ethylene glycol) Block Copolymer/SiRNA Polyplexes. *Bioconjug Chem* 17, 1209-18.
- (39) Jere, D., Xu, C.-X., Arote, R., Yun, C.-H., Cho, M.-H., and Cho, C.-S. (2008) Poly([beta]-amino ester) as a carrier for si/shRNA delivery in lung cancer cells. *Biomaterials* 29, 2535-2547.
- (40) Mulligan, R. C. (1993) The basic science of gene therapy. *Science* 260, 926-32.
- (41) Rudnick, S. I., Swaminathan, J., Sumaroka, M., Liebhaber, S., and Gewirtz, A. M. (2008) Effects of local mRNA structure on posttranscriptional gene silencing. *Proceedings of the National Academy of Sciences* 105, 13787-13792.
- (42) Bennett, R. M., Cornell, K. A., Merritt, M. J., Bakke, A. C., Mourich, D., and Hefeneider, S. H. (1992) Idiotypic mimicry of a cell surface DNA receptor: evidence for anti-DNA antibodies being a subset of anti-anti-DNA receptor antibodies. *Clin Exp Immunol* 90, 428-33.
- (43) Winston, W. M., Molodowitch, C., and Hunter, C. P. (2002) Systemic RNAi in *C. elegans* Requires the Putative Transmembrane Protein SID-1. *Science* 295, 2456-2459.
- (44) Mintzer, M. A., and Simanek, E. E. (2009) Nonviral vectors for gene delivery. *Chem Rev* 109, 259-302.
- (45) von Harpe, A., Petersen, H., Li, Y., and Kissel, T. (2000) Characterization of commercially available and synthesized polyethylenimines for gene delivery. *J Control Release* 69, 309-22.
- (46) Boussif, O., Lezoualc'h, F., Zanta, M. A., Mergny, M. D., Scherman, D., Demeneix, B., and Behr, J. P. (1995) A versatile vector for gene and oligonucleotide transfer into cells in culture and in vivo: polyethylenimine. *Proc Natl Acad Sci U S A* 92, 7297-301.

-
- (47) Hong, S., Leroueil, P. R., Janus, E. K., Peters, J. L., Kober, M. M., Islam, M. T., Orr, B. G., Baker, J. R., Jr., and Banaszak Holl, M. M. (2006) Interaction of polycationic polymers with supported lipid bilayers and cells: nanoscale hole formation and enhanced membrane permeability. *Bioconjug Chem* 17, 728-34.
- (48) Batrakova, E. V., and Kabanov, A. V. (2008) Pluronic block copolymers: evolution of drug delivery concept from inert nanocarriers to biological response modifiers. *J Control Release* 130, 98-106.
- (49) Breunig, M., Lungwitz, U., Liebl, R., and Goepferich, A. (2007) Breaking up the correlation between efficacy and toxicity for nonviral gene delivery. *Proc Natl Acad Sci U S A* 104, 14454-9.
- (50) Davis, M. E. (2009) The first targeted delivery of siRNA in humans via a self-assembling, cyclodextrin polymer-based nanoparticle: from concept to clinic. *Mol Pharm* 6, 659-68.
- (51) Immordino, M. L., Dosio, F., and Cattell, L. (2006) Stealth liposomes: review of the basic science, rationale, and clinical applications, existing and potential. *Int J Nanomedicine* 1, 297-315.
- (52) Erbacher, P., Bettinger, T., Belguise-Valladier, P., Zou, S., Coll, J. L., Behr, J. P., and Remy, J. S. (1999) Transfection and physical properties of various saccharide, poly(ethylene glycol), and antibody-derivatized polyethylenimines (PEI). *J Gene Med* 1, 210-22.
- (53) Petersen, H., Fechner, P. M., Martin, A. L., Kunath, K., Stolnik, S., Roberts, C. J., Fischer, D., Davies, M. C., and Kissel, T. (2002) Polyethylenimine-graft-poly(ethylene glycol) copolymers: influence of copolymer block structure on DNA complexation and biological activities as gene delivery system. *Bioconjug Chem* 13, 845-54.
- (54) Hatakeyama, H., Itho, E., Akita, H., Oishi, M., Nagasaki, Y., Futaki, S., and Harashima, H. (2009) A pH-sensitive fusogenic peptide facilitates endosomal escape and greatly enhances the gene silencing of siRNA-containing nanoparticles in vitro and in vivo. *J Control Release*.
- (55) Mounkes, L. C., Zhong, W., Cipres-Palacin, G., Heath, T. D., and Debs, R. J. (1998) Proteoglycans mediate cationic liposome-DNA complex-based gene delivery in vitro and in vivo. *J Biol Chem* 273, 26164-70.

-
- (56) Thomas, M., Lu, J. J., Ge, Q., Zhang, C., Chen, J., and Klibanov, A. M. (2005) Full deacylation of polyethylenimine dramatically boosts its gene delivery efficiency and specificity to mouse lung. *Proc Natl Acad Sci U S A* 102, 5679-84.
- (57) Zintchenko, A., Philipp, A., Dehshahri, A., and Wagner, E. (2008) Simple modifications of branched PEI lead to highly efficient siRNA carriers with low toxicity. *Bioconjug Chem* 19, 1448-55.
- (58) Patnaik, S., Aggarwal, A., Nimesh, S., Goel, A., Ganguli, M., Saini, N., Singh, Y., and Gupta, K. C. (2006) PEI-alginate nanocomposites as efficient in vitro gene transfection agents. *J Control Release* 114, 398-409.
- (59) Liu, Y., Nguyen, J., Steele, T., Merkel, O., and Kissel, T. A new synthesis method and degradation of hyper-branched polyethylenimine grafted polycaprolactone block mono-methoxyl poly (ethylene glycol) copolymers (hy-PEI-g-PCL-b-mPEG) as potential DNA delivery vectors. *Polymer In Press, Accepted Manuscript*.
- (60) Shuai, X., Merdan, T., Unger, F., and Kissel, T. (2005) Supramolecular gene delivery vectors showing enhanced transgene expression and good biocompatibility. *Bioconjug Chem* 16, 322-9.
- (61) Gusachenko Simonova, O., Kravchuk, Y., Konevets, D., Silnikov, V., Vlassov, V. V., and Zenkova, M. A. (2009) Transfection efficiency of 25-kDa PEI-cholesterol conjugates with different levels of modification. *J Biomater Sci Polym Ed* 20, 1091-110.
- (62) Dehshahri, A., Oskuee, R. K., Shier, W. T., Hatefi, A., and Ramezani, M. (2009) Gene transfer efficiency of high primary amine content, hydrophobic, alkyl-oligoamine derivatives of polyethylenimine. *Biomaterials*.
- (63) Boeckle, S., Fahrmeir, J., Roedl, W., Ogris, M., and Wagner, E. (2006) Melittin analogs with high lytic activity at endosomal pH enhance transfection with purified targeted PEI polyplexes. *J Control Release* 112, 240-8.
- (64) Jere, D., Jiang, H. L., Kim, Y. K., Arote, R., Choi, Y. J., Yun, C. H., Cho, M. H., and Cho, C. S. (2009) Chitosan-graft-polyethylenimine for Akt1 siRNA delivery to lung cancer cells. *Int J Pharm*.
- (65) Liu, Z. M., Lee, S. Y., Sarun, S., Peschel, D., and Groth, T. (2009) Immobilization of poly (ethylene imine) on poly (L: -lactide) promotes MG63 cell proliferation and function. *J Mater Sci Mater Med*.

-
- (66) Peer, D., Karp, J. M., Hong, S., Farokhzad, O. C., Margalit, R., and Langer, R. (2007) Nanocarriers as an emerging platform for cancer therapy. *Nat Nano* 2, 751-760.
- (67) Bartlett, D. W., Su, H., Hildebrandt, I. J., Weber, W. A., and Davis, M. E. (2007) Impact of tumor-specific targeting on the biodistribution and efficacy of siRNA nanoparticles measured by multimodality in vivo imaging. *Proc Natl Acad Sci U S A* 104, 15549-54.
- (68) Li, S. D., Chen, Y. C., Hackett, M. J., and Huang, L. (2008) Tumor-targeted delivery of siRNA by self-assembled nanoparticles. *Mol Ther* 16, 163-9.
- (69) Kunath, K., von Harpe, A., Fischer, D., and Kissel, T. (2003) Galactose-PEI-DNA complexes for targeted gene delivery: degree of substitution affects complex size and transfection efficiency. *J Control Release* 88, 159-72.
- (70) Diebold, S. S., Kursa, M., Wagner, E., Cotten, M., and Zenke, M. (1999) Mannose polyethylenimine conjugates for targeted DNA delivery into dendritic cells. *J Biol Chem* 274, 19087-94.
- (71) Kircheis, R., Kichler, A., Wallner, G., Kursa, M., Ogris, M., Felzmann, T., Buchberger, M., and Wagner, E. (1997) Coupling of cell-binding ligands to polyethylenimine for targeted gene delivery. *Gene Ther* 4, 409-18.
- (72) Elfinger, M., Maucksch, C., and Rudolph, C. (2007) Characterization of lactoferrin as a targeting ligand for nonviral gene delivery to airway epithelial cells. *Biomaterials* 28, 3448-55.
- (73) von Gersdorff, K., Ogris, M., and Wagner, E. (2005) Cryoconserved shielded and EGF receptor targeted DNA polyplexes: cellular mechanisms. *Eur J Pharm Biopharm* 60, 279-85.
- (74) Germershaus, O., Merdan, T., Bakowsky, U., Behe, M., and Kissel, T. (2006) Trastuzumab-polyethylenimine-polyethylene glycol conjugates for targeting Her2-expressing tumors. *Bioconjug Chem* 17, 1190-9.
- (75) Li, D., Wang, Q. Q., Tang, G. P., Huang, H. L., Shen, F. P., Li, J. Z., and Yu, H. (2006) Receptor-mediated gene delivery using polyethylenimine (PEI) coupled with polypeptides targeting FGF receptors on cells surface. *J Zhejiang Univ Sci B* 7, 906-11.
- (76) Ma, N., Wu, S. S., Ma, Y. X., Wang, X., Zeng, J., Tong, G., Huang, Y., and Wang, S. (2004) Nerve growth factor receptor-mediated gene transfer. *Mol Ther* 9, 270-81.

-
- (77) Guo, W., and Lee, R. L. (1999) Receptor-targeted gene delivery via folate-conjugated polyethylenimine. *AAPS PharmSci* 1, E19.
- (78) Kunath, K., Merdan, T., Hegener, O., Haberlein, H., and Kissel, T. (2003) Integrin targeting using RGD-PEI conjugates for in vitro gene transfer. *J Gene Med* 5, 588-99.
- (79) Jiang, G., Park, K., Kim, J., Kim, K. S., and Hahn, S. K. (2009) Target specific intracellular delivery of siRNA/PEI-HA complex by receptor mediated endocytosis. *Mol Pharm* 6, 727-37.
- (80) Li, S., Tan, Y., Viroonchatapan, E., Pitt, B. R., and Huang, L. (2000) Targeted gene delivery to pulmonary endothelium by anti-PECAM antibody. *Am J Physiol Lung Cell Mol Physiol* 278, L504-11.
- (81) Leserman, L. D., Barbet, J., Kourilsky, F., and Weinstein, J. N. (1980) Targeting to cells of fluorescent liposomes covalently coupled with monoclonal antibody or protein A. *Nature* 288, 602-4.
- (82) Zhou, J., Li, H., Li, S., Zaia, J., and Rossi, J. J. (2008) Novel dual inhibitory function aptamer-siRNA delivery system for HIV-1 therapy. *Mol Ther* 16, 1481-9.
- (83) Messerschmidt, S. K., Musyanovych, A., Altvater, M., Scheurich, P., Pfizenmaier, K., Landfester, K., and Kontermann, R. E. (2009) Targeted lipid-coated nanoparticles: delivery of tumor necrosis factor-functionalized particles to tumor cells. *J Control Release* 137, 69-77.
- (84) Beuttler, J., Rothdiener, M., Muller, D., Frejd, F. Y., and Kontermann, R. E. (2009) Targeting of epidermal growth factor receptor (EGFR)-expressing tumor cells with sterically stabilized affibody liposomes (SAL). *Bioconjug Chem* 20, 1201-8.
- (85) Huang, L., Gai, L. O., Caveliers, V., Vanhove, C., Keyaerts, M., De Baetselier, P., Bossuyt, A., Revets, H., and Lahoutte, T. (2008) SPECT imaging with ^{99m}Tc-labeled EGFR-specific nanobody for in vivo monitoring of EGFR expression. *Mol Imaging Biol* 10, 167-75.
- (86) Pardridge, W. M. (2002) Drug and gene targeting to the brain with molecular Trojan horses. *Nat Rev Drug Discov* 1, 131-9.
- (87) Svenson, S., and Tomalia, D. A. (2005) Dendrimers in biomedical applications--reflections on the field. *Adv Drug Deliv Rev* 57, 2106-29.
- (88) Tang, M. X., Redemann, C. T., and Szoka, F. C., Jr. (1996) In vitro gene delivery by degraded polyamidoamine dendrimers. *Bioconjug Chem* 7, 703-14.

-
- (89) Bielinska, A. U., Kukowska-Latallo, J. F., and Baker, J. R., Jr. (1997) The interaction of plasmid DNA with polyamidoamine dendrimers: mechanism of complex formation and analysis of alterations induced in nuclease sensitivity and transcriptional activity of the complexed DNA. *Biochim Biophys Acta* 1353, 180-90.
- (90) Harada, A., Kawamura, M., Matsuo, T., Takahashi, T., and Kono, K. (2006) Synthesis and characterization of a head-tail type polycation block copolymer as a nonviral gene vector. *Bioconjug Chem* 17, 3-5.
- (91) Kukowska-Latallo, J. F., Bielinska, A. U., Johnson, J., Spindler, R., Tomalia, D. A., and Baker, J. R., Jr. (1996) Efficient transfer of genetic material into mammalian cells using Starburst polyamidoamine dendrimers. *Proc Natl Acad Sci U S A* 93, 4897-902.
- (92) Lee, J. H., Lim, Y. B., Choi, J. S., Lee, Y., Kim, T. I., Kim, H. J., Yoon, J. K., Kim, K., and Park, J. S. (2003) Polyplexes assembled with internally quaternized PAMAM-OH dendrimer and plasmid DNA have a neutral surface and gene delivery potency. *Bioconjug Chem* 14, 1214-21.
- (93) Kim, T. I., Seo, H. J., Choi, J. S., Jang, H. S., Baek, J. U., Kim, K., and Park, J. S. (2004) PAMAM-PEG-PAMAM: novel triblock copolymer as a biocompatible and efficient gene delivery carrier. *Biomacromolecules* 5, 2487-92.
- (94) Wada, K., Arima, H., Tsutsumi, T., Chihara, Y., Hattori, K., Hirayama, F., and Uekama, K. (2005) Improvement of gene delivery mediated by mannosylated dendrimer/alpha-cyclodextrin conjugates. *J Control Release* 104, 397-413.
- (95) Wada, K., Arima, H., Tsutsumi, T., Hirayama, F., and Uekama, K. (2005) Enhancing effects of galactosylated dendrimer/alpha-cyclodextrin conjugates on gene transfer efficiency. *Biol Pharm Bull* 28, 500-5.
- (96) Kono, K., Akiyama, H., Takahashi, T., Takagishi, T., and Harada, A. (2005) Transfection activity of polyamidoamine dendrimers having hydrophobic amino acid residues in the periphery. *Bioconjug Chem* 16, 208-14.
- (97) Arima, H., Kihara, F., Hirayama, F., and Uekama, K. (2001) Enhancement of gene expression by polyamidoamine dendrimer conjugates with alpha-, beta-, and gamma-cyclodextrins. *Bioconjug Chem* 12, 476-84.
- (98) Zinselmeyer, B. H., Mackay, S. P., Schatzlein, A. G., and Uchegbu, I. F. (2002) The lower-generation polypropylenimine dendrimers are effective gene-transfer agents. *Pharm Res* 19, 960-7.

-
- (99) Shah, D. S., Sakthivel, T., Toth, I., Florence, A. T., and Wilderspin, A. F. (2000) DNA transfection and transfected cell viability using amphipathic asymmetric dendrimers. *Int J Pharm* 208, 41-8.
- (100) Ohsaki, M., Okuda, T., Wada, A., Hirayama, T., Niidome, T., and Aoyagi, H. (2002) In vitro gene transfection using dendritic poly(L-lysine). *Bioconjug Chem* 13, 510-7.
- (101) Kim, T. I., Baek, J. U., Zhe Bai, C., and Park, J. S. (2007) Arginine-conjugated polypropylenimine dendrimer as a non-toxic and efficient gene delivery carrier. *Biomaterials* 28, 2061-7.
- (102) Schatzlein, A. G., Zinselmeyer, B. H., Elouzi, A., Dufes, C., Chim, Y. T., Roberts, C. J., Davies, M. C., Munro, A., Gray, A. I., and Uchegbu, I. F. (2005) Preferential liver gene expression with polypropylenimine dendrimers. *J Control Release* 101, 247-58.
- (103) Akinc, A., Thomas, M., Klivanov, A. M., and Langer, R. (2005) Exploring polyethylenimine-mediated DNA transfection and the proton sponge hypothesis. *J Gene Med* 7, 657-63.
- (104) Kawano, T., Okuda, T., Aoyagi, H., and Niidome, T. (2004) Long circulation of intravenously administered plasmid DNA delivered with dendritic poly(L-lysine) in the blood flow. *J Control Release* 99, 329-37.
- (105) Okuda, T., Sugiyama, A., Niidome, T., and Aoyagi, H. (2004) Characters of dendritic poly(L-lysine) analogues with the terminal lysines replaced with arginines and histidines as gene carriers in vitro. *Biomaterials* 25, 537-44.
- (106) Koc, F., Wyszogrodzka, M., Eilbracht, P., and Haag, R. (2005) Highly regioselective synthesis of amino-functionalized dendritic polyglycerols by a one-pot hydroformylation/reductive amination sequence. *J Org Chem* 70, 2021-5.
- (107) Maszewska, M., Leclaire, J., Cieslak, M., Nawrot, B., Okruszek, A., Caminade, A. M., and Majoral, J. P. (2003) Water-soluble polycationic dendrimers with a phosphoramidothioate backbone: preliminary studies of cytotoxicity and oligonucleotide/plasmid delivery in human cell culture. *Oligonucleotides* 13, 193-205.
- (108) Weber, N., Ortega, P., Clemente, M. I., Shcharbin, D., Bryszewska, M., de la Mata, F. J., Gómez, R., and Muñoz-Fernández, M. A. (2008) Characterization of carbosilane dendrimers as effective carriers of siRNA to HIV-infected lymphocytes. *Journal of Controlled Release* 132, 55-64.

-
- (109) Mintzer, M. A., Merkel, O. M., Kissel, T., and Simanek, E. (2009) Polycationic triazine-based dendrimers: Effect of peripheral groups on transfection efficiency. *New Journal of Chemistry* doi: 10.1039/b908735d.
- (110) Fire, A., Xu, S., Montgomery, M. K., Kostas, S. A., Driver, S. E., and Mello, C. C. (1998) Potent and specific genetic interference by double-stranded RNA in *Caenorhabditis elegans*. *Nature* 391, 806-11.
- (111) Hammond, S. M., Boettcher, S., Caudy, A. A., Kobayashi, R., and Hannon, G. J. (2001) Argonaute2, a link between genetic and biochemical analyses of RNAi. *Science* 293, 1146-50.
- (112) Katiyar-Agarwal, S., Morgan, R., Dahlbeck, D., Borsani, O., Villegas, A., Jr., Zhu, J. K., Staskawicz, B. J., and Jin, H. (2006) A pathogen-inducible endogenous siRNA in plant immunity. *Proc Natl Acad Sci U S A* 103, 18002-7.
- (113) Navarro, L., Dunoyer, P., Jay, F., Arnold, B., Dharmasiri, N., Estelle, M., Voinnet, O., and Jones, J. D. (2006) A plant miRNA contributes to antibacterial resistance by repressing auxin signaling. *Science* 312, 436-9.
- (114) Agrawal, N., Dasaradhi, P. V., Mohammed, A., Malhotra, P., Bhatnagar, R. K., and Mukherjee, S. K. (2003) RNA interference: biology, mechanism, and applications. *Microbiol Mol Biol Rev* 67, 657-85.
- (115) Kariko, K., Bhuyan, P., Capodici, J., and Weissman, D. (2004) Small interfering RNAs mediate sequence-independent gene suppression and induce immune activation by signaling through toll-like receptor 3. *J Immunol* 172, 6545-9.
- (116) Elbashir, S. M., Harborth, J., Lendeckel, W., Yalcin, A., Weber, K., and Tuschl, T. (2001) Duplexes of 21-nucleotide RNAs mediate RNA interference in cultured mammalian cells. *Nature* 411, 494-8.
- (117) Elbashir, S. M., Lendeckel, W., and Tuschl, T. (2001) RNA interference is mediated by 21- and 22-nucleotide RNAs. *Genes Dev* 15, 188-200.
- (118) Heidel, J. D., Hu, S., Liu, X. F., Triche, T. J., and Davis, M. E. (2004) Lack of interferon response in animals to naked siRNAs. *Nat Biotechnol*.
- (119) Dorsett, Y., and Tuschl, T. (2004) siRNAs: applications in functional genomics and potential as therapeutics. *Nat Rev Drug Discov* 3, 318-29.
- (120) Gomase, V. S., and Tagore, S. (2008) RNAi--a tool for target finding in new drug development. *Curr Drug Metab* 9, 241-4.

-
- (121) Dykxhoorn, D. M., and Lieberman, J. (2006) Running interference: prospects and obstacles to using small interfering RNAs as small molecule drugs. *Annu Rev Biomed Eng* 8, 377-402.
- (122) Braasch, D. A., Paroo, Z., Constantinescu, A., Ren, G., Oz, O. K., Mason, R. P., and Corey, D. R. (2004) Biodistribution of phosphodiester and phosphorothioate siRNA. *Bioorg Med Chem Lett* 14, 1139-43.
- (123) Palliser, D., Chowdhury, D., Wang, Q.-Y., Lee, S. J., Bronson, R. T., Knipe, D. M., and Lieberman, J. (2006) An siRNA-based microbicide protects mice from lethal herpes simplex virus 2 infection. *Nature* 439, 89-94.
- (124) Zhang, X., Shan, P., Jiang, D., Noble, P. W., Abraham, N. G., Kappas, A., and Lee, P. J. (2004) Small interfering RNA targeting heme oxygenase-1 enhances ischemia-reperfusion-induced lung apoptosis. *J Biol Chem* 279, 10677-84.
- (125) Lomas-Neira, J. L., Chung, C. S., Wesche, D. E., Perl, M., and Ayala, A. (2005) In vivo gene silencing (with siRNA) of pulmonary expression of MIP-2 versus KC results in divergent effects on hemorrhage-induced, neutrophil-mediated septic acute lung injury. *J Leukoc Biol* 77, 846-53.
- (126) Giladi, H., Ketzinel-Gilad, M., Rivkin, L., Felig, Y., Nussbaum, O., and Galun, E. (2003) Small interfering RNA inhibits hepatitis B virus replication in mice. *Mol Ther* 8, 769-76.
- (127) Song, E., Lee, S. K., Wang, J., Ince, N., Ouyang, N., Min, J., Chen, J., Shankar, P., and Lieberman, J. (2003) RNA interference targeting Fas protects mice from fulminant hepatitis. *Nat Med* 9, 347-51.
- (128) Manoharan, M. (2004) RNA interference and chemically modified small interfering RNAs. *Curr Opin Chem Biol* 8, 570-9.
- (129) Geary, R. S., Watanabe, T. A., Truong, L., Freier, S., Lesnik, E. A., Sioufi, N. B., Sasmor, H., Manoharan, M., and Levin, A. A. (2001) Pharmacokinetic properties of 2'-O-(2-methoxyethyl)-modified oligonucleotide analogs in rats. *J Pharmacol Exp Ther* 296, 890-7.
- (130) Viel, T., Boisgard, R., Kuhnast, B., Jego, B., Siquier-Pernet, K., Hinnen, F., Dolle, F., and Tavitian, B. (2008) Molecular imaging study on in vivo distribution and pharmacokinetics of modified small interfering RNAs (siRNAs). *Oligonucleotides* 18, 201-12.
- (131) Judge, A. D., Robbins, M., Tavakoli, I., Levi, J., Hu, L., Fronda, A., Ambegia, E., McClintock, K., and MacLachlan, I. (2009) Confirming the RNAi-mediated

- mechanism of action of siRNA-based cancer therapeutics in mice. *J Clin Invest* 119, 661-73.
- (132) Sioud, M., Furset, G., and Cekaite, L. (2007) Suppression of immunostimulatory siRNA-driven innate immune activation by 2'-modified RNAs. *Biochem Biophys Res Commun* 361, 122-6.
- (133) Bartlett, D. W., and Davis, M. E. (2008) Impact of tumor-specific targeting and dosing schedule on tumor growth inhibition after intravenous administration of siRNA-containing nanoparticles. *Biotechnol Bioeng* 99, 975-85.
- (134) Zimmermann, T. S., Lee, A. C., Akinc, A., Bramlage, B., Bumcrot, D., Fedoruk, M. N., Harborth, J., Heyes, J. A., Jeffs, L. B., John, M., Judge, A. D., Lam, K., McClintock, K., Nechev, L. V., Palmer, L. R., Racie, T., Rohl, I., Seiffert, S., Shanmugam, S., Sood, V., Soutschek, J., Toudjarska, I., Wheat, A. J., Yaworski, E., Zedalis, W., Koteliansky, V., Manoharan, M., Vornlocher, H. P., and MacLachlan, I. (2006) RNAi-mediated gene silencing in non-human primates. *Nature* 441, 111-4.
- (135) Dykxhoorn, D. M., Palliser, D., and Lieberman, J. (2006) The silent treatment: siRNAs as small molecule drugs. *Gene Ther* 13, 541-52.
- (136) Giljohann, D. A., Seferos, D. S., Prigodich, A. E., Patel, P. C., and Mirkin, C. A. (2009) Gene Regulation with Polyvalent siRNA Nanoparticle Conjugates. *Journal of the American Chemical Society* 131, 2072.
- (137) Gao, S., Dagnaes-Hansen, F., Nielsen, E. J. B., Wengel, J., Besenbacher, F., Howard, K. A., and Kjems, J. (2009) The Effect of Chemical Modification and Nanoparticle Formulation on Stability and Biodistribution of siRNA in Mice. *Mol Ther* 17, 1225-1233.
- (138) Kunath, K., von Harpe, A., Petersen, H., Fischer, D., Voigt, K., Kissel, T., and Bickel, U. (2002) The structure of PEG-modified poly(ethylene imines) influences biodistribution and pharmacokinetics of their complexes with NF-kappaB decoy in mice. *Pharm Res* 19, 810-7.
- (139) Merdan, T., Kunath, K., Petersen, H., Bakowsky, U., Voigt, K. H., Kopecek, J., and Kissel, T. (2005) PEGylation of poly(ethylene imine) affects stability of complexes with plasmid DNA under in vivo conditions in a dose-dependent manner after intravenous injection into mice. *Bioconjug Chem* 16, 785-92.
- (140) de Wolf, H. K., Snel, C. J., Verbaan, F. J., Schiffelers, R. M., Hennink, W. E., and Storm, G. (2007) Effect of cationic carriers on the pharmacokinetics and tumor

- localization of nucleic acids after intravenous administration. *Int J Pharm* 331, 167-75.
- (141) Burke, R. S., and Pun, S. H. (2008) Extracellular barriers to in Vivo PEI and PEGylated PEI polyplex-mediated gene delivery to the liver. *Bioconjug Chem* 19, 693-704.
- (142) Merkel, O. M., Librizzi, D., Pfestroff, A., Schurrat, T., Buyens, K., Sanders, N. N., De Smedt, S. C., Behe, M., and Kissel, T. (2009) Stability of siRNA polyplexes from poly(ethylenimine) and poly(ethylenimine)-g-poly(ethylene glycol) under in vivo conditions: Effects on pharmacokinetics and biodistribution measured by Fluorescence Fluctuation Spectroscopy and Single Photon Emission Computed Tomography (SPECT) imaging. *J Control Release* 10.1016/j.jconrel.2009.05.016.
- (143) Bitko, V., Musiyenko, A., Shulyayeva, O., and Barik, S. (2005) Inhibition of respiratory viruses by nasally administered siRNA. *Nat Med* 11, 50-5.
- (144) Li, B. J., Tang, Q., Cheng, D., Qin, C., Xie, F. Y., Wei, Q., Xu, J., Liu, Y., Zheng, B. J., Woodle, M. C., Zhong, N., and Lu, P. Y. (2005) Using siRNA in prophylactic and therapeutic regimens against SARS coronavirus in Rhesus macaque. *Nat Med* 11, 944-51.
- (145) Wiseman, J. W., Goddard, C. A., McLelland, D., and Colledge, W. H. (2003) A comparison of linear and branched polyethylenimine (PEI) with DCChol/DOPE liposomes for gene delivery to epithelial cells in vitro and in vivo. *Gene Ther* 10, 1654-62.
- (146) Kleemann, E., Neu, M., Jekel, N., Fink, L., Schmehl, T., Gessler, T., Seeger, W., and Kissel, T. (2005) Nano-carriers for DNA delivery to the lung based upon a TAT-derived peptide covalently coupled to PEG-PEI. *J Control Release* 109, 299-316.
- (147) Rudolph, C., Schillinger, U., Plank, C., Gessner, A., Nicklaus, P., Muller, R., and Rosenecker, J. (2002) Nonviral gene delivery to the lung with copolymer-protected and transferrin-modified polyethylenimine. *Biochim Biophys Acta* 1573, 75-83.
- (148) Sakae, M., Ito, T., Yoshihara, C., Iida-Tanaka, N., Yanagie, H., Eriguchi, M., and Koyama, Y. (2008) Highly efficient in vivo gene transfection by plasmid/PEI complexes coated by anionic PEG derivatives bearing carboxyl groups and RGD peptide. *Biomed Pharmacother* 62, 448-53.

-
- (149) Chen, J., Gao, X., Hu, K., Pang, Z., Cai, J., Li, J., Wu, H., and Jiang, X. (2008) Galactose-poly(ethylene glycol)-polyethylenimine for improved lung gene transfer. *Biochem Biophys Res Commun* 375, 378-83.
- (150) Kamlah, F., Eul, B. G., Li, S., Lang, N., Marsh, L. M., Seeger, W., Grimminger, F., Rose, F., and Hanze, J. (2009) Intravenous injection of siRNA directed against hypoxia-inducible factors prolongs survival in a Lewis lung carcinoma cancer model. *Cancer Gene Ther* 16, 195-205.
- (151) Robbins, M., Judge, A., Ambegia, E., Choi, C., Yaworski, E., Palmer, L., McClintock, K., and MacLachlan, I. (2008) Misinterpreting the therapeutic effects of small interfering RNA caused by immune stimulation. *Hum Gene Ther* 19, 991-9.
- (152) Gillespie, D. L., Whang, K., Ragel, B. T., Flynn, J. R., Kelly, D. A., and Jensen, R. L. (2007) Silencing of Hypoxia Inducible Factor-1{alpha} by RNA Interference Attenuates Human Glioma Cell Growth In vivo. *Clin Cancer Res* 13, 2441-2448.
- (153) Reich, S. J., Fosnot, J., Kuroki, A., Tang, W., Yang, X., Maguire, A. M., Bennett, J., and Tolentino, M. J. (2003) Small interfering RNA (siRNA) targeting VEGF effectively inhibits ocular neovascularization in a mouse model. *Mol Vis* 9, 210-6.
- (154) Dorn, G., Patel, S., Wotherspoon, G., Hemmings-Mieszczak, M., Barclay, J., Natt, F. J., Martin, P., Bevan, S., Fox, A., Ganju, P., Wishart, W., and Hall, J. (2004) siRNA relieves chronic neuropathic pain. *Nucleic Acids Res* 32, e49.
- (155) Thakker, D. R., Natt, F., Husken, D., van der Putten, H., Maier, R., Hoyer, D., and Cryan, J. F. (2005) siRNA-mediated knockdown of the serotonin transporter in the adult mouse brain. *Mol Psychiatry* 10, 782-9, 714.
- (156) Morrissey, D. V., Lockridge, J. A., Shaw, L., Blanchard, K., Jensen, K., Breen, W., Hartsough, K., Macherer, L., Radka, S., Jadhav, V., Vaish, N., Zinnen, S., Vargeese, C., Bowman, K., Shaffer, C. S., Jeffs, L. B., Judge, A., MacLachlan, I., and Polisky, B. (2005) Potent and persistent in vivo anti-HBV activity of chemically modified siRNAs. *Nat Biotechnol* 23, 1002-7.
- (157) Sato, Y., Murase, K., Kato, J., Kobune, M., Sato, T., Kawano, Y., Takimoto, R., Takada, K., Miyanishi, K., Matsunaga, T., Takayama, T., and Niitsu, Y. (2008) Resolution of liver cirrhosis using vitamin A-coupled liposomes to deliver siRNA against a collagen-specific chaperone. *Nat Biotechnol* 26, 431-42.

-
- (158) Woodrow, K. A., Cu, Y., Booth, C. J., Saucier-Sawyer, J. K., Wood, M. J., and Saltzman, W. M. (2009) Intravaginal gene silencing using biodegradable polymer nanoparticles densely loaded with small-interfering RNA. *Nat Mater* 8, 526-33.
- (159) Merkel, O. M., Beyerle, A., Librizzi, D., Pfestroff, A., Behr, T. M., Sproat, B., Barth, P. J., and Kissel, T. H. (2009) Non-viral siRNA delivery to the lung investigation of PEG-PEI polyplexes and their in vivo performance. *Molecular Pharmaceutics* doi:10.1021/mp900107v.
- (160) Sanhai, W. R., Sakamoto, J. H., Canady, R., and Ferrari, M. (2008) Seven challenges for nanomedicine. *Nat Nanotechnol* 3, 242-4.
- (161) Spanoudaki, V. C., and Ziegler, S. I. (2008) PET & SPECT instrumentation. *Handb Exp Pharmacol*, 53-74.
- (162) Riemann, B., Schafers, K. P., Schober, O., and Schafers, M. (2008) Small animal PET in preclinical studies: opportunities and challenges. *Q J Nucl Med Mol Imaging* 52, 215-21.
- (163) Mather, S. (2009) Molecular imaging with bioconjugates in mouse models of cancer. *Bioconjug Chem* 20, 631-43.
- (164) Schnockel, U., Hermann, S., Stegger, L., Law, M., Kuhlmann, M., Schober, O., Schafers, K., and Schafers, M. (2009) Small-animal PET: A promising, non-invasive tool in pre-clinical research. *Eur J Pharm Biopharm.*
- (165) Fischman, A. J., Alpert, N. M., Livni, E., Ray, S., Sinclair, I., Elmaleh, D. R., Weiss, S., Correia, J. A., Webb, D., Liss, R., and et al. (1991) Pharmacokinetics of 18F-labeled fluconazole in rabbits with candidal infections studied with positron emission tomography. *J Pharmacol Exp Ther* 259, 1351-9.
- (166) Phelps, M. E. (2000) PET: the merging of biology and imaging into molecular imaging. *J Nucl Med* 41, 661-81.
- (167) Malek, A., Merkel, O., Fink, L., Czubayko, F., Kissel, T., and Aigner, A. (2009) In vivo pharmacokinetics, tissue distribution and underlying mechanisms of various PEI(-PEG)/siRNA complexes. *Toxicology and Applied Pharmacology* 236, 97-108.
- (168) Van de Water, F. M., Boerman, O. C., Wouterse, A. C., Peters, J. G., Russel, F. G., and Masereeuw, R. (2006) Intravenously administered siRNA accumulates in the kidney and selectively suppresses gene function in renal proximal tubules. *Drug Metab Dispos* 34, 1393-7.
- (169) Merkel, O. M., Librizzi, D., Pfestroff, A., Schurrat, T., Behe, M., and Kissel, T. (2009) In vivo SPECT and real-time gamma camera imaging of biodistribution and

- pharmacokinetics of siRNA delivery using an optimized radiolabeling and purification procedure. *Bioconjug Chem* 20, 174-82.
- (170) Aillon, K. L., Xie, Y., El-Gendy, N., Berkland, C. J., and Forrest, M. L. (2009) Effects of nanomaterial physicochemical properties on in vivo toxicity. *Adv Drug Deliv Rev* 61, 457-66.
- (171) Lanone, S., and Boczkowski, J. (2006) Biomedical applications and potential health risks of nanomaterials: molecular mechanisms. *Curr Mol Med* 6, 651-63.
- (172) Ebtekar, M. (2006) Air pollution induced asthma and alterations in cytokine patterns. *Iran J Allergy Asthma Immunol* 5, 47-56.
- (173) Upadhyay, S., Stoeger, T., Harder, V., Thomas, R. F., Schladweiler, M. C., Semmler-Behnke, M., Takenaka, S., Karg, E., Reitmeir, P., Bader, M., Stampfl, A., Kodavanti, U. P., and Schulz, H. (2008) Exposure to ultrafine carbon particles at levels below detectable pulmonary inflammation affects cardiovascular performance in spontaneously hypertensive rats. *Part Fibre Toxicol* 5, 19.
- (174) Krzyzanowski, M. (2008) WHO Air Quality Guidelines for Europe. *J Toxicol Environ Health A* 71, 47-50.
- (175) von Klot, S., Wolke, G., Tuch, T., Heinrich, J., Dockery, D. W., Schwartz, J., Kreyling, W. G., Wichmann, H. E., and Peters, A. (2002) Increased asthma medication use in association with ambient fine and ultrafine particles. *Eur Respir J* 20, 691-702.
- (176) Nel, A. (2005) Atmosphere. Air pollution-related illness: effects of particles. *Science* 308, 804-6.
- (177) Donaldson, K., Stone, V., Clouter, A., Renwick, L., and MacNee, W. (2001) Ultrafine particles. *Occup Environ Med* 58, 211-6, 199.
- (178) Hajeri, P. S., and Singh, S. K. (2009) siRNAs:-their potential as therapeutic agents. Part I Designing of siRNAs. *Drug Discov Today*.
- (179) Sioud, M. (2005) Induction of inflammatory cytokines and interferon responses by double-stranded and single-stranded siRNAs is sequence-dependent and requires endosomal localization. *J Mol Biol* 348, 1079-90.
- (180) Judge, A. D., Sood, V., Shaw, J. R., Fang, D., McClintock, K., and MacLachlan, I. (2005) Sequence-dependent stimulation of the mammalian innate immune response by synthetic siRNA. *Nat Biotechnol* 23, 457-62.

-
- (181) Jackson, A. L., Bartz, S. R., Schelter, J., Kobayashi, S. V., Burchard, J., Mao, M., Li, B., Cavet, G., and Linsley, P. S. (2003) Expression profiling reveals off-target gene regulation by RNAi. *Nat Biotechnol* 21, 635-7.
- (182) Clark, P. R., Pober, J. S., and Kluger, M. S. (2008) Knockdown of TNFR1 by the sense strand of an ICAM-1 siRNA: dissection of an off-target effect. *Nucleic Acids Res* 36, 1081-97.
- (183) Chen, P. Y., Weinmann, L., Gaidatzis, D., Pei, Y., Zavolan, M., Tuschl, T., and Meister, G. (2008) Strand-specific 5'-O-methylation of siRNA duplexes controls guide strand selection and targeting specificity. *Rna* 14, 263-74.
- (184) Judge, A. D., Bola, G., Lee, A. C., and MacLachlan, I. (2006) Design of noninflammatory synthetic siRNA mediating potent gene silencing in vivo. *Mol Ther* 13, 494-505.
- (185) Elmen, J., Thonberg, H., Ljungberg, K., Frieden, M., Westergaard, M., Xu, Y., Wahren, B., Liang, Z., Orum, H., Koch, T., and Wahlestedt, C. (2005) Locked nucleic acid (LNA) mediated improvements in siRNA stability and functionality. *Nucleic Acids Res* 33, 439-47.
- (186) Swayze, E. E., Siwkowski, A. M., Wancewicz, E. V., Migawa, M. T., Wyrzykiewicz, T. K., Hung, G., Monia, B. P., and Bennett, C. F. (2007) Antisense oligonucleotides containing locked nucleic acid improve potency but cause significant hepatotoxicity in animals. *Nucleic Acids Res* 35, 687-700.
- (187) Chang, C. I., Yoo, J. W., Hong, S. W., Lee, S. E., Kang, H. S., Sun, X., Rogoff, H. A., Ban, C., Kim, S., Li, C. J., and Lee, D. K. (2009) Asymmetric shorter-duplex siRNA structures trigger efficient gene silencing with reduced nonspecific effects. *Mol Ther* 17, 725-32.
- (188) Moghimi, S. M., Symonds, P., Murray, J. C., Hunter, A. C., Debska, G., and Szweczyk, A. (2005) A two-stage poly(ethylenimine)-mediated cytotoxicity: implications for gene transfer/therapy. *Mol Ther* 11, 990-5.
- (189) Akhtar, S., and Benter, I. (2007) Toxicogenomics of non-viral drug delivery systems for RNAi: potential impact on siRNA-mediated gene silencing activity and specificity. *Adv Drug Deliv Rev* 59, 164-82.
- (190) Kabanov, A. V., Batrakova, E. V., Sriadibhatla, S., Yang, Z., Kelly, D. L., and Alakov, V. Y. (2005) Polymer genomics: shifting the gene and drug delivery paradigms. *J Control Release* 101, 259-71.

- (191) Nel, A., Xia, T., Madler, L., and Li, N. (2006) Toxic potential of materials at the nanolevel. *Science* 311, 622-7.
- (192) Kagan, V. E., Bayir, H., and Shvedova, A. A. (2005) Nanomedicine and nanotoxicology: two sides of the same coin. *Nanomedicine* 1, 313-6.

**PART I: NON-VIRAL *IN VITRO*
DELIVERY OF pDNA**

2 Integrin alpha-v-beta-3 targeted gene delivery using RGD peptidomimetic conjugates with copolymers of PEGylated poly(ethylene imine)

Published in Bioconjugate Chemistry 20 (2009) 1270-1280

2.1 Abstract

This study describes the synthesis and characterization of five conjugates of poly(ethylene glycol) modified polyethylenimine (PEG-PEIs) coupled in two different synthesis routes to a non-peptidic pentacyclic RDG-mimetic for integrin receptor-targeted gene delivery. Synthesis of this panel of different conjugates allowed for systematic analysis of structure-activity relationships. Conjugates were therefore characterized concerning molecular composition, DNA condensation, size and zeta potential of self-assembled polyplexes. In vitro characterization included investigation of blood compatibility, binding affinity to receptor-positive and receptor-negative cells measured by flow cytometry, cellular uptake quantified by scintillation counting, and efficiency and specificity of transfection assayed by reporter gene expression. In a first synthetic approach, low molecular weight PEI (LMW-PEI) was PEGylated using a heterobifunctional PEG linker and coupling of the RGD-mimetic was achieved at the distal end of PEG chains. In a second synthesis route, the RGD-mimetic was directly coupled to AB-block-copolymers of PEI (25 kDa) and PEG (30 kDa). Interactions of RGD-PEG-LMW-PEI conjugates with DNA were strongly impaired, whereas PEG-PEI-RGD conjugates were more promising candidates due to their physico-chemical properties and higher receptor specificity. The binding-, uptake- and transfection-efficiency in receptor positive cells was strongly increased upon conjugation of the RGD-mimetic to AB-block-copolymers of PEG-PEI and depended on the degree of peptide substitution. The conjugates of PEG-PEI AB-block-copolymers with low ligand density of the RGD-mimetic appear to be promising candidates for in vivo cancer gene therapy.

2.2 Introduction

The integrin receptor $\alpha_v\beta_3$ is a known marker of angiogenic vascular tissue (1). The so-called vitronectin receptor represents a highly interesting therapeutic target because of its role in a wide range of pathologies which have been reviewed elsewhere, e.g. angiogenesis (2). Vitronectin, fibronectin and fibrinogen, contain the tripeptide motif Arg-Gly-Asp, abbreviated as RGD, which is recognized by integrin receptors. Extensive neovascularization in tumors makes integrin receptor $\alpha_v\beta_3$ a promising target for cancer gene therapy. Targeted delivery of pDNA (3-5) and siRNA (6) condensed by poly(ethylene imine)-graft-poly(ethylene glycol) (PEG-PEI) copolymers bearing cyclic RGD peptides

was reported earlier in the context of cancer gene therapy. In fact, the N-alkylated cyclic pentapeptide c(-RGDf[NMe]V-) is currently being tested in phase II clinical trials under the name “Cilengitide” as an angiogenesis inhibitor in glioblastoma multiforme (7). Because of metabolic instability of peptides and bioavailability reasons, non-peptidic small molecule RGD-mimetics were developed, such as β -amino acid-based azacarba analogues with increased lipophilicity (8), hydantoin scaffolds (9), aminobenzoyl and isonipecotyl groups as arginine mimetic and C-terminal tryptophan to maintain ionic and hydrophobic interaction (10) or attachment of aliphatic carbamate linkers (11). Another class of substances which is similar to the one used in our study was described by Ishikawa et al. (12), suggesting that a cyclic guanidine at the N-terminus generates suitable adhesion, receptor inhibition and water solubility. None of the RGD-mimetics mentioned above have so far been used for targeted gene delivery.

In this study, we used as a targeting ligand thiol and maleimide derivatives of a pentacyclic peptidomimetic substance of a class of 1- α -Z-2,3-diaminopropionic acid substituted 4-amino-1H-pyrimidin-2-ones previously reported to exhibit high affinities to the vitronectin receptor in the nanomolar range (13). This ligand was coupled to different derivatives of PEI using two different synthetic approaches to generate five different bioconjugates for targeted gene delivery based on a novel RGD-mimetic. The position and ligand density was varied to identify the most suitable synthetic strategy and composition of the conjugates.

2.3 Materials and Methods

Materials:

PEI 25 kDa (Polymin TM, 25 kDa) was a gift from BASF (Ludwigshafen, Germany), low molecular weight poly(ethylene imine) (LMW-PEI) with a low degree of branching (14) and the block copolymer poly(ethylene glycol)-poly(ethylene imine) (PEI25k-PEG30k) (15) were synthesized as described earlier.

RGD-mimetics (RGD-M) were obtained as maleimide derivative (C₃₄H₃₆N₈O₇, Mw 668.70 g/mol) or as sulfhydryl derivative (C₃₀H₃₅N₇O₅S, Mw 605.71 g/mol) from Abbott Laboratories (Abbott Park, IL, USA) as shown in Figure 1. Orthopyridyl-disulfide poly(ethylene glycol)-succinimidyl propionic acid (NHS-PEG2kDa-OPSS) was purchased from Nektar Therapeutics (San Carlos, CA, USA), the luciferase encoding plasmid pCMV-Luc from The Plasmid Factory (Bielefeld, Germany), Luciferase Assay Reagent (LAR) and

Cell Culture Lysis Reagent (CCLR) were bought from Promega (Mannheim, Germany), ion exchange columns SP Sepharose HP from Amersham Pharmacia Biotech (Freiburg, Germany), and centricon YM-30 from Millipore (Millipore, Schwalbach, Germany). Fluorescein-5-isothiocyanate (FITC), Dithiothreitol (DTT), and 2,4,6-Trinitrobenzenesulfonic Acid (TNBS), were purchased from Sigma-Aldrich Laborchemikalien GmbH (Seelze, Germany), dimethylacetamide (DMAc), and all other chemicals were used of analytical grade.

Conjugate Synthesis:

Conjugates were synthesized using two different approaches. Either (i) prePEGylated PEI (PEI25k-PEG30k), synthesized as described previously (15), was coupled directly with a maleimide-derivative of the RGD-M, or (ii) LMW-PEI (PEI 5 kDa) was PEGylated with a 2 kDa SPA-PEG2k-OPSS linker which was activated with DTT before coupling to a thiol-derivative of the RGD-M. For the first synthetic approach (i), shown in Figure 2, 23.3 mg PEG-PEI, corresponding to 10 mg PEI (0.4 μmol), was diluted to 500 μl with in either double distilled water (conjugate 10-1) or HEPES buffered saline (HBS, 20 mM HEPES, 150 mM NaCl, pH 7.5) (conjugates 10-2 and 5-2) in a 1.5 ml Eppendorf cup. RGD-M was dissolved in dimethylacetamide (DMAc) and amounts of 2.67 mg (4.0 μmol) (conjugates 10-1 and 10-2) or 1.33 mg (2.0 μmol) (conjugate 5-2) were added to the polymer solution, vortexed for 30 sec and incubated under constant shaking on a sample shaker TH 15 (Edmund Bühler, Hechingen, Germany) at room temperature for 24 h. After incubation, purification was accomplished by ultrafiltration using centricon YM-30 spin columns.

The second synthetic approach (ii), (Figure 3), involved coupling of a PEG linker to LMW-PEI. For this step, 5 mg LMW-PEI (1 μmol) were dissolved in HEPES buffered saline, pH 7.5, and reacted for 8 h with either 11.5 mg (5 μmol) (conjugate I) or 23 mg (10 μmol) (conjugate II) PEG linker, which had been dissolved in 200 μl absolute ethanol. Purification of the conjugates was achieved by modified ion exchange chromatography on an ÄKTA FPLC system equipped with 2 SP Sepharose HP cation exchange columns (ÄKTA Prime, Amersham Pharmacia Biotech, Freiburg, Germany) as previously described (16, 17). The intermediate products, namely the PEGylated PEI precursors which were eluted with a high ionic strength buffer (3 M NaCl, 20 mM HEPES) from the ion exchange column, were desalted using centricon YM-3 spin columns as recommended by the manufacturer. They were characterized concerning their PEI concentration by copper complexation (18, 19) and concerning their coupling degree by a pyridon-2-thion release assay (20). For this assay and

for activation of the PEG-linker, PEG-PEIs were treated with a 10-fold molar excess of DTT for 4 h at room temperature. Pyridon-2-thion release was measured spectrophotometrically at 343 nm and the activated PEG-PEIs were purified using centricon YM-3 spin columns in presence of 10 mM EDTA to avoid metal catalyzed sulfhydryl oxidation (21). The activated, purified and characterized precursors were mixed with a 3-fold (Conjugate I) or 10-fold (Conjugate II) molar excess of a sulfhydryl derivative of the RGD-M dissolved in DMAc and were coupled by formation of disulfide bonds. After another ultrafiltration step, coupling degree of all conjugates was determined spectrophotometrically at 297 nm, the wavelength that had shown maximal absorption in a wvescan of RGD-M. Measured absorption was compensated with the blank value of the non-coupled precursor.

Fluorescent Labeling of Polymers and Conjugates:

Polymers were labeled as previously reported (22). Briefly, 20 mg polymer were dissolved in 2 ml 0.1 M sodium bicarbonate buffer, pH 9.0, and mixed with 1 mg FITC in 200 ml DMSO, stirred in the dark for 3 h at room temperature and purified by ultrafiltration using centricon YM-10 spin columns with a MWCO of 10 kDa. The concentration of the purified sample was determined at 405 nm after formation of a picrate with 2,4,6-Trinitrobenzenesulfonic Acid (TNBS) in an assay previously described (23). The absorbance of the fluorescent dye was found not to interfere with the results from the TNBS assay.

FITC-labeled conjugates were obtained by labeling the pre-synthesized conjugates as described above. Since the targeting ligand, namely the RGD-M, does not contain primary amines, we presumed that post-labeling would not negatively affect the conjugates, whereas pre-labeling could interfere with the coupling steps of either RGD-Mal or the PEG-linker.

Radioactive Labeling of Conjugate 5-2:

Similar to the fluorescent labeling, conjugate 5-2 was dissolved in 1 ml 0.1 M sodium bicarbonate buffer, pH 9.0, at a concentration of 10 mg/ml, mixed with p-SCN-Bn-DTPA (Macrocylics, Dallas, TX, USA) in DMSO at a final concentration of 1 mg/ml and reacted for one hour at room temperature. The reaction was stopped by addition of 0.1 M citrate buffer, pH 5.0, before the reaction mixture was purified by ultrafiltration using centricon YM-10 spin columns with a MWCO of 10 kDa. The concentration of the purified sample was determined at 405 nm using the TNBS-assay (23).

An amount of 100 µg of DTPA coupled polymer or conjugate were diluted in 0.1 M acetate buffer, pH 4.5, and mixed with 10 MBq $^{111}\text{InCl}_3$ for 30 min at room temperature, followed by size exclusion chromatography using a PD-10 Sephadex G25 prepacked column from Amersham Pharmacia Biotech (Freiburg, Germany).

Polyplex formation:

Polyplexes were formed by mixing equal volumes (25 µl each) of pDNA and polymer or conjugate diluted in 150 mM NaCl solution to obtain the desired nitrogen to DNA phosphate ratio (N/P ratio). Briefly, the appropriate amount of polymer was added to a pDNA dilution (0.04 µg/µl) to yield a final concentration of 0.02 µg DNA per µl, vortexed for 10 sec and incubated for equilibration for 10 min.

Dynamic Light Scattering (DLS) and Laser Doppler Anemometry (LDA):

For measurements of hydrodynamic diameters, polyplexes were prepared as described above. 50 µl of the polyplex solution were pipetted into a disposable cuvette (UVette, Eppendorf, Wesseling-Berzdorf, Germany) and measured in the “General Purpose” mode, which best fits the correlation function of sizes measured with polyplexes. Attenuator and position were optimized by the device. Subsequently, polyplex solutions were diluted with 5 % glucose solution to 800 µl and pipetted into a folded capillary cell (Malvern Instruments, Herrenberg, Germany) for zeta potential measurement. Measurements were performed in replicates of five using a Zetasizer Nano ZS (Malvern Instruments, Herrenberg, Germany) equipped with a 4 mW He–Ne laser at a wavelength of 633 nm at 25 °C. Scattered light was detected at a 173° backward scattering angle. The viscosity and refractive index of water at 25 °C was used for data analysis with the Dispersion Technology Software 5.00 (Malvern Instruments, Herrenberg, Germany). The accuracy of the instrument was validated using reference polymer particles (Nanosphere Size Standards of 50, 100 and 200 nm, Duke Scientific Corp., Palo Alto, CA, USA) and with Zeta Potential Transfer Standard (Malvern Instruments, Herrenberg, Germany).

Ethidium Bromide Quenching Assay:

To investigate if condensation efficiency of the polymers used for conjugate synthesis would be influenced by coupling of PEG or the targeting ligand, 4 µg of herring testes DNA (Sigma-Aldrich Chemie GmbH, Schnelldorf, Germany) were complexed with polymers or conjugates at different N/P ratios. After incubation for 20 min at room

temperature, 20 μ l of a 0.1 mg/ml ethidium bromide solution (Carl Roth GmbH, Karlsruhe, Germany) were added and shortly incubated in the dark after intensive mixing. Intercalation-caused fluorescence was quantified using a fluorescence plate reader (LS 50 B, Perkin-Elmer, Rodgau-Jügesheim, Germany) at 518 nm excitation and 605 nm emission wavelengths. Experiments were performed in triplicates, results are given as mean relative fluorescence intensity values where intercalation of free DNA represents 100 % fluorescence and non-intercalating ethidium bromide in buffer represents 0 % remaining fluorescence.

Hemolytic Activity:

Surface activity leading to hemolysis was quantified after treating human erythrocytes with polyplexes made of polymers or conjugates. Therefore, erythrocytes were isolated from fresh citrated blood from healthy volunteers by centrifugation, washed with PBS buffer and diluted to $5 \cdot 10^8$ cells/ml. Polyplexes of 0.1 μ g pDNA per ml were prepared at N/P 5, and 50 μ l aliquots of polyplex solutions, 1 % Triton-X 100 (100 % lysis) or 150 mM NaCl (0 % lysis) were mixed with 50 μ l erythrocyte suspension. After incubation for 30 min at 37 °C, samples were centrifuged at 400 g. Hemolysis of replicates of three was measured spectrophotometrically in supernatants at 541 nm and is given as mean percentage of the released hemoglobin normalized to total hemolysis induced by 1% Triton-X 100.

Cell culture:

MeWo (human malignant skin melanoma; ATCC: HTB-65) and A549 (human non-small-cell lung carcinoma; ATCC: CCL-185) cells were purchased from ATCC (Teddington, UK) and maintained in DMEM (PAA Laboratories, Cölbe, Germany) supplemented with 10% fetal calf serum (Cytogen, Sinn, Germany) in humidified atmosphere with 5% CO₂ at 37 °C.

Immunofluorescence Staining of Integrin $\alpha_v\beta_3$ Receptors on the Cell Surface:

MeWo and A549 cells were seeded with 60000 cells per well on 24 well plates (Nunc, Wiesbaden, Germany). After incubation for 24 h, cells were washed with Earle's Balanced Salt Solution (EBSS, Hyclone, Thermo Fisher, Schwerte, Germany) and incubated with either 3 % bovine serum albumin in phosphate buffered saline (PBS/BSA) only (blank cells and secondary antibody only cells) or with integrin $\alpha_v\beta_3$ antibody ([BV3] (ab7166), Abcam, Cambridge, MA, USA) at a concentration of 1 μ g/ml in PBS/BSA for 1 hour in the dark.

Cells were washed three times with ice cold PBS before all wells except for blanks were treated with a 1:100 dilution of a FITC-labeled goat polyclonal to mouse IgG H&L (ab6785, Abcam, Cambridge, MA, USA) antibody in PBS/BSA for 30 min in the dark. Afterwards, cells were washed three times with ice cold PBS before they were trypsinized with 100 μ l trypsin/EDTA (PAA Laboratories, Cölbe, Germany) and fixed with 200 μ l of a 1:1 mixture of FACSFlow (BD Biosciences, San Jose, CA) and 4% paraformaldehyde in PBS. Cell suspensions were stored refrigerated in the dark until analysis by flow cytometry. All experiments were performed with replicates of three.

Binding Assay:

MeWo and A549 cells were seeded with 60,000 cells per well in 24 well plates (Nunc, Wiesbaden, Germany). After incubation for 24 h, medium was aspirated and cells were supplied with cold serum-containing medium before they were transfected with polyplexes containing 1 μ g DNA per well and FITC-labeled polymer or conjugate at N/P 5. Triplicates of cells were incubated with the polyplexes for 15 min at 4 °C before they were washed three times with PBS, trypsinized and fixed with a 1:1 mixture of FACSFlow (BD Biosciences, San Jose, CA) and 4% paraformaldehyde in PBS. Cell suspensions were stored refrigerated in the dark until analysis by flow cytometry.

Flow Cytometry:

Suspensions of fixed cells were measured on a FACScan (BD Biosciences, San Jose, CA) with excitation at 488 nm and the emission filter set to a 530/30 bandpass. Cells were gated, 10,000 viable cells were evaluated in each experiment, and results are given as the mean of 3 independent measurements. Data acquisition and analysis was performed using CellQuest Pro (BD Biosciences, San Jose, CA) and FCS Express V3.00 (DeNovo Software, Thornhill, Canada). Results were statistically analyzed using one-way ANOVA with Bonferroni post-hoc test.

Quantification of Uptake:

MeWo and A549 cells were seeded with 60,000 cells per well in 24 well plates (Nunc, Wiesbaden, Germany). After incubation for 24 h, triplicates of cells were treated with polyplexes prepared of various amounts of pCMV-Luc and radiolabeled conjugate 5-2 at N/P 5. Cells were incubated for 4 h before they were treated as described by Haigler et al. (24) to make sure only internalized activity was measured. Briefly, the cells were first

treated with 0.5 ml acetic acid (0.2 M NaAc containing 0.5 M NaCl, pH 2.5) for 6 min at 4°C followed by a quick washing with an additional amount of 0.5 ml acetic acid to remove any remaining membrane-bound activity. The cell-associated activity, which was extracted by treating the cells with 0.5 ml 1 M NaOH for 80 min at 37°C, was considered to be internalized. The extracts in 0.5 ml NaOH were collected and the wells were then washed with an additional 0.5 ml NaOH. Before analysis in the gamma counter, the samples were adjusted to neutral pH by adding drops of 3 M HCl.

In vitro Cell Transfection:

MeWo and A549 cells were seeded with 30000 cells per well in 24 well plates (Nunc, Wiesbaden, Germany). After incubation for 24 h, cells were treated with polyplexes prepared of the “gold standard” PEI 25 kDa, LMW-PEI, PEG-PEI or the various conjugates at N/P 5. After 4 h of incubation, medium was changed and cells were incubated for another 44 h before they were washed with PBS and lysed with cell culture lysis reagent (CCLR, Promega, Mannheim, Germany). Lysates of triplicates were assayed for luciferase expression with a commercial luciferase assay reagent (LAR, Promega, Mannheim, Germany) on a luminescence plate reader LUMIstar OPTIMA (BMG Labtech, Offenburg, Germany).

Competitive Inhibition of in vitro Cell Transfection:

For competitive inhibition of cell transfection, MeWo and A549 cells were seeded with 30000 cells per well in 24 well plates (Nunc, Wiesbaden, Germany). After incubation for 24 h, cells were pre-treated with increasing amounts increasing from 0.05 to 1.5 nmol per ml of the free targeting ligand for 15 min at 37 °C. Polyplexes prepared of PEG-PEI or conjugate 5-2 at N/P 5 were added into the RGD-M containing medium. Replicates of 3 were incubated for 4 h before medium was changed and thereafter treated as described above.

2.4 Results and Discussion

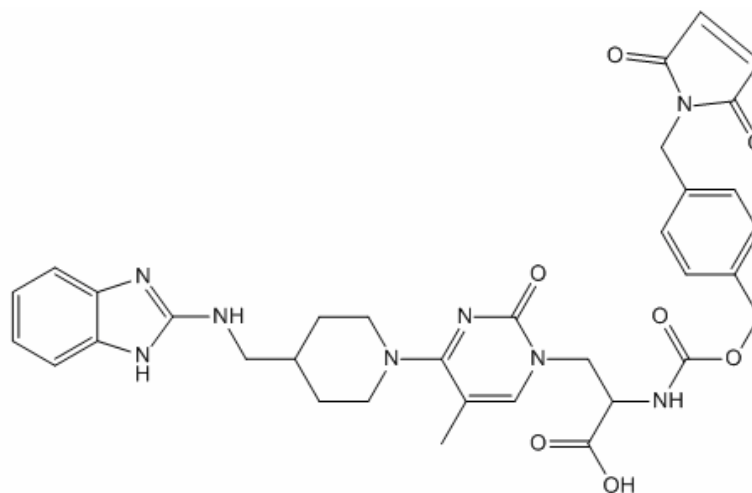
Synthetic Outcome:

RGD-peptides were reported to be good targeting ligands for tumor endothelium using non-viral lipopolyplexes (25, 26) or polyplexes containing siRNA (6, 27, 28) and pDNA (4, 5) or

protein delivery systems bearing antisense oligonucleotides (29). Integrin targeting is an approach adopted from nature: several pathogenic organisms, such as adenoviruses (30), use the integrin receptor to promote their cellular internalisation. While RGD-PEG-PEI has successfully been reported to efficiently deliver nucleic acids into tumors (6), cRGD bearing micelles did not show enhanced uptake but modulated intracellular trafficking (4). RGD-mimetics, on the other hand, have, to our knowledge, so far only been used as therapeutic agents, e.g. as angiogenesis inhibitors (31), inhibitors of monocyte-derived macrophages (32), enhancers of osseointegration (33), as imaging tracers for atherosclerotic plaques (34), and were recently described as ligands for 5-FU (35) or TNF α carrying liposomes (36). In this study we describe for the first time synthesis of five RGD-M conjugates of different molecular composition in two different coupling approaches (compare Figures 2 and 3) for non-viral gene delivery by coupling of a 1- α -Z-2,3-diaminopropionic acid substituted 4-amino-1H-pyrimidin-2-one. This small molecule (13), exhibits nanomolar affinity to the vitronectin receptor (IC₅₀ = 1.3 nM) as determined by ELISA and therefore binds stronger than the physiologic ligand vitronectin (IC₅₀ = 6 nM (37)) and is comparable to the cyclic pentapeptide Cilengitide (IC₅₀ = 0.86 nM (38)) which is being studied in clinical trials. The advantages of this targeting ligand compared to peptides are its metabolic stability and low molecular weight. Two types of conjugates were synthesized either consisting of AB-block-copolymers of PEI (25 kDa) and PEG (30 kDa) directly coupled with RGD-M ligands attached to PEI amines (Figure 2) or of a low molecular weight PEI core which was PEGylated using a heterobifunctional PEG linker that was decorated with RGD-M molecules at the distal end of the PEG chains (Figure 3), similar to (6, 28). Coupling of PEG to LMW-PEI in HBS buffer, pH 7.5, yielded coupling degrees of 70-80 % of the feed, as shown in Figures 3. Coupling of RGD-M to activated PEG did not only depend on the excess of RGD-M but also on the amount of PEG-linker present. Synthesis of Conjugate I, for which a 5-fold molar excess of PEG over PEI and 3-fold molar excess of RGD-M over PEI was used, resulted in a conjugate which can be described as LMW-PEI-(PEG2k)₄-RGD_{0.2} (final yield of LMW-PEI: 10.0%), whereas Conjugate II, for which the feed contained a 10-fold molar excess of PEG linker and a 10-fold molar excess of RGD-M over PEI, yielded the conjugate LMW-PEI-(PEG2k)₇-RGD₆ (final yield of LMW-PEI: 5.8%). Coupling of RGD-mimetic-Maleimide turned out to be strongly influenced by pH. PEG-PEI dissolved in double-distilled water produced a pH of 10, where most of the amines in PEI are deprotonated and available for addition to RGD-mimetic-Maleimide. Mixing the two components yielded quantitative reaction, whereas

only 50 % of the feed reacted with PEG-PEI in HEPES buffered saline adjusted to pH 7.5. Thus, Conjugate 10-1, where a 10-fold molar excess of RGD-M over PEI was added to PEG-PEI in water, reacted to a compound which can be described as PEG30k-PEI25k-RGD₁₀ (final yield of PEG-PEI: 86.0%). Conjugates 10-2 and 5-2, where 10- and 5-fold excess of RGD-M, respectively, was added to PEG-PEI in HBS, yielded in PEG30k-PEI25k-RGD₅ (final yield of PEG-PEI: 84.0%), and PEG30k-PEI25k-RGD_{2.5} (final yield of PEG-PEI: 88.0%). While LMW-PEI-PEG-RGD conjugates were purified in several steps by ion exchange chromatography and buffer was additionally exchanged by ultrafiltration, PEG-PEI-RGD conjugates were only ultrafiltrated and revealed much higher yields. All conjugates and their synthesis are depicted schematically in Figures 2 and 3 and Table 1.

A

Chemical Formula: $C_{34}H_{36}N_8O_7$

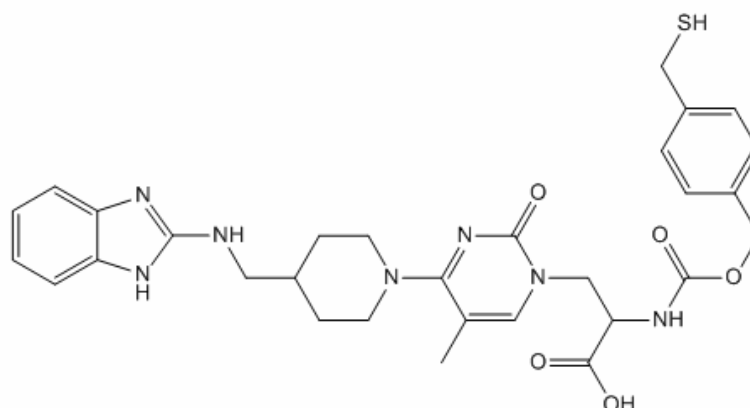
Exact Mass: 668.27

Molecular Weight: 668.7

m/z: 668.27 (100.0%), 669.27 (40.0%), 670.28 (6.8%), 670.27 (2.5%), 671.28 (1.3%)

Elemental Analysis: C, 61.07; H, 5.43; N, 16.76; O, 16.75

B

Chemical Formula: $C_{30}H_{35}N_7O_5S$

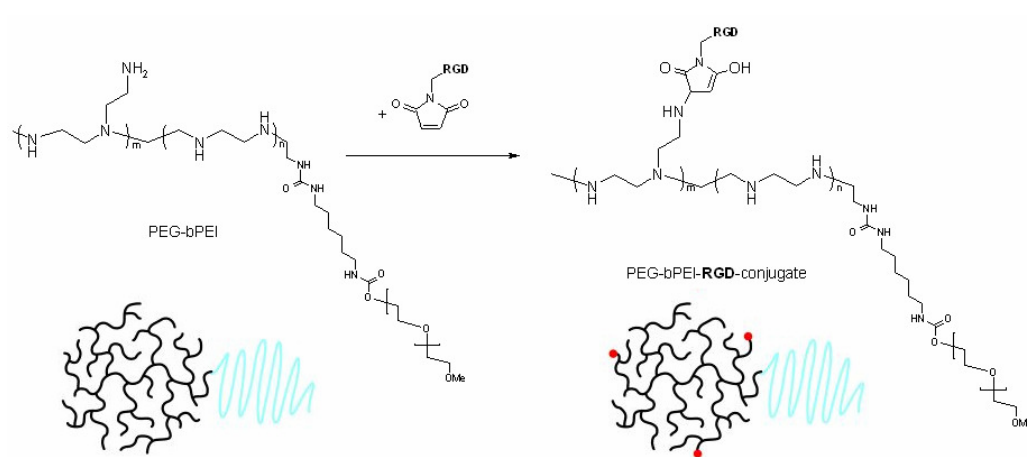
Exact Mass: 605.24

Molecular Weight: 605.71

m/z: 605,24 (100,0%), 606,25 (33,0%), 607,25 (6,3%), 607,24 (5,7%), 606,24 (3,4%), 608,24 (1,5%),
608,25 (1,0%)

Elemental Analysis: C, 59.49; H, 5.82; N, 16.19; O, 13.21; S, 5.29

Figure 1: A) Maleimide- and B) thiol-derivatives of the 1- α -Z-2,3-diaminopropionic acid substituted 4-amino-1H-pyrimidin-2-one RGD-Mimetic with a 2-aminobenzimidazole moiety connected to the piperidine ring via one methylene group which were used for coupling via PEG-linker (A) or direct coupling (B).



Variation of Coupling Degree by Feed Ratio and pH

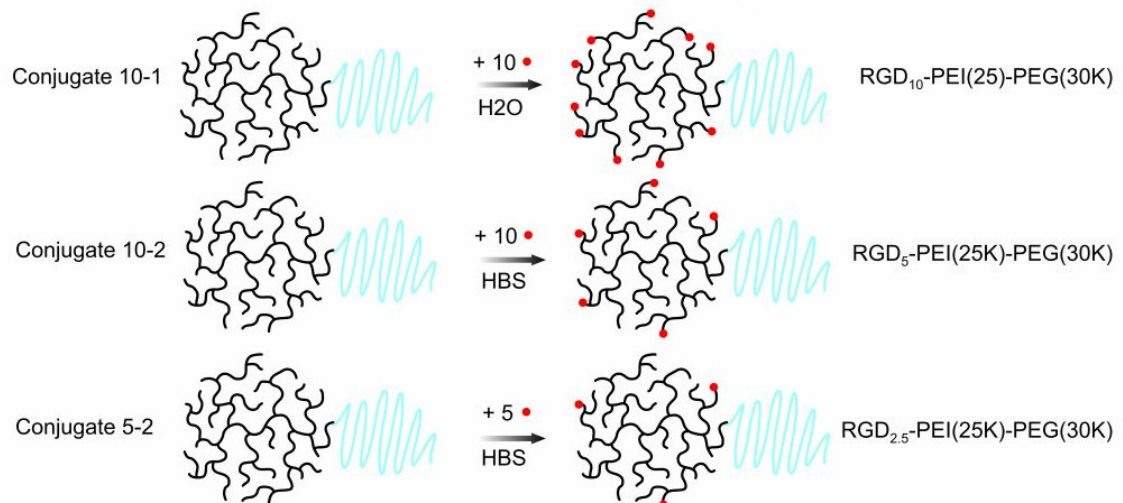


Figure 2: Synthesis of PEG-bPEI-RGD conjugates via direct coupling and. Feeds of different fold excess of RGD-Mimetic and synthesis at different pH yielded 3 conjugates (Conjugate 10-1, 10-2, and 5-2) schematically illustrated below the synthesis scheme.

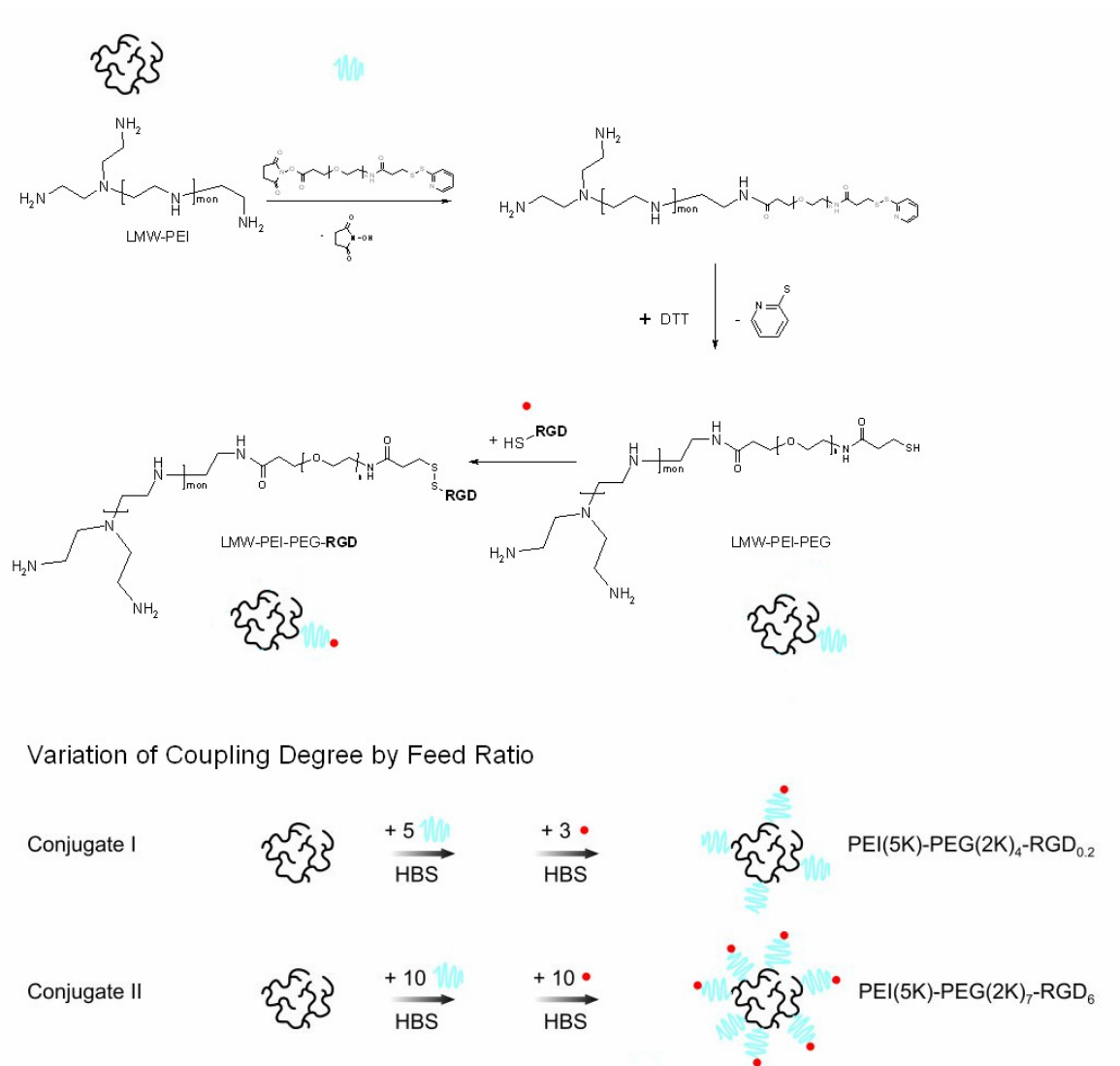


Figure 3: Synthesis of LMW-PEI-PEG-RGD conjugates via heterobifunctional PEG. Feeds of different fold excess of RGD-Mimetic and PEG linker yielded 2 different conjugates (Conjugate I & II) schematically illustrated below the synthesis scheme.

	PEI 25k	PEG- PEI	Con 5-2	Con 10-2	Con 10-1	LMW- PEI	Con I	Con II
PEI Mw [kDa]	25	25	25	25	25	5	5	5
PEG Mw [kDa]	-	1*30	1*30	1*30	1*30	-	4*2	7*2
RGD [mol/ mol]	-	-	2.5	5	10	-	0.2	6
Coupled	-	-	directly	directly	directly	-	via PEG	via PEG
Size [nm]	90.1 ± 10.1	162 ± 5.34	387 ± 101	271 ± 6.3	92.1 ± 3.23	116 ± 2.07	677 ± 211	597 ± 111
Zeta [mV]	28.2 ± 2.16	10.9 ± 1.21	2.79 ± 0.35	9.33 ± 1.03	4.88 ± 0.72	20.2 ± 1.02	-27.9 ± 1.08	-32.5 ± 6.05

Table 1: Molecular composition of polymers and conjugates, and size and zeta potential of their complexes with pDNA.

Hydrodynamic Diameter and Zeta Potential:

Both PEI and PEGylated PEIs are known to efficiently form polyplexes with p-DNA (39), hence we measured hydrodynamic diameters of self-assembled complexes containing plasmid DNA and conjugates and compared their sizes to polyplexes prepared with the polymers that had been used for synthesis. It was reported earlier, that PEI 25kDa formed smaller particles than LMW-PEI at low N/P ratios (40), which is in good agreement with our findings (compare Figure 4). Interestingly, conjugation of RGD-M to PEG-PEI influenced size of particles in different ways. In theory, conjugation shifts the ratio of primary:secondary:tertiary amines and thus the protonation profile. Additionally, the targeting ligand itself can be protonated and influence interaction with polyanions. Therefore its spatial orientation is most relevant. In our case, Conjugate 10-1, bearing 10 molecules RGD-M, formed particles smaller (92.1 ± 3.23 nm) than unmodified PEG-PEI (162 ± 5.34 nm). Conjugate 5-2, on the other hand, which bears the smallest amount of

RGD-M molecules, formed larger complexes (387 ± 101 nm) than PEG-PEI, and Conjugate 10-2 (271 ± 6.3 nm), bearing twice as many RGD-M molecules than Conjugate 5-2 and half as many as Conjugate 10-1, still formed bigger complexes than PEG-PEI but smaller ones than the conjugate bearing the least targeting ligands. Obviously, the targeting moiety affected complex formation, which resulted in the smallest complexes formed by the conjugate bearing the highest density of RGD-M. Surprisingly, conjugates of lower coupling degree formed significantly larger particles. This can be explained by spatial orientation of the targeting ligands which do not seem to be involved in complex formation if coupled in low density but may be oriented towards the surface of the complexes yielding non-spherical particles which can only hardly be measured concerning hydrodynamic diameters by dynamic light scattering. Conjugates I and II, on the other hand, both exhibited a strong hindrance in nanoplex formation compared to LWM-PEI. The LMW-PEI used in our study was less branched than PEI 25kDa, and coupling of PEG decreased electrostatic interaction of LMW-PEI with negatively charged DNA both by a shift of the ratio of primary:secondary:tertiary amines and by modification of a small (5 kDa) ionic polymer with a relatively large (2 kDa) non-ionic polymer, yielding in a small portion of PEI in the overall copolymer conjugates, in fact less than 50 %. The increased number of targeting ligands in Conjugate II seemed to decrease size of polyplexes, which is a sign for interaction between the targeting ligand and DNA. But differences in size between Conjugate I (677 ± 211 nm) and II (597 ± 111 nm) were not significant. In a previously published paper, it was reported that branched PEI 25k even after coupling of 40 molecules PEG and RGD peptide still formed small particles of about 200 nm at N/P ratio > 1 (28). Therefore, we hypothesized that LMW-PEI, which additionally to its shorter chain length contains a lower branching degree is not suitable for DNA condensation after PEGylation. It is known that particles < 200 nm in size are taken up by most cell lines and that larger particles sediment faster and thereby enhancing transfection efficiency under in vitro conditions (41). Polyplexes showing aggregation, on the other hand, are not suitable for systemic administration. Aggregation tendency, of course, has to be evaluated in the context of surface charge. Therefore, zeta potentials of the various complexes were measured by LDA, as shown in Figure 4. Polyplexes formed with PEI 25k revealed the highest surface charge, which can easily be understood as a function of the high number of protonable amines. LMW-PEI polyplexes, which have a lower branching degree (14) and therefore a smaller number of primary amines, exhibited a decreased zeta potential, followed by PEG-PEI polyplexes, where the positive surface charge is believed to be shielded by non-ionic

PEG (42, 43). Polyplexes prepared with RGD-PEG-PEI conjugates showed slightly lower surface charges compared to PEG-PEI. This could be explained by the coupling of the targeting ligands which most probably are attached to secondary amines, which exhibit a high electron density but lower steric hindrance than tertiary amines. By coupling, secondary amines are turned into tertiary ones which are less prone to protonation than secondary amines, decreasing the protonation of the conjugate compared to the polymer. Additionally, it is possible that the targeting ligand, if oriented towards the surface of the polyplex, may shield the positive surface charges of the polyplexes as described for transferrin-PEI polyplexes (44), PEG-PEI conjugates with anti-OA3 Fab' (45) and PEG-PEI conjugates with trastuzumab (46). LMW-PEI-PEG conjugates, on the other hand, formed polyplexes with net negative surface charge which was probably caused by insufficient condensation of DNA. As already seen in size measurements, PEGylation of LMW-PEI impaired condensation of DNA. In the case of LMW-PEI conjugates, a relatively small polymer (5 kDa) was substantially modified with several comparably large PEG chains (2 kDa). Although the targeting moiety is a small molecule, the assumption that conjugation can influence complex formation (47) explained the differences in sizes between LMW-PEI conjugate complexes and LMW-PEI complexes.

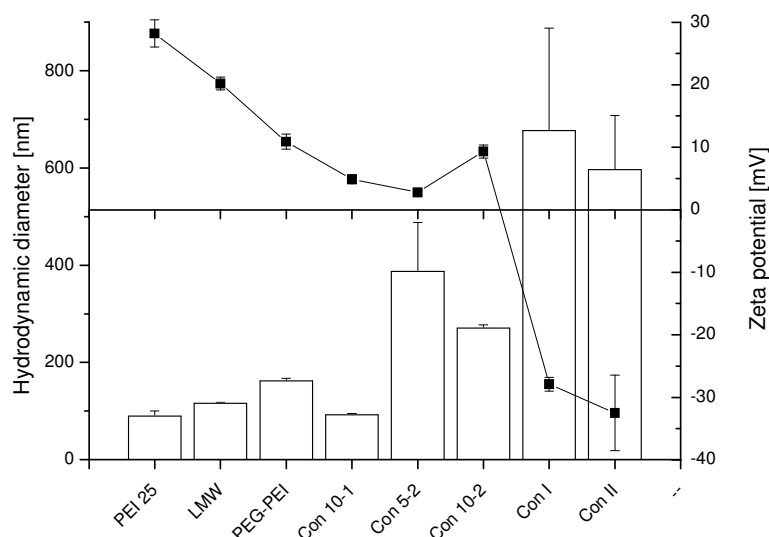


Figure 4: Size (bars) and zeta potential (squares) of pDNA complexes formed with polymers and conjugates at N/P 5 were significantly affected by conjugation. Conjugates I and II synthesized by PEGylation of LMW-PEI were not able to condense DNA into small particles, also shown by the negative zeta potential, whereas sizes of directly

coupled PEG-PEI-RGD conjugates decrease with increasing ligand density and exhibit only slight differences in surface charge.

Condensation of DNA:

A means to quantify condensation and protection of DNA inside the core of polyplexes is detection of intercalation-caused fluorescence of double strands that are available for reaction with ethidium bromide. DNA condensation efficiency of the different polymers and conjugates at different N/P ratios was therefore measured in ethidium bromide quenching assays. PEG-PEI conjugates (see Figure 5A) showed an obvious trend: Unmodified PEI 25k incorporated and protected DNA best, showing full condensation at N/P 3 whereas PEG-PEI reached full condensation at N/P > 5. By increasing the amount of RGD-M molecules per PEG-PEI, condensation efficiency was gradually increased, and Conjugate 10-1 showed similar values as PEI 25k. This was in line with the trends observed in dynamic light scattering, where Conjugate 10-1 formed polyplexes as small as PEI 25k. Better condensation and higher stability of PEG-PEI conjugate complexes compared to their unmodified counterpart were previously described for trastuzumab-coupled PEG-PEI conjugates (46). LMW-PEI-PEG conjugates (Figure 5B) yielded condensation properties strongly different from LMW-PEI. The latter exhibited condensation efficiency almost as good as PEI 25k with complete condensation above N/P 5. Conjugate I, on the other hand did not show sigmoidal dose-responsive condensation efficiency but a linear trend, which proves impairment of the usual condensation behavior of DNA by PEI. As already seen in size and zeta potential measurements, DNA seemed to be loosely bound to the conjugates at N/P 5 and was not well condensed into small polyplexes. Interestingly, at N/P 10, full condensation was reached, and it can be hypothesized that the small amount of targeting ligand in this conjugate gained importance only at higher N/P ratios. Conjugate II exhibited another profile, which was attributed to the higher graft density of RGD-M. At low N/P ratios, Conjugate II showed better condensation than Conjugate I, but full condensation was not reached at N/P 10. This assay of course only mirrors in vitro condensation. Complex stability in presence of serum is currently being addressed in our present study, and in vivo stability will eventually be subject to an in vivo study if biocompatibility of the conjugates proves to be suitable.

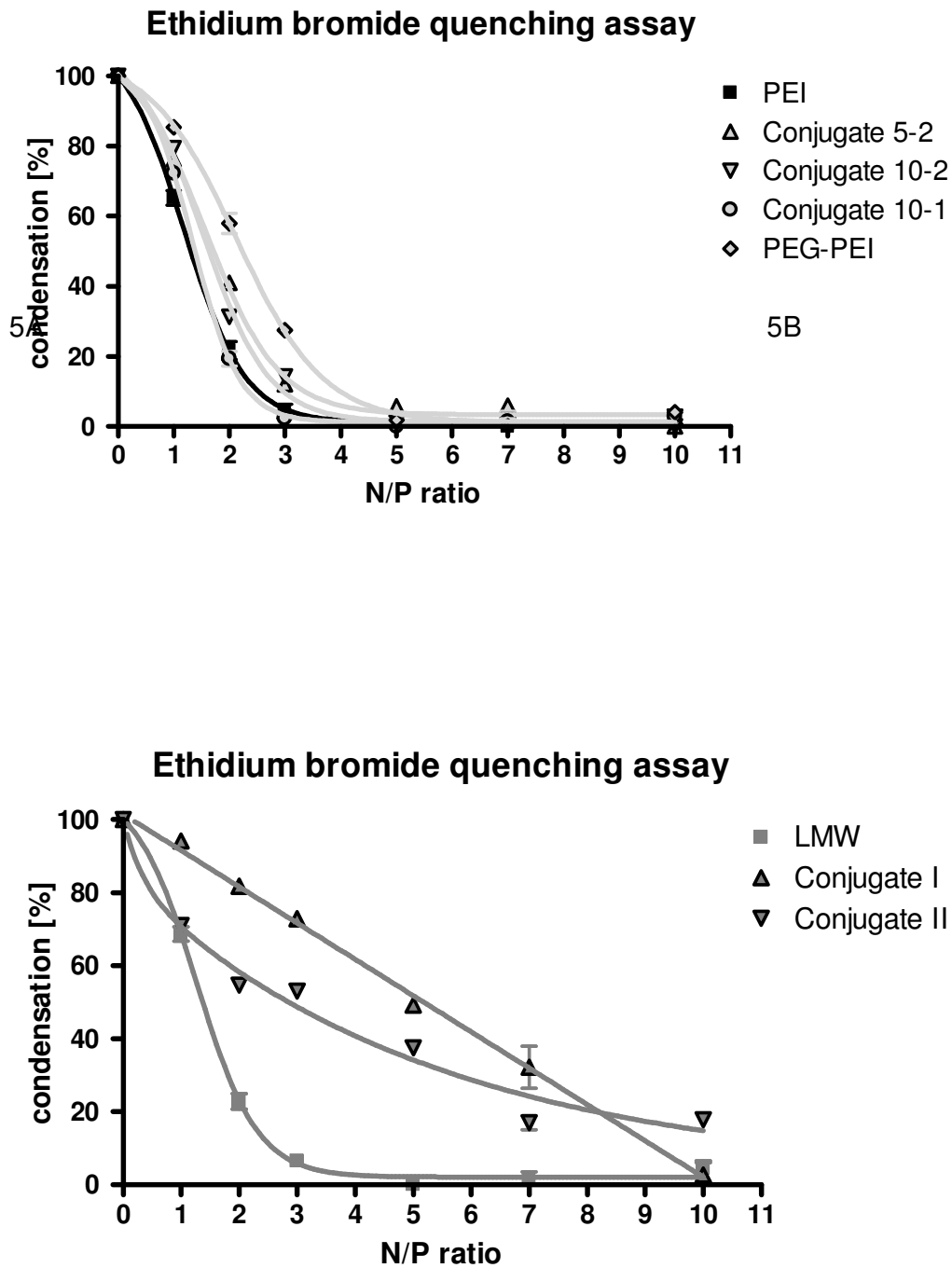


Figure 5: Quenching of intercalation caused ethidium bromide fluorescence upon condensation of DNA with A: PEI 25k, PEG-PEI or PEG-PEI conjugates and B: LMW-PEI or LMW-PEI-PEG conjugates. Increase of ligand density increased condensation of DNA. While only minor differences were observed among PEG-PEI and its conjugates, condensation of LMW-PEI was strongly influenced upon conjugation.

Biocompatibility:

Non-specific interaction of polyplexes with cell surfaces is known for polycations such as PEI, PPI, PLL or PAMAM and can provoke nano hole formation caused toxicity (48). PEGylation of polycations is an effective shielding approach to decrease interaction with blood components (15). Since all of the conjugates showed nearly neutral or even negative zeta potentials, strong decrease of non-specific interactions was expected. In order to investigate blood compatibility of the conjugates, red blood cells were treated with polyplexes composed of DNA and polymers or conjugates and analyzed for hemolysis (see Figure 6). Polyplexes prepared with PEI 25k caused the strongest hemolytic effects, LMW-PEI and PEG-PEI polyplexes showed significantly (** $p < 0.001$) decreased hemolytic activity. Interestingly, conjugation with the targeting ligand increased hemolysis: Conjugate II, despite of its negative surface charge, caused significantly (* $p < 0.05$) higher hemolysis than LMW-PEI, and Conjugates 10-1 (* $p < 0.05$), 10-2 (** $p < 0.01$), and 5-2 (** $p < 0.001$) showed stronger hemolysis than PEG-PEI. This could be an indication of surface activity or different spatial orientation of the targeting ligand depending on the coupling degree. RGD sequences do not only interact with integrin alpha v beta 3 (49). Since erythrocytes do not carry integrins but rather an integrin-associated protein (IAP) CD47 (50), non-specific interactions in this assay could lead to cross reactivity of the conjugates with CD47. Agglutination of the red blood was strongly observed in cells treated with unmodified PEI 25k and slightly in LMW-PEI treated cells. PEG-PEI and conjugates did not cause agglutination despite of the slightly higher hemolytic effects of the conjugates (data not shown). In order to test the conjugates in an in vivo study, minimal hemolysis and crosslinking of cells is a prerequisite. Further toxicity assays will show if the conjugates we synthesized are safe enough to be applied intravenously in a tumor model. Other options could be intratumoral injections or local administration.

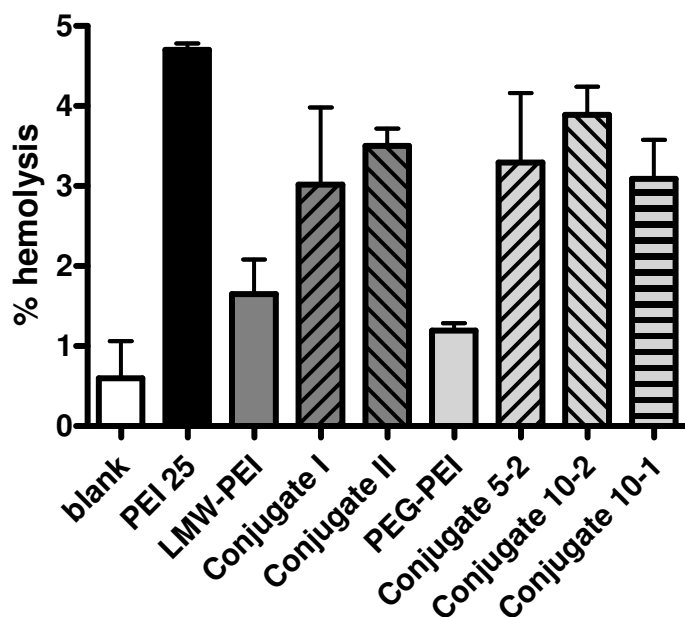


Figure 6: Percentage of hemolytic activity of pDNA complexes formed with PEI 25k, LMW-PEI, LMW-PEI-PEG conjugates, PEG-PEI or PEG-PEI conjugates compared to total hemolysis caused by 1 % Triton X. Both LMW-PEI and PEG-PEI caused less haemolytic effects than PEI 25 kDa while their conjugates displayed lower biocompatibility but still less hemolysis than PEI 25 kDa.

Expression of Integrin Receptor:

To test specific bioactivity of the conjugates in $\alpha_v\beta_3$ integrin overexpressing cells compared to cells that do not show overexpression of this receptor, expression status of MeWo human melanoma and A549 carcinomic human alveolar basal epithelial cells, two cell lines previously used for integrin targeted gene delivery (51), was quantified after immunostaining by flow cytometry (Figure 7A). A549 cells treated with primary and secondary antibody did not show significantly stronger fluorescence than after treatment with secondary antibody only, proving that fluorescence was only cause by non-specific binding of the secondary antibody. MeWo cells, on the other hand, showed clear overexpression of CD51/CD61. A549 cells were therefore considered receptor-negative, whereas MeWo cells were considered receptor-positive.

Cell Binding of Polyplexes:

Binding of fluorescently labeled polyplexes to the receptor expressing or non-expressing cell surface of MeWo or A549 cells, respectively, was tested at 4 °C, where energy dependent processes such as receptor mediated endocytosis are deactivated. Flow cytometric analysis proved that only Conjugates 10-2 and 5-2 with substitution degrees of 5 and 2.5 RGD-M per molecule displayed differences concerning binding to receptor positive or receptor negative cells (Figure 7B). Conjugate 10-1, on the other hand, which bears the highest number of RGD-M molecules, did not show significantly higher binding to MeWo compared to A549 cells. Due to higher stability of the complex possibly at least parts of the targeting ligand in Conjugate 10-1 are involved in complex formation and are therefore either oriented towards the inside of the complex or hidden by DNA with which they interact. Therefore, Conjugate 10-1 forms the smallest particles, condenses DNA as well as PEI 25k and does not bind to MeWo cells specifically stronger than to A549 cells. Concerning substitution degree, linker chemistry and their correlation to specificity, there are contrary reports in literature. While Garg et al. (35) reported increasing specific uptake with increasing amounts of targeting ligand in a range of coupling degree below 8-10 mol %, they also described lipoplex destabilization above that degree. This amount is still much below the coupling degree of all the conjugates in our study and it is possible, that polyplexes could as well be destabilized at high coupling degrees. It must also be kept in mind that the RGD-M used for conjugate synthesis is a receptor antagonist. Vitronectin-receptor antagonists are known to cause detachment of cells. The high amount of RGD-M present in Conjugate 10-1 did therefore detach cells effectively interacting with Conjugate 10-1, what could be observed macroscopically. The detached cells were aspirated in one of the washing steps leading to low fluorescence values measured by flow cytometry. It was earlier reported that integrin dimerization, cluster formation and activation of downstream effects depend on ligand density and affinity (52). This could explain that conjugates bearing a higher ligand density have a stronger inhibitory effect on cell attachment than those with lower ligand density.

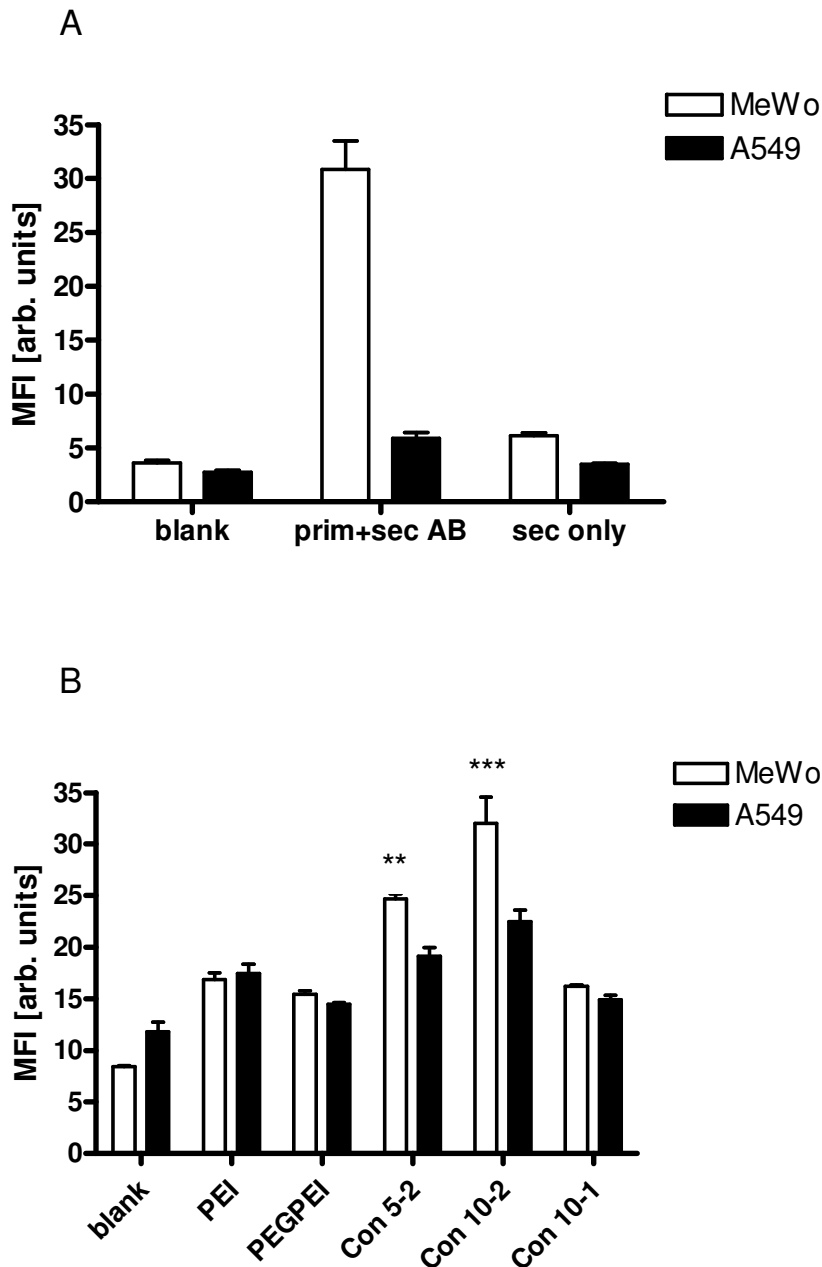


Figure 7A: Flow cytometric analysis of relative expression of integrin alpha v beta 3 in A549 and MeWo cells compared to blank cells and cells treated with the fluorescently labeled secondary antibody only. MeWo cells known to express a noticeable amount of integrin receptors proved significantly stronger binding of the primary antibody. 7B: Flow cytometric binding analysis of fluorescently labeled polymer and conjugate complexes to the surface of A549 and MeWo cells. Conjugate 10-2 with a medium ligand density shows the strongest differences concerning binding to receptor positive and receptor negative cells. Cells treated with Conjugate 10-1 were macroscopically observed to be detached from the plate.

Transfection Efficacy:

To investigate if the strong interaction of the conjugates with MeWo cells was only a concentration-dependent surface effect of the targeting ligand, uptake, which was assumed to be receptor-mediated endocytosis due to a previous report (53), was studied in a radioactive assay. Here, surface-bound material could be removed and distinct information about internalization could be obtained. In order to test for concentration dependent effects, MeWo and A549 cells were treated with increasing concentrations of Conjugate 5-2/DNA polyplexes, which had caused strong non-specific effects in the hemolysis assay, which could be interpreted as an indication of a surface effect. But scintillation counting of cell lysates confirmed cell specificity of uptake at each concentration as shown in Figure 8. Up to 1 μg of DNA per well, an increasing abundance of RGD-M leads to increasing uptake of polyplexes without any sign of cell detachment.

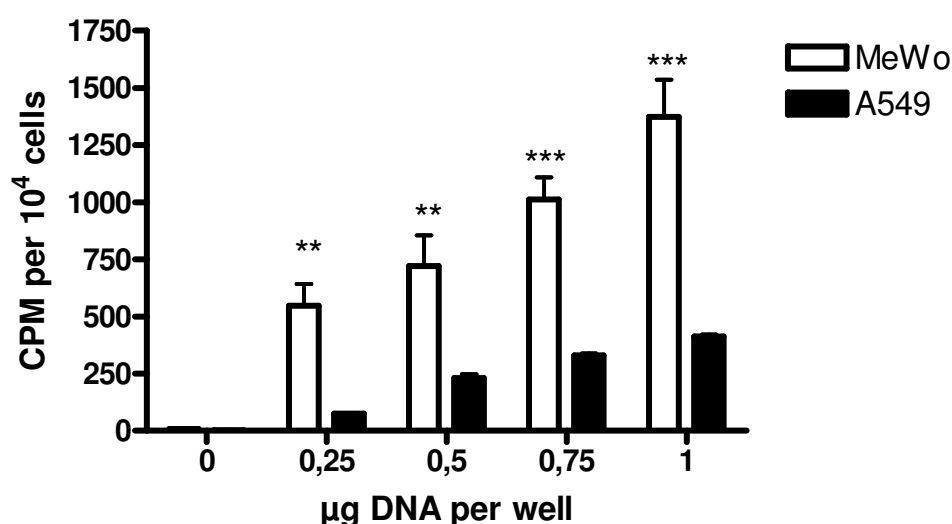


Figure 8: Radioactive internalization analysis of radiolabeled conjugate 5-2 complexes into A549 and MeWo cells at different concentrations. Up to 1 μg DNA per ml, increasing uptake of radiolabeled polyplex is maintained with increasing concentration.

Finally, transgene expression after transfection of receptor-positive and receptor-negative cells with polymer and conjugate complexes was measured. PEI 25k, the “gold standard” in polymeric non-viral gene delivery was used for comparison in each experiment (compare Figure 9A). LMW-PEI and PEG-PEI complexes exhibited lower transfection efficiency compared to PEI25kDa, due to decreased non-specific cell interaction. LMW-PEI-PEG conjugates were even inferior to LMW-PEI concerning transfection efficiency which can be explained by insufficient condensation and protection of DNA inside the complex. In a

previous study, it was shown that attaching the targeting ligand to PEI via PEG spacer achieved higher transfection efficiency than direct coupling (46), but in this panel of conjugates, PEGylated LMW-PEI conjugates did not exhibit desirable qualities. By PEGylation of LWM-PEI the interaction between polycation and polyanion was obviously impaired, shown by poor condensation and large polyplex sizes. In another report, conjugation of an RGD peptide to PEI via PEG was inefficient whereas coupling via SPDP-mediated efficient and specific transfection efficiency (51), which is in accordance with our results. Directly coupled Conjugate 10-1 yielded higher transfection efficiency than PEG-PEI but no specific differences in between the cell lines. This comparably low transfection efficacy of Conjugate 10-1 can again be explained by cell detachment which falsified the results. Conjugate 5-2, on the other hand showed 28-fold higher transgene expression in MeWo cells than PEG-PEI and highly significantly ($***p < 0.001$) stronger expression than in A549. The low ligand density in this conjugate obviously did not cause any inhibitory effects on cell attachment. Conjugate 10-2 achieved very good and specific ($**p < 0.01$) transfection efficiency in MeWo, as well, which was comparable to that of the PEI 25 kDa but might be decreased compared to Conjugate 5-2 due to cell detachment. The fact that some of the conjugates also showed better transfection efficiency in A549 cells compared to non-targeted PEG-PEI, can be explained by a constitutive expression of integrin receptor on almost all cells which was shown to be much lower in A549 than in MeWo cells but not fully absent (Figure 7A).

Specificity of Transfection Efficacy:

To ascertain receptor specificity of transfection efficiency, which had also yielded higher values for conjugates in A549 cells, uptake of conjugate complexes was competitively inhibited by free ligand. Eventually, transfection efficiency was measured and compared to that of non-targeted PEG-PEI complexes, as shown in Figure 9B. Conjugate 5-2 complexes again caused significantly higher ($***p < 0.001$) transfection efficiency in MeWo than PEG-PEI complexes, but transgene expression was decreased by increasing amounts of free ligand. At 0.1 nmol inhibitor per ml and higher concentrations, transfection efficiency in MeWo cells was not significantly different from that of PEG-PEI complexes. Interestingly, Conjugate 5-2 complexes also again caused slightly higher transgene expression in A549 cells than PEG-PEI complexes, and this increase was reversed in A549 cells, too, in presence of free targeting ligand. Since A549 cells do express a low number of integrin receptors, this result is not very surprising. Conjugate 5-2 was exemplarily investigated in

this assay as it has shown the highest transfection efficacy in the absence of competing free RGD-M. Since we were able to prove the specificity of its receptor-mediated delivery of pDNA, we hypothesize that this uptake route is also true in case of the other conjugates.

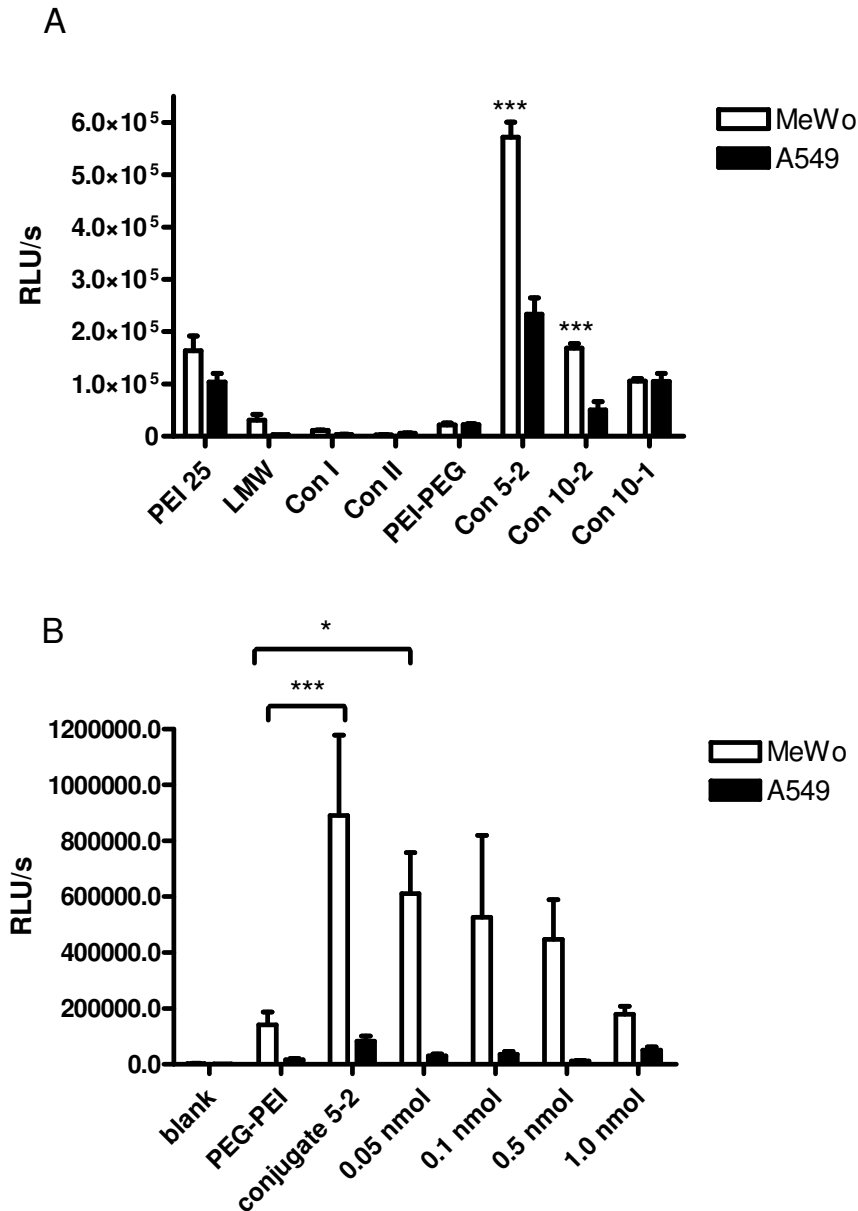


Figure 9A: Transfection efficiency of polymer and conjugate complexes in A549 and MeWo cells. Conjugate 5-2 with the lowest ligand density revealed the highest transgene expression. 9B: Competitive inhibition of transfection efficiency of conjugate complexes in A549 and MeWo cells. At a concentration of 0.1 nmol/ml of free targeting ligand or higher, transfection efficiency of Conjugate 5-2 could be comparatively inhibited to values significantly higher than that of PEG-PEI.

2.5 Conclusion

In conclusion, with our panel of differently synthesized conjugates, we have been able to investigate structure function relationships. The high affinity small molecule we used for integrin receptor targeting proved to be a suitable coupling reagent for in vitro gene delivery systems. Depending on the coupling route, more and less effective conjugates were obtained. Obviously, LMW-PEI lost its ability to condense DNA into small particles and to protect it upon coupling of substantial amounts of PEG. The RGD-M-coupled LMW-PEI-PEG conjugates therefore did not perform well in vitro and did not generate high transgene expression. The PEG-PEI conjugates, where the targeting ligand was coupled to the PEI domain of a diblock-like copolymer, on the other hand, seemed to be very promising compounds. PEG-PEI was not strongly affected concerning DNA condensation upon conjugation which is shown by ethidium bromide quenching and size measurements of the polyplexes. The coupling degree of the targeting moiety had an impact on sizes, zeta potentials and complexation of DNA but even more strongly influenced bioactivity. Whereas Conjugate 10-1 lacked specific interaction with MeWo cells, Conjugates 10-2 and 5-2 exhibited significantly higher binding and transgene expression in integrin receptor overexpressing cells, which could be inhibited by free targeting ligand. In these conjugates, DNA was tightly bound, but targeting ligands were obviously well accessible for interaction with cell surface receptors. Considering the biologic effect of the RGD-M, conjugates with a rather low coupling degree revealed the best results in vitro, with transfection efficacy inversely correlating with coupling degree. In this study we were able to identify Conjugates 10-2 and especially 5-2 as promising candidates for in vivo cancer gene therapy.

2.6 Acknowledgements

We are grateful to Dr. Cornelia Brendel (FACS laboratory, Department of Hematology, Oncology and Immunology, University Hospital Marburg) and Prof. Dr. Thomas Behr (Nuclear Medicine Department, University Hospital Marburg) for the generous use of equipment and facilities and to Eva Mohr (Department of Pharmaceutics and Biopharmacy, Philipps Universität Marburg) for excellent technical support.

2.7 References

- (1) Brooks, P. C., Clark, R. A., and Cheresh, D. A. (1994) Requirement of vascular integrin $\alpha v \beta 3$ for angiogenesis. *Science* 264, 569-71.
- (2) Hovidala-Dilke, K. (2008) $\alpha v \beta 3$ integrin and angiogenesis: a moody integrin in a changing environment. *Curr Opin Cell Biol* 20, 514-9.
- (3) Kim, W. J., Yockman, J. W., Jeong, J. H., Christensen, L. V., Lee, M., Kim, Y. H., and Kim, S. W. (2006) Anti-angiogenic inhibition of tumor growth by systemic delivery of PEI-g-PEG-RGD/pCMV-sFlt-1 complexes in tumor-bearing mice. *J Control Release* 114, 381-8.
- (4) Oba, M., Aoyagi, K., Miyata, K., Matsumoto, Y., Itaka, K., Nishiyama, N., Yamasaki, Y., Koyama, H., and Kataoka, K. (2008) Polyplex Micelles with Cyclic RGD Peptide Ligands and Disulfide Cross-Links Directing to the Enhanced Transfection via Controlled Intracellular Trafficking. *Mol Pharm.*
- (5) Oba, M., Fukushima, S., Kanayama, N., Aoyagi, K., Nishiyama, N., Koyama, H., and Kataoka, K. (2007) Cyclic RGD peptide-conjugated polyplex micelles as a targetable gene delivery system directed to cells possessing $\alpha v \beta 3$ and $\alpha v \beta 5$ integrins. *Bioconjug Chem* 18, 1415-23.
- (6) Schiffelers, R. M., Ansari, A., Xu, J., Zhou, Q., Tang, Q., Storm, G., Molema, G., Lu, P. Y., Scaria, P. V., and Woodle, M. C. (2004) Cancer siRNA therapy by tumor selective delivery with ligand-targeted sterically stabilized nanoparticle. *Nucleic Acids Res* 32, e149.
- (7) Reardon, D. A., Fink, K. L., Mikkelsen, T., Cloughesy, T. F., O'Neill, A., Plotkin, S., Glantz, M., Ravin, P., Raizer, J. J., Rich, K. M., Schiff, D., Shapiro, W. R., Burdette-Radoux, S., Dropcho, E. J., Wittemer, S. M., Nippgen, J., Picard, M., and Nabors, L. B. (2008) Randomized phase II study of cilengitide, an integrin-targeting arginine-glycine-aspartic acid peptide, in recurrent glioblastoma multiforme. *J Clin Oncol* 26, 5610-7.
- (8) Peyman, A., Wehner, V., Knolle, J., Stilz, H. U., Breipohl, G., Scheunemann, K. H., Carniato, D., Ruxer, J. M., Gourvest, J. F., Gadek, T. R., and Bodary, S. (2000) RGD mimetics containing a central hydantoin scaffold: $\alpha v \beta 3$ vs $\alpha IIb \beta 3$ selectivity requirements. *Bioorg Med Chem Lett* 10, 179-82.

-
- (9) Sulyok, G. A., Gibson, C., Goodman, S. L., Holzemann, G., Wiesner, M., and Kessler, H. (2001) Solid-phase synthesis of a nonpeptide RGD mimetic library: new selective $\alpha v \beta 3$ integrin antagonists. *J Med Chem* 44, 1938-50.
 - (10) Pollina, E. (1996) Design and Synthesis of RGD Mimetics as Potent Inhibitors of Platelet Aggregation. *J. Undergrad. Sci* 3, 119-126.
 - (11) Burnett, C. A., Xie, J., Quijano, J., Shen, Z., Hunter, F., Bur, M., Li, K. C., and Danthi, S. N. (2005) Synthesis, in vitro, and in vivo characterization of an integrin $\alpha(v)\beta(3)$ -targeted molecular probe for optical imaging of tumor. *Bioorg Med Chem* 13, 3763-71.
 - (12) Ishikawa, M., Kubota, D., Yamamoto, M., Kuroda, C., Iguchi, M., Koyanagi, A., Murakami, S., and Ajito, K. (2006) Tricyclic pharmacophore-based molecules as novel integrin $\alpha(v)\beta(3)$ antagonists. Part 2: synthesis of potent $\alpha(v)\beta(3)/\alpha(IIb)\beta(3)$ dual antagonists. *Bioorg Med Chem* 14, 2109-30.
 - (13) Zechel, C., Backfisch, G., Delzer, J., Geneste, H., Graef, C., Hornberger, W., Kling, A., Lange, U. E., Lauterbach, A., Seitz, W., and Subkowski, T. (2003) Highly potent and selective $\alpha v \beta 3$ -receptor antagonists: solid-phase synthesis and SAR of 1-substituted 4-amino-1H-pyrimidin-2-ones. *Bioorg Med Chem Lett* 13, 165-9.
 - (14) Fischer, D., Bieber, T., Li, Y., Elsasser, H. P., and Kissel, T. (1999) A novel non-viral vector for DNA delivery based on low molecular weight, branched polyethylenimine: effect of molecular weight on transfection efficiency and cytotoxicity. *Pharm Res* 16, 1273-9.
 - (15) Petersen, H., Fechner, P. M., Fischer, D., and Kissel, T. (2002) Synthesis, Characterization, and Biocompatibility of Polyethylenimine-graft-poly(ethylene glycol) Block Copolymers. *Macromolecules* 35, 6867-6874.
 - (16) Kircheis, R., Kichler, A., Wallner, G., Kursa, M., Ogris, M., Felzmann, T., Buchberger, M., and Wagner, E. (1997) Coupling of cell-binding ligands to polyethylenimine for targeted gene delivery. *Gene Ther* 4, 409-18.
 - (17) Germershaus, O., Merdan, T., Bakowsky, U., Behe, M., and Kissel, T. (2006) Trastuzumab-polyethylenimine-polyethylene glycol conjugates for targeting Her2-expressing tumors. *Bioconjug Chem* 17, 1190-9.
 - (18) von Harpe, A. (2000) in *Department Pharmaceutics and Biopharmacy*, Philipps-Universität, Marburg.

-
- (19) Ungaro, F., De Rosa, G., Miro, A., and Quaglia, F. (2003) Spectrophotometric determination of polyethylenimine in the presence of an oligonucleotide for the characterization of controlled release formulations. *J Pharm Biomed Anal* 31, 143-9.
- (20) Carlsson, J., Drevin, H., and Axen, R. (1978) Protein thiolation and reversible protein-protein conjugation. N-Succinimidyl 3-(2-pyridyldithio)propionate, a new heterobifunctional reagent. *Biochem J* 173, 723-37.
- (21) Hermanson, G. T. (1996) *Bioconjugate Techniques*, Academic Press, San Diego.
- (22) Merdan, T., Kunath, K., Fischer, D., Kopecek, J., and Kissel, T. (2002) Intracellular processing of poly(ethylene imine)/ribozyme complexes can be observed in living cells by using confocal laser scanning microscopy and inhibitor experiments. *Pharm Res* 19, 140-6.
- (23) Snyder, S. L., and Sobocinski, P. Z. (1975) An improved 2,4,6-trinitrobenzenesulfonic acid method for the determination of amines. *Anal Biochem* 64, 284-8.
- (24) Haigler, H. T., Maxfield, F. R., Willingham, M. C., and Pastan, I. (1980) Dansylcadaverine inhibits internalization of ¹²⁵I-epidermal growth factor in BALB 3T3 cells. *J Biol Chem* 255, 1239-41.
- (25) Temming, K., Schiffelers, R. M., Molema, G., and Kok, R. J. (2005) RGD-based strategies for selective delivery of therapeutics and imaging agents to the tumour vasculature. *Drug Resist Updat* 8, 381-402.
- (26) Zuhorn, I. S., Kalicharan, D., Robillard, G. T., and Hoekstra, D. (2007) Adhesion receptors mediate efficient non-viral gene delivery. *Mol Ther* 15, 946-53.
- (27) Schiffelers, R. M., Mixson, A. J., Ansari, A. M., Fens, M. H., Tang, Q., Zhou, Q., Xu, J., Molema, G., Lu, P. Y., Scaria, P. V., Storm, G., and Woodle, M. C. (2005) Transporting silence: design of carriers for siRNA to angiogenic endothelium. *J Control Release* 109, 5-14.
- (28) Schiffelers, R. M., and Storm, G. (2006) ICS-283: a system for targeted intravenous delivery of siRNA. *Expert Opin Drug Deliv* 3, 445-54.
- (29) Kang, H., Alam, M. R., Dixit, V., Fisher, M., and Juliano, R. L. (2008) Cellular Delivery and Biological Activity of Antisense Oligonucleotides Conjugated to a Targeted Protein Carrier. *Bioconjug Chem*.

-
- (30) Bai, M., Campisi, L., and Freimuth, P. (1994) Vitronectin receptor antibodies inhibit infection of HeLa and A549 cells by adenovirus type 12 but not by adenovirus type 2. *J Virol* 68, 5925-32.
- (31) Kerr, J. S., Wexler, R. S., Mousa, S. A., Robinson, C. S., Wexler, E. J., Mohamed, S., Voss, M. E., Devenny, J. J., Czerniak, P. M., Gudzelak, A., Jr., and Slee, A. M. (1999) Novel small molecule alpha v integrin antagonists: comparative anti-cancer efficacy with known angiogenesis inhibitors. *Anticancer Res* 19, 959-68.
- (32) Ballana, E., Pauls, E., Senserrich, J., Clotet, B., Perron-Sierra, F., Tucker, G. C., and Este, J. A. (2008) Cell adhesion through alphaV-containing integrins is required for efficient HIV-1 infection in macrophages. *Blood*.
- (33) Petrie, T. A., Reyes, C. D., Burns, K. L., and Garcia, A. J. (2008) Simple application of fibronectin-mimetic coating enhances osseointegration of titanium implants. *J Cell Mol Med*.
- (34) Burtea, C., Laurent, S., Murariu, O., Rattat, D., Toubeau, G., Verbruggen, A., Vanstherem, D., Vander Elst, L., and Muller, R. N. (2008) Molecular imaging of alpha v beta3 integrin expression in atherosclerotic plaques with a mimetic of RGD peptide grafted to Gd-DTPA. *Cardiovasc Res* 78, 148-57.
- (35) Garg, A., Tisdale, A. W., Haidari, E., and Kokkoli, E. Targeting colon cancer cells using PEGylated liposomes modified with a fibronectin-mimetic peptide. *International Journal of Pharmaceutics In Press, Corrected Proof*.
- (36) Demirgoz, D., Garg, A., and Kokkoli, E. (2008) PR_b-Targeted PEGylated Liposomes for Prostate Cancer Therapy. *Langmuir*.
- (37) Orlando, R. A., and Cheresch, D. A. (1991) Arginine-glycine-aspartic acid binding leading to molecular stabilization between integrin alpha v beta 3 and its ligand. *J Biol Chem* 266, 19543-50.
- (38) Mitjans, F., Meyer, T., Fittschen, C., Goodman, S., Jonczyk, A., Marshall, J. F., Reyes, G., and Piulats, J. (2000) In vivo therapy of malignant melanoma by means of antagonists of alphav integrins. *Int J Cancer* 87, 716-23.
- (39) Petersen, H., Fechner, P. M., Martin, A. L., Kunath, K., Stolnik, S., Roberts, C. J., Fischer, D., Davies, M. C., and Kissel, T. (2002) Polyethylenimine-graft-poly(ethylene glycol) copolymers: influence of copolymer block structure on DNA complexation and biological activities as gene delivery system. *Bioconjug Chem* 13, 845-54.

-
- (40) Kunath, K., von Harpe, A., Fischer, D., Petersen, H., Bickel, U., Voigt, K., and Kissel, T. (2003) Low-molecular-weight polyethylenimine as a non-viral vector for DNA delivery: comparison of physicochemical properties, transfection efficiency and in vivo distribution with high-molecular-weight polyethylenimine. *J Control Release* 89, 113-25.
- (41) Mahato, R. I., Rolland, A., and Tomlinson, E. (1997) Cationic lipid-based gene delivery systems: pharmaceutical perspectives. *Pharm Res* 14, 853-9.
- (42) Lucas, B., Remaut, K., Sanders, N. N., Braeckmans, K., De Smedt, S. C., and Demeester, J. (2005) Studying the intracellular dissociation of polymer-oligonucleotide complexes by dual color fluorescence fluctuation spectroscopy and confocal imaging. *Biochemistry* 44, 9905-12.
- (43) Mao, S., Neu, M., Germershaus, O., Merkel, O., Sitterberg, J., Bakowsky, U., and Kissel, T. (2006) Influence of Polyethylene Glycol Chain Length on the Physicochemical and Biological Properties of Poly(ethylene imine)-graft-Poly(ethylene glycol) Block Copolymer/SiRNA Polyplexes. *Bioconjug Chem* 17, 1209-18.
- (44) Ogris, M., Brunner, S., Schuller, S., Kircheis, R., and Wagner, E. (1999) PEGylated DNA/transferrin-PEI complexes: reduced interaction with blood components, extended circulation in blood and potential for systemic gene delivery. *Gene Ther* 6, 595-605.
- (45) Merdan, T., Callahan, J., Petersen, H., Kunath, K., Bakowsky, U., Kopeckova, P., Kissel, T., and Kopecek, J. (2003) Pegylated polyethylenimine-Fab' antibody fragment conjugates for targeted gene delivery to human ovarian carcinoma cells. *Bioconjug Chem* 14, 989-96.
- (46) Germershaus, O., Neu, M., Behe, M., and Kissel, T. (2008) HER2 targeted polyplexes: the effect of polyplex composition and conjugation chemistry on in vitro and in vivo characteristics. *Bioconjug Chem* 19, 244-53.
- (47) Ogris, M., Steinlein, P., Carotta, S., Brunner, S., and Wagner, E. (2001) DNA/polyethylenimine transfection particles: influence of ligands, polymer size, and PEGylation on internalization and gene expression. *AAPS PharmSci* 3, E21.
- (48) Hong, S., Leroueil, P. R., Janus, E. K., Peters, J. L., Kober, M. M., Islam, M. T., Orr, B. G., Baker, J. R., Jr., and Banaszak Holl, M. M. (2006) Interaction of polycationic polymers with supported lipid bilayers and cells: nanoscale hole formation and enhanced membrane permeability. *Bioconjug Chem* 17, 728-34.

- (49) Takagi, J. (2004) Structural basis for ligand recognition by RGD (Arg-Gly-Asp)-dependent integrins. *Biochem Soc Trans* 32, 403-6.
- (50) Brown, E., Hooper, L., Ho, T., and Gresham, H. (1990) Integrin-associated protein: a 50-kD plasma membrane antigen physically and functionally associated with integrins. *J Cell Biol* 111, 2785-94.
- (51) Kunath, K., Merdan, T., Hegener, O., Haberlein, H., and Kissel, T. (2003) Integrin targeting using RGD-PEI conjugates for in vitro gene transfer. *J Gene Med* 5, 588-99.
- (52) Boontheekul, T., Kong, H. J., Hsiong, S. X., Huang, Y. C., Mahadevan, L., Vandeburgh, H., and Mooney, D. J. (2008) Quantifying the relation between bond number and myoblast proliferation. *Faraday Discuss* 139, 53-70; discussion 105-28, 419-20.
- (53) Schraa, A. J., Kok, R. J., Berendsen, A. D., Moorlag, H. E., Bos, E. J., Meijer, D. K., de Leij, L. F., and Molema, G. (2002) Endothelial cells internalize and degrade RGD-modified proteins developed for tumor vasculature targeting. *J Control Release* 83, 241-51.

3 Polycationic triazine-based dendrimers: Effect of peripheral groups on transfection efficiency

Published in the New Journal of Chemistry (2009), *doi: 10.1039/b908735d*

3.1 Abstract

A panel of eight, generation two triazine dendrimers differing in the number of amines, guanidines, hydroxyls and aliphatic groups on the periphery was synthesized and assayed for gene transfer in an attempt to correlate the effects of surface functionality on transfection efficiency. The physicochemical and biological properties of the dendrimers and dendriplexes, such as condensation of DNA, size, surface charge and morphology of dendriplexes, toxic and ultimately transfection efficiency in MeWo cells, was analyzed. The results from an ethidium bromide exclusion assay showed that the complexation efficiency of the dendrimers with DNA is moderately affected by surface groups. Increasing the number of surface amines, reducing the number of surface hydroxyl groups, or replacing the amine moiety with guanidines all help strengthen the complex formed. Results from dynamic light scattering and zeta potential analyses indicate that the smallest particles result from complexes that exhibit the highest zeta potentials. Cytotoxicity was low for all compounds, particularly for the G2-5 dendrimer containing alkyl groups on the periphery, suggesting the benefit of incorporating such neutral functionality onto the surface of the triazine dendrimers. Highest transfection efficiency was observed for the dendrimers that formed the smallest complexes, suggesting that this physicochemical property is the most accurate predictor for determining which dendrimers will show the highest transfection efficiency.

3.2 Introduction

While gene therapy has shown promise in clinical trials for the treatment of a variety of diseases, complications, including immunogenicity and the potential for genetic recombination, that are associated with using viral vectors as DNA carriers has motivated numerous chemists to design non-viral carrier systems (1). Non-viral vector systems include cationic polymers (2), peptides (3), liposomes (4), and dendrimers (5). While nearly all of these systems show reduced transfection efficiency compared to viral analogues, their potential for large-scale production and reduced toxicity make these systems a more attractive alternative (6).

Among the non-viral vector systems, dendrimers are advantageous because they can be synthesized to afford monodisperse products with multi-functional peripheries. Various dendrimers including polyamidoamine (PAMAM) (7), polypropylenimine (PPI) (8),

dendritic poly-L-lysine (PLL) (9), phosphorus-containing dendrimers (10), and carbosilane dendrimers (11) have all shown success in a number of transfection studies. However, a thorough analysis of dendrimers based on melamine as candidates for gene therapy is, thus far, unavailable. Cationic triazine dendrimers have shown low cytotoxicity *in vitro* and *in vivo* (12). In addition, the synthesis of these compounds allows for the incorporation of multiple functionalities on the surface (13) to aid in overcoming the barriers associated with gene therapy. With the recently completed kilogram-scale synthesis of a dendrimer based on melamine (14), commercial availability of these types of compounds could follow.

The obstacles encountered for non-viral vector mediated gene transfer can generally be classified into three main groups: 1) toxicity of the vector, 2) affinity of the complex for the cell surface and cell penetration, and 3) stability of the vector-DNA complex. Cytotoxicity of most non-viral carriers stems from their cationic nature, and accordingly, incorporating non-ionic groups to improve biocompatibility is common. Derivatizing cationic dendrimers with neutral groups such as polyethylene glycol (PEG) (15), hydroxyl groups (16), or lipids (17) has helped reduce cytotoxicity. Our library focuses on the potential of hydroxyl groups as well as alkyl groups to help reduce the toxicity of triazine dendrimers.

To improve the association of non-viral complexes with the cell surface and to increase cell penetration, studies often aim at incorporating functionalities onto the surface of dendrimers that can mimic the effects seen for arginine-rich peptides (18-20). Guanidinylation is an effective and synthetically simple way to probe this effect. Our library includes structures to compare amines and guanidinium groups. Studies have also shown that PAMAM dendriplexes with hydrophobic groups on the surface display enhanced affinity for the cell surface (21). The hydrophobic nature of our dendrimer cores as well as the incorporation of alkyl groups on the surface are hypothesized to promote interactions with cell surface phospholipids. Finally, the number of surface amine groups was varied to gain insight into dendrimer-DNA complex formation.

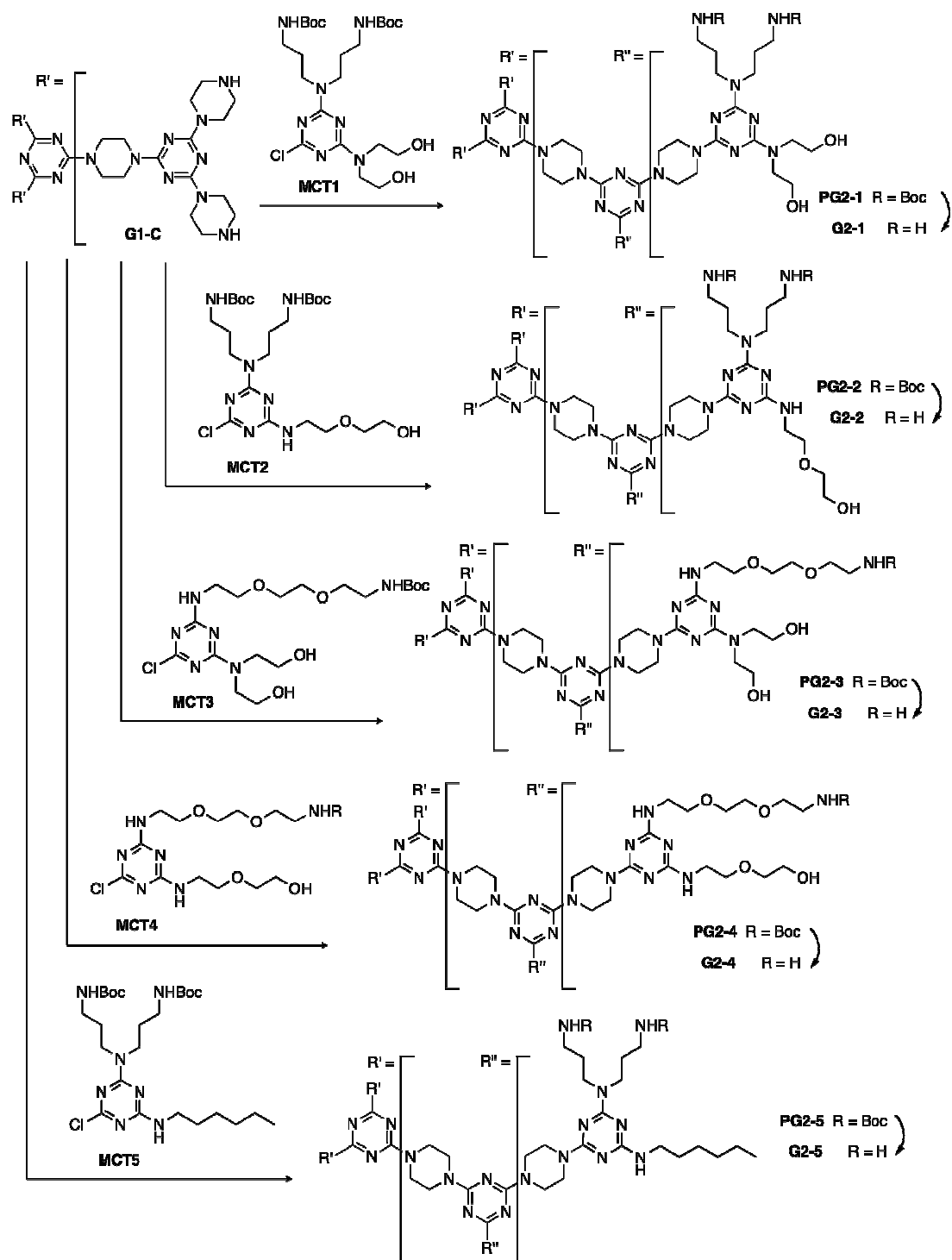
In this paper we report the synthesis of a library of monodisperse dendrimers with various surface functional groups to investigate the effect of triazine dendrimer peripheries on transfection efficiency. The physicochemical and biological properties of these structures, including complexation efficiency, zeta potential, hydrodynamic diameter, cytotoxicity, and finally transfection efficiency, were all assayed. Correlations between these properties and the functionality on the peripheries of the triazine dendrimers are reported.

3.3 Results and Discussion

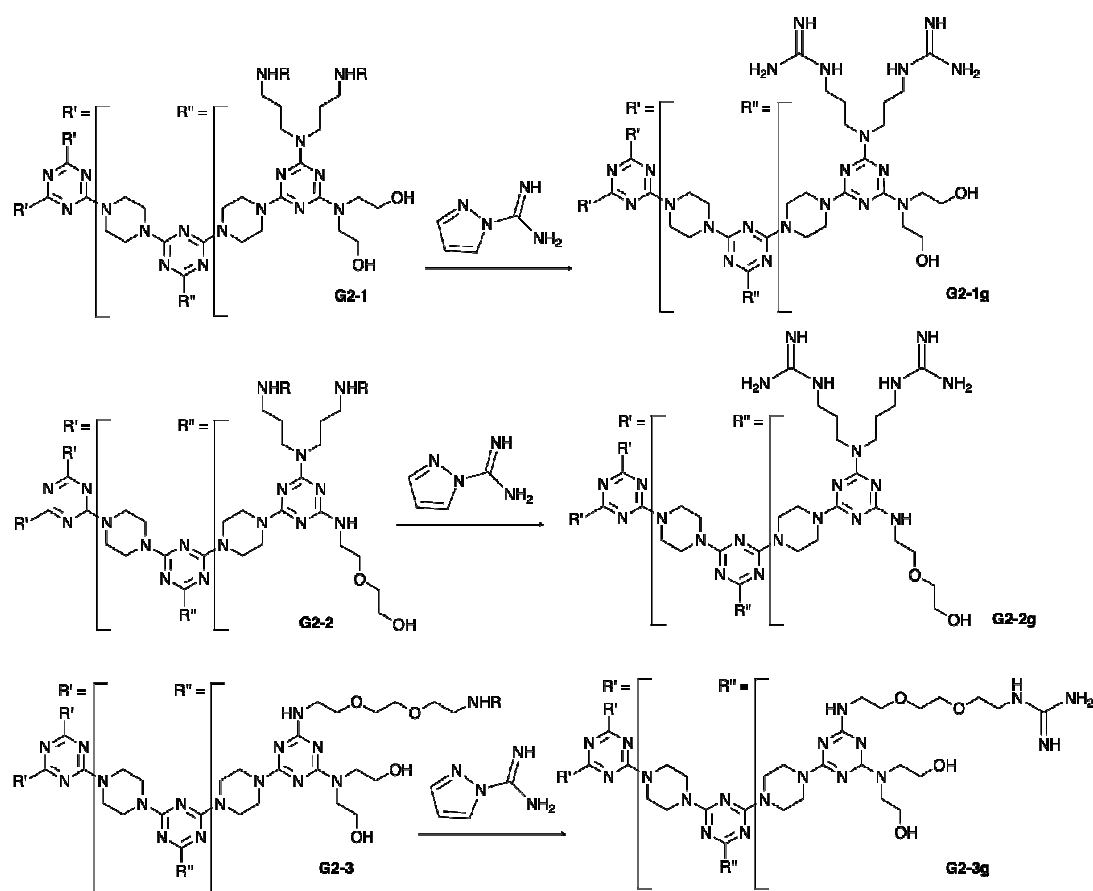
Synthesis

Synthesis of the dendrimers used in this study follows a divergent route in which a first generation triazine core, **G1-C**, which was synthesized as described elsewhere (22), is reacted with various monochlorotriazines (**MCT1** to **MCT5**) to form the second generation structures (**PG2-1** to **PG2-5**). These Boc-protected structures were then deprotected to form dendrimers **G2-1** through **G2-5** (**Scheme 1a**). Subsequently dendrimers **G2-1** to **G2-3** were guanidinylated following previously described procedures (22) to form **G2-1g** to **G2-3g** (**Scheme 1b**). All of the intermediates and products were characterized by ^1H and ^{13}C NMR and/or mass spectrometry as described in the experimental section. The results show nearly complete monodispersity for all of the final products.

a)



b)



Scheme 1: (a) Synthesis of amine terminated triazine based dendrimers proceeds by divergent route, (b) synthesis of guanidinylated triazine dendrimers

Ethidium bromide quenching assay

The association of dendrimers and DNA, a so-called dendriplex, can result in the formation of both tightly or loosely associated complexes, with the latter resulting in DNA being more accessible to nucleases and other species. To quantify the extent of unassociated DNA, an ethidium bromide intercalation assay is utilized. In this assay, dendrimer and DNA are complexed and then exposed to ethidium bromide. If unassociated DNA exists, ethidium bromide intercalates and fluoresces. If only tightly bound DNA is present, intercalation is hindered and fluorescence is absent. Therefore, compounds that exhibit low fluorescence typically correlate with highly compacted and protected DNA complexes, which is favorable for in vivo studies. The extent of intercalation quenching by triazine dendrimers is reported in **Figure 1** and various trends that correlate the packaging of DNA with the surface functionality of the dendrimers are evident.

The choice of the peripheral group of the triazine dendimers appears to have notable effect on the packaging of DNA. In all cases, the dendrimers that contain only six surface amines (**G2-3** and **G2-4**) complexed weakly to DNA as compared to the analogues that contain twelve surface amines (**G2-1** and **G2-2** respectively). This suggests that condensation efficiency is moderately affected by the number of surface amines, with improved complexation seen for dendrimers with a higher number of surface amines. Guanidinylation appears to significantly increase packaging over primary amine analogues in nearly all cases. This has been seen in earlier studies in which guanidylated cholesterol derivatives were reported to interact more strongly with DNA than similar amine structures (23). Like the amine analogues, more strongly complexed structures were formed using dendrimers with twelve peripheral guanidines (**G2-1g** and **G2-2g**) as compared to dendrimers with only six guanidines (**G2-3g**).

The formation of strongly complexed structures decreases with increasing number of surface hydroxyl groups, suggesting that this neutral functionality may hinder interactions with DNA. However, for the alkyl group of **G2-5**, the formation of a strongly complexed dendriplex is observed. In fact the alkylated compound outperforms PEI in complexation efficiency, suggesting this compound should be competitive in transfection efficiency assays.

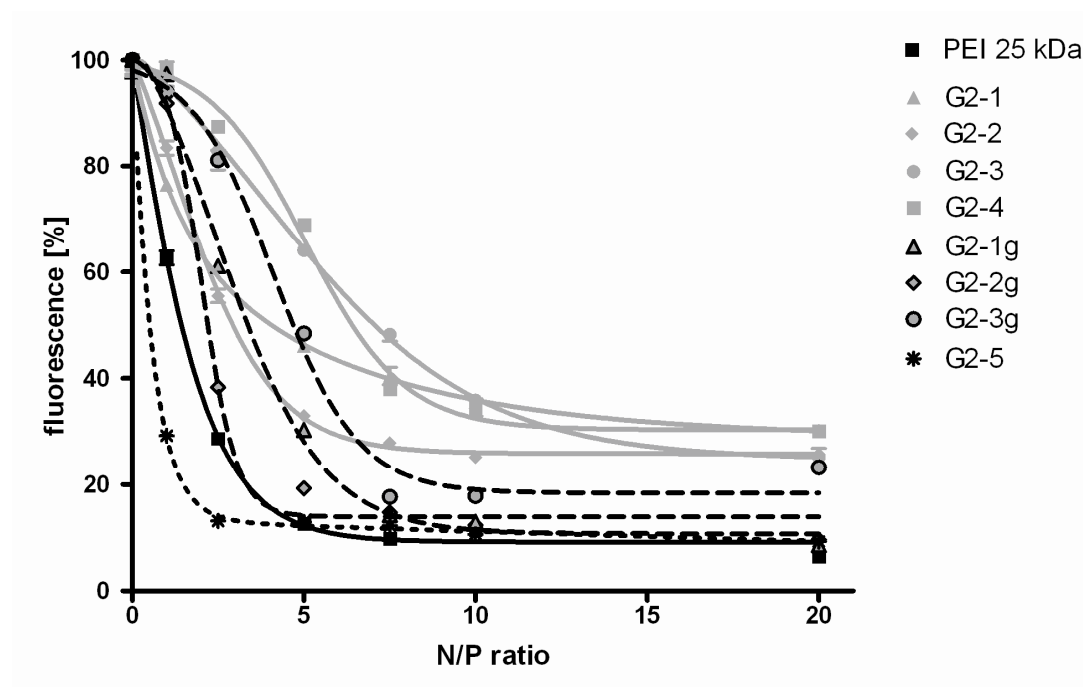


Figure 110: DNA condensation efficiency was quantified by ethidium bromide quenching assay.

Dynamic light scattering and zeta potential measurements

Dynamic light scattering was used to determine the size of the triazine dendrimer-DNA complexes (**Figure 2a**). In general, the size of the complex can affect both transfection efficiency and toxicity. For in vitro studies, large polyplexes can sediment faster and may result in high transfection efficiency, but can also result in high cytotoxicity (24). However, complexes with diameters of less than 200 nm are endocytosed by most cell lines and are believed to be more practical for in vivo and clinical applications.

In general, complex size appears to be independent of peripheral functionality. The smallest complexes were formed using dendrimers **G2-1** and **G2-5**, suggesting these compounds should be the most competitive in transfection efficiency assays. Alternatively, both **G2-1g** and **G2-2g** formed complexes with sizes of approximately 1 μm , which is generally a size for which sedimentation occurs, suggested that the compounds may also exhibit notable transfection efficiency in vitro.

Zeta potential measurements were used to determine the surface charge of the dendrimplexes (**Figure 2b**). In general, positively charged particles associate well with the cell surface and are internalized by the cell via endocytosis while negatively charged particles are usually repelled by the negatively charged plasma membrane. Overall, the results of the zeta potential analysis are complementary to the data collected from DLS. The dendrimers that showed the highest surface charge (**G2-1**, **G2-4**, **G2-3g**, and **G2-5**) also formed the smallest complexes suggesting that these structures may exhibit notable transfection efficiency. Only dendrimer **G2-3** showed a negative zeta potential at an N/P ratio of 5, indicating that this compound will not likely be an effective gene transfer agent.

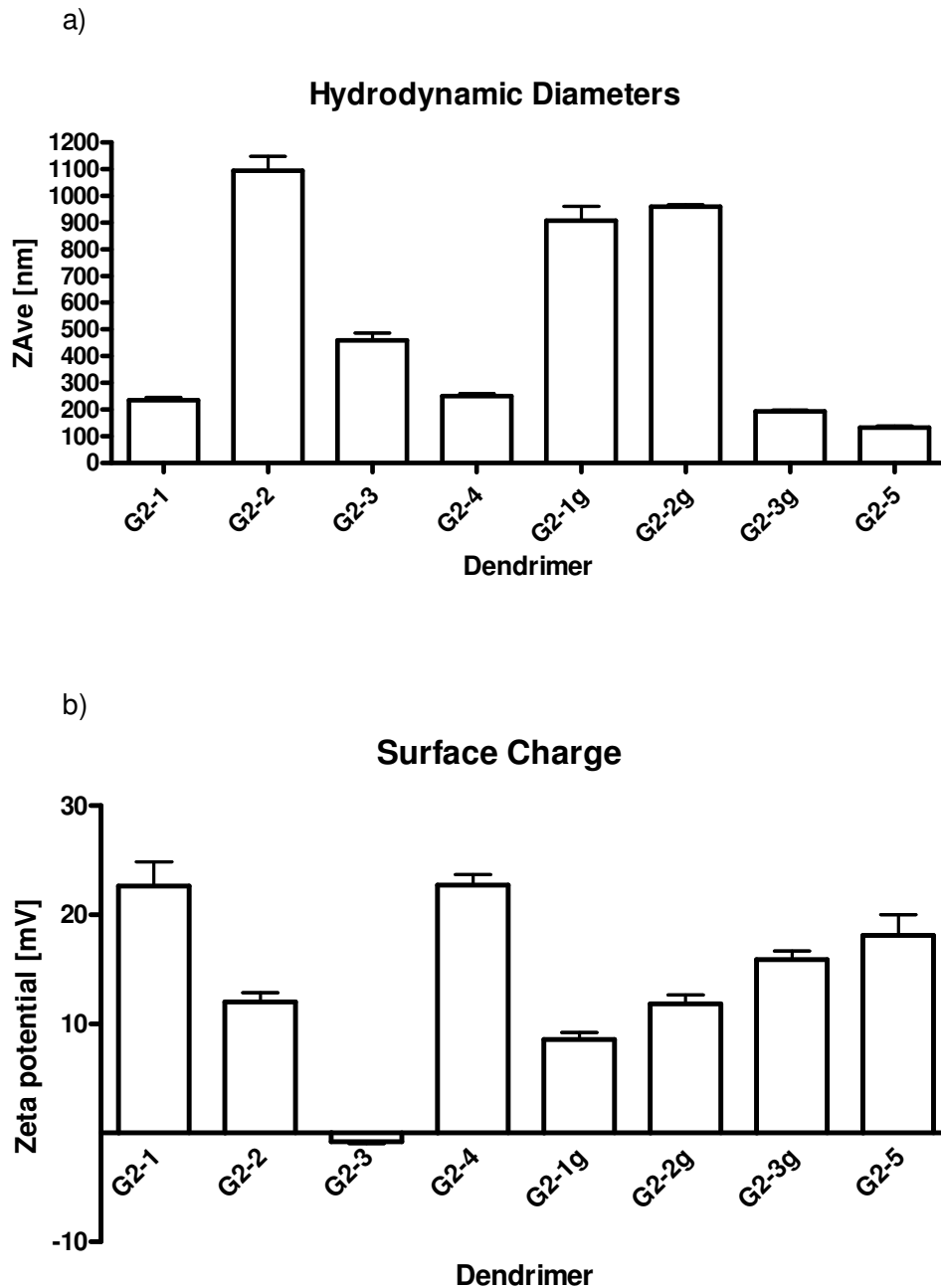


Figure 211: Hydrodynamic diameters (a) and zeta potentials (b) of various endriplexes at an N/P of 5 were determined in 10 mM HEPES buffer, pH 7.4.

MTT-assays

The cytotoxicity observed in this study derives from incubation of various concentrations of the dendrimer (0.001 – 0.5 mg/mL) with murine L929 fibroblasts. The cell viability is quantified by mitochondrial enzyme activity, which reduces yellow 3-(4,5-dimethylthiazol-2-yl)-2,5-diphenyltetrazolium bromide (MTT) to its purple formazan. The reduction is

quantified spectrophotometrically. The quantified toxicity represents the “worst case scenario”: dendriplexes should display reduced toxicity due to the masking of cationic groups, and this trend has been reported in previous studies investigating the use of PPI for gene delivery (8). The results are shown in **Figure 3**.

The cytotoxicity results from this study correlate well with an earlier report that revealed an IC_{50} value of 0.1 mg/mL for a related triazine dendrimer (12). In general there are no clear trends for correlating cytotoxicity with surface functionality. None of the triazine dendrimers used in this study showed substantial cytotoxicity, indicating that this will not be a substantial factor that influences gene transfer activity.

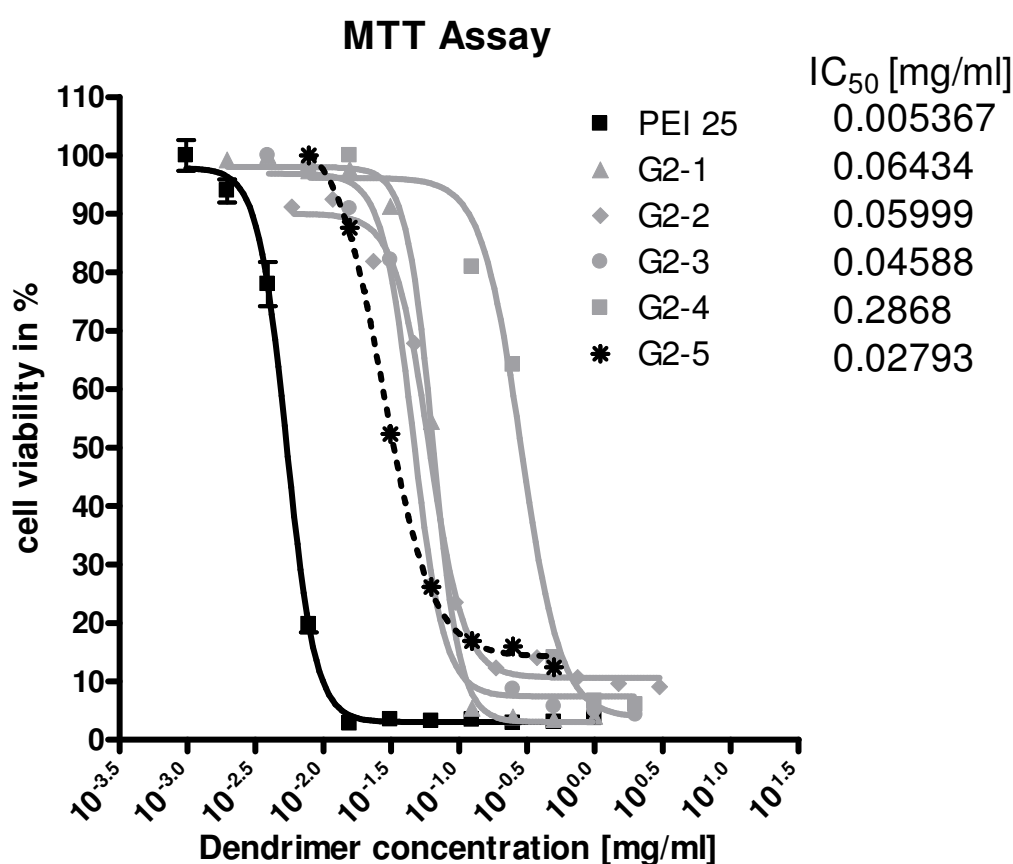


Figure 312: Toxicity profiles of all the water soluble dendrimers according to the MTT assay were compared to that of PEI 25 kDa. For clarity, IC_{50} values are given.

Transfection efficiency

Transfection efficiency of the dendriplexes at three different N/P ratios was quantified using a commercial luciferase assay in a human melanoma cell line (MeWo). The data is

reported in relative light units on a log scale. The gene transfer activity was compared to 25 kDa PEI, a gold standard in transfection (**Figure 4**).

The highest transfection efficiency was seen for DNA complexed with either **G2-1** or **G2-5**. These complexes have relatively small sizes (< 250 nm), which correlates with earlier studies that showed that high transfection efficiency is seen for small complexes (25, 26). However, at high N/P ratios (N/P = 7.5) high transfection efficiency was also seen for complexes with twelve guanidine surface groups despite the large size of these complexes. This high transfection efficiency may be due to a sedimentation effect exerted on these large complexes. However, due to their large size these compounds would not be suitable for in vivo gene delivery studies. For all of the complexes that contain only 6 terminal amines (**G2-3**, **G2-4** and **G2-3g**), poor transfection efficiency correlates with low cation number.

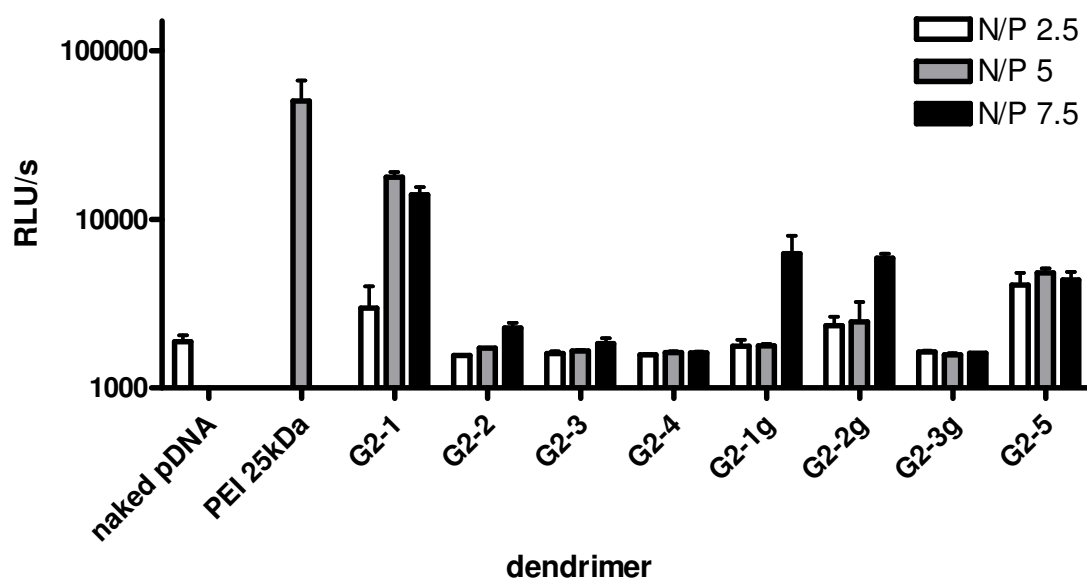


Figure 413: Transfection efficiency of all the water soluble dendrimers at various N/P ratios in MeWo cells are given as relative light units detected by luciferase assay.

3.4 Conclusion

Triazine dendrimers join the growing list of macromolecules capable of facilitating gene delivery. Even within this small subset of architectures, trends in activity emerge that validate observations made in other classes of molecules. Perhaps surprisingly, small structural perturbations in the periphery of triazine dendrimers influence transfection efficiency. The competitive efficacy seen with **G2-1** bodes well for future studies,

including those aimed at examining the influence of generation and core structure which we hope to communicate in due course.

3.5 Experimental

Materials

All chemicals used for synthesis were of analytical grade. The intermediate structures **G1-C** and **MCT-2** were synthesized as described elsewhere.^{13,22}

Synthesis

Monochlorotriazine 1 (MCT1). Cyanuric chloride (0.92 g, 5.00 mmol) and Boc-protected 3,3'-bisaminopropylamine (1.66 g, 5.00 mmol) were each dissolved in 60 mL tetrahydrofuran and cooled to 0 °C. The Boc-protected triamine was added dropwise to cyanuric chloride followed by the addition of DIPEA (1.75 mL, 10.05 mmol). After 3 hours, diethanolamine (0.53 g, 5.02 mmol) and DIPEA (1.75 mL, 10.05 mmol) were dissolved in 60 mL tetrahydrofuran, cooled to 0 °C, and added dropwise to the reaction mixture. The mixture was warmed to room temperature. After 20 hours the solvent was evaporated under reduced pressure. The crude product was dissolved in dichloromethane and washed with distilled water. The organic layer was dried and purified by column chromatography (10:1 CH₂Cl₂:ethyl acetate) to yield **MCT1** (2.49 g, 91%). ¹H NMR (300 MHz, CDCl₃) δ: 5.76 (b, 1H, OH) 5.36 (t, 2H, NHBoc), 3.77 (d, 4H, CH₂OH), 3.67 (d, 4H, NCH₂CH₂OH), 3.51-3.43 (br, 4H, NCH₂CH₂CH₂), 3.01 (m, 4H, CH₂NHBoc), 1.79-1.67 (m, 4H, CH₂CH₂CH₂), 1.37 (s, 18H, C(CH₃)₃). ¹³C NMR (75 MHz, CDCl₃) δ: 168.4 (C₃N₃), 165.0 (C₃N₃), 164.1 (C₃N₃), 156.3 (CO), 79.3 (OC(CH₃)₃), 61.7 (CH₂OH), 51.7 (NCH₂CH₂OH), 44.6 (NCH₂CH₂CH₂), 38.0 (CH₂NHBoc), 28.2 (C(CH₃)₃), 27.7 (CH₂CH₂CH₂). MS (ESI): calcd 547.29 (M⁺); found 548.30 (M + H⁺).

Monochlorotriazine 3 (MCT3). Mono-Boc-protected 2,2'-(ethylenedioxy)bis(ethylamine) (0.33 g, 1.32 mmol) and cyanuric chloride (0.24 g, 1.33 mmol) were each dissolved in 20mL tetrahydrofuran, and cooled to 0 °C. The diamine solution was added dropwise to the cyanuric chloride solution followed by the addition of DIPEA (0.75mL, 4.31 mmol). After 3 hours, diethanolamine (0.11 g, 1.326 mmol) and DIPEA (0.75mL, 4.31 mmol) were dissolved in 20 mL tetrahydrofuran, cooled to 0 °C, and added dropwise to the reaction mixture. The solution was warmed to room temperature. After 18 hours the reaction mixture was dried under reduced pressure. The crude product was dissolved in

dichloromethane and washed with distilled water. The dichloromethane layer was dried and purified using column chromatography (10:1 CH₂Cl₂:ethyl acetate) to afford **MCT3** (0.49 g, 80%). ¹H NMR (300 MHz, CDCl₃) δ: 6.11 (br, 1H, OH), 5.38 (br, 1H, NHBoc), 3.89 (br, 4H, NCH₂CH₂OH), 3.77 (br, 2H, NHCH₂CH₂O) 3.60 (s, 4H, OCH₂CH₂O), 3.54 (m, 6H, OCH₂CH₂NHBoc, NCH₂CH₂OH), 3.29, (q, 2H, CH₂NHBoc), 1.96 (br, 2H, OH), 1.42 (s, 9H, C(CH₃)₃). ¹³C NMR (300 MHz, CDCl₃) δ: 168.7 (C₃N₃), 165.9 (C₃N₃), 165.2 (C₃N₃), 156.4 (CO), 70.6 (CH₂OCH₂CH₂OCH₂), 69.5 (OCH₂CH₂O), 61.8 (CH₂OH), 52.3 (NCH₂CH₂OH), 41.0 (HNCH₂), 40.5 (CH₂NHBoc), 28.6 (C(CH₃)₃). MS (ESI): calcd 464.22 (M⁺); found 465.17 (M + H⁺).

Monochlorotriazine 4 (MCT4). Mono-Boc-protected 2,2'-(ethylenedioxy)bis(ethylamine) (0.10 g, 0.40 mmol) and cyanuric chloride (0.07 g, 0.40 mmol) were each dissolved in 7 mL tetrahydrofuran and cooled to 0 °C. The diamine solution was added dropwise to the cyanuric chloride solution followed by the addition of DIPEA (0.21 mL, 1.21 mmol). After 3 hours, 2-(2-aminoethoxy)ethanol (0.04 mL, 0.40 mmol) and DIPEA (0.21 mL, 1.21 mmol) were mixed in 7 mL tetrahydrofuran, cooled to 0 °C, and added dropwise to reaction mixture. The solution was allowed to warm to room temperature. After 18 hours the reaction mixture dried under reduced pressure, dissolved in dichloromethane, and washed with distilled water. The dichloromethane layer was dried and the product was purified by column chromatography (1:1 CH₂Cl₂:ethyl acetate → 1:1 CH₂Cl₂:ethyl acetate with 10% CH₃OH) to afford **MCT4** (0.16 g, 85%). ¹H NMR (300 MHz, CDCl₃) δ: 3.72 (s, 4H, NCH₂), 3.62 (s, 8H, OCH₂CH₂O), 3.53 (t, 6H, OCH₂CH₂NH), 3.31 (t, 2H, CH₂NHBoc), 2.75 (s, 1H, OH), 1.42 (s, 9H, C(CH₃)₃). ¹³C NMR (300 MHz, CDCl₃) δ: 166.2 (C₃N₃), 165.8 (C₃N₃), 156.3 (CO), 79.3 (OC(CH₃)₃), 72.6 (OCH₂CH₂O), 70.6 (OCH₂CH₂NH), 61.8 (CH₂OH), 40.8 (NHCH₂), 40.5 (CH₂NHBoc), 28.6 (C(CH₃)₃). MS (ESI): calcd 464.22 (M⁺); found 465.23 (M + H⁺).

Monochlorotriazine 5 (MCT5). Boc-protected 3,3'-bisaminopropylamine (0.48 g, 1.45 mmol) and cyanuric chloride (0.27 g, 1.45 mmol) were each dissolved in 4:1 CH₂Cl₂:CH₃OH (30 mL) and cooled to 0 °C. The triamine solution was added dropwise to cyanuric chloride followed by the addition of DIPEA (0.25 mL, 1.44 mmol). After 3 hours, hexylamine (0.15 g, 1.45 mmol) and DIPEA (0.25 mL, 1.44 mmol) were dissolved in 15 mL of 4:1 CH₂Cl₂:CH₃OH, cooled to 0 °C, and added dropwise to the reaction mixture. After 12 hours reaction mixture was dried under reduced pressure, dissolved in dichloromethane, and washed with distilled water. The dichloromethane layer was dried

and the crude product was purified by column chromatography (10:1 CH₂Cl₂:ethyl acetate) to afford **MCT5** (0.72 g, 91%). ¹H NMR (300 MHz, CDCl₃) δ: 3.59-3.49 (t, 4H, NCH₂), 3.37 (q, 2H, NHCH₂), 3.09 (m, 4H, CH₂NHBoc), 1.78-1.69 (m, 4H, CH₂CH₂CH₂), 1.57 (m, 2H, NHCH₂CH₂), 1.44 (s, 18H, C(CH₃)₃), 1.31 (s, 6H, CH₂), 0.88 (t, 3H, CH₃). ¹³C NMR (300 MHz, CDCl₃) δ: 168.7 (C₃N₃), 165.6 (C₃N₃), 165.4 (C₃N₃), 156 (CO), 79.1 (OC(CH₃)₃), 44.0 (NCH₂CH₂CH₂), 43.6 (NHCH₂), 41.2 (NHCH₂CH₂), 37.8 (CH₂NHBoc), 37.0 (CH₂NHBoc), 31.7 (CH₂CH₂CH₃), 28.6 (C(CH₃)₃), 28.0 (CH₂CH₂CH₂), 26.7 (NHCH₂CH₂CH₂), 22.8 (CH₂CH₃), 14.2 (CH₃). MS (ESI): calcd 543.33 (M⁺); found 544.33 (M + H⁺).

Protected G2-1 (P-G2-1). **MCT1** (0.57 g, 1.04 mmol) and **G1-C** (0.18 g, 0.17 mmol) were each dissolved in 10 mL of 9:1 CH₂Cl₂:CH₃OH. The solutions were mixed at room temperature followed by the addition of DIPEA (0.5mL, 2.9 mmol). The reaction mixture was heated to 70 °C. After 10 days the reaction mixture was dried, re-dissolved in dichloromethane, and washed with distilled water. The organic layer was condensed and purified by column chromatography (4:1 CH₂Cl₂:ethyl acetate with 1 → 3% CH₃OH) to yield **P-G2-1** (0.43 g, 61%). ¹H NMR (300 MHz, CDCl₃) δ: 5.64 (s, 12H, OH) 5.09 (s, 12H, NHBoc), 3.87 (br, 24H, CH₂OH), 3.81 (br, 72H, piperazine), 3.77 (br, 24H, NCH₂CH₂OH), 3.61 (br, 24H, NCH₂CH₂CH₂), 3.11 (br, 24H, CH₂NHBoc), 1.67 (br, 24H, CH₂CH₂CH₂), 1.44 (s, 108H, C(CH₃)₃). ¹³C NMR (300 MHz, CDCl₃) δ: 165.6 (C₃N₃), 165.5 (C₃N₃), 156.2 (CO), 79.2 (OC(CH₃)₃), 62.0 (CH₂OH), 51.3 (NCH₂CH₂OH), 44.2 (NCH₂CH₂CH₂), 43.6 (piperazine), 38.2 (CH₂NHBoc), 28.7 (C(CH₃)₃), 27.9 (CH₂CH₂CH₂). MS (MALDI): calcd 4142.57 (M⁺); found 4142.71 (M + H⁺).

G2-1. **P-G2-1** (0.38 g, 0.09 mmol) was dissolved in 3 M HCl:CH₃OH. After 2 days the reaction was condensed and neutralized with NaCO₃ to pH=7. NaCl byproduct was removed from the mixture using an Amicon apparatus and a millipore membrane with NMWL = 1,000 under 35 psi N₂. The solution remaining inside the Amicon vessel was dried *in vacuo* to afford **G2-1** (0.25 g, 93%). MS (MALDI): calcd 2941.94 (M⁺); found 4142.90 (M + H⁺). HPLC (2:1 H₂O with 0.14% TFA:acetonitrile): 3.196 min.

G2-1g. **G2-1** (21.9 mg, 7.4 μmol) was dissolved in 1mL distilled water. 1H-pyrazole-1-carboxamidinium•HCl (0.13 g, 890 μmol) and DIPEA (0.31 mL, 1.78 mmol) were mixed in 1mL acetonitrile. When the acetonitrile solution became clear, the distilled water solution was added, and the mixture was stirred at room temperature. After 5 days the solvents were removed and the mixture was re-dissolved in diionized water. Excess starting material was removed from the solution using an Amicon apparatus and a millipore membrane with

NMWL = 1,000 under 35 psi N₂. The solution remaining inside the Amicon vessel was dried *in vacuo* to afford **G2-1g** dendrimer (18.1 mg, 71%). MS (MALDI): calcd 3446.21 (M⁺); found 3447.00 (M + H⁺).

Protected G2-2 (P-G2-2). MCT2 (0.30 g, 0.55 mmol) and G1-C (0.10 g, 0.09 mmol) were each dissolved in 3 mL 9:1 CHCl₃:CH₃OH. The monochlorotriazine solution was added dropwise to the G1-C solution followed by the addition of DIPEA (0.40 mL, 2.30 mmol). After 5 days the reaction mixture was dried under reduced pressure, re-dissolved in dichloromethane, and washed with distilled water. The organic layer was dried and purified by column chromatography (4:1 CH₂Cl₂:ethyl acetate and 3→7% CH₃OH) to afford **P-G2-2** dendrimer (0.22 g, 58%). ¹H NMR (300 MHz, CDCl₃) δ: 5.26 (br, 18H, NHBoc), 3.82 (br, 72H, piperazine), 3.75 (br, 36H, CH₂OCH₂CH₂OH), 3.64 (br, 12H, NHCH₂), 3.61 (br, 24, NCH₂), 3.08 (br, 24H, CH₂NHBoc), 1.73 (br, 24H, CH₂CH₂CH₂), 1.44 (s, 108H, C(CH₃)₃). ¹³C NMR (300 MHz, CDCl₃) δ: 165.6 (C₃N₃), 165.2 (C₃N₃), 156.2 (CO), 79.3 (OC(CH₃)₃), 72.5 (OCH₂CH₂OH), 70.2 (NHCH₂CH₂O), 61.8 (CH₂OH), 43.3 (piperazine), 42.5 (NCH₂CH₂CH₂), 40.8 (NHCH₂CH₂O), 37.4 (CH₂NHBoc), 28.7 (C(CH₃)₃), 28.0 (CH₂CH₂CH₂). MS (MALDI): calcd 4142.57 (M⁺); found 4143.15 (M + H⁺).

G2-2. **P-G2-2** (0.22 g, 0.05 mmol) was dissolved in 3M HCl:CH₃OH. After 3 days the reaction mixture was condensed, dissolved in distilled water and neutralized with 1M NaOH. NaCl byproduct was removed from the solution using an Amicon apparatus and a millipore membrane with NMWL = 1,000 under 35 psi N₂. The solution remaining inside the Amicon vessel was dried *in vacuo* to afford **G2-2** dendrimer (0.09 g, 59%). MS (MALDI): calcd 2941.94 (M⁺); found 4142.96 (M + H⁺). HPLC (2:1 H₂O with 0.14% TFA:acetonitrile): 3.256 min.

G2-2g. **G2-2** (14.6 mg, 5.0 μmol) was dissolved in 1 mL distilled water. 1H-pyrazole-1-carboxamidinium•HCl (0.09 g, 590 μmol) and DIPEA (0.21 mL, 1.21 mmol) were mixed in 1mL acetonitrile. When the acetonitrile solution became clear, the distilled water solution was added, and the mixture was stirred at room temperature. After five days the solvents were removed and the mixture was redissolved in diionized water. Excess starting material was removed from the solution using an Amicon apparatus and a millipore membrane with NMWL = 1,000 under 35 psi N₂. The solution remaining inside the Amicon vessel was dried *in vacuo* to afford **G2-2g** (12.7 mg, 74%). MS (MALDI): calcd 3446.21 (M⁺); found 3447.12 (M + H⁺).

Protected G2-3 (P-G2-3). MCT3 (0.30 g, 0.65 mmol) and G1-C (0.12 g, 0.11 mmol) were each dissolved in 3 mL 9:1 CH₂Cl₂:CH₃OH. The monochlorotriazine solution was

added to the **G1-C** solution followed by the addition of DIPEA (0.34 mL, 1.95 mmol). The reaction mixture was heated to 70 °C. After 4 days the reaction mixture was dried under reduced pressure, dissolved in dichloromethane, and washed with distilled water. The organic layer was dried and purified by column chromatography using 4:1 CH₂Cl₂:ethyl acetate with 7% CH₃OH to afford **P-G2-3** (0.18 g, 47%). ¹H NMR (300 MHz, CDCl₃) δ: 5.39 (br, 12H, NH), 3.82 (br, 24 + 12 + 72H, NCH₂CH₂OH, NHCH₂, piperazine), 3.57 (s, 36H, OCH₂CH₂O, NCH₂) 3.53 (t, 24H, OCH₂CH₂NHBoc), 3.31 (q, 12H, OCH₂CH₂NHBoc), 1.88 (br, 12H, OH), 1.43 (s, 54H, C(CH₃)₃). ¹³C NMR (300 MHz, CDCl₃) δ: 167.2 (C₃N₃), 165.5 (C₃N₃), 164.6 (C₃N₃), 156.7 (CO), 79.4 (OC(CH₃)₃), 70.5 (CH₂OCH₂CH₂OCH₂), 70.1 (OCH₂CH₂O), 63.1 (CH₂OH), 51.6 (NCH₂CH₂OH), 43.4 (piperazine), 40.6 (NHCH₂, CH₂NHBoc), 28.6 (C(CH₃)₃). MS (MALDI): calcd 3644.13 (M⁺); found 3645.86 (M + H⁺).

G2-3. **P-G2-3** (0.18 g, 0.05 mmol) was dissolved in 3M HCl:CH₃OH (10 mL). After 5 days the solvent was evaporated under reduced pressure and the product was re-dissolved in distilled water and neutralized with NaCO₃ to pH=7. NaCl byproduct was removed from the solution using an Amicon apparatus and a millipore membrane with NMWL = 1,000 under 35 psi N₂. The solution remaining inside the Amicon vessel was dried *in vacuo* to afford **G2-3** (0.12 g, 77%). MS (MALDI): calcd 3043.82 (M⁺); found 3044.37 (M + H⁺). HPLC (2:1 H₂O with 0.14% TFA:acetonitrile): 3.345 min.

G2-3g. **G2-3** (19.3 mg, 6.3 μmol) was dissolved in 1 mL distilled water. 1*H*-pyrazole-1-carboxamidinium•HCl (0.06 g, 380 μmol) and DIPEA (0.13 mL, 750 μmol) were mixed in 1mL acetonitrile. When the acetonitrile solution became clear, the distilled water solution was added and the mixture was stirred at room temperature. After five days the solvents were removed and the mixture was re-dissolved in diionized water. Excess starting material was removed from the solution using an Amicon apparatus and a millipore membrane with NMWL = 1,000 under 35 psi N₂. The solution remaining inside the Amicon vessel was condensed *in vacuo* to afford **G2-3g** (18.3mg, 88%). MS (MALDI): calcd 3295.95 (M⁺); found 2396.51 (M + H⁺).

Protected G2-4 (P-G2-4). **MCT4** (0.15 g, 0.32 mmol) and **G1-C** (0.06 g, 0.05 mmol) were each dissolved in 3 mL 9:1 CH₂Cl₂:CH₃OH. The monochlorotriazine solution was added to the **G1-C** solution at room temperature followed by the addition of DIPEA (0.16 mL, 0.92 mmol). The reaction was heated to 70 °C. After 4 days the reaction mixture was dried *in vacuo*, dissolved in dichloromethane, and washed with distilled water. The organic layer was dried to afford **P-G2-4** (0.18 g, 93%). ¹H NMR (300 MHz, CDCl₃) δ: 5.39 (br,

18H, NH), 3.80 (br, 72H, piperazine), 3.71 (br, 12, OCH₂CH₂OH), 3.61 (br, 96H, CH₂), 3.31 (br, 12H, CH₂NHBoc), 1.43 (s, 54H, C(CH₃)₃). ¹³C NMR (300 MHz, CDCl₃) δ: 166.2 (C₃N₃), 165.6 (C₃N₃), 165.2 (C₃N₃), 156.3 (CO), 79.3 (OC(CH₃)₃), 72.7 (CH₂OCH₂CH₂OCH₂), 70.4 (OCH₂CH₂O), 61.7 (CH₂OH), 43.3 (piperazine), 40.6 (NHCH₂, CH₂NHBoc), 28.6 (C(CH₃)₃). MS (MALDI): calcd 3644.13 (M⁺); found 3645.49 (M + H⁺).

G2-4. P-G2-4 (0.16 g, 0.04 mmol) was dissolved in 3M HCl:CH₃OH. After 5 days the solvent was evaporated under reduced pressure and the product re-dissolved in distilled water and neutralized with NaCO₃ to pH=7. NaCl byproduct was removed from the solution using an Amicon apparatus and a millipore membrane with NMWL = 1,000 under 35 psi N₂. The solution remaining inside the Amicon vessel was condensed *in vacuo* to afford **G2-4** (0.05 g, 40%). MS (MALDI): calcd 3043.82 (M⁺); found 3043.62 (M + H⁺).

Protected G2-5 (P-G2-5). **MCT5** (0.36 g, 0.67 mmol) and **G1-C** (0.06 g, 0.06 mmol) were each dissolved in 5 mL of 10:1 CH₂Cl₂:CH₃OH. The monochlorotriazine solution was added to the **G1-C** solution at room temperature followed by the addition of DIPEA (0.25 mL, 1.44 mmol). The reaction was heated to 70 °C. After 5 days the reaction mixture was dried *in vacuo*, dissolved in dichloromethane, and washed three times with distilled water. The organic layer was dried to afford **P-G2-5** (0.20 g, 86%). ¹H NMR (300 MHz, CDCl₃) δ: 5.25 (br, 5H, NH), 4.91 (br, 8H, NH), 3.82 (s, 72H, piperazine), 3.58 (br, 24H, NCH₂), 3.39 (q, 12H, NHCH₂), 3.08 (br, 24H, CH₂NHBoc), 1.77 (br, 24H, CH₂CH₂CH₂), 1.59 (p, 12H, NHCH₂CH₂), 1.44 (s, 108H, C(CH₃)₃), 1.32 (br, 36H, CH₂), 0.89 (t, 18H, CH₃). ¹³C NMR (300 MHz, CDCl₃) δ: 165.6 (C₃N₃), 165.5 (C₃N₃), 165.3 (C₃N₃), 156.2 (CO), 79.2 (OC(CH₃)₃), 43.3 (NCH₂CH₂CH₂, NHCH₂, piperazine), 41.0 (NHCH₂CH₂), 31.8 (CH₂CH₂CH₃), 30.1 (CH₂), 28.7 (C(CH₃)₃, CH₂CH₂CH₂), 26.8 (NHCH₂CH₂CH₂), 22.8 (CH₂CH₃), 14.3 (CH₃). MS (MALDI): calcd 4118.82 (M⁺); found 4121.46 (M + H⁺).

G2-5. P-G2-5 (0.18 g, 0.04 mmol) was dissolved in 5 mL CH₃OH. Concentrated HCl (5 mL) was added to the methanol solution. After 18 hours the reaction mixture was condensed *in vacuo* and neutralized with 5 M NaOH. At basic pH, product precipitated to yield **G2-5** (0.12 g, 98%). MS (MALDI): calcd 2918.19 (M⁺); found 2919.32 (M + H⁺).

Cell Culture. L929 and MeWo cells were purchased from LG Promochem, Wesel, Germany, and were maintained in Dulbecco's Modified Eagle Medium (DMEM) at low or high glucose (PAA Laboratories, Cölbe, Germany), respectively, supplemented with 10%

fetal calf serum (Cytogen, Sinn, Germany) in humidified atmosphere with 5% CO₂ at 37 °C.

Preparation of dendriplexes. Dendriplexes were formed by adding a solution of calculated concentration of dendrimer to an equal volume of DNA solution (pCMV-Luc, Plasmid Factory, Bielefeld, Germany). The two components were mixed and left for 20 minutes to allow for complex formation. Both pDNA and dendrimer dilutions were prepared in 10 mM HEPES buffer, pH 7.4, and the amount of dendrimer needed to afford a certain N/P ratio was calculated by considering the “protonable unit” of each dendrimer which represents the mass of dendrimer per protonable nitrogen atom. For comparison, bulk polyethylenimine (Polymin, 25 kDa), a gift from BASF (Ludwigshafen, Germany), was used .

Ethidium bromide quenching assay. In order to investigate condensation efficiency of the dendrimers, 4 µg of herring testes DNA (Sigma-Aldrich Chemie GmbH, Schnellendorf, Germany) were mixed with increasing amounts of dendrimers in a final volume of 280 µL 10 mM HEPES buffer and pipetted into opaque FluoroNunc™ 96 well plates (Nunc, Thermo Fisher Scientific, Langenselbold, Germany).. After incubation for 20 minutes at room temperature, 20 µL of a 0.1 mg/mL ethidium bromide solution (Carl Roth GmbH, Karlsruhe, Germany) were added to each well and briefly incubated in the dark under constant shaking. Intercalation-induced fluorescence was quantified using a fluorescence plate reader (LS 50 B, Perkin-Elmer, Rodgau-Jügesheim, Germany) at 518 nm excitation and 605 nm emission wavelengths. Results are given as mean relative fluorescence intensity values with intercalation of free DNA representing 100% fluorescence and non-intercalating ethidium bromide in buffer representing 0% remaining fluorescence. Results are given as means of triplicate measurements +/- standard deviation (SD).

Dynamic light scattering and zeta potential analysis. For measurements of size and zeta potential by dynamic light scattering (DLS) and laser Doppler anemometry (LDA), respectively, dendriplexes of 0.6 µg pCMV-Luc and the according amount of dendrimer were formed as described above. Complexes were incubated for 20 minutes and diluted to a total volume of 800 µL with 10 mM HEPES buffer, pH 7.4, to be measured into a folded capillary cell (Malvern Instruments, Herrenberg, Germany) using a Zetasizer Nano ZS,

Malvern, Herrenberg, Germany. Measurements were conducted in triplicates in the “General Purpose” mode, where position and attenuator were optimized by the device..

MTT assay. The influence of dendrimers on metabolic cell activity was investigated using the MTT assay. For this proliferation assay, murine L929 fibroblasts were seeded on 96-well plates (Nunc, Wiesbaden, Germany) at a density of 8000 cells per well 24 hours before they were treated with dendrimer solutions of increasing concentrations in the range of 0.001 to 1 mg/mL. After another 24 hours, the medium was changed, and the MTT solution was added into fresh serum-free medium and incubated for 4 hours. Cells were lysed with 200 μ L DMSO per well, and remaining mitochondrial enzyme activity compared to untreated cells was determined by measuring the absorbance of enzymatically formed formazan at 580 nm with 690 nm background correction.

Transfection experiments. Human melanoma cells (MeWo) were seeded in 96-well plates (Nunc, Wiesbaden, Germany) at a seeding density of 8000 cells per well. Twenty four hours later, cells were transfected with dendriplexes made of 0.25 μ g pCMV-Luc per well and the according amount of dendrimer calculated to be N/P ratios of 2.5, 5, or 7.5. Branched 25 kDa PEI was used as a positive and free plasmid as a negative control. Dendriplexes were added to full serum-containing medium and cells were incubated for 4 hours before medium was changed. After additional 44 hours, cells were washed with PBS, lysed with Cell Culture Lysis Reagent, CCLR (Promega, Mannheim, Germany), and assayed for luciferase expression with a commercial luciferase assay kit (Promega, Mannheim, Germany) on a LUMIstar OPTIMA plate luminometer (BMG Labtech, Offenburg, Germany).

3.6 Acknowledgements

We thank Eva Mohr and Sandra Engel (DPB, Marburg, Germany) for their support in the cell culture lab. EES acknowledges support of the NIH (NIGMS R01 45640). MM acknowledges a predoctoral fellowship from NSF (GK12-DGE 0538547).

3.7 Notes and references

- (1) Mintzer, M. A., and Simanek, E. E. (2009) Nonviral vectors for gene delivery. *Chem Rev* 109, 259-302.

- (2) Merdan, T., Kopecek, J., and Kissel, T. (2002) Prospects for cationic polymers in gene and oligonucleotide therapy against cancer. *Adv Drug Deliv Rev* 54, 715-58.
- (3) Niidome, T., and Katayama, Y. (2005) Use of Synthetic Peptides for Non-viral Gene Delivery, in *Non-viral Gene Therapy* (Taira, K., Ed.), Springer, Berlin.
- (4) Li, W., and Szoka, F. C., Jr. (2007) Lipid-based nanoparticles for nucleic acid delivery. *Pharm Res* 24, 438-49.
- (5) Guillot-Nieckowski, M., Joester, D., Stohr, M., Losson, M., Adrian, M., Wagner, B., Kansy, M., Heinzlmann, H., Pugin, R., Diederich, F., and Gallani, J. L. (2007) Self-assembly, DNA complexation, and pH response of amphiphilic dendrimers for gene transfection. *Langmuir* 23, 737-46.
- (6) Behr, J. P. (2002) Synthetic gene-transfer vectors. *Accounts of Chemical Research* 26, 274-278.
- (7) Haensler, J., and Szoka, F. C., Jr. (1993) Polyamidoamine cascade polymers mediate efficient transfection of cells in culture. *Bioconjug Chem* 4, 372-9.
- (8) Zinselmeyer, B. H., Mackay, S. P., Schatzlein, A. G., and Uchegbu, I. F. (2002) The lower-generation polypropylenimine dendrimers are effective gene-transfer agents. *Pharm Res* 19, 960-7.
- (9) Shah, D. S., Sakthivel, T., Toth, I., Florence, A. T., and Wilderspin, A. F. (2000) DNA transfection and transfected cell viability using amphipathic asymmetric dendrimers. *Int J Pharm* 208, 41-8.
- (10) Loup, C., Zanta, M.-A., Caminade, A.-M., Majoral, J.-P., and Meunier, B. (1999) Preparation of Water-Soluble Cationic Phosphorus-Containing Dendrimers as DNA Transfecting Agents. *Chemistry - A European Journal* 5, 3644-3650.
- (11) Weber, N., Ortega, P., Clemente, M. I., Shcharbin, D., Bryszewska, M., de la Mata, F. J., Gómez, R., and Muñoz-Fernández, M. A. (2008) Characterization of carbosilane dendrimers as effective carriers of siRNA to HIV-infected lymphocytes. *Journal of Controlled Release* 132, 55-64.
- (12) Neerman, M. F., Zhang, W., Parrish, A. R., and Simanek, E. E. (2004) In vitro and in vivo evaluation of a melamine dendrimer as a vehicle for drug delivery. *Int J Pharm* 281, 129-32.
- (13) Steffensen, M. B., and Simanek, E. E. (2004) Synthesis and manipulation of orthogonally protected dendrimers: building blocks for library synthesis. *Angew Chem Int Ed Engl* 43, 5178-80.

-
- (14) Chouai, A., and Simanek, E. E. (2008) Kilogram-scale synthesis of a second-generation dendrimer based on 1,3,5-triazine using green and industrially compatible methods with a single chromatographic step. *J Org Chem* 73, 2357-66.
- (15) Gajbhiye, V., Kumar, P. V., Tekade, R. K., and Jain, N. K. (2007) Pharmaceutical and Biomedical Potential of PEGylated Dendrimers *Current Pharmaceutical Design* 13, 415-429.
- (16) Lee, J. H., Lim, Y.-b., Choi, J. S., Lee, Y., Kim, T.-i., Kim, H. J., Yoon, J. K., Kim, K., and Park, J.-s. (2003) Polyplexes Assembled with Internally Quaternized PAMAM-OH Dendrimer and Plasmid DNA Have a Neutral Surface and Gene Delivery Potency. *Bioconjugate Chemistry* 14, 1214-1221.
- (17) Toth, I., Sakthivel, T., Wilderspin, A. F., H.Bayeley, O'Donnell, M., Perry, D. J., Pasi, K. J., Lee, C. A., and Florence, A. T. (1999) Novel cationic lipidic peptide dendrimer vectors In vitro gene delivery *STP Pharma Sciences* 9, 93.
- (18) Choi, J. S., Nam, K., Park, J. Y., Kim, J. B., Lee, J. K., and Park, J. S. (2004) Enhanced transfection efficiency of PAMAM dendrimer by surface modification with L-arginine. *J Control Release* 99, 445-56.
- (19) Kim, T. I., Baek, J. U., Zhe Bai, C., and Park, J. S. (2007) Arginine-conjugated polypropylenimine dendrimer as a non-toxic and efficient gene delivery carrier. *Biomaterials* 28, 2061-7.
- (20) Okuda, T., Sugiyama, A., Niidome, T., and Aoyagi, H. (2004) Characters of dendritic poly(L-lysine) analogues with the terminal lysines replaced with arginines and histidines as gene carriers in vitro. *Biomaterials* 25, 537-44.
- (21) Kono, K., Akiyama, H., Takahashi, T., Takagishi, T., and Harada, A. (2005) Transfection activity of polyamidoamine dendrimers having hydrophobic amino acid residues in the periphery. *Bioconjug Chem* 16, 208-14.
- (22) Chen, H. T., Neerman, M. F., Parrish, A. R., and Simanek, E. E. (2004) Cytotoxicity, hemolysis, and acute in vivo toxicity of dendrimers based on melamine, candidate vehicles for drug delivery. *J Am Chem Soc* 126, 10044-8.
- (23) Aissaoui, A., Oudrhiri, N., Petit, L., Hauchecorne, M., Kan, E., Sainlos, M., Julia, S., Navarro, J., Vigneron, J. P., Lehn, J. M., and Lehn, P. (2002) Progress in gene delivery by cationic lipids: guanidinium-cholesterol-based systems as an example. *Curr Drug Targets* 3, 1-16.
- (24) Mahato, R. I., Rolland, A., and Tomlinson, E. (1997) Cationic lipid-based gene delivery systems: pharmaceutical perspectives. *Pharm Res* 14, 853-9.

- (25) Prabha, S., Zhou, W. Z., Panyam, J., and Labhasetwar, V. (2002) Size-dependency of nanoparticle-mediated gene transfection: studies with fractionated nanoparticles. *Int J Pharm* 244, 105-15.
- (26) Xu, D. M., Yao, S. D., Liu, Y. B., Sheng, K. L., Hong, J., Gong, P. J., and Dong, L. (2007) Size-dependent properties of M-PEIs nanogels for gene delivery in cancer cells. *Int J Pharm* 338, 291-6.

4 Triazine dendrimers as non-viral gene delivery systems: Effects of molecular structure on biological activity

Bioconjugate Chemistry (2009), *doi: 10.1021/bc900243r*

4.1 Abstract

A family of generation one, two and three triazine dendrimers differing in their core flexibility was prepared and evaluated for their ability to accomplish gene transfection. Dendrimers and dendriplexes were analyzed concerning their physicochemical and biological properties such as condensation of DNA, size, surface charge, morphology of dendriplexes, toxic and hemolytic effects and ultimately transfection efficiency in L929 and MeWo cells. Flexibility of the backbone was found to play an important role with generation 2 dendrimer displaying higher transfection efficiencies than poly(ethylene imine) 25 kDa or SuperFect™ with lower cytotoxicity. This result is surprising as PAMAM dendrimers require generations 4 or 5 to become effective transfection reagents. The ability to delineate effects of molecular structure and generation of triazine dendrimers with biological properties yields valuable information for further modifying this promising class of non-viral delivery systems.

4.2 Introduction

Gene therapy has gained importance in recent years due to its potential for targeting genetic diseases and inhibiting tumor growth. However, clinical application is limited by numerous biological barriers to delivering plasmid DNA (1). Both viral and non-viral vector systems have been developed to overcome these hurdles. Viral delivery systems, which include retroviruses, lentiviruses, and adenoviruses, have encountered potential safety problems such as recombination, insertional mutagenesis, and immunogenicity as well as scale-up difficulties (2). Therefore, synthesis and evaluation of non-viral vector systems becomes increasingly important in spite of their comparatively lower transfection efficiency (3).

Non-viral vectors such as cationic liposomes, linear and branched polycations and dendrimers have been shown to be effective transfection agents and offer advantages over viral vectors regarding safety and manufacturing. Several non-viral gene delivery systems based on poly(amidoamine) (PAMAM) (4-6), poly(propylene imine) (PPI) (7, 8), and poly(ethylene imine) (PEI) (9, 10) have yielded efficient transfection *in vivo* with relatively low toxicity. The potential of triazine dendrimers as gene delivery systems is largely unexplored, but has been described by us in a study involving generation 2 rigid structures (11), which reveal an optimized peripheral group for further study. These dendrimers may be attractive candidates as they can be synthesized in high yields via a divergent strategy

that creates multiple surface functionalities in a completely monodisperse manner (12). In addition, triazine dendrimers show low toxicity, both in vitro and in vivo: mice tolerate i.p. doses up to 40 mg/kg (13). This level of toxicity is comparable to PAMAM (14) suggesting that triazine dendrimers could be considered as a platform for transfection studies. Here, the physicochemical properties, cytotoxicities and transfection efficiencies of a panel of triazine dendrimers were evaluated to establish structure function relationships. The effect of dendrimer size (generations) as well as core structure is probed in an attempt to maximize transfection efficiency. Increasing generation increases size and the number of available cations. Changing the composition of the core affords dendrimers that differ in the flexibility, a characteristic that is thought to influence interactions with p-DNA (6). The dendrimers used in this study are shown in Figure 1. Here we present results from the synthesis, physicochemical and biological in vitro evaluation of a panel of 5 triazine dendrimers and compare them to commercially available PAMAM dendrimers of different generations to define structural parameters such as generation and core flexibility for the design of triazine dendrimers as non-viral gene delivery systems.

4.3 Materials and Methods

Materials

Poly(ethylene imine) (Polymin™, 25 kDa) was a gift from BASF (Ludwigshafen, Germany), PAMAM (ethylenediamine core, amino surface) 2nd and 3rd generation was bought from Sigma-Aldrich Laborchemikalien GmbH, Seelze, Germany, and SuperFect™ from Qiagen, Hilden, Germany. All chemicals used for synthesis were obtained from Sigma-Aldrich (St. Louis, MO).

Synthesis

The synthesis of all dendrimers used in this study proceeded via a divergent strategy originating from cyanuric chloride. The rigid, first generation dendrimer was synthesized by reacting a tris(piperazyl) triazine core with **MCT1**, followed by deprotection. The rigid, second generation dendrimer, **G2-1**, was synthesized as previously described (11). To form the third generation rigid dendrimer, **G3-1**, the rigid, deprotected G1-dendrimer, **G1-C** was reacted with di(Boc-piperazyl)monochlorotriazine. This second generation structure was deprotected and reacted with **MCT1** to form the protected third generation compound,

which was deprotected using HCl (Supplementary Materials). A detailed description of the synthesis is provided in the supplementary material section.

The flexible core dendrimer, **F2-1**, was synthesized by reacting cyanuric chloride with mono-Boc-protected *O,O'*-bis(3-aminopropyl)diethylene glycol. This core was deprotected with HCl, reacted with Boc-piperazyl-dichlorotriazine, and capped with Boc-piperazine. After removal of the protecting groups with HCl, the compounds were reacted with **MCT1** and deprotected to form the flexible, second generation dendrimer, **F2-1** (Supplementary Materials). A detailed description of the synthesis is provided in the supplementary material section.

Finally, the second generation bow-tie structure, **B2-1**, was synthesized by reacting di(Boc-piperazyl)monochlorotriazine with *O,O'*-bis(3-aminopropyl)diethylene glycol. This core structure was deprotected with HCl and reacted with di(Boc-piperazyl)monochlorotriazine to form a first generation bow-tie structure. This structure was deprotected, reacted with **MCT1**, and deprotected again to afford the dendrimer **B2-1** (Supplementary Materials). A detailed description of the synthesis is provided in the supplementary material section.

Cell Culture: L929 murine fibroblasts and MeWo human melanoma cells were purchased from LG Promochem, Wesel, Germany, and maintained in DMEM low or high glucose (PAA Laboratories, Cölbe, Germany), respectively, and supplemented with 10% fetal calf serum (Cytogen, Sinn, Germany) in humidified atmosphere with 5% CO₂ at 37°C.

Preparation of Dendriplexes

Dendriplexes were formed by adding 25 µl of a calculated concentration (depending on “protonable unit” and N/P ratio) of dendrimer to an equal volume of the DNA solution (pCMV-Luc, Plasmid Factory, Bielefeld, Germany) and then mixing the two components before letting them mature for 20 minutes. The final concentration of pDNA in the dendriplex solution was 0.02 µg/µl. Both pDNA and dendrimers were diluted with 10 mM HEPES buffer, pH 7.4, and the appropriate amount of dendrimer was calculated by considering the desired N/P ratio and the “protonable unit” of each dendrimer, which represents the mass of dendrimer per protonable nitrogen atom. For comparison, standard transfection reagents, including poly(ethylene imine) (PEI 25 kDa), second and third generation PAMAM (ethylenediamine core, amino surface), and SuperFect (Qiagen, Hilden, Germany) were used. Polyplexes with PEI 25 kDa and dendriplexes with

PAMAMs of 2nd and 3rd generation were formed as described above, whereas dendriplexes with SuperFect were prepared as recommended by the manufacturer.

Ethidium Bromide Quenching Assay

To quantify condensation efficiency of the dendrimers, an indirect dye-quenching assay was performed as previously reported (15). Briefly, 4 µg of herring testes DNA (Sigma-Aldrich Chemie GmbH, Schnelldorf, Germany) was complexed with increasing amounts of dendrimer in a final volume of 280 µl 10 mM HEPES buffer. After incubation for 20 minutes at room temperature, 20 µl of a 0.1 mg/ml ethidium bromide solution (Carl Roth GmbH, Karlsruhe, Germany) was added and incubated for 10 minutes in the dark following intensive mixing. Intercalation-caused fluorescence was quantified using a fluorescence plate reader (LS 50 B, Perkin-Elmer, Rodgau-Jügesheim, Germany) at 518 nm excitation and 605 nm emission wavelengths. Results are given as relative fluorescence intensity values where intercalation of free DNA represents 100% fluorescence and non-intercalating ethidium bromide in buffer represents 0% remaining fluorescence. Results are given as means of triplicate measurements ± standard deviation (SD).

Dynamic Light Scattering and Zeta Potential Analysis

Polyplex size and zeta potential were determined as previously reported (15). Briefly, dendriplexes of 0.6 µg pCMV-Luc and the corresponding amount of dendrimer were prepared as described above. Complexes were incubated for 20 minutes and then diluted to a total volume of 800 µl with 10 mM HEPES buffer, pH 7.4, to be measured using a Zetasizer Nano ZS, Malvern, Herrenberg, Germany. Position and attenuator were optimized by the device. The accuracy of the size measurements was routinely checked using reference polymer particles (Nanosphere Size Standards, 50, 100 and 200 nm, Duke Scientific Corp., Palo Alto, CA, USA), and the zeta potential values were calibrated with the Zeta Potential Transfer Standard (Malvern Instruments, Herrenberg, Germany). The data was analyzed using a High Resolution Multimodal algorithm. All measurements were conducted in triplicates. For better characterization of the size distributions, in addition to Z Average, the PDI of the distribution is given as the mean value of three independent measurements ± SD.

Atomic Force Microscopy

The size and morphology of dried dendriplexes were analyzed by atomic force microscopy as previously described for polyplexes (16). Briefly, dendriplexes were prepared by mixing 1 µg pCMV-Luc and a dendrimer at an N/P ratio of 5 as described above, incubating for 20 minutes, and drying on silicon chips. Microscopy was performed on a NanoWizard (JPK instruments, Berlin, Germany). Commercial NSC16 AIBS-tips (Micromasch, Estonia) on an I-type cantilever with a length of 230 µm and a nominal force constant of 40 N/m were used. All measurements were performed in tapping mode to avoid damage to the sample surface. The scan frequency was 0.6 Hz and scan size was 5x5 µm. Multiple images were recorded, of which one representative topograph is presented.

Erythrocyte Aggregation and Hemolysis

Unspecific cell interaction was visualized by erythrocyte aggregation and quantified by the measurement of hemolysis according to previously described procedures (17). Briefly, human erythrocytes were isolated from fresh citrated blood from healthy volunteers by centrifugation, washed with PBS buffer, and diluted to 500.000.000 cells/ml. Dendriplexes of 0.1 µg pDNA per ml were prepared at N/P 5, and 50 µl aliquots of dendriplex solutions, 1 % Triton-X 100 (100 % lysis) or PBS (0 % lysis) were mixed with 50 µl erythrocyte suspension. After incubation for 30 minutes at 37 °C, samples were centrifuged at 850 g. Hemolysis was measured by VIS-absorption of supernatants at 541 nm and the data is given as a mean percentage (n = 3) of the released hemoglobin ± SD, normalized to total hemolysis induced by 1% Triton-X 100. Pelleted erythrocytes were resuspended in 50 µl PBS and microscopically examined to determine erythrocyte aggregation.

Cell viability

The cytotoxicity of the dendrimers was investigated using an MTT assay (15). Murine L929 fibroblasts were seeded on 96-well plates at a density of 8000 cells per well approximately 24 hours before they were treated with dendrimer solutions of increasing concentrations in the range of 0.001 to 1 mg/ml. Another 24 hrs later, the medium was changed. MTT solution was added into fresh serum-free medium and incubated for 4 hours. The remaining mitochondrial enzyme activity as compared to untreated cells was determined by measuring the absorbance of enzymatically-formed formazane at 580 nm with 690 nm background corrections after cell lysis in 200 µl DMSO. The results are given as mean values of a replicate of 4 ± SD.

Transfection Experiments

To compare transfection efficiency in different cell lines, murine 3T3 fibroblasts (L929) and human melanoma cells (MeWo) were seeded in 96-well plates at a seeding density of 8000 cells per well. Approximately 24 hours later, the cells were transfected with dendriplexes consisting of 0.25 μ g pCMV-Luc per well and the amount of dendrimer calculated to be N/P 2.5, 5 or 7.5. Branched PEI of 25 kDa, second and third generation PAMAM, and 4th generation SuperFect were used as standards and free plasmid was used as a negative control.

Polyplexes were added to full serum-containing medium, and cells were incubated for 4 hours before the medium was changed. Another 44 hours later, the cells were washed with PBS, lysed with CCLR (Promega, Mannheim, Germany), and assayed for luciferase expression using a commercial luciferase assay kit (Promega, Mannheim, Germany) on a BMG LUMIstar OPTIMA luminometer plate reader (BMG Labtech, Offenburg, Germany). Transfection assays were performed in triplicates and the mean values \pm SD are given.

4.4 Results and Discussion

Nomenclature adopted. Throughout the manuscript, the targets are named to reflect common and disparate features in structure with the core/generation-surface groups identified. The cores increase in flexibility from **G** (standard) to **B** (bowtie) to **F** (flexible), and the effect of size is determined over three (**1**, **2**, **3**) generations using the standard core structure. Each dendrimer contains a common surface group (**1**) that was previously reported to avoid obtaining variations in transfection efficiency that result from the peripheral functionalities (*11*).

Synthesis and design criteria

As the products of multistep organic syntheses, triazine dendrimers allow us access to well-defined structures to investigate structure-activity relationships such as the influence of size and backbone structure on transfection efficiency and cytotoxicity. For this purpose, a preliminary panel of dendrimers was synthesized consisting of different generations (**G1**, **G2**, **G3**) with a rigid backbone and a common surface group (**1**), yielding 6, 12 or 24 amino-groups in the periphery. With each increase in generation number, the number of primary amino groups presented in the periphery doubles.

In addition to generation number, the flexibility of the core could hypothetically affect transfection efficiency by influencing the distribution and accessibility of the peripheral groups for interacting with p-DNA (18). The role of flexibility has been supported experimentally by Szoka who showed enhanced transfection efficiency resulting from fragmentation of PAMAM dendrimers (6). In this study, this effect was investigated with second generation triazine dendrimers, each having differing core flexibilities (**G2-1**, **F2-1**, **B2-1**). Synthetic yields and NMR data are provided within the Supporting Information.

The composition of the panel is summarized in Figure 1 and Table 1. Branched poly(ethylene imine) of 25 kDa (PEI 25kDa) was used as a control. The transfection efficiencies of the triazine dendriplexes were additionally compared to SuperFect™, a commercially available 4th generation fractured PAMAM dendrimer and to second and third generation PAMAM as dendrimer standards.

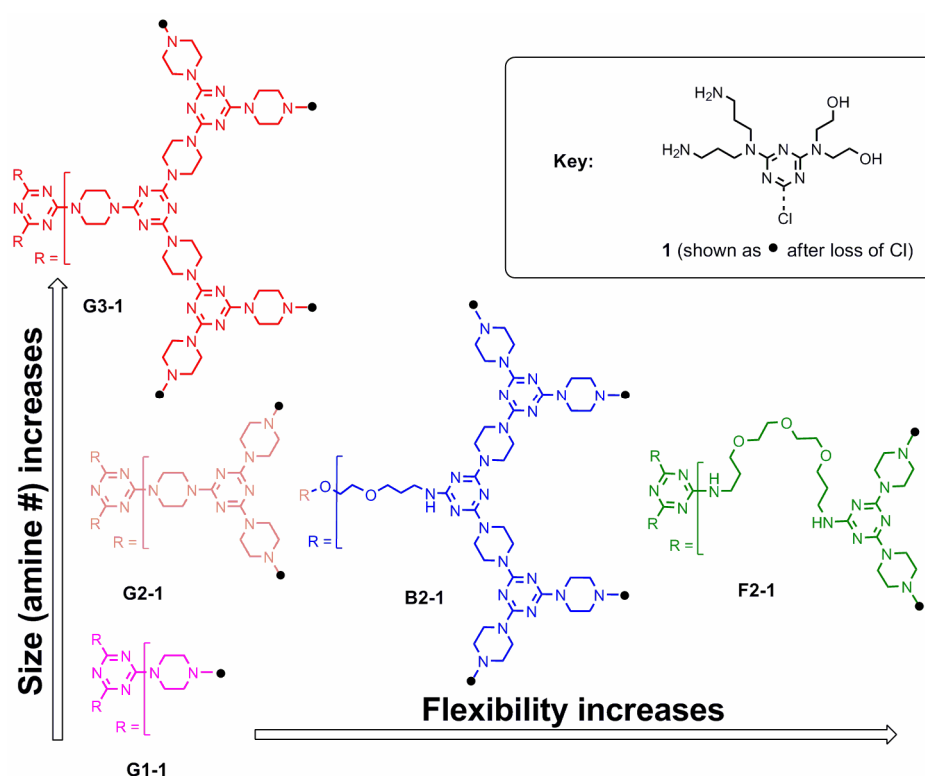


Figure 1. The dendrimer panel is given as chemical structures and sketches in a color code used throughout the study. Structure activity relationships of the dendrimers in Table 1 were investigated in a two-dimensional approach: By variation of the generation (vertical arrows) and the core structure (horizontal arrows), influence of both parameters were investigated.

Condensation properties of triazine dendrimers.

The formation of dendriplexes results from electrostatic interactions between polycationic dendrimers and negatively charged DNA. The quantification of condensation properties was performed using an ethidium bromide quenching assay (15) which reveals the fraction of uncomplexed DNA that is accessible for intercalation with ethidium bromide at a given N/P ratio. PAMAM dendrimers of generation 2 and 3 showed significant residual fluorescence leading to a plateau around N/P 7.5 (compare Figure 2). A similar trend was seen for several triazine dendrimers, including **G1-1**, **G2-1** and **F2-1**. The third generation triazine dendrimer, **G3-1**, yielded higher condensation than PEI, even at low N/P ratios. Interestingly, the bow-tie dendrimer **B2-1** showed better DNA condensation than PEI, with a condensation profile comparable to the third generation rigid dendrimer **G3-1**.

Similar to PAMAM, triazine dendrimers showed an increase in condensation efficiency with increasing generation. The first generation dendrimer **G1-1** condensed DNA less effectively than the second generation analogue, **G2-1**, which in turn was less efficient than the third generation dendrimer, **G3-1**. However, the effect of the core structure on condensation efficiency seems minimal. This may result from the type of amines present in the triazine core. The reason that more flexible dendrimers are thought to complex with DNA more effectively than rigid analogues has been attributed to the increased capacity of flexible dendrimers to interact with DNA, as all amine groups, both inside the core and at the surface, contributed to the electrostatic interactions for binding (19). This increased availability of internalized amines in flexible structures results in the formation of more compact complexes (7, 20, 21). However, in the case of triazine dendrimers, the nitrogen atoms in the core are part of a delocalized electron system and hence not available for protonation under physiologic conditions (pH 7.4). Therefore, only the primary amino functional groups at the dendrimer periphery contribute to DNA condensation due to their accessibility to protonation (22). As the peripheral groups are identical and the triazine core amines remain unprotonated at physiological pH, the trend of increased condensation efficiency for more flexible structures is not apparent; the semi-flexible bow-tie dendrimer **B2-1** more effectively condenses DNA than either the rigid **G2-1** or flexible **F2-1** analogs.

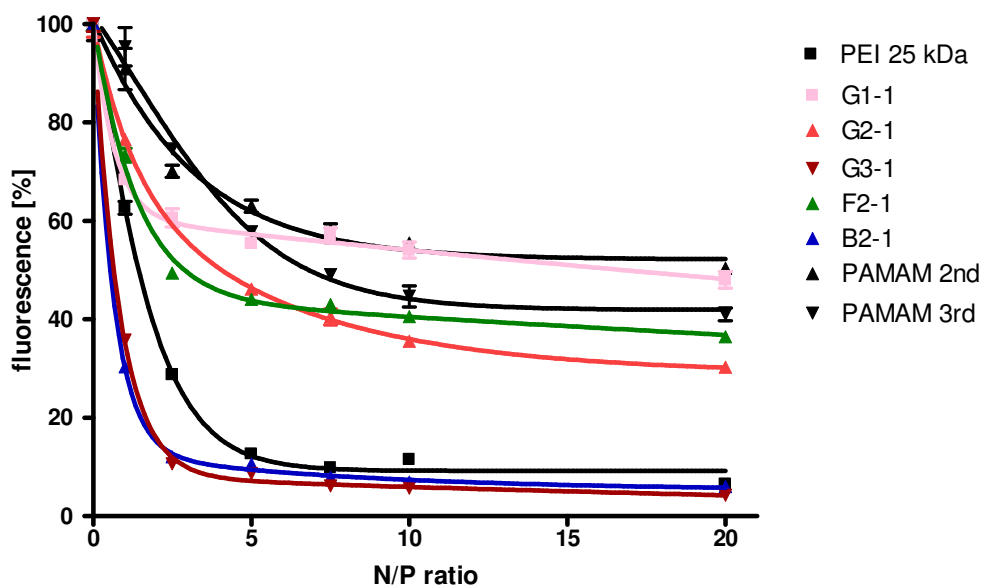


Figure 2. DNA condensation efficiency was quantified by ethidium bromide quenching assays and compared to PAMAMs of the same generations and PEI 25 kDa.

Dendriplex sizes and surface charges.

Polyplexes with diameters < 200 nm in size are internalized by most cell lines (23), while larger particles can sediment faster leading to enhanced transfection efficiency under *in vitro* conditions (24). A positive surface charge generally facilitates endocytosis, whereas negatively charged particles are often repelled by the negatively charged cell surface. Previous studies have shown that the complexation of DNA with PEI decreases polyplex sizes for increasing N/P ratios up to 20 (25). This trend could not be observed for the triazine dendrimers (data not shown). In the case of triazine dendriplexes, there seems to be an optimal N/P ratio at which minimal sizes can be achieved. When this N/P ratio is exceeded, larger dendriplexes (and possibly aggregates) form. By comparing rigid **G1-1**, **G2-1** and **G3-1** dendrimers (Figure 3 A), no clear trend between dendriplex sizes and the generation number emerges. Generally, dendrimers with a higher number of primary amines on the periphery tend to form smaller polyplexes with DNA, as shown for PAMAM in this study. This behavior is not observed for the rigid triazine dendrimers, **G2-1**, **G2-1**, and **G3-1**. Our findings indicated that the rigid second generation dendrimer, **G2-1**, forms the smallest complexes. This may be due to the “nitrogen density” (26) or “charge density” (27, 28), a parameter that is known to influence the interaction of polycations with pDNA. This parameter is defined as the density of protonable amines in the polycation per molecular weight and can also be called the “protonable unit”. The protonable unit can therefore be

measured in g/mol N and helps to characterize polycations. The charge density of PEI, where every third atom is a nitrogen atom, is 43.1 g/mol N (29), which is a comparably high charge density considering that the charge density in our triazine dendrimers is about 200 g/mol N: **G1-1** has a density of primary amines of 211.27 Da/N atom, **G2-1** has a density of 245.3 Da/N atom, and **G3-1** has a density of 262.2 Da/N atom. Therefore, **G2-1** may form smaller complexes as compared to **G3-1** because of the difference in charge density. However, despite the lower charge density of **G2-1**, **G2-2** formed smaller complexes, which can be explained by the twofold increase in primary amines per molecule. The formation of large dendriplexes using the flexible dendrimer, **F2-1** and the bow-tie dendrimer, **B2-1**, may result partially from the low charge densities of these dendrimers (**F2-1**: 262.32 Da/N atom; **B2-1**: 262.2 Da/N atom). These values may be too low for the formation of very small complexes. Additionally, the size of dendriplexes formed with the flexible dendrimer, **F2-1**, were much larger than those of **G2-1**, suggesting that loose structures were obtained, in accordance with data from ethidium bromide quenching assay. The bow-tie dendrimer **B2-1** formed the largest dendriplexes despite its DNA condensation efficiency, possibly caused by the formation of inter-dendriplex aggregates (7). The dendriplex size distributions were monomodal but showed polydispersity indices around 0.2 (Figure 3A) as reported previously for dendriplexes (30-32).

Zeta potentials of the PAMAM dendriplexes generally increased as particle size decreased. For example, the PAMAM 2nd generation dendrimer did not condense DNA efficiently as illustrated by a negative zeta potential and large complexes sizes. As the number of primary amines on the periphery (generation) increases, the PAMAM dendrimers condensed DNA more efficiently (Figure 2) due to their very high number of primary amines (PAMAM G4 = SuperFectTM: 64 surface amines) and charge density (PAMAM G4: 222.10 Da/N atom). The rigid triazine dendrimers (**G1-1**, **G2-1**, and **G3-1**) did not show a clear generation-dependent trend for surface charge. **G1-1** exhibited a zeta potential of -0.0513 mV. The zeta potential of **G2-1** dendriplexes, which had proven to form the smallest particles among the rigid dendrimers, was observed to be strongly positive. By further increasing the generation of the rigid dendrimer, not only sizes increased (Figure 3A), but also the zeta potential decreased (Figure 3B). Taken together, third generation dendrimers condense and protect DNA (Figure 2) efficiently, but may result in larger aggregates in solution. It is possible that, due to their rather low charge density at the same N/P ratio and molecular composition, **G3-1** dendrimers do not shield the negative charge of DNA effectively, which

results in lower electrostatic repulsion and stronger aggregation of dendriplexes. According to the data acquired in the ethidium bromide assay (Figure 2B), the flexible dendrimer **F2-1** only loosely bound DNA and was not able to fully protect the complex. Therefore, it seems reasonable to assume that the net negative charge measured for **F2-1** dendriplexes was caused by segments of free DNA which were not incorporated into any particle but were only bound to the surface of the flexible polycation. The dendriplexes formed with the bow-tie dendrimer **B2-1** exhibited a low but positive surface charge, which can again be explained by inter-dendriplex interaction.

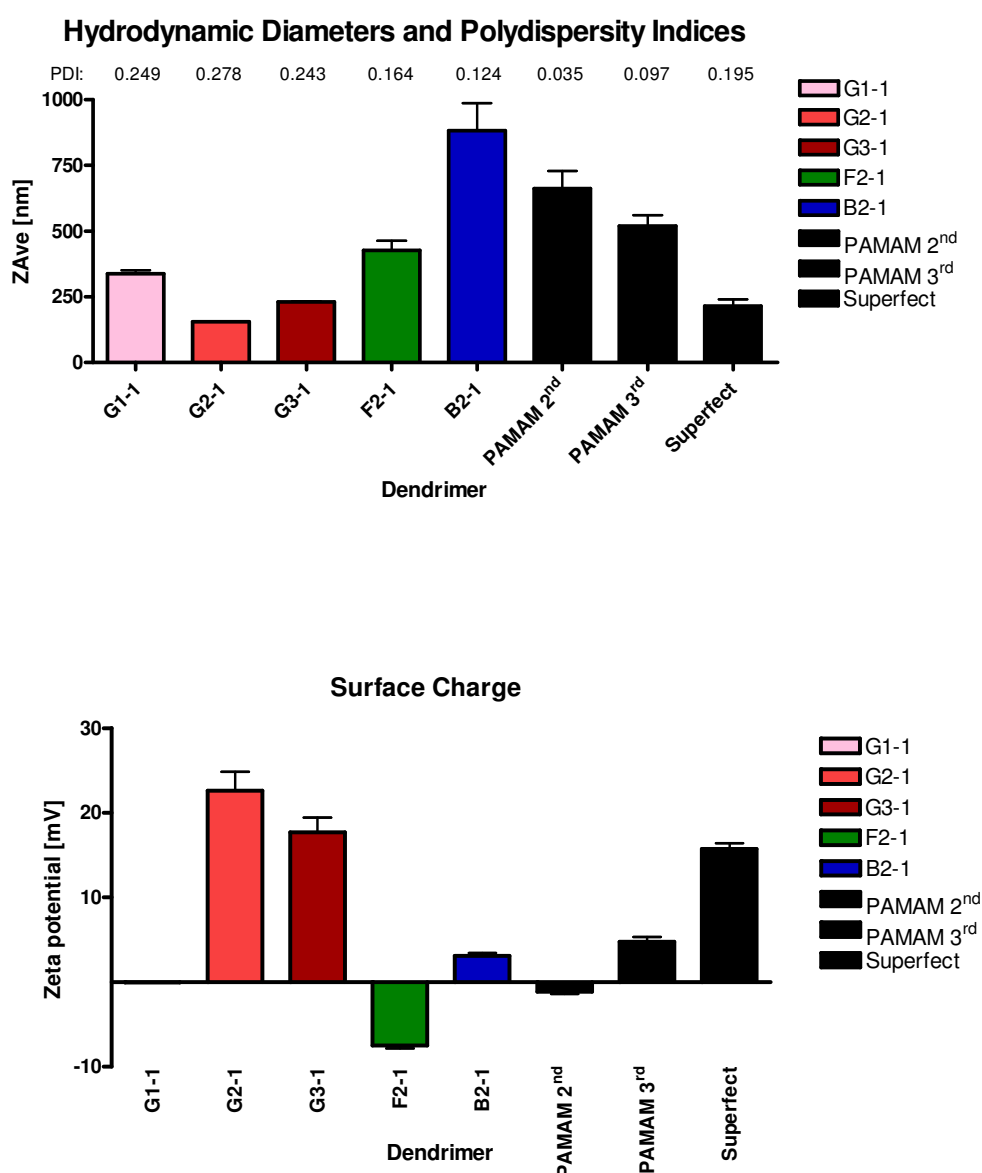


Figure 3. Hydrodynamic diameters (A) and zeta potentials (B) of various dendriplexes at an N/P of 5 were determined in 10 mM HEPES buffer, pH 7.4.

Atomic Force Microscopy.

Although dynamic light scattering is an effective method for measuring particle size, the method is limited because it assumes spherically shaped particles. Therefore atomic force microscopy (AFM) was used to characterize the morphology and heterogeneity of dendriplexes (33). The broad polydispersities observed with the dynamic light scattering experiments was also reflected in the AFM micrographs (Figure 4). The flexible core dendrimer **F2-1**, produced two populations or particles: very small complexes (<50 nm) as well as larger ones (>100 nm). The bow-tie dendrimer, **B2-1**, formed clusters of aggregates, which supports the assumption of inter-dendriplex interactions (7). The third generation dendrimer **G3-1** showed the most uniform distribution.

Both the formation of clusters and the discrepancy between size measurement of dried particles and complexes in solution are not surprising: Similar observations have been made for PAMAM dendriplexes (21). The sizes measured for **F2-1** and **G3-1** dendriplexes by DLS are confirmed by AFM. In AFM, a distribution of 20-100 nm (**F2-1**) and narrow size distribution of particles of 100 nm (**G3-1**) could be observed. The larger sizes measured by DLS can be explained by the high number of short ethylene glycol chains that might be hydrated in solution but carry no weight after drying the sample for AFM. The picture of the **B2-1** dendriplex-clusters confirmed the DLS determined size of ~900.

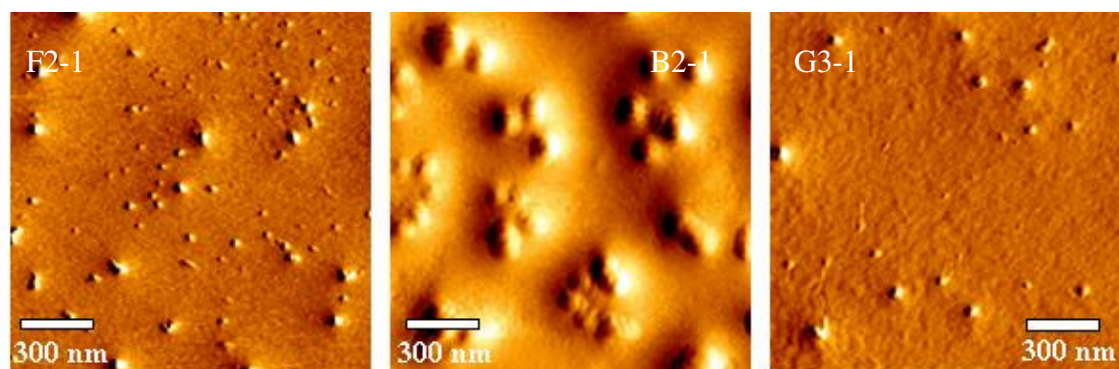


Figure 4. Morphology and density of dendriplexes were investigated by AFM revealing spherically shaped nanoplexes. Differing polyplex sizes as measured by dynamic light scattering are probably due to sample preparation (drying).

Erythrocyte Aggregation and Hemolysis.

Red blood cells can be used to visualize and quantify the membrane interactions of dendriplexes by determining erythrocyte aggregation or hemolysis. Positive surface charges can lead to unspecific binding, membrane interactions and the cytotoxicity associated with

amino groups (34). The concentration dependent hemolysis and perturbation of red blood cells after incubation with PAMAM, diaminobutane (DAB), diamonoethane (DAE) and poly(ethylene oxide) (PEO) grafted carbosilane (CSi-PEO) was reported previously (35). Generation-dependent hemolysis similar to PAMAM was seen with triazine dendrimers as well, though not as pronounced (Figure 5A). The hemolytic activity of triazine dendrimers seems to depend on their core structure, as hemolysis of the flexible dendrimer, **F2-1**, was markedly decreased compared to the rigid analogue, **G2-1**. However, dendriplexes formed from the bow-tie dendrimer, **B2-1**, caused hemolytic effects comparable to **G3-1** dendriplexes. A possible explanation is the strong aggregation of **B2-1** dendriplexes, which could facilitate electrostatic interactions with cells. The extent of hemolytic activity of a dendriplex was clearly shown to be influenced by the zeta potential.

Erythrocyte aggregation

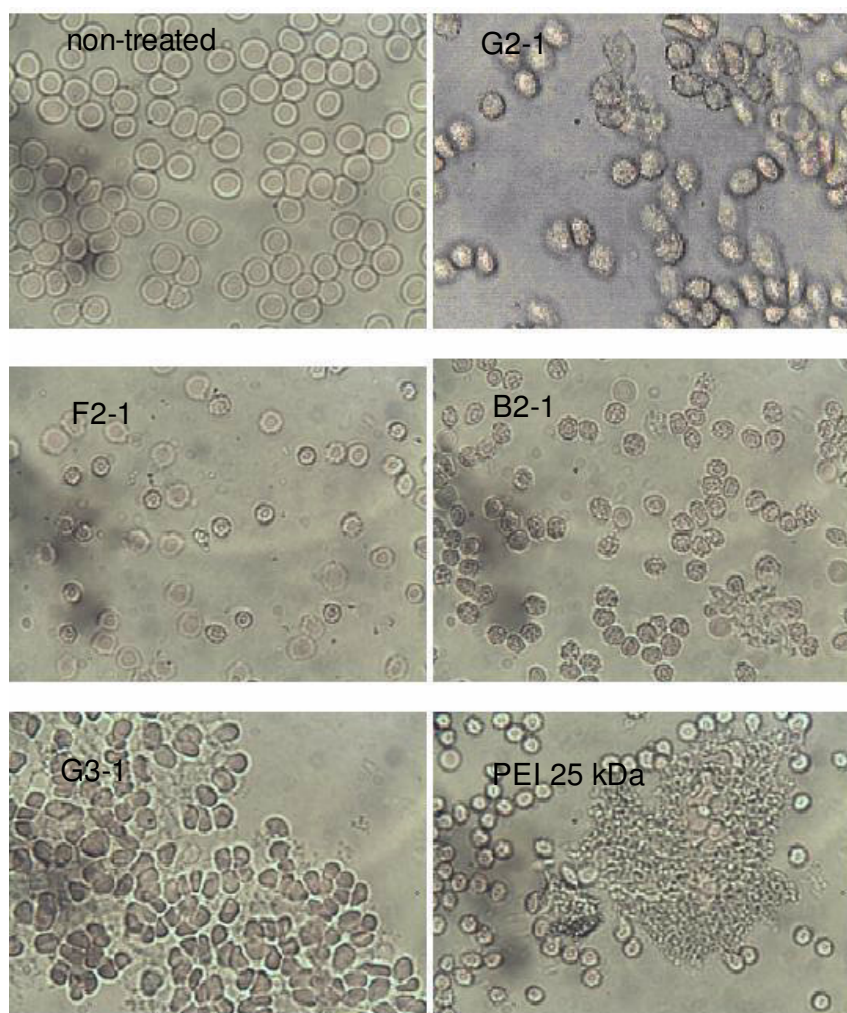
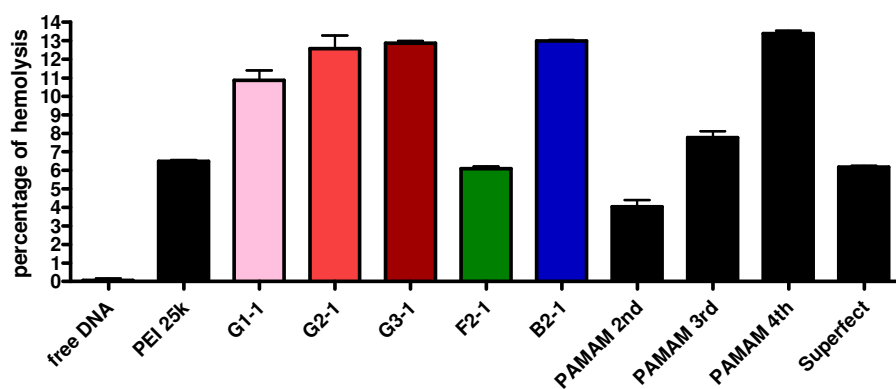


Figure 5. (A) Hemolysis after incubation with dendriplexes at an N/P of 5 was UV-metrically quantified and (B) morphologic changes of erythrocytes were microscopically

captured. Hemolysis depended strongly on the core structure, whereas erythrocyte aggregation increased by generation.

Cytotoxicity.

Cell viability or cytotoxicity can routinely be measured by quantification of mitochondrial enzyme activity using an MTT assay. In order to mimic the “worst case scenario”, murine fibroblasts (L929) were incubated with various concentrations of free dendrimer, ranging from 0.001 to 1 mg/ml (Figure 6). The half enzyme-inhibitory concentrations (IC_{50}) were determined. While PEI 25 kDa exhibited the strongest toxic effects for the panel investigated, there was a clear trend between cytotoxicity and generation number for the rigid triazine dendrimers. For **G1-1**, we determined an IC_{50} value of 501.2 μ g/ml, which is about 100 fold higher than the IC_{50} value of PEI 25 kDa (4.9 μ g/ml, compare Figure 6). The IC_{50} values decreased with increased generation among the rigid dendrimers, which can be explained by the increasing number of peripheral primary amino groups. Nonetheless, **G3-1**, the dendrimer that contains the highest number of primary amines per molecule, was approximately 5 fold less toxic than PEI 25 kDa and showed a 2.5 fold lower IC_{50} value than the third generation PAMAM (35). The **F2-1** dendrimer showed a higher toxicity profile than **G2-1**, which can be explained as resulting from an increased accessibility of both the core and the terminal amine groups, although the hemolytic activity which we measured for F2-1/DNA complexes was comparably low. The effect on remaining cell viability, on the other hand, which is expressed in the IC_{50} values, can have various reasons. Highly surface active substances are expected to strongly impede the phospholipids double layer, leading to decreased cell viability and cell death. But substances that do not exhibit strong membrane toxicity can still alter cellular mechanisms, leading to decreased cell viability. It is therefore not surprising that F2-1, which shows comparably low hemolysis, is more toxic than G2-1 and B2-1, which have higher hemolytic potentials.

The bow-tie dendrimer **B2-1**, on the other hand, exhibited lower toxicity than the rigid dendrimer **G2-1**, despite causing comparable hemolytic effects. For all of the triazine dendrimers, our cytotoxicity results are in line with an earlier report (13) revealing an IC_{50} value of 0.1 mg/ml for a related melamine structure. Triazine dendrimers seem to be less toxic than PEI and therefore more suitable for possible in vivo studies. Moreover, cytotoxicity strongly depends on the core structure and can be significantly reduced by dendriplex formation.

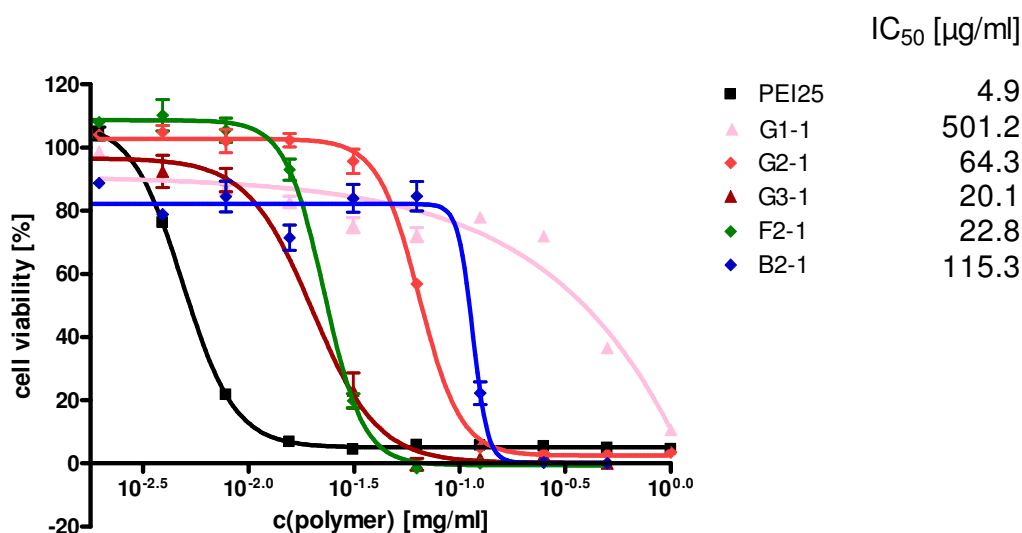


Figure 6. Toxicity profiles of all the dendrimers according to the MTT assays were compared to that of PEI 25 kDa, and for clarity IC₅₀ values are given.

Transfection Efficiency.

The primary interest for non-viral vectors is the efficiency of transfection. This property was studied using a luciferase-expressing plasmid in two different cell lines, namely murine L929 fibroblasts (Figure 7A) and human MeWo (Figure 7B) melanoma cells. The transfection efficiency of dendriplexes at different N/P ratios was quantified using a commercial luciferase assay and was compared to the transfection efficiencies of PEI 25 kDa, SuperFect™, and second and third generation PAMAM.

PAMAM (2nd and 3rd generation) dendrimers showed little transfection efficiency with increasing N/P ratios, as reported in the literature (5). An increase in transfection efficiency with increasing generation was revealed for rigid triazine dendrimers (**G1-1**, **G2-1**, and **G3-1**). The lowest generation dendrimer, **G1-1**, did not induce transgene expression in L929 or MeWo cells, while **G2-1** successfully transfected MeWo and L929 at N/P ratio > 7.5. Interestingly, **G3-1** yielded a maximum luciferase expression at N/P 5 in both cell lines. The reduced transfection efficiency at a higher N/P ratio for the higher generation dendrimer may be caused by cytotoxic effects. In both cell lines, **F2-1** achieved the highest transgene expression, even higher than the expression of PEI 25 or SuperFect. The bow-tie dendrimer, **B2-1**, exhibited moderate transfection efficiency at N/P ratio of 5 in L929 and at N/P 5 and 7.5 in MeWo cells.

These results demonstrate that triazine dendrimers could provide a promising platform for gene delivery systems as they induce transfection at generation two, while established

transfection reagents such as PAMAM are ineffective at that size. Similarly, the phosphorous containing dendrimers of Majoral show a transfection optimum at generation 5 (36). Higher generation, flexible triazine dendrimers are therefore under investigation with the goal of providing more efficient transfection reagents.

Because the flexible dendrimer, **F2-1**, formed larger complexes than the third generation dendrimer, **G3-1**, it presumably sedimented faster (24). This could have contributed to the higher transfection efficiency seen for this dendriplex. However, this route of endocytosis may not prove viable for *in vivo* applications. But also a higher availability to RNA polymerase inside the nucleus of DNA in these less compact dendriplexes, as reported by Yamagata et al. (37), might be an explanation. Hence the colloidal stability and the systematic variation of the triazine dendrimer surface are further goals for synthetic modifications.

Transfection efficiency in fibroblasts and melanoma cells

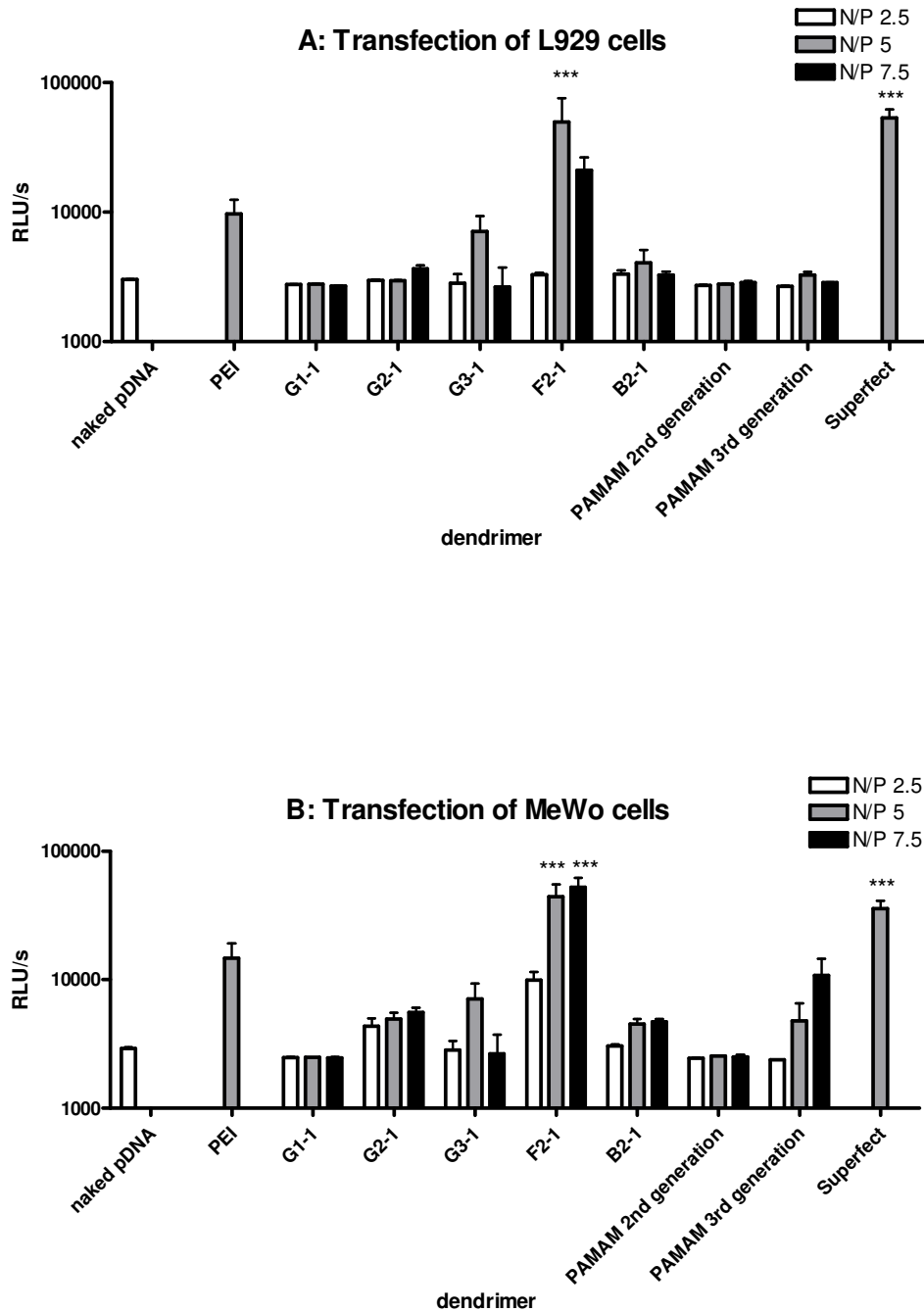


Figure 7. Transfection efficiency of the dendrimers at various N/P ratios in (A) L929 and (B) MeWo cells are given as relative light units detected by luciferase assay. F2-1 and

*Superfect exhibited significantly (***) $p < 0.01$ higher transgene expression than PEI 25 kDa and all other dendrimers.*

	Generation-1	Generation-2	Generation-3	Generation-2	Generation-2
	rigid	rigid	rigid	flexible	bow-tie
Primary amines	6	12	24	12	16
Amine density [Da/N atom]	211.27	245.30	262.20	262.32	262.20
DNA condensation at plateau [%]	48.0	30.2	4.2	36.4	5.9
Size [nm]	338.3	154.8	230.2	426.3	882.0
Zeta potential [mV]	-0.05	22.6	17.7	-7.5	3.1
Hemolysis [%]	12.6	10.9	12.9	6.11	13.0
Toxicity (IC50) [µg/ml]	501.2	64.3	20.1	22.8	115.3
Transfection efficiency (N/P 5, MeWo) [RLU/s]	2480.0	4948.3	7087.3	44184.0	4487.0

Table 1. Summary of properties of the screened dendrimers concerning in vitro parameters

4.5 Conclusion

Efforts to optimize the triazine dendrimers will require consideration of a number of lessons learned from these studies. The first generation rigid dendrimer, **G1-1**, yielded very low condensation efficiency, and although the structure had a good biocompatibility profile it did not show any transfection efficiency. The second generation rigid dendrimer **G2-1** showed improved DNA condensation, formed small dendriplexes, and was less toxic but more hemolytic than PEI. However, it showed intermediate transfection efficiency. The **G3-1** dendrimer condensed DNA well, formed small particles within a narrow size distribution, but exhibited erythrocyte aggregation. Transfection efficiency of this dendrimer was possibly limited by toxic effects at higher N/P ratios.

The change in core structure had the most profound impact on physicochemical as well as biologic properties of the triazine dendrimers. While the rigid, second generation dendrimer, **G2-1**, formed comparably small dendriplexes, both **B2-1** and **F2-1** assembled

DNA into larger complexes with lower or even negative surface charge. DNA condensation was affected differently: DNA condensation with **F2-1** and **G2-1** were similar, whereas **B2-1** protected DNA even better than PEI 25 kDa. The flexible dendrimer **F2-1** was most effective in transfection experiments. The low density particles exhibited the lowest hemolytic effect and almost no erythrocyte aggregation.

The bow-tie dendrimer, **B2-1**, caused the most pronounced hemolytic effects which are attributed to the formation of aggregates and clusters as observed with DLS and AFM. Due to their large size, **B2-1** dendriplexes were not effectively taken up by L929 or MeWo cells, leading to low transfection efficiency. We remain optimistic that triazine dendrimers demonstrate a promising platform for non-viral delivery systems, meriting further investigations, while our most important result is that flexible triazine dendrimers that are well biocompatible may be highly efficient vectors for non-viral gene delivery at comparably low generations. This is especially true for the flexible dendrimer **F2-1**, which exhibits higher transfection efficacy than SuperFect.

4.6 Acknowledgements

We thank Eva Mohr and Sandra Engel (DPB, Marburg, Germany) for their support in the cell culture lab and Michael Dutescu (Dept. of Clinical Chemistry, Marburg, Germany) for providing us with fresh blood samples. EES acknowledges support of the NIH (NIGMS R01 45640).

4.7 References

- (1) Anderson, W. F. (1998) Human gene therapy. *Nature* 392, 25-30.
- (2) Verma, I. M., and Somia, N. (1997) Gene therapy -- promises, problems and prospects. *Nature* 389, 239-42.
- (3) Mintzer, M. A., and Simanek, E. E. (2009) Nonviral vectors for gene delivery. *Chem Rev* 109, 259-302.
- (4) Haensler, J., and Szoka, F. C., Jr. (1993) Polyamidoamine cascade polymers mediate efficient transfection of cells in culture. *Bioconjug Chem* 4, 372-9.
- (5) Kukowska-Latallo, J. F., Bielinska, A. U., Johnson, J., Spindler, R., Tomalia, D. A., and Baker, J. R., Jr. (1996) Efficient transfer of genetic material into mammalian

- cells using Starburst polyamidoamine dendrimers. *Proc Natl Acad Sci U S A* 93, 4897-902.
- (6) Tang, M. X., Redemann, C. T., and Szoka, F. C., Jr. (1996) In vitro gene delivery by degraded polyamidoamine dendrimers. *Bioconjug Chem* 7, 703-14.
- (7) Zinselmeyer, B. H., Mackay, S. P., Schatzlein, A. G., and Uchegbu, I. F. (2002) The lower-generation polypropylenimine dendrimers are effective gene-transfer agents. *Pharm Res* 19, 960-7.
- (8) Hollins, A. J., Benboubetra, M., Omidi, Y., Zinselmeyer, B. H., Schatzlein, A. G., Uchegbu, I. F., and Akhtar, S. (2004) Evaluation of generation 2 and 3 poly(propylenimine) dendrimers for the potential cellular delivery of antisense oligonucleotides targeting the epidermal growth factor receptor. *Pharm Res* 21, 458-66.
- (9) Fischer, D., Bieber, T., Li, Y., Elsasser, H. P., and Kissel, T. (1999) A novel non-viral vector for DNA delivery based on low molecular weight, branched polyethylenimine: effect of molecular weight on transfection efficiency and cytotoxicity. *Pharm Res* 16, 1273-9.
- (10) Kunath, K., von Harpe, A., Fischer, D., Petersen, H., Bickel, U., Voigt, K., and Kissel, T. (2003) Low-molecular-weight polyethylenimine as a non-viral vector for DNA delivery: comparison of physicochemical properties, transfection efficiency and in vivo distribution with high-molecular-weight polyethylenimine. *J Control Release* 89, 113-25.
- (11) Mintzer, M. A., Merkel, O. M., Kissel, T., and Simanek, E. (2009) Polycationic triazine-based dendrimers: Effect of peripheral groups on transfection efficiency. *New Journal of Chemistry* doi: 10.1039/b908735d.
- (12) Lim, J., Guo, Y., Rostollan, C. L., Stanfield, J., Hsieh, J. T., Sun, X., and Simanek, E. E. (2008) The role of the size and number of polyethylene glycol chains in the biodistribution and tumor localization of triazine dendrimers. *Mol Pharm* 5, 540-7.
- (13) Neerman, M. F., Zhang, W., Parrish, A. R., and Simanek, E. E. (2004) In vitro and in vivo evaluation of a melamine dendrimer as a vehicle for drug delivery. *Int J Pharm* 281, 129-32.
- (14) Roberts, J. C., Bhalgat, M. K., and Zera, R. T. (1996) Preliminary biological evaluation of polyamidoamine (PAMAM) Starburst dendrimers. *J Biomed Mater Res* 30, 53-65.

-
- (15) Germershaus, O., Mao, S., Sitterberg, J., Bakowsky, U., and Kissel, T. (2008) Gene delivery using chitosan, trimethyl chitosan or polyethyleneglycol-graft-trimethyl chitosan block copolymers: establishment of structure-activity relationships in vitro. *J Control Release* 125, 145-54.
- (16) Germershaus, O., Merdan, T., Bakowsky, U., Behe, M., and Kissel, T. (2006) Trastuzumab-polyethylenimine-polyethylene glycol conjugates for targeting Her2-expressing tumors. *Bioconjug Chem* 17, 1190-9.
- (17) Germershaus, O., Neu, M., Behe, M., and Kissel, T. (2008) HER2 targeted polyplexes: the effect of polyplex composition and conjugation chemistry on in vitro and in vivo characteristics. *Bioconjug Chem* 19, 244-53.
- (18) Han, M., Chen, P., and Yang, X. (2005) Molecular dynamics simulation of PAMAM dendrimer in aqueous solution. *Polymer* 46, 3481-3488.
- (19) Kabanov, V. A., Sergeyev, V. G., Pyshkina, O. A., Zinchenko, A. A., Zezin, A. B., Joosten, J. G. H., Brackman, J., and Yoshikawa, K. (2000) Interpolyelectrolyte Complexes Formed by DNA and Astramol Poly(propylene imine) Dendrimers. *Macromolecules* 33, 9587-9593.
- (20) Gebhart, C. L., and Kabanov, A. V. (2001) Evaluation of polyplexes as gene transfer agents. *J Control Release* 73, 401-16.
- (21) Tang, M. X., and Szoka, F. C. (1997) The influence of polymer structure on the interactions of cationic polymers with DNA and morphology of the resulting complexes. *Gene Ther* 4, 823-32.
- (22) Wolfert, M. A., Dash, P. R., Nazarova, O., Oupicky, D., Seymour, L. W., Smart, S., Strohm, J., and Ulbrich, K. (1999) Polyelectrolyte vectors for gene delivery: influence of cationic polymer on biophysical properties of complexes formed with DNA. *Bioconjug Chem* 10, 993-1004.
- (23) Wood, K. C., Little, S. R., Langer, R., and Hammond, P. T. (2005) A family of hierarchically self-assembling linear-dendritic hybrid polymers for highly efficient targeted gene delivery. *Angew Chem Int Ed Engl* 44, 6704-8.
- (24) Mahato, R. I., Rolland, A., and Tomlinson, E. (1997) Cationic lipid-based gene delivery systems: pharmaceutical perspectives. *Pharm Res* 14, 853-9.
- (25) Erbacher, P., Bettinger, T., Belguise-Valladier, P., Zou, S., Coll, J. L., Behr, J. P., and Remy, J. S. (1999) Transfection and physical properties of various saccharide, poly(ethylene glycol), and antibody-derivatized polyethylenimines (PEI). *J Gene Med* 1, 210-22.

-
- (26) Kim, T. I., Seo, H. J., Choi, J. S., Jang, H. S., Baek, J. U., Kim, K., and Park, J. S. (2004) PAMAM-PEG-PAMAM: novel triblock copolymer as a biocompatible and efficient gene delivery carrier. *Biomacromolecules* 5, 2487-92.
- (27) Akinc, A., Thomas, M., Klivanov, A. M., and Langer, R. (2005) Exploring polyethylenimine-mediated DNA transfection and the proton sponge hypothesis. *J Gene Med* 7, 657-63.
- (28) Wittmar, M., Ellis, J. S., Morell, F., Unger, F., Schumacher, J. C., Roberts, C. J., Tendler, S. J. B., Davies, M. C., and Kissel, T. (2005) Biophysical and Transfection Studies of an Amine-Modified Poly(vinyl alcohol) for Gene Delivery. *Bioconjugate Chemistry* 16, 1390-1398.
- (29) Kunath, K., von Harpe, A., Petersen, H., Fischer, D., Voigt, K., Kissel, T., and Bickel, U. (2002) The structure of PEG-modified poly(ethylene imines) influences biodistribution and pharmacokinetics of their complexes with NF-kappaB decoy in mice. *Pharm Res* 19, 810-7.
- (30) Khandare, J. J., Jayant, S., Singh, A., Chandna, P., Wang, Y., Vorsa, N., and Minko, T. (2006) Dendrimer versus linear conjugate: Influence of polymeric architecture on the delivery and anticancer effect of paclitaxel. *Bioconjug Chem* 17, 1464-72.
- (31) Patil, M. L., Zhang, M., Betigeri, S., Taratula, O., He, H., and Minko, T. (2008) Surface-modified and internally cationic polyamidoamine dendrimers for efficient siRNA delivery. *Bioconjug Chem* 19, 1396-403.
- (32) Zhou, J., Wu, J., Hafdi, N., Behr, J. P., Erbacher, P., and Peng, L. (2006) PAMAM dendrimers for efficient siRNA delivery and potent gene silencing. *Chem Commun (Camb)*, 2362-4.
- (33) Manunta, M., Tan, P. H., Sagoo, P., Kashefi, K., and George, A. J. (2004) Gene delivery by dendrimers operates via a cholesterol dependent pathway. *Nucleic Acids Res* 32, 2730-9.
- (34) Braun, C. S., Vetro, J. A., Tomalia, D. A., Koe, G. S., Koe, J. G., and Middaugh, C. R. (2005) Structure/function relationships of polyamidoamine/DNA dendrimers as gene delivery vehicles. *J Pharm Sci* 94, 423-36.
- (35) Malik, N., Wiwattanapatapee, R., Klopsch, R., Lorenz, K., Frey, H., Weener, J. W., Meijer, E. W., Paulus, W., and Duncan, R. (2000) Dendrimers: relationship between structure and biocompatibility in vitro, and preliminary studies on the biodistribution of 125I-labelled polyamidoamine dendrimers in vivo. *J Control Release* 65, 133-48.

- (36) Padié, C., Maszewska, M., Majchrzak, K., Nawrot, B., Caminade, A.-M., and Jean-Pierre Majoral. (2009) Polycationic phosphorus dendrimers: synthesis, characterization, study of cytotoxicity, complexation of DNA, and transfection experiments. *New Journal of Chemistry* 33, 318.
- (37) Yamagata, M., Kawano, T., Shiba, K., Mori, T., Katayama, Y., and Niidome, T. (2007) Structural advantage of dendritic poly(L-lysine) for gene delivery into cells. *Bioorg Med Chem* 15, 526-32.

**PART II: NON-VIRAL *IN VITRO* AND
IN VIVO DELIVERY OF siRNA**

5 In vivo SPECT and real-time gamma camera imaging of biodistribution and pharmacokinetics of siRNA delivery using an optimized radiolabeling and purification procedure

Published in Bioconjugate Chemistry 20 (2009) 174-182

5.1 Abstract

Single Photon Emission Computed Tomography (SPECT) imaging provides a three-dimensional method for exactly locating gamma emitters in a non-invasive procedure under in vivo conditions. For characterization of siRNA delivery systems, molecular imaging techniques are extremely helpful to follow biodistribution under in experimental animal studies. Quantification of biodistribution of siRNA and non-viral delivery systems using this technique requires efficient methods to stably label siRNA with a gamma emitter (e.g. ^{111}In or $^{99\text{m}}\text{Tc}$) and to purify labeled material from excesses of radio label or linkers. In the following study, we have optimized labeling and purification of siRNA which was then applied as free siRNA or after complexation with polyethylenimine (PEI) 25 kDa for in vivo real-time gamma camera and SPECT imaging. Quantification of scintillation counts in regions of interest (ROIs) was compared to conventional scintillation counting of dissected organs, and the data acquired by imaging was shown to corroborate that of scintillation counting. This optimization and proof of principle study demonstrates that biodistribution and pharmacokinetics of siRNA and the corresponding polyplexes can be determined using SPECT leading to comparable results as conventional methodology.

5.2 Introduction

Single Photon Emission Computed Tomography (SPECT) imaging is an attractive method which allows three-dimensional localization of gamma emitters such as ^{111}In ($E\gamma=171$ and 245 keV) or $^{99\text{m}}\text{Tc}$ ($E\gamma=140$ keV) using a non-invasive procedure under in vivo conditions. Such techniques would be extremely helpful for assessing siRNA and their corresponding non-viral delivery systems with regard to biodistribution and targeting.

SPECT, compared to Positron Emission Tomography (PET), is less elaborate and expensive and shows additionally a higher resolution in small animals. The disadvantage of SPECT and PET providing only functional but no morphological information can be alleviated by either combining SPECT or PET and Computed Axial Tomography (CT), magnetic resonance imaging (MRI) or anatomical landmarking. For the latter, bones are visualized using radioactively $^{99\text{m}}\text{Tc}$ labeled bisphosphonates. Dual-isotope SPECT recordings can then be recorded in separate channels for each energy window and superimposed to generate 3D images. This dual-isotope SPECT method has not been utilized to investigate siRNA delivery systems so far. Although it doesn't provide the same

information as SPECT/CT or SPECT/MRI, it, of course, gives a better insight than single-isotope SPECT.

The field of siRNA delivery has rapidly evolved in recent years, however, only few in vivo studies combining siRNA delivery with non-invasive molecular imaging techniques such as SPECT or PET appeared in the literature (1, 2). Several groups have labeled siRNA with ^{32}P (3, 4) which is a beta emitter and can only be determined using scintillation counting or autoradiography in an endpoint study but not in in vivo imaging. Phosphodiester and phosphorothioate siRNA has been reported to be labeled with ^{123}I and ^{125}I (5), but radiometal labeling is usually preferred over radiohalogen labeling because of stability reasons (6, 7). In an earlier report, siRNA had been labeled with ^{111}In , but biodistribution was only quantified invasively (8). A recent PET/bioluminescence study (2) using DOTA chelated ^{64}Cu was the first report of assessing siRNA delivery by PET imaging. An earlier study (9) quantitated distribution of $^{99\text{m}}\text{Tc}$ labeled single strands using a gamma camera, but unfortunately allowed only for an estimation of biodistribution of duplexes. SPECT, compared to PET, provides better spatial resolution in small animals and doesn't require synthesis of short live and high energy emitters. Additionally, using high resolution SPECT imaging based on multi pinhole collimation, which is a prototype of the latest small animal scanners, allowed us to use a clinical camera (10).

Quantification of biodistribution of siRNA and their delivery systems using SPECT or two-dimensional gamma camera imaging, requires efficient methods for stably labeling siRNA with a gamma emitting isotope as well as fast and efficient purification of labeled materials from excesses of radiolabel or linkers.

The fate of pDNA after intravenous application of different non-viral vectors, such as poly ethylenimine (PEI) or PEGylated PEI (PEG-PEI), has been reported previously (11, 12), but it cannot be assumed that siRNA polyplexes would perform identically under in vivo conditions. In fact, several studies demonstrated differences between siRNA and DNA containing polyplexes (13, 14). Hence, dual isotope SPECT would be of interest for in vivo live imaging the biodistribution of siRNA polyplexes. As $^{111}\text{Indium}$ can be complexed with chelators such as p-SCN-Bn-DTPA, we have developed an optimized a method (8) for covalently labeling amine-modified siRNA and applied this labeled siRNA in real time live imaging of the distribution of our previously in vitro investigated PEI/siRNA polyplexes (15).

5.3 Materials and Methods

Materials:

Amine-modified luciferase GL3 siRNA with a C6-NH₂ linker at each 3' of the double strand was purchased from Dharmacon (Lafayette, CO, USA). 2-(4-isothiocyanatobenzyl)-diethylenetriaminepentaacetic acid (p-SCN-Bn-DTPA) was purchased from Macrocyclics (Dallas, TX, USA), Arsenazo(III), Yttrium(III) chloride and Diethyl pyrocarbonate (DEPC) from Sigma-Aldrich Laborchemikalien GmbH (Seelze, Germany). The purification columns miRACLE were purchased from Stratagene (La Jolla, CA, USA), RNeasy Mini from Qiagen (Hilden, Germany), and PD-10 from Amersham Pharmacia Biotech (Freiburg, Germany). The radioactive substances ¹¹¹InCl₃ and ^{99m}Tc-alendronate were purchased from Covidien Deutschland GmbH (Neustadt a.d. Donau, Germany), and balb/c mice from Charles River WIGA (Sulzfeld, Germany).

Polyethylenimine, PEI 25 kDa (Polymin™, 25 kDa) was a gift from BASF (Ludwigshafen, Germany), all other chemicals used were of analytical grade. All buffers were treated with 0.1 % Diethyl pyrocarbonate (DEPC).

Methods:

p-SCN-Bn-DTPA-coupling:

Amine-modified luciferase GL3 siRNA was dissolved in siRNA buffer provided by the manufacturer. Coupling of p-SCN-Bn-DTPA was accomplished by a previously described method (8). Briefly, 20 nmol siRNA in 10 µl siRNA buffer, adjusted to pH 8.5 with an equal volume of 0.2 M NaHCO₃, was mixed with a 50 fold excess of the chelator dissolved in 36 µl DMSO. In our experiments, we used the amine reactive variant of DTPA (p-SCN-Bn-DTPA) instead of DTPA-dianhydride (cDTPA). Incubation times were varied from 45 minutes as reported to 3 hours. The coupling degree was determined after purification by quantification of DTPA in a non-radioactive assay described by Pippin et al.(16). Briefly, absorption of a complex of Arsenazo(III) and Yttrium(III) at 652 nm is measured, and sample DTPA content can be calculated or a calibration curve can be recorded due to decreasing absorption of the complex falling apart after addition of DTPA.

PD-10 size exclusion chromatography (SEC):

One method used for separation of labeled siRNA from p-SCN-Bn-DTPA or radiolabel was size exclusion chromatography SEC employing a PD-10 Sephadex G25 prepacked column.

The column was equilibrated with 50 ml DEPC-treated PBS before the reaction mixture was applied to the column. Fractions of 13 droplets each were collected. RNA content was measured UV-metrically at 260 nm using a Pharmacia Ultrospec 2000 UV/VIS, Pharmacia Biotech (Freiburg, Germany), and radioactive signal in 10 μ l of each fraction was determined using a Gamma Counter Packard 5005 (Packard Instruments, Meriden, CT, USA).

miRACLE and RNeasy purification:

Spin column purification was conducted as described for the miRACLE columns. Briefly, 1 or 100 μ g siRNA for miRACLE or RNeasy columns, respectively, were diluted to 600 μ l with 2 M sodium acetate, ethanol and guanidinium salts containing “Binding Buffer” provided in the miRACLE kit and applied to a spin column. Columns were centrifuged for 2 minutes at 16,000 g, and washed 3 times with 600 μ l “Low Salt Wash Buffer” by centrifugation for 1 minute at 16,000 g. The membranes were dried by a fifth centrifugation step without applying any solution. RNA was then eluted by incubating the membrane with 50 μ l 60 °C warm DEPC-treated RNase free water for 2 minutes and following centrifugation for 1 minute at 16,000 g. This step was repeated and followed by a third incubation where 25 μ l DEPC-treated 0.5 M sodium acetate, pH 4.5, were applied instead of water to achieve a final concentration of 0.1 M sodium acetate in the siRNA solution.

Radio labeling:

Radio labeling of the p-SCN-Bn-DTPA-coupled siRNA was accomplished in 0.1 M sodium acetate buffer, pH 4.5. For the validation of the method, small amounts of 10 nmol siRNA were incubated with 16.2 MBq InCl_3 for 30 minutes at room temperature. For in vivo experiments, 111 nmol siRNA were incubated with 28.9 MBq InCl_3 for 30 minutes at room temperature, followed by either PD-10 SEC or spin column binding, washing and elution or a combination of both methods. For in vivo experiments, siRNA was purified using a PD-10 column first. Fractions 5-9 (compare figures 4A and 4B), which showed both a high radioactive signal and the strongest UV absorption at 260 nm and don't contain any free p-SCN-Bn-DTPA or Indium, were combined and further purified as well as concentrated using RNeasy columns as described above.

Animal studies:

All animal experiments were carried out according to the German law of protection of animal life and approved by an external review committee for laboratory animal care.

For in vivo experiments in 4 weeks old balb/c mice (~ 20 g), 35 µg Bn-DTPA coupled thiourea derivative of siRNA, corresponding to 2.57 nmol and 0.255 MBq, were either administered as free siRNA or after complexation at an N/P of 6 with 25 kDa branched PEI. Free siRNA or complexes were injected i.v. to the tail vein and biodistribution was followed by perfusion live imaging and static imaging acquired with a Siemens e.cam gamma camera (Siemens AG, Erlangen, Germany). Biodistribution 2 hours post injection was investigated by high-resolution SPECT imaging using a custom built multiplexing multipinhole collimator, mounted on the Siemens e.cam gamma camera, quantified by analysis of regions of interest (ROIs) in the planar gamma camera images and was eventually compared to conventional gamma counting of dissected organs.

For anatomical landmarking in the SPECT images, mice were additionally injected with 4 MBq ^{99m}Tc-labeled phosphonate 4 hours before imaging.

Statistics:

Analytical measurements were conducted in triplicates. Animal experiments include 5 animals per group; results are given as mean values. Two way ANOVA and statistical evaluation was accomplished using GraphPad Prism 4.03 (GraphPad Software, LaJolla, USA).

5.4 Results and Discussion

While labeling of amine modified siRNA with p-SCN-Bn-DTPA was accomplished different from the method previously reported (8), and could not be improved by variation of incubation time, purification of the reaction mixture, on the other hand, was extensively optimized. For coupling the amine modified siRNA, we preferred the use of p-SCN-Bn-DTPA over cyclic DTPA anhydride (cDTPA) (8) since in the coupling reaction with the latter one of the chelating teeth is used for amide formation in a ring opening reaction. The advantage of formation of a thiourea derivative in a standard reaction of amines and the benzyl-isothiocyanate modified DTPA is the fact that each chelating tooth is available for complex formation after DTPA is unaffected by the reaction of the benzyl spaced isothiocyanate, which is shown in Figure 1.

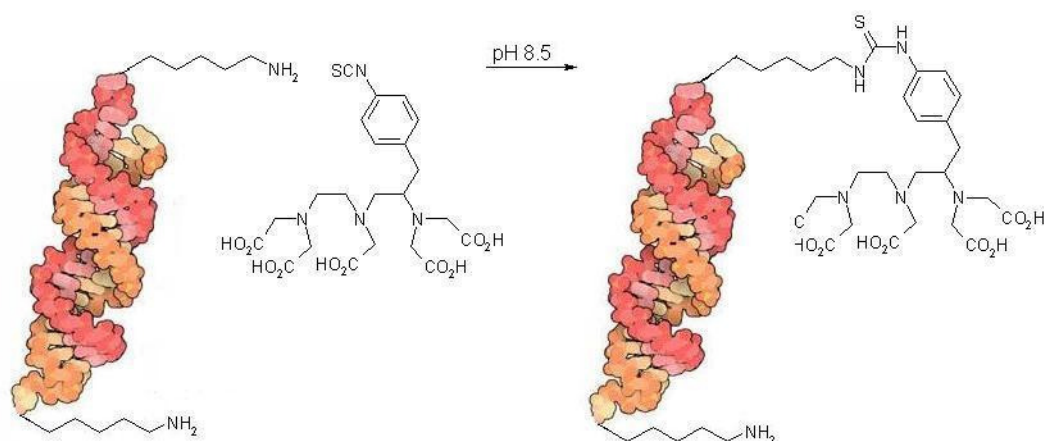


Figure 1: Reaction of amine-modified siRNA and p-SCN-Bn-DTPA in formation of a thiourea derivative. Both strands bear a C6-NH₂ linker, but a coupling degree of 2 mol/mol could not be achieved.

In search of a faster purification method than extensive dialysis which would yield in a higher percentage of siRNA recovery and protect the siRNA from degradation, a method was employed which is known from RNA isolation from cells or tissues. First of all, spin columns specifically developed for miRNA isolation (miRACLE, Stratagene) were used to validate the method and to quantify the yield. The basic principle of this purification or isolation method is the binding of RNA in presence of chaotropic salts to the silica membrane of the spin columns. Additionally, RNA is made insoluble by a high concentration of ethanol of at least 70 % v/v in the presence of 10 % v/v 2 M sodium acetate buffer, and therefore can be washed extensively but fast with low salt buffers containing 70 % v/v ethanol. Finally, the RNA is eluted with water or TE buffer. Due to the chelating activity of EDTA in TE buffer, which could later complex parts of radioactive Indium, all siRNA was eluted with DEPC-treated water.

The miRACLE spin columns proved to be applicable for siRNA as the yield of eluted siRNA was 92.6 ± 6.4 % and the coupling degree determined after purification was 16.9 ± 2.1 % (compare Figure 2A). Because of their low binding capacity (1 μ g RNA per column) and bigger reaction feeds needed for in vivo application, the use of RNeasy Mini columns (Qiagen) that hold 100 μ g of RNA was validated in the next step. Since the buffer composition of the binding and washing buffers in the RNeasy kit is proprietary, buffers from the miRACLE kit, which were assured to be free of chelators, were used for all spin column purifications. The yield of the siRNA recovery could extensively be increased from

40 % which had been eluted with 25 °C warm DEPC-water to 79.6 ± 4.1 % after incubating the siRNA on the membrane for 2 minutes with 60 °C warm DEPC-water.

Coupling degree of such purified siRNA was determined to be 32.9 ± 1.8 % as shown in Figure 2A.

A

Purification method	Yield [%]	Coupling Degree [mol/mol]
PD-10 GPC	108.5 +/- 20.5	3.23 +/- 0.141
miRACLE spin columns	92.6 +/- 6.4	0.17 +/- 0.002
RNeasy spin columns	79.6 +/- 4.1	0.33 +/- 0.002

B

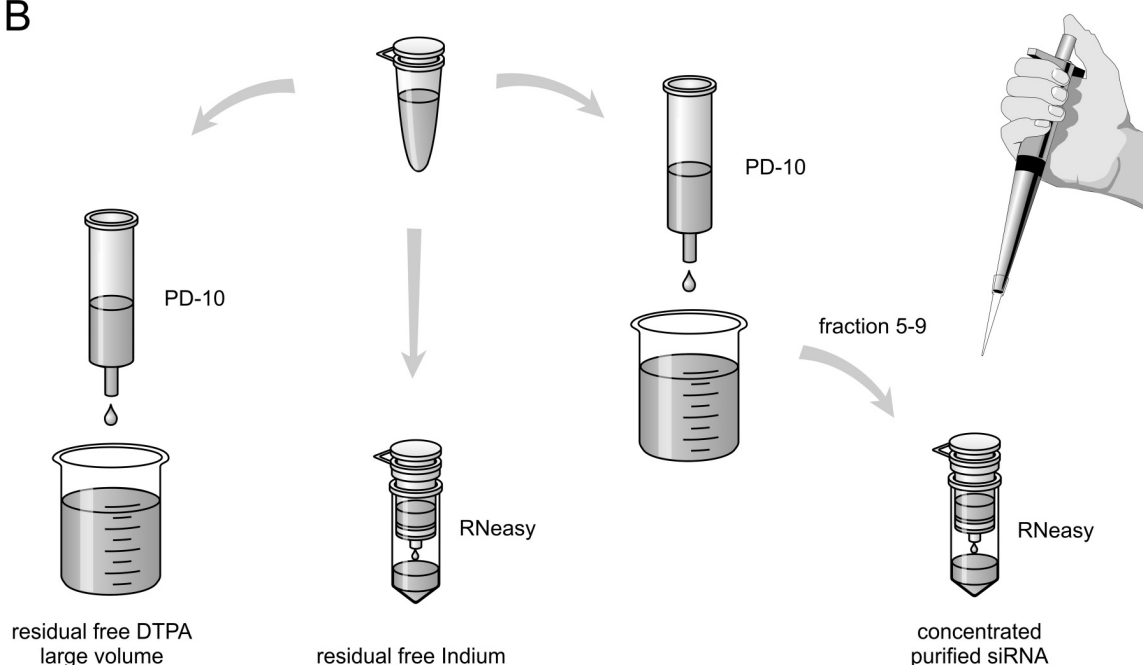


Figure 2A: Yields and *p*-SCN-Bn-DTPA coupling degrees analyzed after different methods of siRNA purification, 2B: Purification with a PD-10 column didn't effectively separate siRNA from an excess of unreacted *p*-SCN-Bn-DTPA, RNeasy columns didn't desalt from InCl_3 , and therefore, a combined purification after annealing was employed.

For purification after radiolabeling, in the first approach, PD-10 (Amersham) SEC was employed as described by Van de Water et al. (8). After analysis of the collected fractions for UV-metrically determined siRNA concentration and gamma-counted radioactivity, RNA peak fraction and peak fraction of the radioactivity seemed to be shifted, as shown in Figure 3A, and the radioactive signal slowly decreased before a second peak appeared. Due to the principle of SEC, big particles are eluted first, smaller ones in later fractions. Since

the siRNA had only been brought into contact with DEPC-treated buffers upon receipt, we precluded degradation. One possible explanation was that siRNA had not been fully annealed, and possibly only the single strands had been effectively labeled with p-SCN-Bn-DTPA. To prove this, radio labeling was repeated a) without annealing and b) with annealing of the siRNA strands by heating up to 94 °C for 2 minutes after p-SCN-Bn-DTPA-labeling, and with c) pre-annealed siRNA. To make sure that the annealed double strands would not be separated on the membranes of the spin columns or under harsh conditions such as 16,000 g centrifugal force, this reaction mixture was purified on a PD-10 column. Here, a mathematically calculated coupling degree of theoretically 323 % and therefore an excess of at least 123 % of free p-SCN-Bn-DTPA was determined, as shown in Figure 2A.

The same amounts of free Indium (grey circles, Figure 3C) or free p-SCN-Bn-DTPA-chelated Indium (grey squares, Figure 3C) which had been in the reaction mixtures were each applied to a PD-10 column in separate experiments. This allowed us to detect when free Indium and when Indium chelated by residual free p-SCN-Bn-DTPA would be eluted from the PD-10 column and which peak in the chromatographs represented each of those two compounds. Free Indium showed a peak at fraction 17, p-SCN-Bn-DTPA-Indium at fraction number 12. The overlay of each Indium signal in Figure 3C allowed to clearly identify the second, smaller peak in 3A and 3B to be the free Indium.

Re-annealing of the pre-coupled siRNA strands finally caused concurrence of the radioactivity and the siRNA peak, which is shown in Figure 3B. Without annealing, again a shift of both peaks was observed (compare Figure 3A). But still the decrease of the radioactivity signal of the re-annealed sample (3B) fell less steep than the RNA signal. In the pre-annealed sample (black circles in Figure 3C), that obviously contained a high amount of free p-SCN-Bn-DTPA (compare Figure 2A), the Indium peak was even broader and didn't show a free Indium-peak after fraction 15.

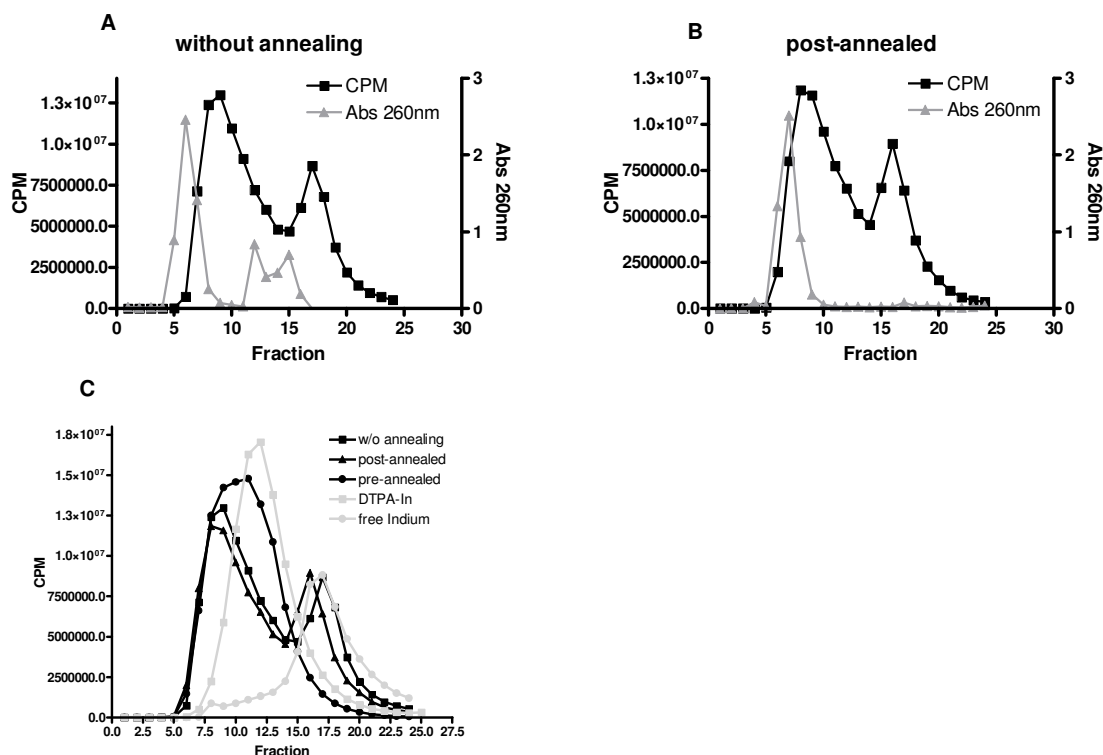


Figure 3: PD-10 size exclusion chromatographs of purified siRNA. A: RNeasy purified siRNA without annealing. Radioactivity and RNA peaks are shifted. B: RNeasy purified siRNA after post-annealing. Peaks are concurrent but radioactivity signal decreases slowly. C: Overlay of radioactivity signals. *p*-SCN-Bn-DTPA-Indium appears after fraction 7 and is the reason for slow decrease of signal in RNeasy purified siRNA and the broad peak in PD-10 purified pre-annealed siRNA (black circles). Free Indium peaks at fraction 17 and is not apparent in PD-10 purified pre-annealed siRNA due to excess of free *p*-SCN-Bn-DTPA.

Since spin column purification after *p*-SCN-Bn-DTPA coupling had proven to be extremely more effective than SEC, it was next employed for purification after radiolabeling of another sample of which small aliquots were either applied to a PD-10 column for quality control without further treatment (Figure 4A) or after re-annealing (Figure 4B). The chromatographs of those two aliquots didn't show significant differences, but finally the peaks of RNA concentration and radioactivity matched both in peak and valley. But as a second, smaller peak appeared again after fraction 15, it must be admitted, that the spin column purification is highly effective for separation of siRNA (approx. 13.6 kDa) from small molecules like *p*-SCN-Bn-DTPA (650 Da), but cannot fully separate siRNA from large excesses of salts like InCl₃. The best strategy therefore seemed to be a combination of SEC and spin column purification, as another benefit of a following spin column

purification is the fact that the peak fractions from SEC can be combined and concentrated on the columns, as shown in Figure 2. Annealing of siRNA should be accomplished after p-SCN-Bn-DTPA coupling to achieve a high coupling degree.

The final yield after combined purification of 125 nmol siRNA of which 111 nmol siRNA were labeled with 28.8 MBq was 81.2 % with a specific activity of 99 MBq/ μ mol.

Functionality of the labeled siRNA was investigated in vitro and found not to be significantly different from a non-labeled duplex of the same sequence (data not shown).

Quality Control of Spin Column Purified siRNA

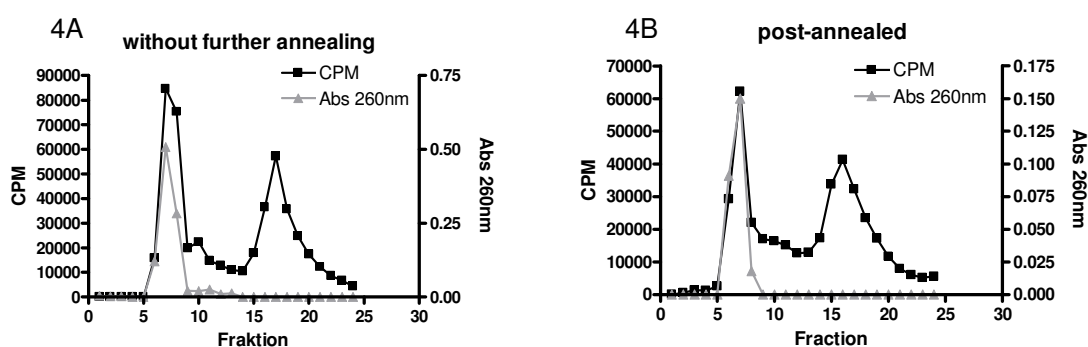


Figure 4: PD-10 size exclusion chromatographs of siRNA that was purified with RNeasy spin columns after coupling and after radiolabeling. RNA and radioactivity peaks are concurrent in climax and anticlimax but substantial amount of free Indium is left in solution.

In the in vivo experiments, labeled and purified siRNA was either administered as free siRNA, as reported earlier (8), or after complexation with 25 kDa branched PEI, which has earlier been characterized concerning in vivo biodistribution and pharmacokinetics after complexation of pDNA and ODNs (11, 17, 18) and has lately been used for in vivo siRNA delivery (19-24).

In the real-time perfusion study, rapid accumulation of PEI-complexed siRNA in the liver and in the kidneys could be observed, as well as an increasing signal in the bladder, as shown in Figures 5B, 6B, and Movie 4, supplementary data. Quantification of scintillation counts in the ROIs as a function of time, as shown in Figure 6B, reveal that the half life of PEI-complexed siRNA in the blood pool (triangles, Figure 6B and 6C) is only 168.5 seconds, which is in good agreement with published data (25). The signal in liver and kidneys decreases to a plateau after initial accumulation (circles, Figure 6B) and the signal of residual radioactive material in the injection site (diamonds, Figure 6B) decreases as well

to a certain extent. Free siRNA, on the other hand, showed initial uptake into liver and kidneys, as shown in Figure 6A (circles), but no accumulation. Our real time perfusion recording shows very rapid excretion into the bladder (Figure 5A and Movie 1), which is visualized and quantified in Figure 6A. While activity in the liver and kidneys decreases (Figure 6A, circles), it increases to the same extent in the bladder (Figure 6A, squares).

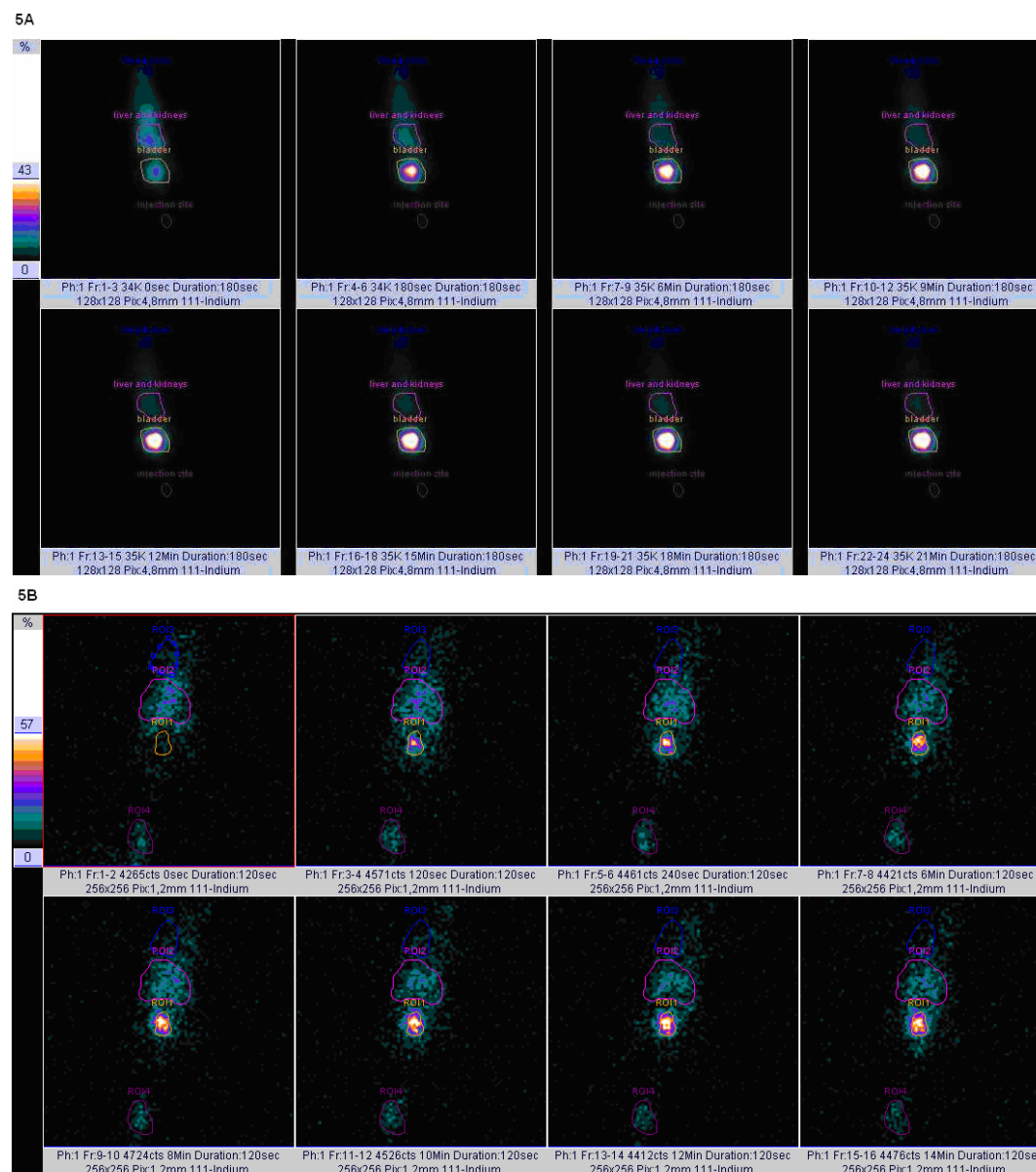
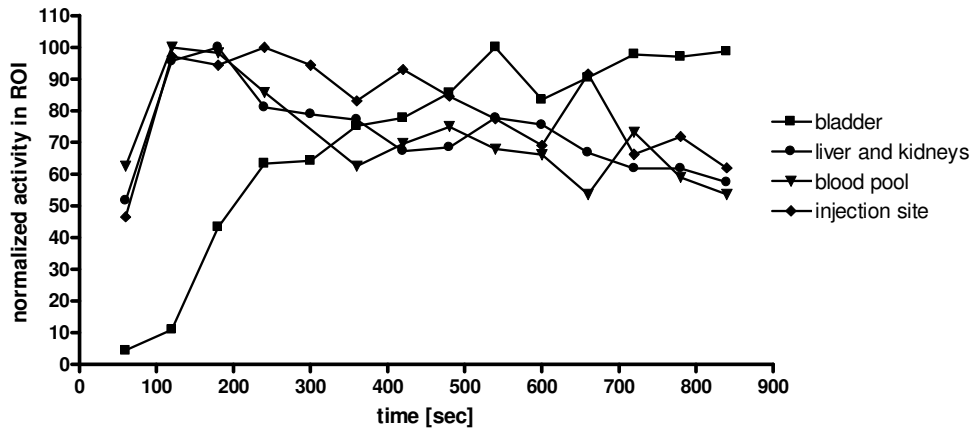
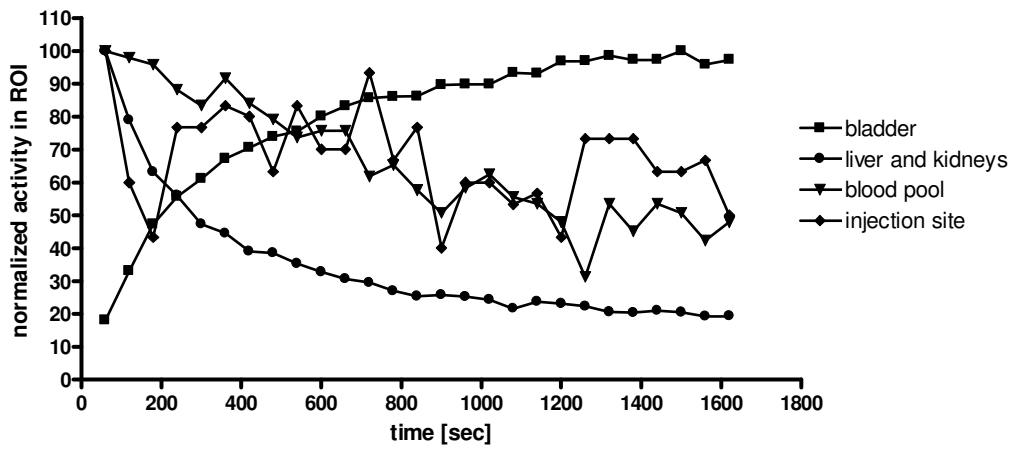


Figure 5: Planar gamma camera perfusion movie with regions of interest for lifetime quantification after injection of $35\ \mu\text{g}$ siRNA, corresponding to $2.57\ \text{nmol}$ and $0.255\ \text{MBq}$ ^{111}In , A: as free siRNA and B: complexed at N/P of 6 with $25\ \text{kDa}$ bPEI.

6A



6B



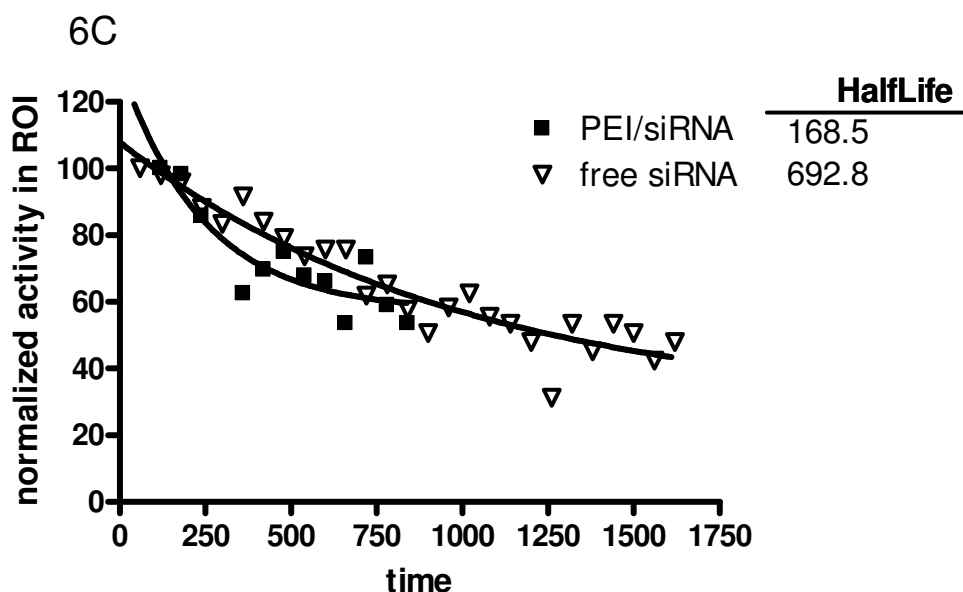


Figure 6: Normalized graphical analysis of activity in regions of interest in Figures 5A and 5B. 6A: PEI-complexed siRNA, 6B: Free siRNA, 6C: Pharmacokinetic analysis of siRNA in circulation.

SPECT images recorded 2 hours post injection corroborated the observation of accumulation of PEI complexed siRNA in liver, kidneys and bladder by providing more three-dimensional, regional information (compare Figure 7B and Movie 2), and gamma scintillation counting of dissected organs confirmed that PEI 25 kDa-complexed siRNA accumulated in the liver and was renally excreted as it was found to be in the urine and not in the bladder tissue (compare Figure 8A). Confirmation of non-invasive data by invasive data which has been reported in drug delivery (26) and gene therapy (27) studies was the critical part of this investigation and was successfully achieved.

Free siRNA could be measured in the kidneys, as earlier reported (8), partly in the liver but was also eliminated through the bowel. Due to their instability in serum, free siRNA duplexes are rapidly degraded upon injection. Therefore, small fragments bearing the label supposedly circulate in the blood pool and show a different behavior than macromolecules or nanoplexes.

Fast renal clearance and a high signal in the urine in biodistribution studies with PEI/pDNA polyplexes had so far been interpreted as degraded plasmid being excreted (28). In our study, on the other hand, we found higher signals in the urine for PEI-complexed siRNA compared to free siRNA, 2 hours after injection. One reason could be that the free siRNA had been excreted to the bladder faster than PEI complexed siRNA and got lost by urination

before the the animals were sacrificed. But the signal in the urine can not only be caused by degradation products, knowing that renal clearance might even be faster than siRNA degradation (25). In fact, free siRNA, which for sure had partly been degraded after injection, showed a different profile from complexed siRNA. In the case of free siRNA, no distinct deposition in any certain organ could be observed (Figure 8A), and the percentage of injected dose which was still in circulation after 2 hours was 9 % per ml blood compared to 1 % for PEI25-complexed siRNA (Figure 8). Half life of free siRNA was 692.8 seconds (compare Figures 6A and 6C). SPECT images of mice treated with free siRNA (Figure 7A) showed no distinct deposition in any organ either, except for the bladder. One explanation for this could be long circulation and almost no deposition of small fragments of degraded siRNA or a binding of amine-modified siRNA to blood components. It is known that siRNA is degraded rapidly in vivo by serum nucleases and that this can be prevented or retarded by chemical modification of the nucleotides or by complexation with an appropriate delivery system (29-31). In our earlier publication, we showed that bPEI 25 kDa as well as PEGylated derivatives do have the potential to protect siRNA from RNase degradation (15). As formulation with the polymer seemed to drive kinetics and distribution, PEI-complexed siRNA showed a clear accumulation in the liver of 15 % injected dose per organ (Figure 8A), although not as prominent as observed with pDNA, which had been reported to be up to 40 % (11). Accumulation in the spleen could not be observed either, although more labeled polymer (2.9 %, data not shown) than labeled siRNA (0.9 %, Figure 8A) was found to be taken up – possibly by macrophages. This again supports the assumption by Merdan et al (11) of polyplexes at least partly falling apart into free polymer, which is then especially taken up by the liver and spleen, and into siRNA, which is excreted or degraded upon release from the complex.

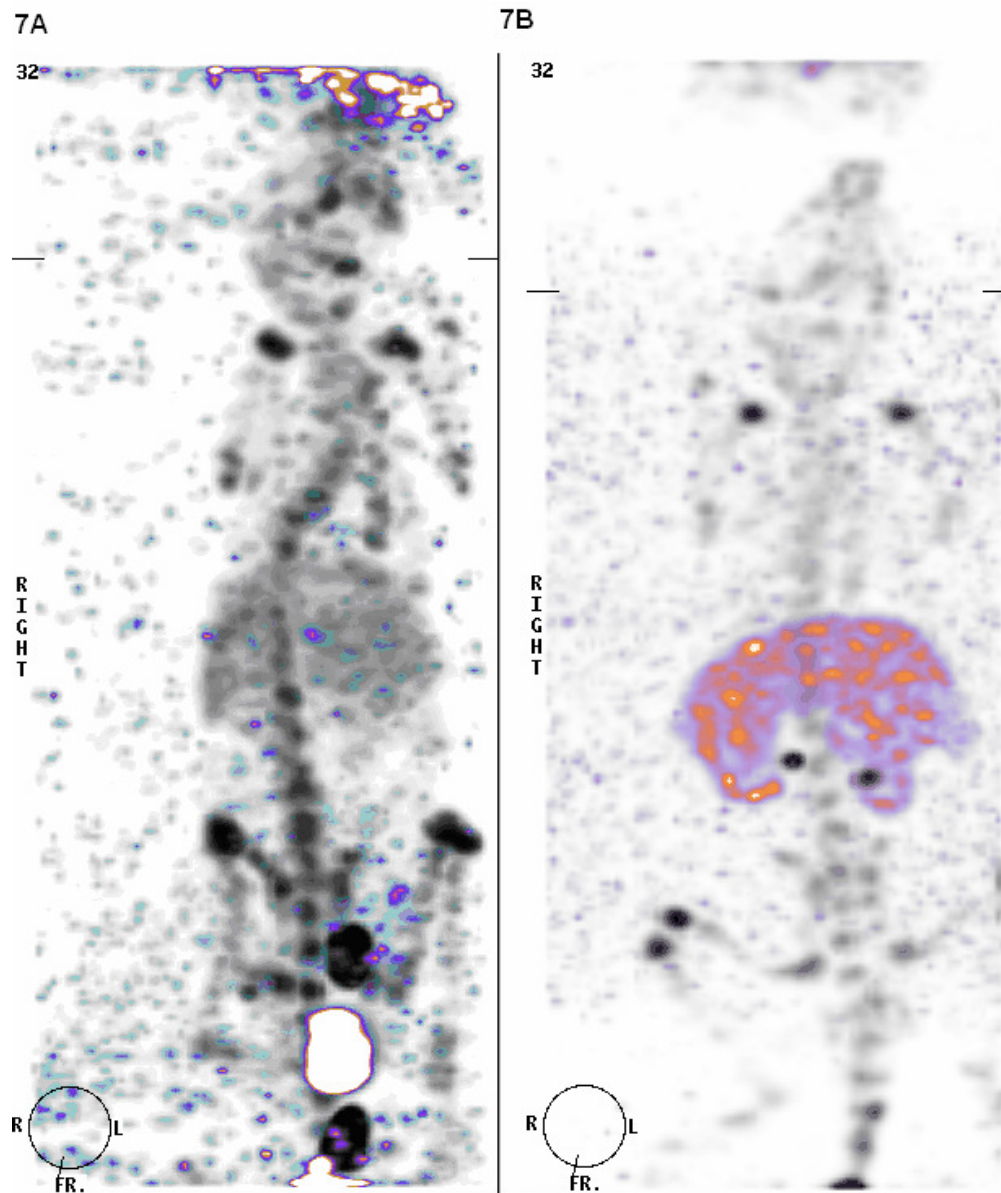


Figure 7: SPECT image of 4 weeks old male balb/c mouse injected with 35 μg siRNA, corresponding to 2.57 nmol and 0.255 MBq ^{111}In (purple, blue and orange), and 8 MBq $^{99\text{m}}\text{Tc}$ -labeled phosphonate (greyscale) for anatomical landmarking. A: free siRNA, B: complexes at N/P 6 with 25 kDa bPEI.

A primary deposition in the lungs and secondary redistribution, which had been assumed for PEI/pDNA complexes earlier (11, 32), could not be observed in our perfusion studies. Neither did we observe acute or lethal toxicity which had been described by several groups investigating biodistribution and kinetics of PEI/pDNA polyplexes (33). The fact that we did not observe any lethality or lung accumulation is in good agreement with former reports that explained death of laboratory animals after embolism to be caused by entrapment of aggregates of polyplexes and blood components in the lung capillaries (34).

The disadvantage of imaging techniques not differentiating between free label, degraded or intact labeled compound can only be overcome by verification using autoradiography or after specific siRNA isolation and purification of intact 21mers and photometric quantification.

This aspect also stresses the importance of efficient purification after the labeling process.

A shortcoming of the imaging compared to gamma scintillation of dissected organs is the fact that planar pictures don't allow for differentiation between organs in the same plane of projection, such as liver and kidneys or urine and bladder (Figure 8). Regions of interest always express the total scintillation counts of all organs in the plane of projection and organs, that don't show significant uptake, can hardly be analyzed. In our study, only the liver, kidneys, urine and bladder showed strong signals and could easily be detected in planar images, but the significant difference in uptake to the liver of free siRNA and PEI/siRNA polyplexes could only be shown after dissection of organs (Figure 8A).

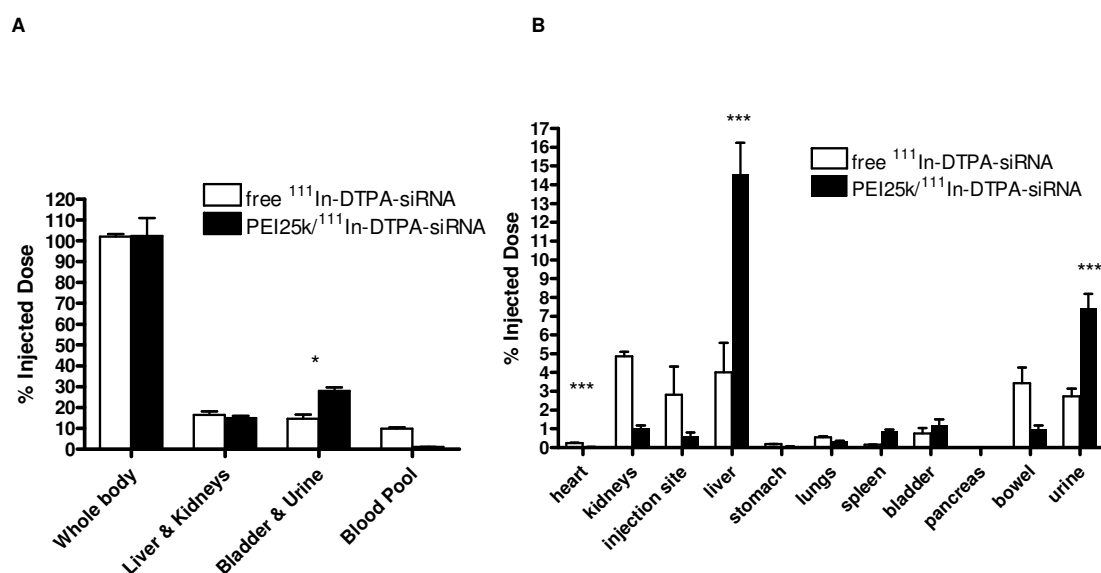


Figure 8A: Scintillation analysis of regions of interest 2 hours after injection. 8B: Scintillation analysis of dissected organs 2 hours after injection expressed as % injected dose per organ.

5.5 Conclusion

In summary, we developed an optimized and simple method for coupling p-SCN-Bn-DTPA to siRNA and purification of those radiolabeled siRNA complexes with high yields of these expensive materials. Once the siRNA bears the radioactive label, it can be applied in non-invasive perfusion, kinetics and biodistribution studies which corroborate the results from

end point scintillation counting methods but offer the advantage of live imaging and examination at various time points in the same animal, reducing the number of animals needed compared to conventional techniques. Dual isotope SPECT and gamma camera imaging are very useful methods to follow biodistribution of polyplexes especially with respect to the kinetic of distribution. For determination of exact scintillation counts in every single organ, the latter have to be dissected. But imaging clearly is able to assess siRNA delivery, biodistribution and even pharmacokinetics, if a ROI is placed in the blood pool, without sacrificing animals. This proof of principle allows us to investigate distribution and kinetics of a variety of our vectors by multiple methods, including double labeling of vector and load, in the future.

5.6 Acknowledgment

The authors are grateful to Ulla Cramer and Klaus Keim for excellent technical support, and to Helmut Höffken, MD, for expert medical advice. The financial support of Deutsche Forschungsgemeinschaft (DFG Forschergruppe 627) is gratefully acknowledged.

5.7 Supporting Information

Supporting online information are two animated gif files of SPECT images comparable to Figures 7A and 7B, and two gif files of the perfusion studies shown in Figures 5A and 5B.

5.8 References

- (1) Bartlett, D. W. and Davis, M. E. (2008). Impact of tumor-specific targeting and dosing schedule on tumor growth inhibition after intravenous administration of siRNA-containing nanoparticles. *Biotechnol Bioeng* 99: 975-85
- (2) Bartlett, D. W., Su, H., Hildebrandt, I. J., Weber, W. A. and Davis, M. E. (2007). Impact of tumor-specific targeting on the biodistribution and efficacy of siRNA nanoparticles measured by multimodality in vivo imaging. *Proc Natl Acad Sci U S A* 104: 15549-54
- (3) de Martimprey, H., Bertrand, J.-R., Fusco, A., Santoro, M., Couvreur, P., Vauthier, C. and Malvy, C. (2007). siRNA nanoformulation against the Ret/PTC1 junction

- oncogene is efficient in an in vivo model of papillary thyroid carcinoma. *Nucl. Acids Res.* 36: e2
- (4) Wolfrum, C., Shi, S., Jayaprakash, K. N., Jayaraman, M., Wang, G., Pandey, R. K., Rajeev, K. G., Nakayama, T., Charrise, K., Ndungo, E. M., Zimmermann, T., Koteliansky, V., Manoharan, M. and Stoffel, M. (2007). Mechanisms and optimization of in vivo delivery of lipophilic siRNAs. *Nat Biotechnol* 25: 1149-57
- (5) Braasch, D. A., Paroo, Z., Constantinescu, A., Ren, G., Oz, O. K., Mason, R. P. and Corey, D. R. (2004). Biodistribution of phosphodiester and phosphorothioate siRNA. *Bioorg Med Chem Lett* 14: 1139-43
- (6) Barendswaard, E. C., Scott, A. M., Divgi, C. R., Williams, C., Jr., Coplan, K., Riedel, E., Yao, T. J., Gansow, O. A., Finn, R. D., Larson, S. M., Old, L. J. and Welt, S. (1998). Rapid and specific targeting of monoclonal antibody A33 to a colon cancer xenograft in nude mice. *Int J Oncol* 12: 45-53
- (7) Clarke, K., Lee, F.-T., Brechbiel, M. W., Smyth, F. E., Old, L. J. and Scott, A. M. (2000). In Vivo Biodistribution of a Humanized Anti-Lewis Y Monoclonal Antibody (hu3S193) in MCF-7 Xenografted BALB/c Nude Mice. *Cancer Res* 60: 4804-4811
- (8) Van de Water, F. M., Boerman, O. C., Wouterse, A. C., Peters, J. G., Russel, F. G. and Masereeuw, R. (2006). Intravenously administered siRNA accumulates in the kidney and selectively suppresses gene function in renal proximal tubules. *Drug Metab Dispos* 34: 1393-7.
- (9) Liu, N., Ding, H., Vanderheyden, J. L., Zhu, Z. and Zhang, Y. (2007). Radiolabeling small RNA with technetium-99m for visualizing cellular delivery and mouse biodistribution. *Nucl Med Biol* 34: 399-404

-
- (10) Schramm, N. U. E., G.; Engeland, U.; Schurrat, T.; Behe, M.; Behr, T.M. (2003). High-resolution SPECT using multipinhole collimation. *Nuclear Science, IEEE Transactions on 50*: 315 - 320
- (11) Merdan, T., Kunath, K., Petersen, H., Bakowsky, U., Voigt, K. H., Kopecek, J. and Kissel, T. (2005). PEGylation of poly(ethylene imine) affects stability of complexes with plasmid DNA under in vivo conditions in a dose-dependent manner after intravenous injection into mice. *Bioconjug Chem 16*: 785-92
- (12) Kunath, K., von Harpe, A., Petersen, H., Fischer, D., Voigt, K., Kissel, T. and Bickel, U. (2002). The structure of PEG-modified poly(ethylene imines) influences biodistribution and pharmacokinetics of their complexes with NF-kappaB decoy in mice. *Pharm Res 19*: 810-7
- (13) Gary, D. J., Puri, N. and Won, Y. Y. (2007). Polymer-based siRNA delivery: perspectives on the fundamental and phenomenological distinctions from polymer-based DNA delivery. *J Control Release 121*: 64-73
- (14) Tseng, S.-j. and Tang, S.-C. (2007). Development of Poly(amino ester glycol urethane)/siRNA Polyplexes for Gene Silencing. *Bioconjugate Chem. 18*: 1383-1390
- (15) Mao, S., Neu, M., Germershaus, O., Merkel, O., Sitterberg, J., Bakowsky, U. and Kissel, T. (2006). Influence of Polyethylene Glycol Chain Length on the Physicochemical and Biological Properties of Poly(ethylene imine)-graft-Poly(ethylene glycol) Block Copolymer/SiRNA Polyplexes. *Bioconjug Chem 17*: 1209-18
- (16) Pippin, C. G., Parker, T. A., McMurry, T. J. and Brechbiel, M. W. (1992). Spectrophotometric method for the determination of a bifunctional DTPA ligand in DTPA-mono-clonal antibody conjugates. *Bioconjug Chem 3*: 342-5

-
- (17) Kunath, K., von Harpe, A., Fischer, D., Petersen, H., Bickel, U., Voigt, K. and Kissel, T. (2003). Low-molecular-weight polyethylenimine as a non-viral vector for DNA delivery: comparison of physicochemical properties, transfection efficiency and in vivo distribution with high-molecular-weight polyethylenimine. *J Control Release* 89: 113-25
- (18) Fischer, D., Osburg, B., Petersen, H., Kissel, T. and Bickel, U. (2004). Effect of Poly(ethylene imine) molecular weight and PEGylation on organ distribution and pharmacokinetics of polyplexes with oligodeoxynucleotides in mice. *Drug Metab Dispos* 32: 983-992.
- (19) Urban-Klein, B., Werth, S., Abuharbeid, S., Czubayko, F. and Aigner, A. (2005). RNAi-mediated gene-targeting through systemic application of polyethylenimine (PEI)-complexed siRNA in vivo. *Gene Ther* 12: 461-6
- (20) Schiffelers, R. M. and Storm, G. (2006). ICS-283: a system for targeted intravenous delivery of siRNA. *Expert Opin Drug Deliv* 3: 445-54
- (21) Schiffelers, R. M., Ansari, A., Xu, J., Zhou, Q., Tang, Q., Storm, G., Molema, G., Lu, P. Y., Scaria, P. V. and Woodle, M. C. (2004). Cancer siRNA therapy by tumor selective delivery with ligand-targeted sterically stabilized nanoparticle. *Nucleic Acids Res* 32: e149
- (22) Kim, S. H., Jeong, J. H., Lee, S. H., Kim, S. W. and Park, T. G. (2008). Local and systemic delivery of VEGF siRNA using polyelectrolyte complex micelles for effective treatment of cancer. *J Control Release* 129: 107-16
- (23) Grzelinski, M., Urban-Klein, B., Martens, T., Lamszus, K., Bakowsky, U., Hobel, S., Czubayko, F. and Aigner, A. (2006). RNA interference-mediated gene silencing of pleiotrophin through polyethylenimine-complexed small interfering RNAs in

- vivo exerts antitumoral effects in glioblastoma xenografts. *Hum Gene Ther* 17: 751-66
- (24) Ge, Q., Filip, L., Bai, A., Nguyen, T., Eisen, H. N. and Chen, J. (2004). Inhibition of influenza virus production in virus-infected mice by RNA interference. *Proc Natl Acad Sci U S A* 101: 8676-81
- (25) Dykxhoorn, D. M., Palliser, D. and Lieberman, J. (2006). The silent treatment: siRNAs as small molecule drugs. *Gene Ther* 13: 541-52
- (26) Wang, D., Sima, M., Mosley, R. L., Davda, J. P., Tietze, N., Miller, S. C., Gwilt, P. R., Kopeckova, P. and Kopecek, J. (2006). Pharmacokinetic and biodistribution studies of a bone-targeting drug delivery system based on N-(2-hydroxypropyl)methacrylamide copolymers. *Mol Pharm* 3: 717-25
- (27) de Vries, E. F., Buursma, A. R., Hospers, G. A., Mulder, N. H. and Vaalburg, W. (2002). Scintigraphic imaging of HSVtk gene therapy. *Curr Pharm Des* 8: 1435-50
- (28) Kawabata, K., Takakura, Y. and Hashida, M. (1995). The fate of plasmid DNA after intravenous injection in mice: involvement of scavenger receptors in its hepatic uptake. *Pharm Res* 12: 825-30
- (29) Bumcrot, D., Manoharan, M., Koteliansky, V. and Sah, D. W. (2006). RNAi therapeutics: a potential new class of pharmaceutical drugs. *Nat Chem Biol* 2: 711-9
- (30) Behlke, M. A. (2006). Progress towards in vivo use of siRNAs. *Mol Ther* 13: 644-70
- (31) Morrissey, D. V., Lockridge, J. A., Shaw, L., Blanchard, K., Jensen, K., Breen, W., Hartsough, K., Macherer, L., Radka, S., Jadhav, V., Vaish, N., Zinnen, S., Vargeese, C., Bowman, K., Shaffer, C. S., Jeffs, L. B., Judge, A., MacLachlan, I. and Polisky, B. (2005). Potent and persistent in vivo anti-HBV activity of chemically modified siRNAs. *Nat Biotechnol* 23: 1002-7

- (32) Ishiwata, H., Suzuki, N., Ando, S., Kikuchi, H. and Kitagawa, T. (2000). Characteristics and biodistribution of cationic liposomes and their DNA complexes. *J Control Release* 69: 139-48
- (33) Ogris, M., Brunner, S., Schuller, S., Kircheis, R. and Wagner, E. (1999). PEGylated DNA/transferrin-PEI complexes: reduced interaction with blood components, extended circulation in blood and potential for systemic gene delivery. *Gene Ther* 6: 595-605
- (34) Chollet, P., Favrot, M. C., Hurbin, A. and Coll, J. L. (2002). Side-effects of a systemic injection of linear polyethylenimine-DNA complexes. *J Gene Med* 4: 84-91

6 Stability of siRNA polyplexes from poly(ethylenimine) and poly(ethylenimine)-g-poly(ethylene glycol) under in vivo conditions: Effects on pharmacokinetics and biodistribution measured by Fluorescence Fluctuation Spectroscopy and Single Photon Emission Computed Tomography (SPECT) imaging

Published in the Journal of Controlled Release 138 (2009) 148-159

6.1 Abstract

In search of optimizing siRNA delivery systems for systemic application, one critical parameter remains their stability in blood circulation. In this study, we have traced pharmacokinetics and biodistribution of each component of siRNA polyplexes formed with polyethylenimine 25 kDa (PEI) or PEGylated PEIs by in vivo real-time gamma camera recording, SPECT imaging, and scintillation counting of blood samples and dissected organs. In vivo behavior of siRNA and polymers were compared and interpreted in the context of in vivo stability of the polyplexes which had been measured by fluorescence fluctuation spectroscopy (FFS). Both pharmacokinetics and biodistribution of polymer-complexed siRNA were dominated by the polymer. PEGylated polymers and their siRNA polyplexes showed significantly less uptake into liver (13.6-19.7 % ID of PEGylated polymer and 9.5-10.2 % ID of siRNA) and spleen compared to PEI 25 kDa (liver deposition: 36.2 % ID of polymer and 14.6 % ID of siRNA). With non-invasive imaging methods we were able to predict both kinetics and deposition in living animals allowing the investigation of organ distribution in real time and at different time points. FFS measurements proved stability of the applied polyplexes under in vivo conditions which explained the different behavior of complexed from free siRNA. Despite their stability in circulation, we observed that polyplexes dissociated upon liver passage. Therefore, siRNA/(PEG-)PEI delivery systems are not suitable for systemic administration, but only if the first-pass effect can be circumvented, which is the case in local application.

6.2 Introduction

Systemic delivery of siRNA remains a challenging objective. Uncomplexed siRNA which is not chemically stabilized by modification of backbone or sugars will be fast degraded under in vivo conditions by serum nucleases (1-5). Therefore, appropriate formulations of siRNA are a prerequisite for systemic application, and biocompatible vectors that are stable in circulation and release their payload after endocytosis are required. A new method which allows quantification of integrity of siRNA/carrier systems under serum concentration comparable to in vivo conditions, Fluorescence Fluctuation Spectroscopy (FFS), has lately been described (6) and allows the measurement of polyplex integrity in serum-containing fluids as well as prediction of in vivo stability. As earlier described, FFS uses ultra-sensitive

avalanche photodiode detectors to monitor fluorescence intensity fluctuations caused by the diffusion of fluorescently labeled molecules throughout the excitation volume of a microscope (6).

As we reported earlier, Single Photon Emission Computed Tomography (SPECT) and planar imaging offers the possibility of assessing real-time pharmacokinetics and biodistribution in living animals (7). Radionuclide imaging with PET and SPECT, especially, combine the advantages of high sensitivity and good three-dimensional (3D) imaging (8). Pharmacokinetic parameters have, to our knowledge, only been reported for siRNA (9, 10), but not for their vectors. Other reports describing biodistribution of siRNA only mentioned fast renal clearance (11, 12) or effect on pharmacokinetics by formulation with cationic carriers (13), but in none of these, pharmacokinetic parameters, such as elimination half-lives, area under the curve (AUC) or clearance were determined. Soutschek et al. were the first to compare elimination half-lives and clearance of free and cholesterol-conjugated siRNA (10). Free siRNA was rapidly excreted through the kidneys with a half-life of 6 minutes, whereas the conjugate was shown to bind albumin and circulated much longer, exhibiting an elimination half-life of 95 minutes.

Our group previously described the fate of pDNA/(PEG-)PEI polyplexes after intravenous application of different non-viral vectors. But siRNA displayed different complexation behavior and siRNA complexes showed differences in physico-biological parameters compared to pDNA complexes (14-16). Therefore, monitoring pharmacokinetics and biodistribution of siRNA complexes by real-time gamma camera imaging, 3D localization using SPECT and scintillation counting of blood and organ samples were thought to give a more detailed insight into the biological performance and distribution of siRNA polyplexes after intravenous (i.v.) application in mice. In our earlier study, we were able to show that PEI 25 kDa as well as its PEGylated derivatives efficiently complex siRNA and offer protection against RNase degradation in vitro (17). But instability of pDNA/PEI complexes in vivo has been assumed in several reports (18-21). A double labeling approach of pDNA polyplexes showed differences in kinetics and deposition of load and vector and led to the conclusions that polyplexes dissociate after i.v. injection (20). Stability of siRNA/PEI complexes has, to our knowledge, not yet been quantified under in vivo conditions. As previously reported, we have already investigated stability of siRNA/(PEG-)PEI polyplexes in a competition assay with the polyanion heparin under in vitro conditions (17). But to determine in vivo stability, which would allow for predicting their behavior after i.v. injection, we made now use of fluorescence fluctuation spectroscopy (FFS). Combining this

method and determination of pharmacokinetic parameters and biodistribution of both vector and load permitted to finally quantify in vivo stability of siRNA/(PEG-)PEI delivery systems.

Additionally, PEGylation of cationic polymers has been reported to increase colloidal stability of the polyplexes and to reduce non-specific interaction with blood components (22), which in turn results in decreased uptake by the reticuloendothelial system (RES) and significant prolongation of circulation time of the PEGylated polyplexes (23). On the other hand, PEGylated polyplexes were reported to be less stable in blood, concerning integrity of the pDNA/PEG-PEI system (20, 24). This was explained by steric hindrance of polyplex formation due to PEG chains in the core of the polyplexes, a decreased number of primary amines and thermodynamic destabilization (20, 25). Yet, three other groups demonstrated significant prolongation of pDNA blood levels using PEGylated cationic polymers for packaging of the plasmid (23, 26, 27).

Another assumption which so far has not been investigated for siRNA/PEG-PEI polyplexes is the observation of a primary deposition of pDNA complexes in the lungs and a secondary redistribution (20, 28). Ishikawa et al. showed quantitative accumulation of pDNA-bearing positively charged liposomes in the lungs, which decreased from 90 % ID to 20 % ID over 120 minutes (28). In order to investigate if positively charged siRNA-bearing polyplexes would exhibit the same behavior, we employed planar gamma camera imaging and 3D SPECT imaging which allow for in vivo real-time and 3D-recording of pharmacokinetics and biodistribution, respectively (7).

6.3 Materials and Methods

Materials:

Amine-modified luciferase GL3 siRNA with a C6-NH₂ linker at each 3' of the double strand as well as the unaltered GL3 duplex and a non-specific siCONTROL duplex number IX was purchased from Dharmacon, Lafayette, CO, USA. Fluorescently labeled GL3 siRNA with Alexa488 ($\lambda_{\text{ex}} = 495 \text{ nm}$, $\lambda_{\text{em}} = 519 \text{ nm}$) at the 5' end of the sense strand was purchased from Eurogentec (Seraing, Belgium). 2-(4-isothiocyanatobenzyl)-diethylenetriaminepentaacetic acid (p-SCN-Bn-DTPA) was purchased from Macrocyclics (Dallas, TX, USA), Arsenazo(III), Yttrium(III) chloride, 2,4,6-Trinitrobenzenesulfonic Acid (TNBS), and Diethyl- pyrocarbonate (DEPC) from Sigma-Aldrich Laborchemikalien GmbH (Seelze, Germany). The miRACLE purification columns were purchased from

Stratagene (La Jolla, CA, USA), RNeasy Mini from Qiagen (Hilden, Germany), centricon YM-10 from Millipore (Millipore, Schwalbach, Germany), Vivaspin 2 MWCO 30 kDa from Sartorius Stedim Biotech GmbH (Göttingen, Germany), and PD-10 from Amersham Pharmacia Biotech (Freiburg, Germany). The radioactive substance $^{111}\text{InCl}_3$ was purchased from Covidien Deutschland GmbH (Neustadt a.d. Donau, Germany), and balb/c mice from Charles River WIGA (Sulzfeld, Germany). OptiMEM was purchased from Invitrogen (Merelbeke, Belgium), DMEM from PAA Laboratories (Cölbe, Germany), and fetal bovine serum (FBS) from Cytogen (Sinn, Germany). Polyethylenimine, PEI 25 kDa (PolyminTM, 25 kDa) was a gift from BASF (Ludwigshafen, Germany), polyethylene glycol grafted PEIs (PEG-PEIs) were synthesized as described previously (22), all other chemicals used were of analytical grade. All buffers used for siRNA-coupling were treated with 0.1 % DEPC.

Methods:

DTPA-coupling:

Amine-modified luciferase GL3 siRNA was coupled with p-SCN-Bn-DTPA as previously described (7, 29). Briefly, siRNA in siRNA buffer, adjusted to pH 8.5 with 0.2 M NaHCO_3 , was mixed with a 50 fold excess of p-SCN-Bn-DTPA dissolved in DMSO. The reaction mixture was incubated under constant shaking for 1 hour at room temperature, before 0.1 M citrate buffer, pH 5.0, were added to stop the reaction.

For DTPA-coupling of polymer, 5 mg PEI or 10.9 mg PEG-PEI (equivalent to 5 mg PEI) were dissolved in 250 μl water and adjusted to pH 8.5 with 0.2 M NaHCO_3 buffer. In order to achieve a DTPA coupling degree which would yield an amount of chelator per N/P 6 polyplex comparable to the amount obtained with the labeled siRNA, 2.9 μmol of the amines in 5 mg should be modified with DTPA. Therefore, 0.5 mg of p-SCN-Bn-DTPA in 29 μl DMSO were added to the polymer solution and reacted for one hour at room temperature. This reaction as well was stopped by addition of 0.1 M citrate buffer, pH 5.0, before the reaction mixture was purified by ultrafiltration using centricon YM-10 spin columns (Millipore, Schwalbach, Germany) as described below.

RNeasy spin column purification:

The DTPA-siRNA conjugate was purified from the excess of p-SCN-Bn-DTPA by using RNeasy columns. First of all, an ethanol precipitation was used to remove DMSO, which might interfere with the spin columns. This was accomplished by adding 737,5 μl 2 M sodium acetate buffer, pH 4.0, and 5.2 ml ethanol, which yielded in a total percentage of 70

% ethanol. The mixture was stored at -80 °C for 2 hours before it was centrifuged at 13,000 g for 15 minutes. The supernatant was discarded and the pelleted siRNA was resolved in 2.0 ml guanidinium salts containing “Binding Buffer” provided in the miRACLE kit, a kit especially designed for miRNA isolation. Purification was accomplished as previously described using RNeasy Mini spin columns (7). The coupling degree was determined after purification by quantification of DTPA in a non-radioactive UV-metric assay described by Pippin et al. (30).

Ultrafiltration:

Purification of polymers from non reacted p-SCN-Bn-DTPA was performed by ultrafiltration using centricon YM-10 ultrafiltration spin columns (Millipore, Millipore, Schwalbach, Germany) with a cut-off of 10 kDa. These columns were used as recommended by the manufacturer. Briefly, the reaction mixture was added to the column and centrifuged for about 2 hours at 5,000 g, until, except for a small amount of solution the whole sample had flown through. The columns were filled with water up to the 2 ml mark and the filtration procedure was repeated twice. After the second desalting step, the residual volume in the column was saved and diluted with 0.1 M sodium acetate buffer, pH 4.5, to 1 ml. The concentration of the purified sample was determined at 405 nm after formation of a picrate with 2,4,6-Trinitrobenzenesulfonic Acid (TNBS) in an assay previously described (31).

Radiolabeling:

Radiolabeling of the DTPA-coupled siRNA or polymer was accomplished in 0.1 M sodium acetate buffer, pH 5.4. Briefly, DTPA-coupled siRNA was annealed at 94 °C for 2 minutes and incubated with 30 MBq InCl₃ for 30 minutes at room temperature, followed by PD-10 size exclusion chromatography (SEC) and spin column concentration of peak fractions as described earlier (7). For polymer labeling, 300 µg DTPA-PEI (equivalent to 653 µg PEG-PEI) in 0.1 M sodium acetate buffer, pH 5.4, were incubated with 30 MBq ¹¹¹InCl₃ for 30 minutes at room temperature, followed by PD-10 SEC and concentration of peak fractions using centricon ultrafiltration.

PD-10 size exclusion chromatography (SEC):

SEC using PD-10 Sephadex G25 prepacked columns is a fast and easy method for desalting and can be used to remove free Indium after radiolabeling macromolecules. Radiolabeled

siRNA was treated as previously described (7), radiolabeled polymer was applied to the PD-10 column in the same way. Briefly, the column was equilibrated with PBS, the sample was applied and the flow through collected in fractions of 13 droplets each. RNA content was measured UV-metrically at 260 nm using a Pharmacia Ultrospec 2000 UV/VIS, Pharmacia Biotech, Freiburg, Germany, and radioactive signal in 10 μ l of each fraction was determined using a Gamma Counter Packard 5005, Packard Instruments, Meriden, CT, USA.

Those fractions that showed both a high radioactive signal and the strongest UV absorption at 260 nm for siRNA and at 405 nm for PEI after addition of TNBS, were combined and further purified as well as concentrated using spin columns as described above.

Polyplex preparation:

Polyplexes were formed in a self-assembly process relying on electrostatic interactions (32). A defined amount of positively charged polymer was added to a solution of negatively charged siRNA to yield different N/P ratios. For instance, 1.8 ng PEI correspond to 1 pmol of a 21mer duplex, if an N/P ratio of 1 is desired. Polyplexes were formed in 10 mM HEPES buffer by adding the polymer solution to the siRNA solution. Polyplexes were incubated for 10 minutes before they were further utilized for measurements or transfections.

FFS measurements:

Fluorescence fluctuation spectroscopy (FFS) measurements were performed on a MRC1024 Bio-Rad confocal laser scanning microscope equipped with a water immersion objective lens (Plan Apo 60X, NA 1.2, collar rim correction, Nikon, Japan). The laser beam was focused at about 100 μ m on a glass slide (Menzel-Gläser, Braunschweig, Germany), which contained the free Alexa488-siRNA or Alexa488-siRNA containing polyplexes (final concentration of 88.9 nM Alexa488-siRNA in all samples, except for blanks, for in vitro like experiments). Polyplexes were prepared in 10 mM HEPES buffer, pH 7.4 as described above, at N/P ratios 5, 10, and 15, and were added to either OptiMEM, OptiMEM containing FBS or pure fetal bovine serum (FBS) to result in 0 %, 10 % or 90 % FBS.

In order to mimic in vivo conditions, in a second setup, polyplexes of a concentration of 17.33 μ M siRNA were prepared at an N/P ratio of 6, of which 30 μ l were added to 400 μ l FBS, resulting in final concentration of 1.2 μ M siRNA and 93 % serum. The polyplexes were prepared by mixing polyplexes containing Alexa488-labeled (0.068 μ M final

concentration) and polyplexes containing non-labeled siRNA (1.14 μM final concentration). This approach was first of all chosen to avoid too many fluorescent particles that would generate overlapping peaks and would therefore impede the determination of an accurate baseline value, and second to adjust the fluorescence to that in the aforementioned measurements. Acquisition time for each measurement was 30 seconds. The first measurement was started after addition of polyplexes to medium, kinetics were observed over 60 minutes (0, 10, 20, 30, 60 minutes time points). The intensity of the two baselines (free and complexed siRNA) in the fluorescence fluctuations profiles were determined as previously described (6).

Size and Zeta-Potential measurements:

Dynamic light scattering (DLS) was employed to determine hydrodynamic diameters of the polyplexes, and laser Doppler anemometry (LDA) was utilized to measure their zeta potentials. Polyplexes were formed as described above by mixing 50 pmol DTPA-coupled or unaltered siRNA and the according amount of polymer for N/P 10. Complexes were incubated for 10 minutes and diluted to a total volume of 800 μl with 10 mM HEPES buffer, pH 7.4, to be measured using a Zetasizer Nano ZS (Malvern, Herrenberg, Germany). Position and attenuator were optimized by the device. Measurements were conducted in triplicates.

Cell Culture:

HeLa cells were purchased from Clontech (Saint-Germain-en-Laye, France) and transfected with a Luciferase Reporter Vector pTRE2hyg-Luc (Clontech, Saint-Germain-en-Laye, France) containing the luciferase reporter gene and a hygromycine resistance gene, as previously reported (33). Briefly, the plasmid was mixed with Lipofectamine and PLUS reagent (Invitrogen, Karlsruhe, Germany) as recommended by the manufacturer. Stably transfected cells were selected by treating the cells with a culture medium containing 200 $\mu\text{g/ml}$ hygromycine B (Invitrogen, Karlsruhe, Germany). Clones were propagated and characterized concerning luciferase expression and proliferation rate. One of the clones was picked to be further propagated. Cells were maintained in DMEM (PAA Laboratories, Cölbe, Germany), supplemented with 10 % fetal bovine serum (Cytogen, Sinn, Germany), in humidified atmosphere with 5 % CO_2 at 37°C.

In vitro transfection experiments:

For transfections, HeLa/Luc cells were seeded in 96 well plates (Thermo Fisher Scientific (Nunc GmbH & Co. KG), Langenselbold, Germany) with a density of 8,000 cells per well. Medium was changed 24 hours later and polyplexes of 20 pmol siGL3 or siCONTROL per well (88.9 nM) and an N/P ratio of 10 were added in the full serum-containing medium. Control cells were treated with free siRNA only. As a positive control, siGL3 was added as lipoplexes formed with Lipofectamine2000 (Invitrogen, Karlsruhe, Germany); lipoplexes of Lipofectamine and siCONTROL were considered the negative control. The medium was changed 4 hours post transfection, and cells were incubated for another 44 hours before they were washed with PBS, lysed with CCLR (Promega, Mannheim, Germany), and assayed for luciferase expression with a commercial luciferase assay kit (Promega, Mannheim, Germany) on a BMG LUMIstar OPTIMA luminometer plate reader (BMG Labtech, Offenburg, Germany).

Albumin binding assay:

Binding of siRNA to plasma proteins like albumin was detected in an albumin binding assay previously described by Geary et al. (34). Briefly, an albumin stock solution of 450 mg/ml and 0.005 % Tween 80 was prepared in phosphate buffered saline (PBS), pH 7.4. Polyplexes at N/P 6 or free radioactively labeled siRNA were added to DMEM containing no, 4.5 mg/ml or 45 mg/ml albumin, which is a physiological concentration. According to Zini et al. (35), these concentrations equal monomer concentrations of 3.37 or 16.77 mg/ml, respectively, assuming a K_d of 150 μ M for the monomer-dimer equilibrium. Final siRNA concentration was chosen to be 1.2 μ M as in the in vivo experiments. Solutions were incubated for one hour at 37 °C and loaded to low binding polyethersulfone (PES) Vivaspin columns (Sartorius Stedim Biotech GmbH, Göttingen, Germany) with a molecular weight cut-off of 30,000 Da. After centrifugation for 15 minutes at 735 g, aliquots of unfiltered and filtered solutions were measured for siRNA content using a scintillation counter.

Animal studies:

All animal experiments were carried out according to the German law of protection of animal life and were approved by an external review committee for laboratory animal care. For in vivo experiments, 4 weeks old balb/c mice (~ 20 g), were injected with 35 μ g DTPA-siRNA, corresponding to 2.57 nmol and 255 kBq. siRNA was either administered as free duplexes or after complexation at N/P 6 with 25 kDa branched PEI, PEI(25kDa)-PEG(2kDa)₁₀, or PEI(25kDa)-PEG(20kDa)₁. Pharmacokinetics of each component were

observed over 2 hours by retroorbitally drawn blood samples of 25 μ l at certain time points. Biodistribution over a period of about 25 minutes, depending on the individual depth of anesthesia in each animal, was observed non-invasively by dynamic real-time gamma camera imaging acquired with a Siemens e.cam gamma camera (Siemens AG, Erlangen, Germany) (7). Static planar and SPECT images were taken at later time points using a custom built multiplexing multipinhole collimator mounted on the Siemens e.cam gamma camera. Two-dimensionally acquired data was quantified by analysis of regions of interest (ROIs) as previously described (7). Two hours after i.v. injection, animals were sacrificed; organs were dissected and analyzed for deposition of radioactive material by gamma scintillation counting on a Packard 5005 Gamma Counter (Packard Instruments, Meriden, CT, USA).

Data analysis and statistics:

Analytical measurements were conducted in triplicates, transfection experiments in quadruplets. Animal experiments included 5 animals per group; results are given as mean values \pm standard deviation (SD). Two way ANOVA and statistical evaluation was performed using Graph Pad Prism 4.03 (Graph Pad Software, LaJolla, USA). Pharmacokinetic parameters were determined using Kinetica 4.4.1 (Thermo Electron Corporation, Karlsruhe, Germany).

6.4 Results and Discussion

Since neither stability under in vivo conditions nor pharmacokinetic parameters of siRNA/(PEG-)PEI polyplexes have so far been investigated, in this study, we addressed the stability issue under serum concentration comparable to in vivo conditions by FFS measurements and the pharmacokinetics by detection of radiolabeled polyplexes. To investigate the influence of PEGylation, we chose three polymers: branched PEI 25 kDa (PEI 25) and two PEGylated derivatives with different grafting degree but the same percentage of PEI content, being 46 % of the copolymer. The PEGylated PEIs used in this study were one copolymer with 10 short 2 kDa PEG chains, which can be described by the formula PEI(25kDa)-PEG(2kDa)₁₀, and another PEI derivative with only one long PEG chain, named PEI(25kDa)-PEG(20kDa)₁.

Radiolabeling:

The optimized procedure for radiolabeling and purification of coupled and labeled siRNA, which we have reported lately (7), enabled us to track kinetics and deposition of siRNA. But in order to investigate in vivo behavior of both vector and load, which would allow us to compare kinetics and distribution of the vector to that of the load, and would therefore provide us with information on in vivo stability of the polyplexes, it was necessary to radiolabel the polymers as well. The polymers could easily be separated from p-SCN-Bn-DTPA by ultrafiltration. This can be explained by their high reactivity due to an excess of primary amines that can be coupled. Therefore, it can be assumed that no or only small amounts of unreacted p-SCN-Bn-DTPA were left in the reaction mixture. Purification after radiolabeling was not necessary as shown in Figure 1A-C. Quality control SEC on a PD-10 column showed neither significant amounts of DTPA (peaks at fractions 10-12) nor of free Indium (peaks at fractions 15-19, compare (7)). In order to investigate if parts of the hot Indium had not stably been chelated by DTPA but non-specifically bound by free valences of PEI and would therefore be released upon complexation of siRNA, we formed complexes with a small aliquot of radiolabeled PEI and applied it on a PD-10 column. In the eluted fractions, the UV signal for siRNA and the radioactive signal showed concurrence, and free Indium was not observed (see Figure 1D).

Quality Control of Labeled Polymer and Polyplex

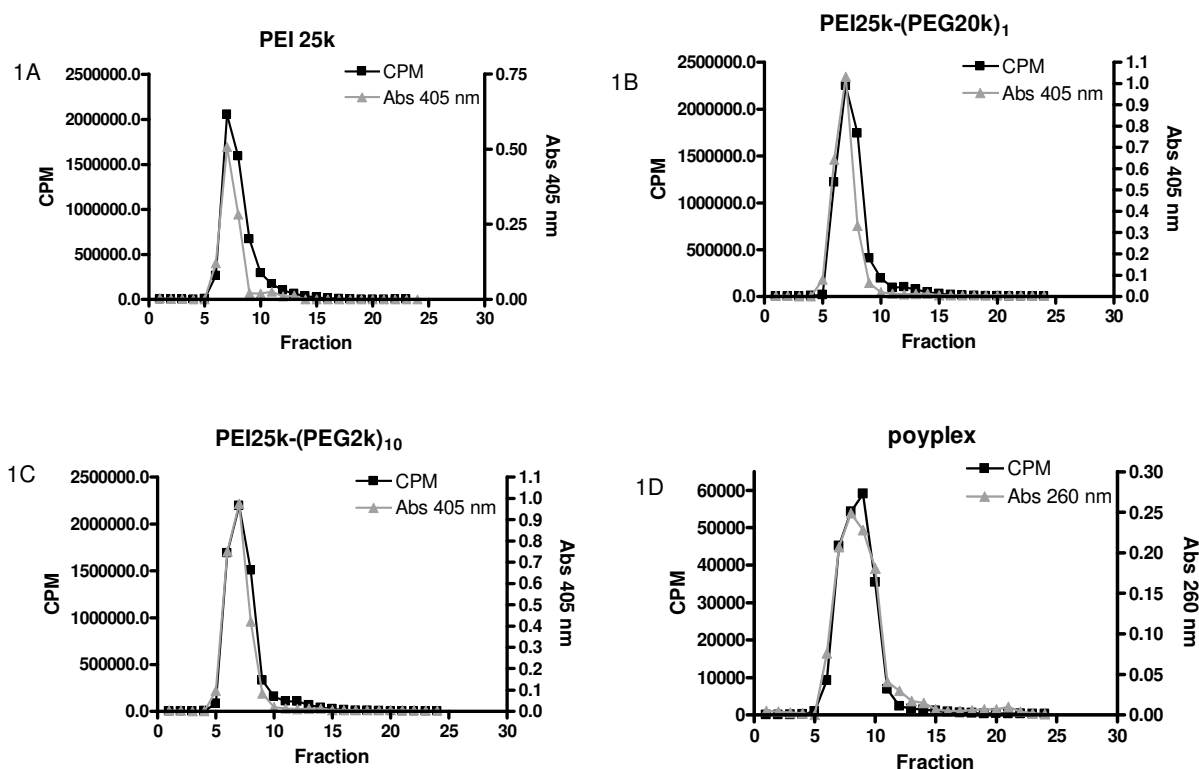


Figure 1: PD-10 size exclusion chromatograph of A-C: radiolabeled polymers. Neither free DTPA nor Indium was observed in later fractions. The tailing of the polymer peak can be explained by the polydispersity of the polymer. D: radiolabeled PEI after complex formation.

Fluorescence Fluctuation Spectroscopy (FFS):

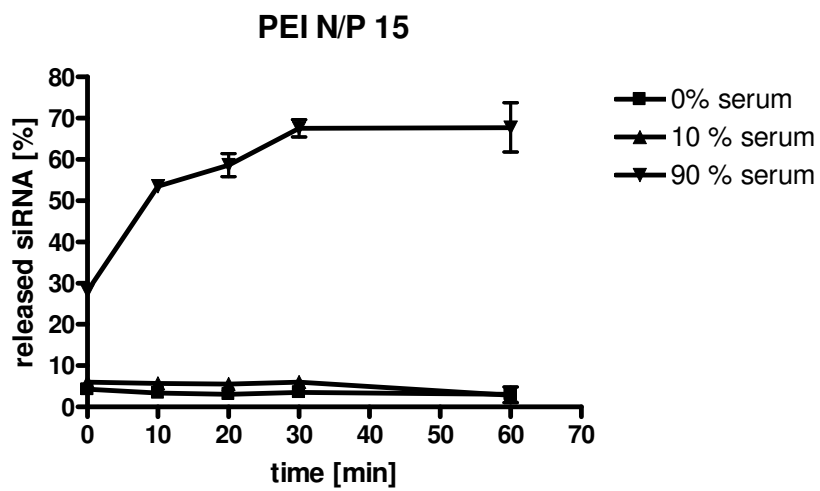
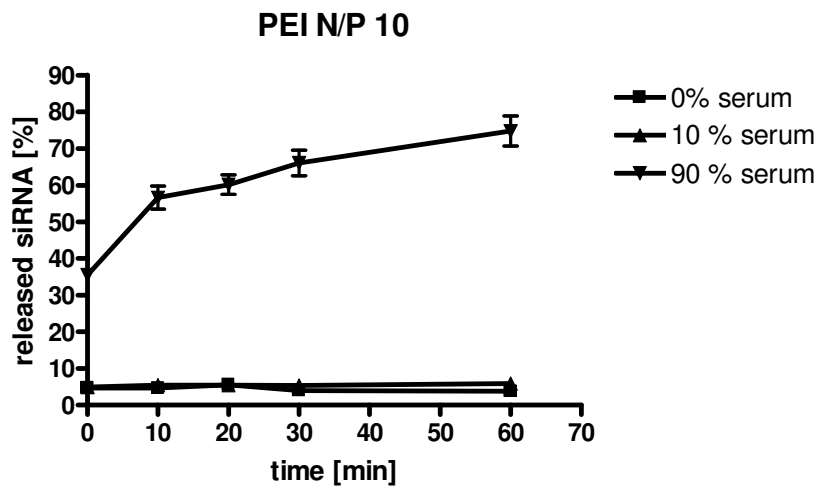
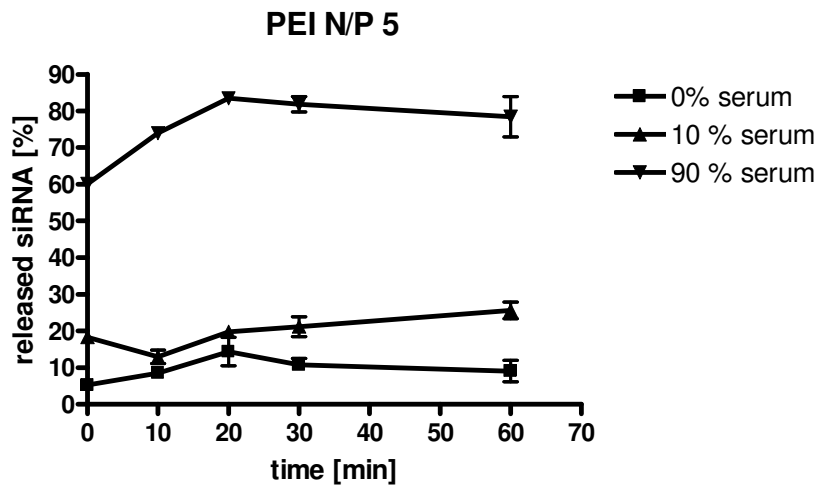
One of the aims of this study was to correlate biodistribution and pharmacokinetics of our polyplexes with their stability in serum. Therefore, we used fluorescence fluctuation spectroscopy (FFS), a sophisticated method for detection of release of siRNA from polyplexes under cell culture and in vivo conditions. As previously described (6), the amount of free fluorescently labeled siRNA can be quantified in presence of serum in an FFS measurement. In a solution of free fluorescently labeled siRNA, the fluorescence signal is proportional to the concentration of siRNA. When the siRNA is complexed in nanoplexes, the fluorescence baseline, caused by freely moving siRNA, drops and highly fluorescent peaks, that originate from nanoplexes containing large amounts of siRNA, occur. Since the fluorescence baseline is proportional to the amount of free siRNA that is present, the degree of association and dissociation can be calculated proportionally to the

differences between the signals for blank, free siRNA, and complexed siRNA as described by Buyens (6).

Little is known about structural changes and instability of polyplexes *in vivo*. To our knowledge, so far polyplexes made of PEG-PEI and siRNA have only been characterized prior to administration which doesn't allow for a prediction of their *in vivo* behavior. Instability (20) and premature polyplex unpacking (21) have been assumed in various reports and have been made responsible for a different *in vivo* biodistribution of polymer and load (20) or the delivery of the load to a lesser extent (21), but this assumption has not been verified by quantification under serum concentration comparable to *in vivo* conditions. The FFS measurements we performed, finally allowed us to interpret biodistribution and pharmacokinetics in the context of complex stability *in vivo*.

In order to mimic *in vitro* conditions of our actual transfection experiments, all concentrations were chosen to match the standard transfection procedure. Since we were interested in the influence of serum on polyplex stability, we observed siRNA release from polyplexes at N/P 5, 10 or 15 at 0 %, 10 % and 90 % FBS, as shown in Figure 2A. While 10 % serum didn't seem to affect stability of PEI complexes at an N/P of 10 or higher, release of 75 % for N/P 5 and about 55 % for N/P 10 and 15 were observed in the first 10 minutes upon addition to 90 % serum-containing medium. After 60 minutes of incubation in this medium, complexes of N/P 5 released almost the total load of siRNA, and complexes of N/P 10 and 15 still showed very low stability and a release of about 70 % of the load. Very similar profiles were observed for the PEGylated PEIs (data not shown). As for cell culture experiments the relevant concentration of serum is 10 %, all release profiles at this concentration are shown in Figure 2B. Interestingly, strong differences could be observed for the various polymers. The unmodified PEI 25 kDa exhibited the most stable complexes, which can easily be explained by the charge density of the polymer. But even the two differently PEGylated PEIs showed remarkable differences in their release profiles. To our surprise, PEI-PEG(20k)₁ offered less stability than PEI-PEG(2k)₁₀ although it had protected siRNA better from RNase degradation in an *in vitro* assay in our earlier publication (17). In the aforementioned assay, polyplexes were formed in 5 % glucose solution and treated with increasing amounts of RNase. No serum or high ionic strength buffers had been used. But in the heparin competition assay, concentrations as low as 0.07 IU/ μ g RNA released almost the complete load (17). The comparison to only about 50 % release of pDNA at a heparin concentration of 0.25 IU/ μ g DNA (36) emphasizes the fact that siRNA/(PEG-)PEI polyplexes are even *in vitro* less stable than pDNA polyplexes.

A



B

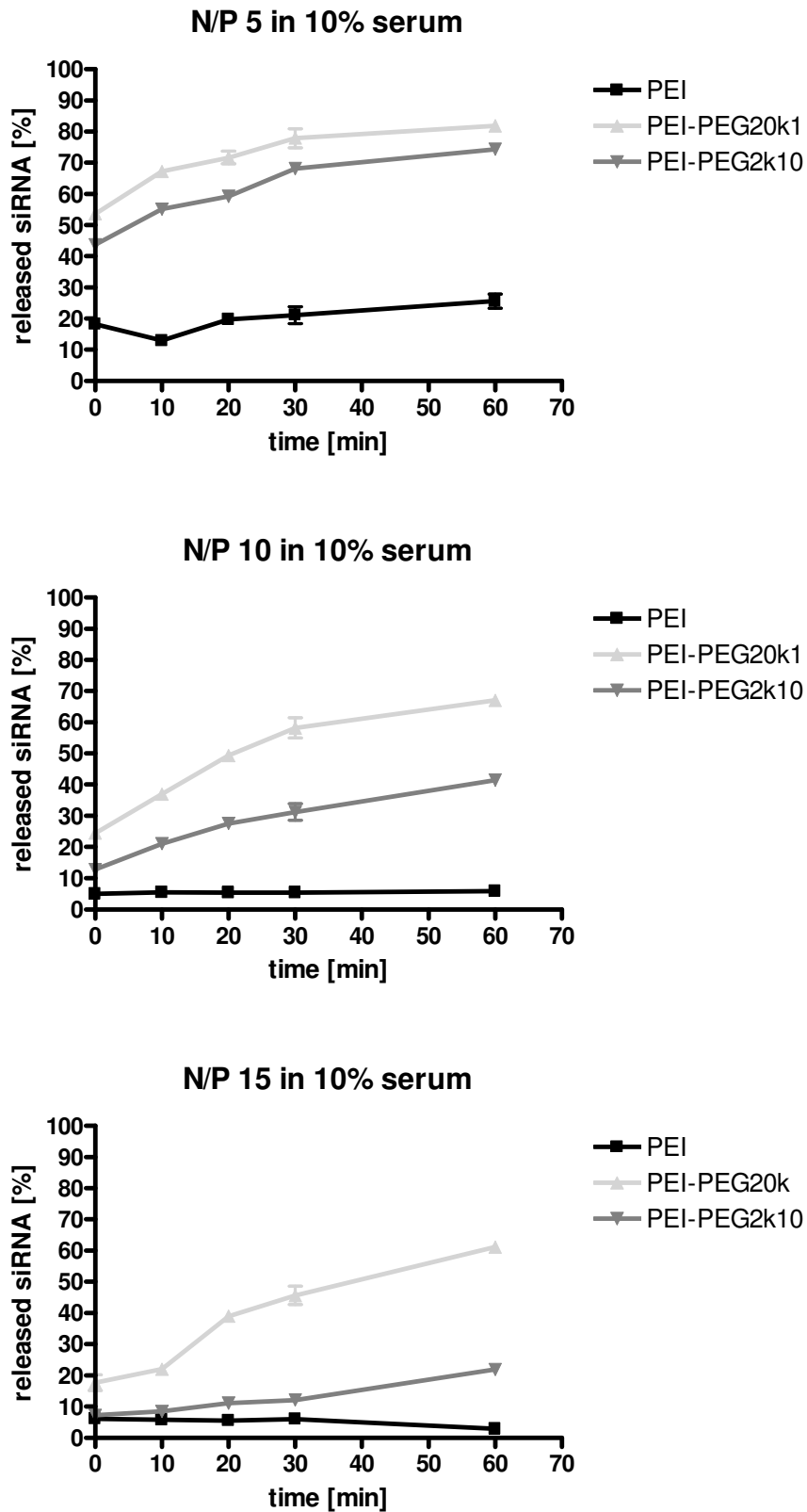


Figure 2A: FFS measurements showing siRNA release from PEI 25 kDa polyplexes prepared at 88.9 nM final siRNA concentration and N/P 5, 10, and 15 in 0-90 % serum-

containing medium. Figure 2B: FFS measurements showing siRNA release from PEI 25 kDa and PEG-PEI polyplexes prepared at 88.9 nM final siRNA concentration and N/P 5, 10, and 15 in 10 % serum-containing medium.

In the FFS assays, relationships (i) between stability and N/P ratio, and (ii) between stability and PEG chain length were found. At N/P 5, both PEGylated polymers were not able to form stable complexes, reflected in a fast and almost complete release of siRNA in 10 % serum-containing medium. But by increasing the N/P ratio to 10, differences in stability depending on the PEGylation pattern became clearer. While PEI-PEG(20k)₁ complexes released more than 50 % of siRNA, PEI-PEG(2k)₁₀ complexes showed only 40 % release during an incubation period of 60 minutes. These differences became even more prominent at N/P 15, where PEI-PEG(2k)₁₀ complexes showed only a slightly different release profile from PEI complexes, but PEI-PEG(20k)₁ complexes still released more than 50 % of their load during 60 minutes of incubation at 37 °C. Stability of polyplexes in 90 % serum-containing medium was observed at the same concentration as used in the *in vivo* experiments and at N/P 6, which had been chosen for i.v. injections. As shown in Figure 3 and assumed earlier (20), stability is very much depending on polyplex concentration. At this about 13.5 fold higher concentration, differences in the profiles of the two PEGylated polymers were much less prominent than at the *in vitro* concentration. PEI 25 kDa again exhibited the most stable polyplexes which showed almost no release of siRNA. The PEGylated polymers, on the other hand, set 12.6 % (PEI-PEG(2k)₁₀) or 15.5 % (PEI-PEG(20k)₁) of their load free over 60 minutes of incubation at 37 °C, which encouraged us to apply polyplexes of an N/P ratio as low as 6 in our *in vivo* study.

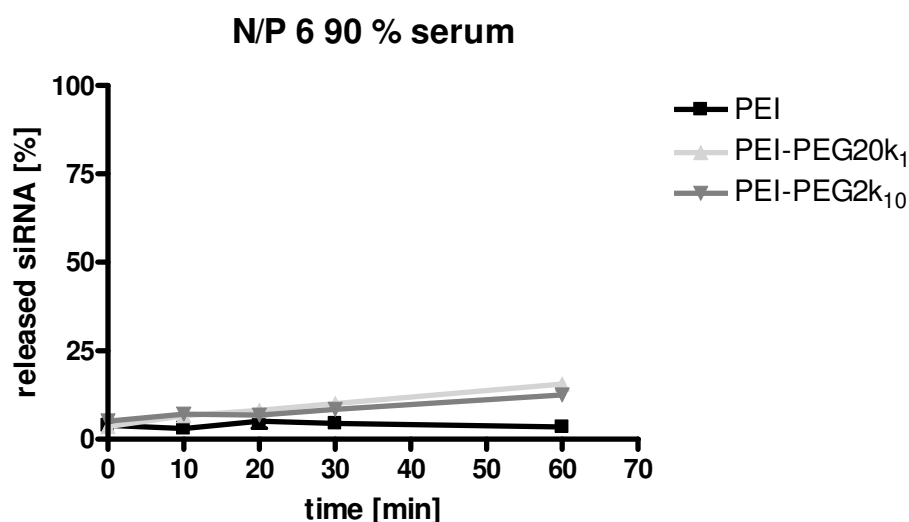
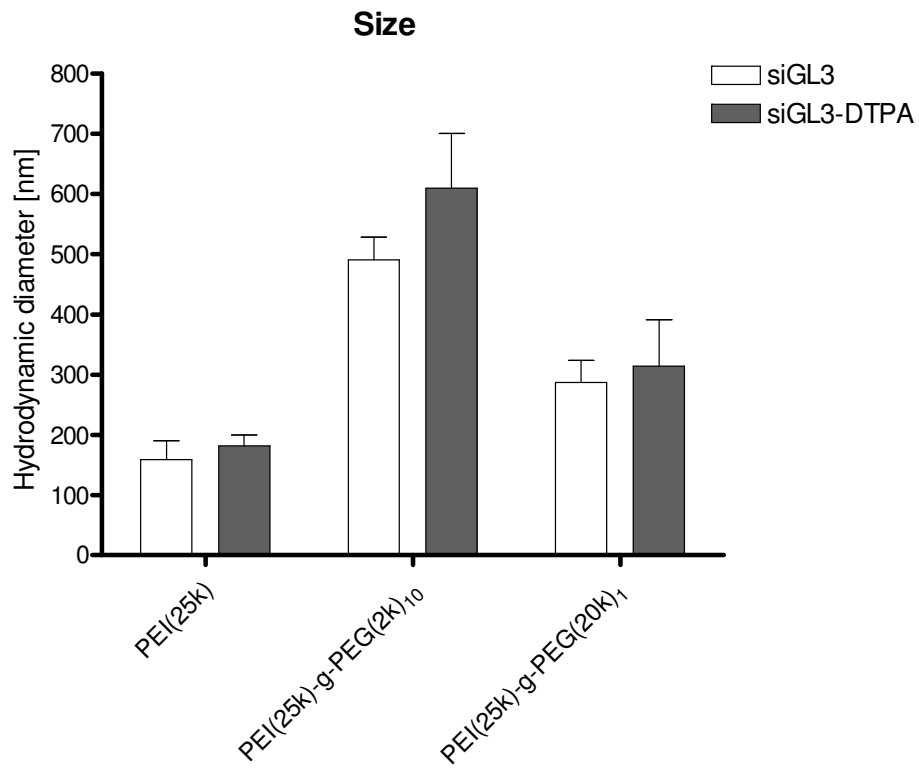


Figure 3: FFS measurements showing siRNA release from PEI 25 kDa and PEG-PEI polyplexes prepared at 1.2 μ M final siRNA concentration and N/P 6 in 90% serum-containing medium.

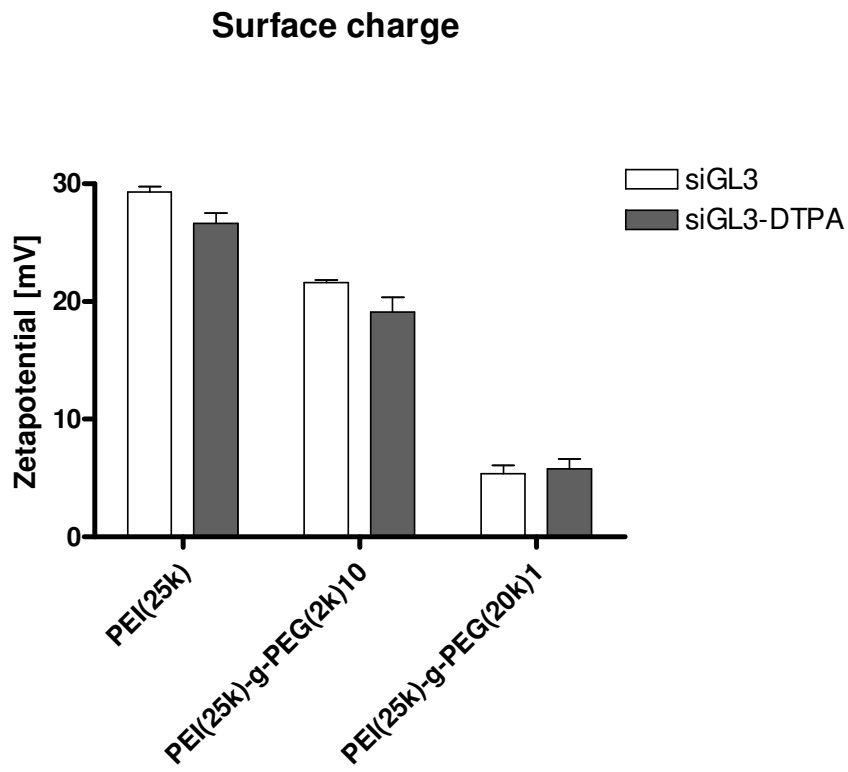
Physical characterization of polyplexes:

To further characterize the polyplexes and to determine if the C₆-thiourea coupled Bn-DTPA would affect siRNA complex formation, we measured sizes and zeta potentials of polyplexes formed with the unmodified duplex siGL3 and the Bn-DTPA coupled thiourea derivative of siGL3. No significant differences ($p > 0.05$) concerning size (Fig. 4A) or surface charge (Fig. 5B) were found in between the groups of the same polymer but different duplexes. Interestingly, PEI-PEG(2k)₁₀ formed much bigger complexes with siRNA in HEPES buffer than PEI or PEG(20k)₁. This is in accordance with our previous findings reporting that a large amount of PEG chains impedes electrostatic interaction between polycation and polyanion and therefore hampers condensation into small particles (17, 37). The influence of PEGylation on zeta potential is shown in Figure 4B and can be explained by the core-shell structure which has been stated by us and others (17, 29, 38). According to the findings of our FFS measurements, this hypothesis of a PEG corona only holds true for measurements in the absence of serum. But this outer PEG shell is drawn for the decrease of surface charge, which is especially dramatic for the copolymer bearing the 20 kDa PEG chain.

4A



4B



4C

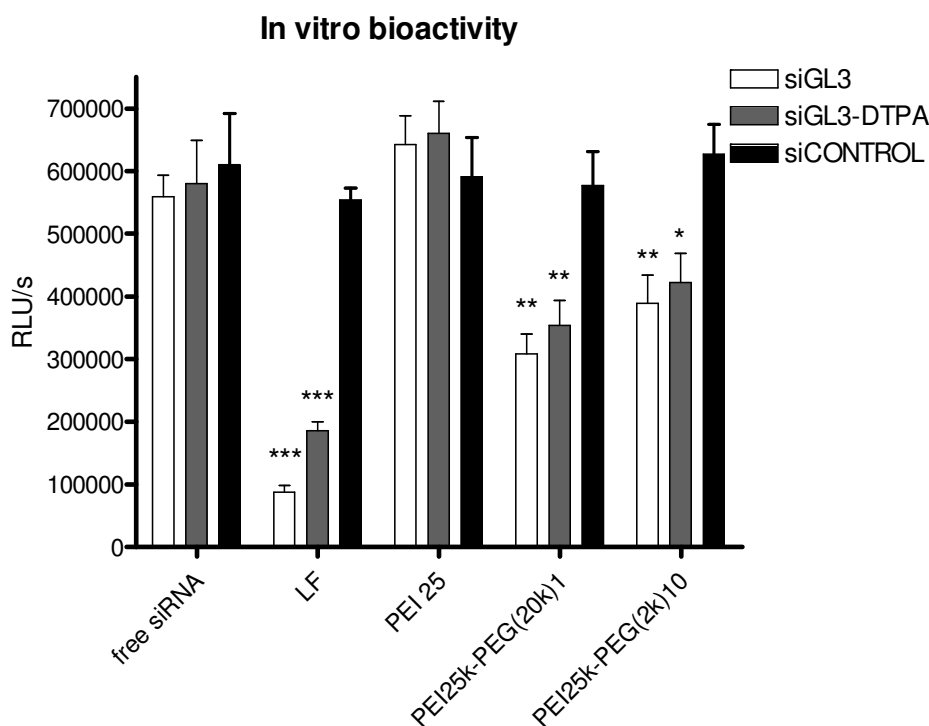


Figure 4A: Sizes of PEI 25 kDa and PEG-PEI polyplexes prepared with siGL3 or the Bn-DTPA coupled thiourea derivative of siGL3 (siGL3-DTPA), determined by dynamic light scattering. 4B: Zeta potentials of PEI 25 kDa and PEG-PEI polyplexes prepared with siGL3 or the Bn-DTPA coupled thiourea derivative of siGL3 (siGL3-DTPA) determined by laser Doppler anemometry. Derivatization of siRNA did neither affect size nor zeta potential significantly. 4C: Transfection of HeLa/Luc cells stably expressing firefly Luciferase with siGL3, the Bn-DTPA coupled thiourea derivative of siGL3 (siGL3-DTPA) or a scrambled control sequence (siCONTROL) after complexation of siRNA with Lipofectamine 2000 (LF), PEI 25 kDa or PEG-PEI. Derivatization of siRNA did not affect knockdown efficacy significantly.

In vitro bioactivity of polyplexes:

Functionality of the labeled siRNA was investigated in vitro in siRNA transfection experiments of the stably luciferase expressing cell line HeLa/Luc. Sequence specific knockdown of luciferase expression was checked for by comparison of the effects of a random control duplex. Since FFS measurements had revealed that PEG-PEI-complexes at

N/P 5 were not stable in 10 % serum, polyplexes were formed at N/P 10 for in vitro transfections.

As a result, we found no significant differences between the knockdown efficiency of the non-labeled and the labeled duplex of the same sequence. Downregulation of luciferase expression in the constitutively luciferase expressing cell line compared to non-specific control was highly significant (***) $p < 0.001$) for Lipofectamine 2000 and significant (** $p < 0.01$, * $p < 0.05$) for PEG-PEI polyplexes (compare Figure 4C). No effect was observed for PEI polyplexes, as earlier reported (17). Considering the stability of these polyplexes, it can be hypothesized that siRNA is too tightly bound to PEI and therefore not available for incorporation into RISC inside the cell. PEI-PEG(20k)₁ which had shown lowest stability in the FFS measurements yielded the highest knockdown efficiency among the polyplexes. PEI-PEG(2k)₁₀ polyplexes which had proven higher stability mediated less downregulation of luciferase expression which could also be explained by the larger size of these polyplexes.

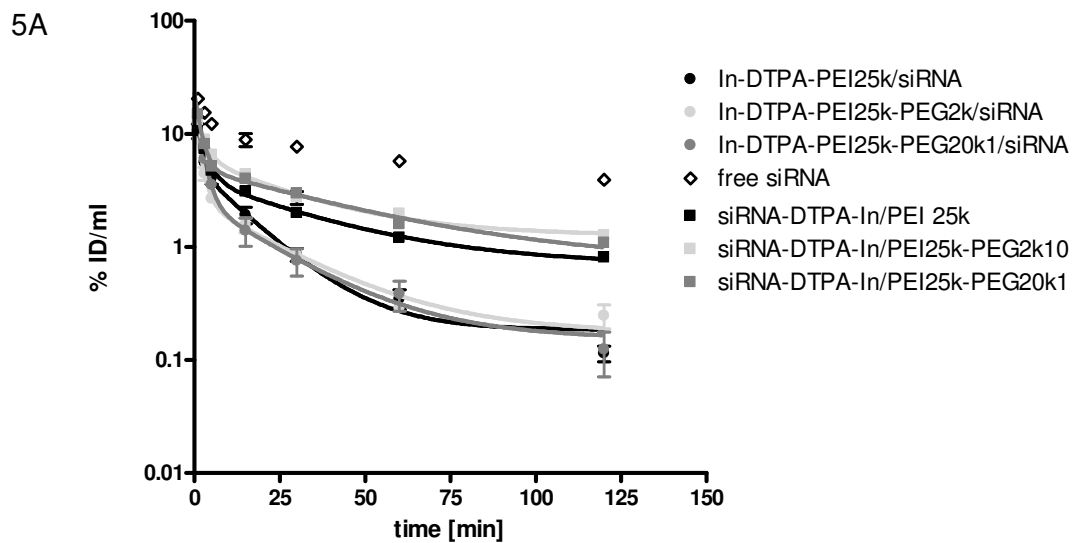
In vivo experiments:

After thorough characterization of the polyplexes, pharmacokinetics and biodistribution of both the vector and the load were determined in two different sets of experiments. An optimal experiment would enable simultaneous detection of double-labeled polyplexes. Double-isotope detection is possible, but the signal of ¹¹¹In would, e.g., interfere with the detection of ^{99m}Tc. Therefore, in the first set, radioactively labeled siRNA was intravenously applied either as free siRNA, as reported earlier (12), or after complexation with PEI or PEG-PEI. These materials have earlier been characterized concerning in vivo biodistribution and pharmacokinetics after complexation of pDNA and ODNs (20, 24, 39) and have recently been used for in vivo siRNA delivery (40-45).

For a better understanding of the fate of each component of the polyplexes, seen in the context of stability of polyplexes, we performed another set of experiments. Here, polyplexes were formed with radiolabeled polymer and non-labeled siRNA. The same amount of polyplex as in the first set was applied by i.v. injection. Data from scintillation counting of blood samples were analyzed with Kinetic 4.1.1 (Thermo Electron Corporation, Karlsruhe, Germany) and fitted to a biphasic exponential IV bolus equation ($C(t) = Ae^{-at} + Be^{-bt}$).

Pharmacokinetics of vector and load:

Analysis of blood clearance of labeled siRNA revealed strong differences between complexed and free siRNA. As shown in Figure 5A, all profiles of complexes, no matter if siRNA or polymers were labeled, exhibited a fast and steep alpha phase, in which the polyplexes are assumed to be deposited in a deeper compartment. Statistic analysis of alpha (elimination constant of alpha phase) and A (coefficient of alpha phase) values revealed neither significant differences between the different polyplexes nor between vector and load ($p > 0.05$). The rapid deposition phase, which lasted only a few minutes for each component observed, can be characterized by $t_{1/2 \text{ alpha}}$ half-lives of 4.0 minutes, 2.7 minutes, and 1.6 minutes for complexed siRNA and 0.6 minutes, 1.3 minutes, and 1.5 minutes for the polymers PEI 25kDa, PEI-PEG(2k)₁₀, and PEI-PEG(20k)₁, respectively (compare Figure 5B). The alpha phase was followed by a flatter beta elimination phase. Half-lives $t_{1/2 \text{ beta}}$ determined for complexed siRNA, were 84.9 minutes (PEI 25kDa), 55.1 minutes (PEI-PEG(2k)₁₀), and 44.8 minutes (PEI-PEG(20k)₁), a trend that mirrors stability of the different polyplexes. The values calculated for the different polymers (10.7 minutes, 20.1 minutes, and 19.9 minutes, respectively) did not reveal strong differences, as shown in both Figures 5A and 5B. Both alpha and beta half-lives of polymers and nucleic acids are in very good agreement with values previously described for pDNA/(PEG-)PEI polyplexes (20). Alpha and beta half-lives of free siRNA are comparable to values reported for ⁶⁴Cu-DOTA labeled 5'-amino-C6-modified siRNA ($t_{1/2 \text{ alpha}} = 2.4$ minutes and $t_{1/2 \text{ beta}} = 61.9$ minutes) that was applied in a comparable concentration (2.5 mg/kg vs. 1.75 mg/kg in our study) and investigated by PET (46).



5B

	AUC [min*%/ml]	±	alpha [min]	±	beta [min]	±	CL [ml/min/kg]	±	MRT [min]	±	V _{ss} [ml/kg]	±
PEI25k/DTPA-siRNA	283,7	55,6	4,0	2,3	84,9	31,6	13,0	1,8	68,5	30,3	1056,3	160,8
PEI25k-PEG(2k)10/DTPA-siRNA	404,0	76,4	2,7	0,8	55,1	6,7	8,6	1,3	70,0	6,8	855,5	237,8
PEI25k-PEG(20k)1/DTPA-siRNA	351,9	13,2	1,6	0,1	44,8	8,1	10,0	1,1	57,1	7,9	770,9	154,7
free DTPA-siRNA	1298,5	181,8	2,9	1,4	93,2	12,1	3,1	0,4	129,0	15,7	404,8	109,7
PEI25k-DTPA/siRNA	114,6	31,8	0,6	0,2	10,7	1,5	30,6	5,6	12,4	2,3	932,1	260,6
PEI25k-PEG(2k)10-DTPA/siRNA	93,1	20,7	1,3	0,4	20,1	2,1	41,5	11,5	22,8	3,4	1197,8	190,9
PEI25k-PEG(20k)1-DTPA/siRNA	104,1	46,5	1,5	0,2	19,9	5,5	38,3	17,3	19,6	8,9	972,3	16,6

Figure 5A: Pharmacokinetics of each single component of polyplexes containing 35 µg siRNA in balb/c mice. Labeled polymers (circles) showed more rapid elimination from circulation than labeled siRNA (squares). 5B: Kinetic parameters of labeled siRNA (upper half), free siRNA and labeled polymers (lower half) are listed in the table. AUC, area under the curve; alpha, half-life in alpha phase; beta, half-life in elimination (beta-) phase; CL, clearance; MRT, mean residence time; V_{ss}, steady state volume of distribution.

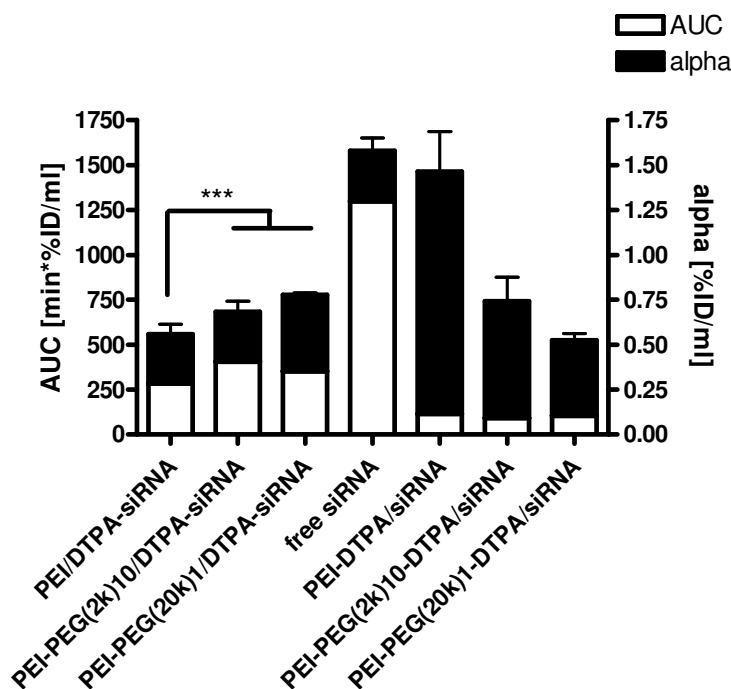


Figure 6: Analysis of kinetics parameters: Analysis of the values for area under the curve (AUC, left y axis in $\text{min} \cdot \% \text{ID}/\text{ml}$) revealed significant differences between PEI and PEG-PEI complexed siRNA ($***p < 0.001$) as well as between load and vector for each type of polyplex. Analysis of alpha (right y axis in $\% \text{ID}/\text{ml}$) showed strong differences in the rapidness of clearance from circulation between PEI and PEG-PEI as well as between load and vector.

Differences between area under the curve (AUC) values of load and vector were highly significant ($p < 0.001$) for each polyplex, which is in agreement with previously reported data concerning pDNA polyplexes (20). AUC of free siRNA was found to be highly significantly ($p < 0.001$) larger than all of the AUC values of complexed siRNA. Interestingly, we also observed highly significant ($***p < 0.001$) differences between AUC of PEI and PEG-PEI complexed siRNA as shown in Figure 6. The difference in this parameter can be explained by a difference in stability of the polyplexes as determined by FFS, but it also has to be seen in context of deposition of the polyplexes. As Figure 8 shows, PEI complexes were held back by the liver to a much higher extent than PEG-PEI complexes. This causes a lower bioavailability, shorter circulation time and smaller AUC value. AUC values and other pharmacokinetic parameters for free and complexed siRNA have previously been reported by Li et al. (9). In their study, FAM-labeled siRNA was applied at a dose of 1.2 mg/kg, and data were acquired by fluorescence detection. The

elimination half-life of only 15 min reported for free siRNA in tumor-free mice is much shorter than in our study or in the one described by Bartelett et al. (46). This is probably due to the C6-modification of the siRNA used by us and Bartelett. Other parameters such as Clearance, AUC, Mean Residence Time (MRT) and Steady State Volume of Distribution (V_{ss}) were affected by this modification, as well. Free siRNA circulated much longer in our study, leading to a longer elimination time, a bigger AUC, a slower clearance, a longer MRT and a larger V_{ss} . The nanoparticles described by Li et al., on the other hand, showed enhanced circulation, characterized by a longer elimination half-life, a strongly greater AUC, a much slower clearance, much longer MRT and smaller V_{ss} in tumor-free mice. Obviously, their nanoparticles were stable and did not show high uptake by the RES.

Albumin binding of modified siRNA:

An unexpected result was that free siRNA seemed to stay in circulation longer than any other component. Since the profiles of complexed siRNA were obviously driven by the polymer, differences between free siRNA and complexed siRNA confirmed that polyplexes were stable in circulation to a certain extent. But unmodified siRNA is actually known to be renally excreted even faster than it can be degraded (47). In our particular case, this was not true and was assumed to be caused by the C6-modification or the coupling of DTPA. As siRNA is degraded rapidly in vivo by serum nucleases, the radioactive signal measured in the blood samples most likely was caused by fragments of siRNA still bearing the label. As previously stated (7), it is one of the major drawbacks of radioactive end-labeling techniques that the signal measured does not differentiate between intact and degraded material. In order to find out, why these labeled fragments remained longer in circulation than complexed siRNA, binding of the C6-modified siRNA to serum proteins was investigated in an albumin binding assay. It has been reported that lipophilic siRNA, such as 2'-O-(2-Methoxyethyl)-modified siRNA (34) or lipid-conjugated siRNA, in contrast to unmodified siRNA (48) substantially binds to albumin which prevents glomerular filtration yielding in prolonged circulation times and higher bioavailability. As shown in Figure 6, the C6-thiurea-DTPA conjugated siRNA we used exhibited strong binding to albumin both at a low concentration of 4.5 mg/ml and the physiologic concentration of 45 mg/ml. But since the addition of an end-label did not protect siRNA from nuclease digestion, the higher AUC value and the longer circulation time observed for our free siRNA has to be interpreted critically. Degradation of siRNA can be prevented or retarded by chemical modification of the nucleotides, the backbone or by complexation with an appropriate delivery system (49-

51). In our earlier publication, we showed that PEI 25 kDa as well as PEGylated derivatives protected siRNA from RNase degradation (17). The albumin binding assay data express the percentage of siRNA which freely diffuses in the solution that had been examined. As expected, siRNA (13.6 kDa) complexed with PEI (25 kDa) or PEG-PEI (45 kDa) formed larger particles than 30 kDa, which cannot be detected in the flow through of the test solution. In the case of free siRNA, we interpreted the low percentage of remaining siRNA after filtration, which was comparable to the amount filtrated after complexation with polymer, as a result of binding to albumin which explained the circulation time and AUC shown in Figures 5A and 5B. It is important though to keep in mind that this behavior did not represent an enhancement of siRNA bioavailability due to lack of protection against enzymatic degradation.

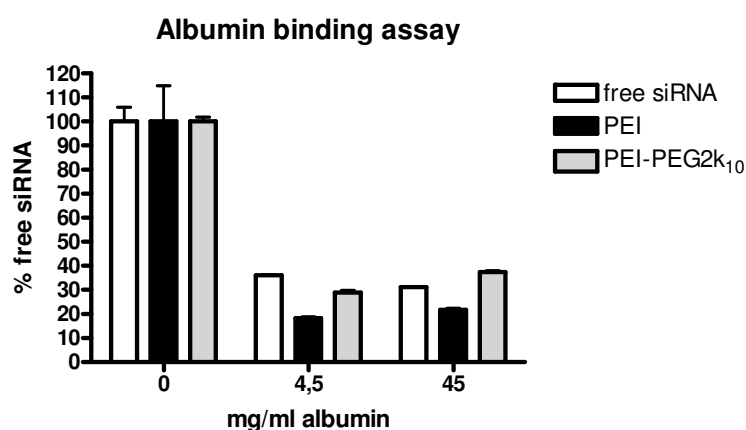


Figure 7: The albumin binding assay proved strong binding of Bn-DTPA coupled siGL3 to serum proteins even at low albumin concentration of 4.5 mg/ml.

Biodistribution of vector and load:

As shown in Figure 8, strong accumulation of PEI 25 kDa (36.2 % injected dose (ID)/organ) was observed in the liver as reported earlier for pDNA/PEI complexes (20, 24, 52). Lower accumulation of both PEG-PEIs and of free or formulated siRNA was statistically significant (**p < 0.001) compared to PEI 25 kDa. This means that even if PEI 25 kDa polyplexes were stable in circulation, they probably dissociated after uptake into the liver. Separation during liver passage was reported for pDNA/PEI complexes and probably resulted from vector unpackaging due to PEI binding to extracellular matrix (ECM) components (21). In that case, PEI was taken up into the liver cells (21), whereas DNA was found in interstitial space (21). The differences in liver deposition of vector and siRNA shown here could explain the dissimilar kinetic profiles. The fate of siRNA can be

explained by taking into account the excretion profiles. Amounts of polymer and complexed siRNA found in the urine were significantly ($***p < 0.001$) different for each pair of vector and load, as well. PEGylated PEIs showed comparably less ($***p < 0.001$) uptake into the liver. This supports our hypothesis of decreased interaction of PEGylated PEIs with blood components and macrophages (20, 24) due to the shielding effect of PEG. In fact, PEG chain length also played an important role in liver uptake, reflected in a significantly ($***p < 0.001$) lower uptake of PEI25k-PEG(20k)₁ compared to PEI25k-PEG(2k)₁₀. This trend is also true for complexed siRNA: PEI 25 kDa-complexed siRNA is deposited in the liver to a significantly ($**p < 0.01$) greater extent than PEG-PEI-complexed siRNA. This again underscores the importance of polyplex stability in blood circulation: PEG-PEIs, which form less stable complexes, release siRNA earlier, yielding lower liver uptake and significantly higher ($**p < 0.01$) excretion of siRNA in the urine. In fact, liver uptake of siRNA correlates very well ($R^2 = 0.9903$) with the amount of siRNA released, as shown in Figure 9. High stability of polyplexes led to stronger uptake of siRNA into the liver. The more siRNA was released from polyplexes in presence of serum, the more it bound to albumin and circulated longer than siRNA that was stably complexed and deposited in the liver. Other organs did not show relevant uptake. Only PEI 25 kDa showed uptake into the lung (3 % ID/ organ) which had earlier been reported to cause lethal events in animal studies investigating pDNA/PEI complexes (20, 23). Lethality and acute toxicity were explained on the basis of embolism due to entrapment of aggregates of polyplexes and blood components in the lung capillaries (53). In our study, we did neither observe accumulation in the lungs, as shown in Figure 8, nor did animals die from the treatment (two mice died from anesthesia). Values of up to 9 % ID/ organ in the case of PEI 25 kDa were measured in the kidneys. Accumulation of radiolabeled siRNA in the kidneys has earlier been reported for free siRNA (12). In our study, deposition of PEI 25 kDa had been even more prominent and can be explained by the lack of glomerular filtration of macromolecules or complexes > 60 kDa (54). Another explanation is that highly positively charged PEI is most probably held back by the negatively charged basal membrane of the bowman's capsules. PEGylated PEIs on the other hand, where the charges are shielded and which are more water soluble, didn't get stuck in the kidneys. Free siRNA didn't show any distinct deposition but accumulation in the bladder and the urine. Fast renal clearance and a high signal in the urine in biodistribution studies with pDNA/PEI polyplexes had so far been interpreted as excretion of degraded plasmid (55). siRNA, on the other hand, is more rapidly excreted than degraded (47). Although radiolabeled siRNA which is released from

polyplexes in circulation or in the liver passages is most likely to be bound to albumin, as discussed above, the amount of radioactivity found in the urine samples of mice treated with free or complexed siRNA is significantly different (PEI 25 kDa * $p < 0.05$, PEI25k-PEG(20k)₁ and PEI25k-PEG(2k)₁₀ *** $p < 0.01$). Our results calculated as % ID per gram (data not shown) prove that PEGylation decreases uptake by macrophages, shown in significantly lower (* $p < 0.05$) uptake of PEG-PEIs into the spleen. In this context it seems to us that post-PEGylation of pre-formed polyplexes could reveal higher stability attributed to PEI-complexes but lower recognition of the particles by the RES. This could be combined with bioreversible crosslinking via disulfide bond formation, which has previously been reported. Mere PEGylation of siRNA would certainly prolong its circulation time, but would not offer protection against nuclease degradation.

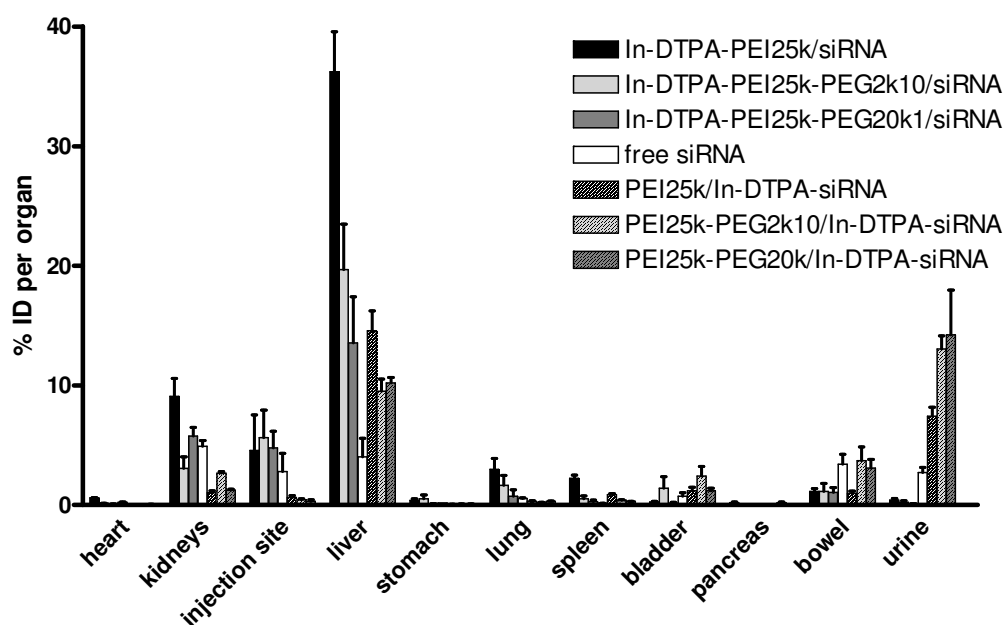


Figure 8: Scintillation analysis of dissected organs 2 hours after injection given as percentage of injected dose per organ.

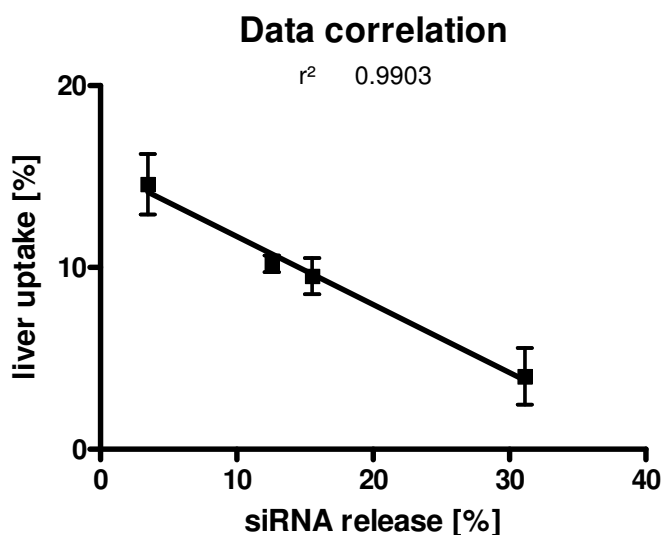


Figure 9: Correlation of siRNA uptake into the liver and siRNA release from polyplexes as measured by FFS

Non-invasive determination of pharmacokinetics and biodistribution:

Additional to scintillation counting of blood samples and organs, we performed real-time perfusion imaging studies to record kinetics and biodistribution during the first 25 minutes after injection. This non-invasive procedure was performed by quantifying radioactivity in “Regions of Interest” (ROIs) in living animals. We generally observed rapid accumulation in liver and kidneys and very fast renal excretion, as shown in Figures 10B (and Supporting Information for each single polymer). As previously described for siRNA/PEI complexes (7), a primary deposition in the lungs and secondary redistribution, which had been quantified for pDNA lipoplexes (28) and assumed for pDNA complexes earlier (20), was neither observed for polymer nor for siRNA in our perfusion studies. Regions of interest were again analyzed 2 hours after injection and are shown in Figure 10A. This graph clearly showed the same trends as Figure 8, but the drawback of two-dimensional imaging is that liver and kidneys, for example, are in the same plane of projection and can therefore not be differentiated. As a result, Figure 10A shows the sum of activity of both kidneys and the liver. Other organs, that did not show accumulation of radioactive material, could not be evaluated at all.

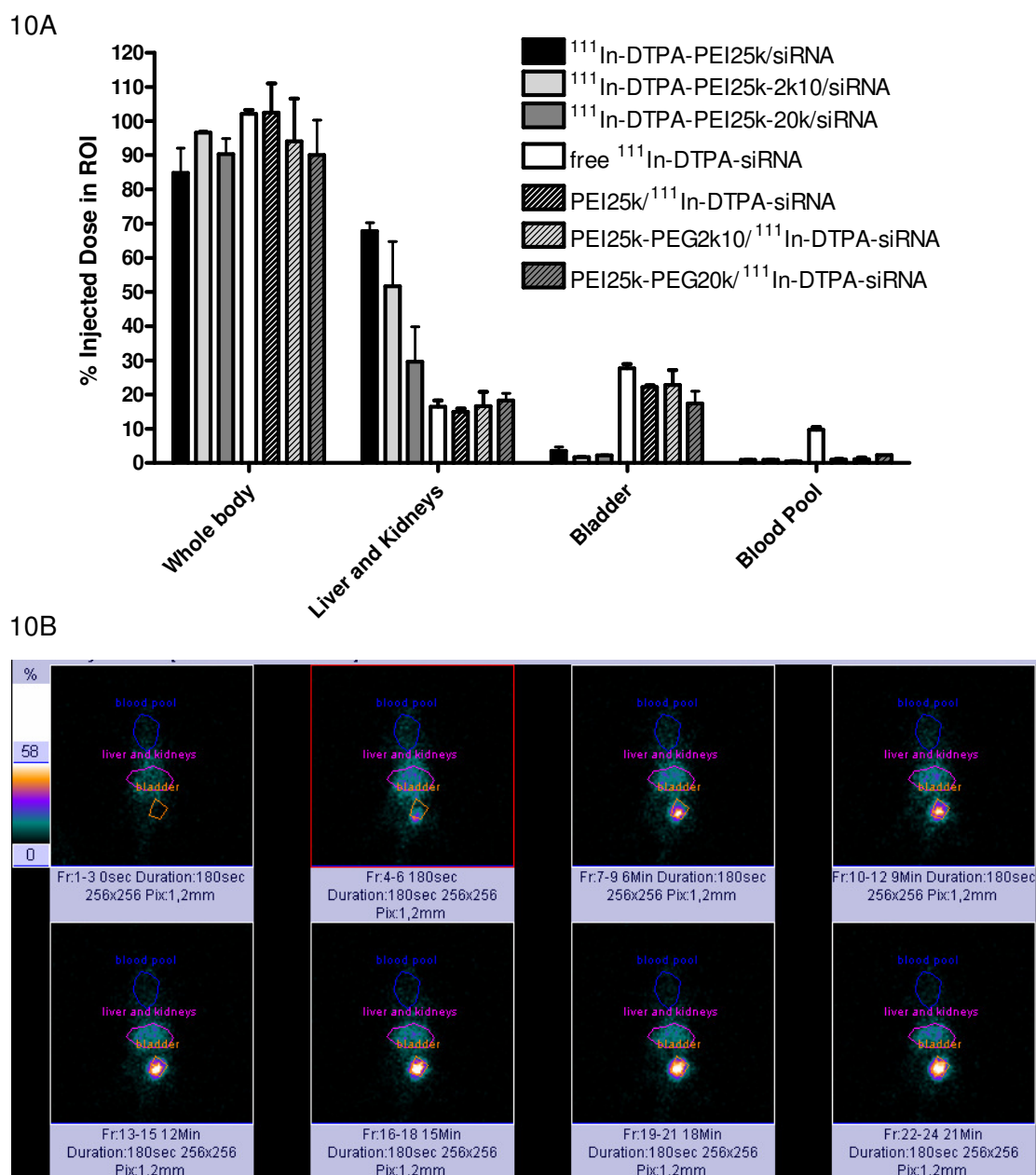


Figure 10A: Scintillation analysis of regions of interest 2 hours after injection for evaluation of biodistribution. 10B: Planar gamma camera perfusion movie with regions of interest for real-time quantification after injection of 35 μg siRNA, corresponding to 2.57 nmol and 0.255 MBq ^{111}In , complexed at an N/P of 6 with 25 kDa bPEI.

The imaging techniques used here provided information on three-dimensional localization of polyplexes and their kinetic behavior. As shown in Movie 1, Supporting Information, polyplexes made of ^{111}In Indium-labeled PEI 25k extensively accumulate in the liver and kidneys. If siRNA is radioactively labeled and the same polyplexes are applied, much less activity is measured in the liver after 2 hours (compare SPECT images Supporting

Information). This again supports the data from scintillation counting of dissected organs (Figure 8). In case of PEG-PEI complexes made of radioactively labeled siRNA, accumulation in the liver is so faint that SPECT images only indicate accumulation in the bladder (compare images Supporting Information).

6.5 Conclusion

Aim of this study was to correlate serum stability of polyplexes with their in vivo behavior and to predict pharmacokinetics and biodistribution. By measuring siRNA release from a vector in presence of serum, using fluorescence fluctuation spectroscopy, we were able to determine stability under serum concentration comparable to in vivo conditions. As expected, complexation of siRNA drove in vivo behavior and the most stable polyplexes experienced fast deposition in the liver. PEGylated polyplexes, which on the one hand are less stable in serum-containing media, showed better transfection efficiency in vitro and less uptake into liver and spleen in vivo, on the other hand. By physico-chemical and in vitro characterization we demonstrated that labeling did not affect polyplex formation or functionality of siRNA.

Additionally, we used nuclear imaging techniques to predict and determine pharmacokinetics, deposition, and to prove that there is no redistribution of polyplexes from the lungs to the liver. During the very first 25 minutes after application, we already observed differences in the behavior of the various polyplexes by real-time gamma camera imaging which are confirmed by scintillation counting of blood samples. Two hours after injection, SPECT images non-invasively exposed differences in organ distribution which had also been found by scintillation counting of dissected organs.

Taken together, we were able to show that stability of polyplexes has a strong influence on kinetics and distribution of each component of the polyplexes and we could prove correlation of stability and liver deposition. After radiolabeling siRNA and polymers, behavior of both vector and load could be followed non-invasively and showed that complexes which were stable in circulation dissociated during liver passage. Polyplexes made of siRNA and (PEG-)PEI are therefore not suitable for systemic but possibly for local application, such as inhalation or direct injection into organs.

In conclusion, this study proved that fluorescence fluctuation spectroscopy and nuclear imaging were able to predict and clarify in vivo behavior of siRNA polyplexes and can be used for optimizing more advanced vectors for systemic application.

6.6 Acknowledgements

The authors are grateful to Eva Mohr and Ulla Cramer for excellent technical support and to Michael Dutescu and Helmut Höffken, MD, for expert medical advice. The financial support of Deutsche Forschungsgemeinschaft (DFG Forschergruppe 627) and MEDITRANS, an Integrated Project funded by the European Commission under the Sixth Framework (NMP4-CT-2006-026668) are gratefully acknowledged.

6.7 References

- (1) Choung, S., Kim, Y. J., Kim, S., Park, H. O., and Choi, Y. C. (2006) Chemical modification of siRNAs to improve serum stability without loss of efficacy. *Biochem Biophys Res Commun* 342, 919-27.
- (2) Hauptenthal, J., Baehr, C., Kiermayer, S., Zeuzem, S., and Piiper, A. (2006) Inhibition of RNase A family enzymes prevents degradation and loss of silencing activity of siRNAs in serum. *Biochem Pharmacol* 71, 702-10.
- (3) Layzer, J. M., McCaffrey, A. P., Tanner, A. K., Huang, Z., Kay, M. A., and Sullenger, B. A. (2004) In vivo activity of nuclease-resistant siRNAs. *Rna* 10, 766-71.
- (4) Xia, J., Noronha, A., Toudjarska, I., Li, F., Akinc, A., Braich, R., Frank-Kamenetsky, M., Rajeev, K. G., Egli, M., and Manoharan, M. (2006) Gene silencing activity of siRNAs with a ribo-difluorotoluyll nucleotide. *ACS Chem Biol* 1, 176-83.
- (5) Turner, J. J., Jones, S. W., Moschos, S. A., Lindsay, M. A., and Gait, M. J. (2007) MALDI-TOF mass spectral analysis of siRNA degradation in serum confirms an RNase A-like activity. *Mol Biosyst* 3, 43-50.
- (6) Buyens, K., Lucas, B., Raemdonck, K., Braeckmans, K., Vercammen, J., Hendrix, J., Engelborghs, Y., De Smedt, S. C., and Sanders, N. N. (2008) A fast and sensitive method for measuring the integrity of siRNA-carrier complexes in full human serum. *J Control Release* 126, 67-76.
- (7) Merkel, O. M., Librizzi, D., Pfestroff, A., Schurrat, T., Behe, M., and Kissel, T. (2009) In vivo SPECT and real-time gamma camera imaging of biodistribution and pharmacokinetics of siRNA delivery using an optimized radiolabeling and purification procedure. *Bioconjug Chem* 20, 174-82.

-
- (8) Massoud, T. F., and Gambhir, S. S. (2003) Molecular imaging in living subjects: seeing fundamental biological processes in a new light. *Genes Dev* 17, 545-80.
 - (9) Li, S. D., Chen, Y. C., Hackett, M. J., and Huang, L. (2008) Tumor-targeted delivery of siRNA by self-assembled nanoparticles. *Mol Ther* 16, 163-9.
 - (10) Soutschek, J., Akinc, A., Bramlage, B., Charisse, K., Constien, R., Donoghue, M., Elbashir, S., Geick, A., Hadwiger, P., Harborth, J., John, M., Kesavan, V., Lavine, G., Pandey, R. K., Racie, T., Rajeev, K. G., Rohl, I., Toudjarska, I., Wang, G., Wuschko, S., Bumcrot, D., Kotliansky, V., Limmer, S., Manoharan, M., and Vornlocher, H. P. (2004) Therapeutic silencing of an endogenous gene by systemic administration of modified siRNAs. *Nature* 432, 173-8.
 - (11) Braasch, D. A., Paroo, Z., Constantinescu, A., Ren, G., Oz, O. K., Mason, R. P., and Corey, D. R. (2004) Biodistribution of phosphodiester and phosphorothioate siRNA. *Bioorg Med Chem Lett* 14, 1139-43.
 - (12) Van de Water, F. M., Boerman, O. C., Wouterse, A. C., Peters, J. G., Russel, F. G., and Masereeuw, R. (2006) Intravenously administered siRNA accumulates in the kidney and selectively suppresses gene function in renal proximal tubules. *Drug Metab Dispos* 34, 1393-7.
 - (13) de Wolf, H. K., Snel, C. J., Verbaan, F. J., Schiffelers, R. M., Hennink, W. E., and Storm, G. (2007) Effect of cationic carriers on the pharmacokinetics and tumor localization of nucleic acids after intravenous administration. *Int J Pharm* 331, 167-75.
 - (14) Gary, D. J., Puri, N., and Won, Y. Y. (2007) Polymer-based siRNA delivery: perspectives on the fundamental and phenomenological distinctions from polymer-based DNA delivery. *J Control Release* 121, 64-73.
 - (15) Malek, A., Czubayko, F., and Aigner, A. (2008) PEG grafting of polyethylenimine (PEI) exerts different effects on DNA transfection and siRNA-induced gene targeting efficacy. *J Drug Target* 16, 124-39.
 - (16) Tseng, S.-j., and Tang, S.-C. (2007) Development of Poly(amino ester glycol urethane)/siRNA Polyplexes for Gene Silencing. *Bioconjugate Chem.* 18, 1383-1390.
 - (17) Mao, S., Neu, M., Germershaus, O., Merkel, O., Sitterberg, J., Bakowsky, U., and Kissel, T. (2006) Influence of Polyethylene Glycol Chain Length on the Physicochemical and Biological Properties of Poly(ethylene imine)-graft-

- Poly(ethylene glycol) Block Copolymer/SiRNA Polyplexes. *Bioconjug Chem* 17, 1209-18.
- (18) Wightman, L., Kircheis, R., Rossler, V., Carotta, S., Ruzicka, R., Kursa, M., and Wagner, E. (2001) Different behavior of branched and linear polyethylenimine for gene delivery in vitro and in vivo. *J Gene Med* 3, 362-72.
- (19) Tseng, W.-C., and Jong, C.-M. (2003) Improved Stability of Polycationic Vector by Dextran-Grafted Branched Polyethylenimine. *Biomacromolecules* 4, 1277-1284.
- (20) Merdan, T., Kunath, K., Petersen, H., Bakowsky, U., Voigt, K. H., Kopecek, J., and Kissel, T. (2005) PEGylation of poly(ethylene imine) affects stability of complexes with plasmid DNA under in vivo conditions in a dose-dependent manner after intravenous injection into mice. *Bioconjug Chem* 16, 785-92.
- (21) Burke, R. S., and Pun, S. H. (2008) Extracellular barriers to in Vivo PEI and PEGylated PEI polyplex-mediated gene delivery to the liver. *Bioconjug Chem* 19, 693-704.
- (22) Petersen, H., Fechner, P. M., Fischer, D., and Kissel, T. (2002) Synthesis, Characterization, and Biocompatibility of Polyethylenimine-graft-poly(ethylene glycol) Block Copolymers. *Macromolecules* 35, 6867-6874.
- (23) Ogris, M., Brunner, S., Schuller, S., Kircheis, R., and Wagner, E. (1999) PEGylated DNA/transferrin-PEI complexes: reduced interaction with blood components, extended circulation in blood and potential for systemic gene delivery. *Gene Ther* 6, 595-605.
- (24) Fischer, D., Osburg, B., Petersen, H., Kissel, T., and Bickel, U. (2004) Effect of poly(ethylene imine) molecular weight and PEGylation on organ distribution and pharmacokinetics of polyplexes with oligonucleotides in mice. *Drug Metab Dispos* 32, 983-992.
- (25) Oupicky, D., Konak, C., Dash, P. R., Seymour, L. W., and Ulbrich, K. (1999) Effect of albumin and polyanion on the structure of DNA complexes with polycation containing hydrophilic nonionic block. *Bioconjug Chem* 10, 764-72.
- (26) Verbaan, F. J., Oussoren, C., Snel, C. J., Crommelin, D. J., Hennink, W. E., and Storm, G. (2004) Steric stabilization of poly(2-(dimethylamino)ethyl methacrylate)-based polyplexes mediates prolonged circulation and tumor targeting in mice. *J Gene Med* 6, 64-75.
- (27) Ward, C. M., Pechar, M., Oupicky, D., Ulbrich, K., and Seymour, L. W. (2002) Modification of pLL/DNA complexes with a multivalent hydrophilic polymer

- permits folate-mediated targeting in vitro and prolonged plasma circulation in vivo. *J Gene Med* 4, 536-47.
- (28) Ishiwata, H., Suzuki, N., Ando, S., Kikuchi, H., and Kitagawa, T. (2000) Characteristics and biodistribution of cationic liposomes and their DNA complexes. *J Control Release* 69, 139-48.
- (29) Van Rompaey, E., Engelborghs, Y., Sanders, N., De Smedt, S. C., and Demeester, J. (2001) Interactions between oligonucleotides and cationic polymers investigated by fluorescence correlation spectroscopy. *Pharm Res* 18, 928-36.
- (30) Pippin, C. G., Parker, T. A., McMurry, T. J., and Brechbiel, M. W. (1992) Spectrophotometric method for the determination of a bifunctional DTPA ligand in DTPA-monoclonal antibody conjugates. *Bioconjug Chem* 3, 342-5.
- (31) Snyder, S. L., and Sobocinski, P. Z. (1975) An improved 2,4,6-trinitrobenzenesulfonic acid method for the determination of amines. *Anal Biochem* 64, 284-8.
- (32) Bakeev, K. N., Izumrudov, V. A., Kuchanov, S. I., Zezin, A. B., and Kabanov, V. A. (1992) Kinetics and mechanism of interpolyelectrolyte exchange and addition reactions. *Macromolecules* 25, 4249-4254.
- (33) Veldhoen, S., Laufer, S. D., Trampe, A., and Restle, T. (2006) Cellular delivery of small interfering RNA by a non-covalently attached cell-penetrating peptide: quantitative analysis of uptake and biological effect. *Nucleic Acids Res* 34, 6561-73.
- (34) Geary, R. S., Watanabe, T. A., Truong, L., Freier, S., Lesnik, E. A., Sioufi, N. B., Sasmor, H., Manoharan, M., and Levin, A. A. (2001) Pharmacokinetic properties of 2'-O-(2-methoxyethyl)-modified oligonucleotide analogs in rats. *J Pharmacol Exp Ther* 296, 890-7.
- (35) Zini, R., Barre, J., Bree, F., Tillement, J. P., and Seville, B. (1981) Evidence for a concentration-dependent polymerization of a commercial human serum albumin. *J Chromatogr* 216, 191-8.
- (36) Neu, M., Germershaus, O., Mao, S., Voigt, K. H., Behe, M., and Kissel, T. (2007) Crosslinked nanocarriers based upon poly(ethylene imine) for systemic plasmid delivery: in vitro characterization and in vivo studies in mice. *J Control Release* 118, 370-80.
- (37) Petersen, H., Fechner, P. M., Martin, A. L., Kunath, K., Stolnik, S., Roberts, C. J., Fischer, D., Davies, M. C., and Kissel, T. (2002) Polyethylenimine-graft-poly(ethylene glycol) copolymers: influence of copolymer block structure on DNA

- complexation and biological activities as gene delivery system. *Bioconjug Chem* 13, 845-54.
- (38) Lucas, B., Remaut, K., Sanders, N. N., Braeckmans, K., De Smedt, S. C., and Demeester, J. (2005) Studying the intracellular dissociation of polymer-oligonucleotide complexes by dual color fluorescence fluctuation spectroscopy and confocal imaging. *Biochemistry* 44, 9905-12.
- (39) Kunath, K., von Harpe, A., Fischer, D., Petersen, H., Bickel, U., Voigt, K., and Kissel, T. (2003) Low-molecular-weight polyethylenimine as a non-viral vector for DNA delivery: comparison of physicochemical properties, transfection efficiency and in vivo distribution with high-molecular-weight polyethylenimine. *J Control Release* 89, 113-25.
- (40) Urban-Klein, B., Werth, S., Abuharbeid, S., Czubayko, F., and Aigner, A. (2005) RNAi-mediated gene-targeting through systemic application of polyethylenimine (PEI)-complexed siRNA in vivo. *Gene Ther* 12, 461-6.
- (41) Schiffelers, R. M., and Storm, G. (2006) ICS-283: a system for targeted intravenous delivery of siRNA. *Expert Opin Drug Deliv* 3, 445-54.
- (42) Schiffelers, R. M., Ansari, A., Xu, J., Zhou, Q., Tang, Q., Storm, G., Molema, G., Lu, P. Y., Scaria, P. V., and Woodle, M. C. (2004) Cancer siRNA therapy by tumor selective delivery with ligand-targeted sterically stabilized nanoparticle. *Nucleic Acids Res* 32, e149.
- (43) Kim, S. H., Jeong, J. H., Lee, S. H., Kim, S. W., and Park, T. G. (2008) Local and systemic delivery of VEGF siRNA using polyelectrolyte complex micelles for effective treatment of cancer. *J Control Release* 129, 107-16.
- (44) Grzelinski, M., Urban-Klein, B., Martens, T., Lamszus, K., Bakowsky, U., Hobel, S., Czubayko, F., and Aigner, A. (2006) RNA interference-mediated gene silencing of pleiotrophin through polyethylenimine-complexed small interfering RNAs in vivo exerts antitumoral effects in glioblastoma xenografts. *Hum Gene Ther* 17, 751-66.
- (45) Ge, Q., Filip, L., Bai, A., Nguyen, T., Eisen, H. N., and Chen, J. (2004) Inhibition of influenza virus production in virus-infected mice by RNA interference. *Proc Natl Acad Sci U S A* 101, 8676-81.
- (46) Bartlett, D. W., Su, H., Hildebrandt, I. J., Weber, W. A., and Davis, M. E. (2007) Impact of tumor-specific targeting on the biodistribution and efficacy of siRNA

- nanoparticles measured by multimodality in vivo imaging. *Proc Natl Acad Sci U S A* 104, 15549-54.
- (47) Dykxhoorn, D. M., Palliser, D., and Lieberman, J. (2006) The silent treatment: siRNAs as small molecule drugs. *Gene Ther* 13, 541-52.
- (48) Wolfrum, C., Shi, S., Jayaprakash, K. N., Jayaraman, M., Wang, G., Pandey, R. K., Rajeev, K. G., Nakayama, T., Charrise, K., Ndungo, E. M., Zimmermann, T., Koteliansky, V., Manoharan, M., and Stoffel, M. (2007) Mechanisms and optimization of in vivo delivery of lipophilic siRNAs. *Nat Biotechnol* 25, 1149-57.
- (49) Behlke, M. A. (2006) Progress towards in vivo use of siRNAs. *Mol Ther* 13, 644-70.
- (50) Bumcrot, D., Manoharan, M., Koteliansky, V., and Sah, D. W. (2006) RNAi therapeutics: a potential new class of pharmaceutical drugs. *Nat Chem Biol* 2, 711-9.
- (51) Morrissey, D. V., Lockridge, J. A., Shaw, L., Blanchard, K., Jensen, K., Breen, W., Hartsough, K., Machermer, L., Radka, S., Jadhav, V., Vaish, N., Zinnen, S., Vargeese, C., Bowman, K., Shaffer, C. S., Jeffs, L. B., Judge, A., MacLachlan, I., and Polisky, B. (2005) Potent and persistent in vivo anti-HBV activity of chemically modified siRNAs. *Nat Biotechnol* 23, 1002-7.
- (52) Germershaus, O., Neu, M., Behe, M., and Kissel, T. (2008) HER2 targeted polyplexes: the effect of polyplex composition and conjugation chemistry on in vitro and in vivo characteristics. *Bioconjug Chem* 19, 244-53.
- (53) Chollet, P., Favrot, M. C., Hurbin, A., and Coll, J. L. (2002) Side-effects of a systemic injection of linear polyethylenimine-DNA complexes. *J Gene Med* 4, 84-91.
- (54) Tryggvason, K., Patrakka, J., and Wartiovaara, J. (2006) Hereditary proteinuria syndromes and mechanisms of proteinuria. *N Engl J Med* 354, 1387-401.
- (55) Kawabata, K., Takakura, Y., and Hashida, M. (1995) The fate of plasmid DNA after intravenous injection in mice: involvement of scavenger receptors in its hepatic uptake. *Pharm Res* 12, 825-30.

7 Non-viral siRNA delivery to the lung – investigation of PEG-PEI polyplexes and their in vivo performance

Published in *Molecular Pharmaceutics* 6 (2009) 1246-1260

7.1 Abstract

Objective: This study describes the physico-biological characterization of PEI- and PEG-PEI polyplexes containing partially 2'-OMe modified 25/27mer dicer substrate siRNAs (DsiRNAs) and their in vivo behavior regarding biodistribution and systemic bioavailability after pulmonary application as well as their ability to knock down gene expression in the lung.

Methods: Biophysical characterization included circular dichroism of siRNA in polyplexes, condensation efficiency of polymers and in vitro stability. After in vivo application, biodistribution and kinetics of radiolabeled polyplexes was quantified and recorded over time in three-dimensional SPECT images and by endpoint scintillation counting. The influence on lung tissue and on the humoral and cellular immunosystem was investigated, and finally knock down of endogenous gene expression in the lung was determined qualitatively.

Results: While all of the polymers used in our study were proven to effectively condense siRNA, stability of the complexes depended on the PEG grafting degree. Interestingly, PEI 25 kDa which showed the least interaction with mucin or surfactant in vitro, performed poorly in vivo. Our nuclear imaging approach enabled us to follow biodistribution of the instilled nanocarriers over time and indicated that PEGylated nanocarriers are more suitable for lung application. While moderate proinflammatory effects were attributed to PEI25k-PEG(2k)10 nanocarriers, none of the treatments caused histological abnormalities. Our preliminary in vivo knock down experiment suggests that PEG-PEI/siRNA complexes are promising nanomedicines for pulmonary siRNA delivery.

Conclusion: These results encouraged us to further investigate possible adverse effects and to quantify in vivo gene silencing in the lung after intratracheal instillation of PEG-PEI/siRNA complexes.

7.2 Introduction

Delivery is still the major hurdle in RNAi therapy. Due to the instability of siRNA and rapid excretion upon systemic injection (*1*), most of the clinical trials involving siRNA based drugs utilize local administration to the eyes, targeting macular degeneration and diabetic retinopathy (Acuity Pharmaceuticals, Alnylam Pharmaceuticals, Inc. and Sirna Therapeutics, Inc), or direct delivery to the brain or the lung (Alnylam Pharmaceuticals,

Inc.), and a recent study has demonstrated the advantages of local pulmonary application of both drugs and nucleic acids over systemic i.v. injection (2). Lung cancer is already the leading cause of cancer death in the United States (3) and the number 8 cause of death worldwide, while lower respiratory infections are number 3, chronic obstructive pulmonary disease is number 4, and tuberculosis is number 7, according to the World Health Organization (WHO) (4). Therefore, efficient therapies that lead to high and prolonged local drug concentration in the lung are needed to avoid any of these respiratory diseases becoming the number one cause of death. The lung with its vast surface area and strong perfusion is indeed well suited to take up small, hydrophobic drug molecules. It is, on the other hand, only permeable to a limited extent for large, hydrophilic biopharmaceuticals, such as siRNA. Yet, successful local siRNA therapy, e.g. protection from SARS infection (5), inhibition of RSV (5, 6) and influenza A (7) virus replication has been reported. While most of the in vivo studies of siRNA based therapy used 21mer duplexes that mimic naturally occurring products of Dicer (8), Kim et al showed that 27mer blunt double strands can be up to 100-fold more potent than 21mer duplexes (9). Different approaches to enhance the stability of siRNA have been reported (10), including modification of the backbone and/or ribose (11). In particular, methylation of the ribose 2' hydroxyl group (2'-OMe) offers the additional benefit of diminishing immunostimulatory effects (12, 13). The first study of pulmonary delivery of siRNA reported successful down regulation of heme oxygenase-1 even after application of naked siRNA (14), and Li et al. only used isotonic dextrose solution (DW5) as carrier⁵. Bitko et al. showed enhanced effects, compared to naked siRNA, with a cationic lipid transfection reagent TransIT-TKO (6), and in the meantime, a limited number of nanocarriers such as surfactants (15), mucoadhesive chitosan (16), and Oligofectamine (17) have been used for improved in vivo pulmonary delivery. In our study, we have investigated how formulation of a 25/27mer 2'-OMe siRNA with polyethylene imine (PEI) and polyethylene glycol (PEG) grafted PEI (PEG-PEI) into nanosized complexes influences biodistribution, absorption, and clearance of vector and load after intratracheal instillation. These parameters were studied by non-invasive nuclear imaging and were compared for PEG-PEIs of different grafting degrees. Additionally, the encapsulation of the modified siRNA, induction of immunostimulatory effects, pulmonary histology after instillation, and finally knock down of target protein expression were investigated.

7.3 Experimental Section

Materials:

Poly(ethylene imine), PEI 25 kDa (Polymin™, 25 kDa) was a gift from BASF (Ludwigshafen, Germany), the block copolymers poly(ethylene glycol)-poly(ethylene imine) PEI25k-PEG(20k)₁ and PEI25k-PEG(2k)₁₀ (18) were synthesized as described earlier. 2'-O-Methylated 25/27mer DsiRNA targeting EGFP (19), fluorescent TYE563- and 5'-sense strand C6-amine modified DsiRNA with the same sequence were obtained from Integrated DNA Technologies (Leuven, Belgium), all other reagents were of analytical quality. BALB/c mice were bought from Harlan Laboratories (Horst, The Netherlands), and C57BL/6-Tg(CAG-EGFP)1Osb/J Actin-EGFP expressing mice were bought from The Jackson Laboratory (Ben Harbour, Maine, USA) and bred in house.

Polyplex formation:

Polyplexes were formed by mixing equal volumes (25 µl each) of siRNA and polymer diluted in 10 mM HEPES buffer, unless otherwise stated, to obtain the desired nitrogen to RNA phosphate ratio (N/P ratio). Briefly, the appropriate amount of polymer was added to an siRNA solution (2 µM) to yield a final concentration of 1 µM siRNA, vortexed for 10 seconds and incubated for polyplex formation for 10-20 minutes.

SYBR® Gold Dye Binding Assay:

To investigate the condensation of siRNA by the various polymers, 1 µg EGFP siRNA (IDT, Leuven, Belgium) was complexed with polymers at different N/P ratios and pipetted into opaque FluoroNunc™ 96 well plates (Nunc, Thermo Fisher Scientific, Langensfeld, Germany). After incubation for 20 minutes at room temperature, 50 µl of a 1x SYBR® Gold solution (Invitrogen, Karlsruhe, Germany) were added to each well and incubated for 10 minutes in the dark under constant shaking on a sample shaker TH 15 (Edmund Bühler, Hechingen, Germany). Intercalation-caused fluorescence was quantified using a fluorescence plate reader (SAFIRE II, Tecan Group Ltd, Männedorf, Switzerland) at 495 nm excitation and 537 nm emission wavelengths. Experiments were performed in replicates of four, and the results are given as mean relative fluorescence intensity values +/- the standard deviation (SD), where intercalation of free siRNA represents 100 % fluorescence and non-intercalating SYBR® Gold in buffer represents 0 % remaining fluorescence.

Fluorescence Quenching Assay:

To investigate the condensation efficiency of the polymers used in this study in a direct approach, 1 μg Tye563-labeled DsiRNA (IDT, Leuven, Belgium) was complexed with polymers at different N/P ratios and pipetted into opaque FluoroNunc™ 96 well plates (Nunc, Thermo Fisher Scientific, Langensfeld, Germany). Remaining fluorescence was quantified using a fluorescence plate reader (SAFIRE II, Tecan Group Ltd, Männedorf, Switzerland) at 549 nm excitation and 563 nm emission wavelengths. Experiments were performed in replicates of four, and the results are given as mean relative fluorescence intensity values \pm SD, where free siRNA represents 100 % fluorescence and polymer in buffer represents 0 % fluorescence.

Circular Dichroism (CD):

To investigate the complexation behavior of the different polymers and their effect on short RNA double strands, we employed circular dichroism spectroscopy, a method widely used in RNA analytics and lately described for characterization of siRNA complexes (20). Briefly, 2 nmol siRNA in 100 μl was mixed with 100 μl polymer solution to form complexes of different N/P ratio. The polyplexes were incubated for 10 minutes before they were diluted with 200 μl 10 mM HEPES buffer, pH 7.4 and pipetted into a 0.2 cm quartz cuvette. CD spectra were recorded on a Jasco J 810s spectropolarimeter (Jasco Labor- und Datentechnik GmbH, Groß-Umstadt, Germany) at 20 °C at a scanning speed of 200 nm/min from 200 nm to 320 nm. As described in (20) the response time was 1 second, the bandwidth and data pitch 1 nm, and each spectrum was the accumulated from 5 scans.

Stability of Polyplexes in the Presence of Mucin and Lung Surfactants:

Stability of polyplexes was determined by release of siRNA from the complex upon interaction with mucin or Alveofact®, respectively. Therefore, an assay similar to the SYBR® Gold dye binding assay was performed with all polyplexes formed at N/P 6. After polyplex formation, 50 μl of a 1x SYBR® Gold solution were added and incubated for 10 minutes in the dark under constant shaking. Afterwards, increasing concentrations of mucin (mucin from porcine stomach Type II, Sigma-Aldrich Chemie GmbH, München, Germany) or Alveofact® (Boehringer-Ingelheim, Germany), (0-0.33 $\mu\text{g}/\mu\text{l}$ final concentration), respectively, were added and incubated with the polyplexes for another 20 minutes before fluorescence was quantified using a fluorescence plate reader (SAFIRE II, Tecan Group Ltd, Männedorf, Switzerland) at 495 nm excitation and 537 nm emission wavelengths.

Experiments were performed in replicates of four, and the results are given as mean relative fluorescence intensity values \pm SD, where free siRNA represents 100 % fluorescence and SYBR® Gold in buffer represents 0 % fluorescence.

In vivo Biodistribution and Kinetics after Intratracheal Application:

All animal experiments were carried out according to the German law of protection of animal life and were approved by an external review committee for laboratory animal care. Polymers and siRNA were radioactively labeled after coupling to p-Bn-SCN-DTPA as previously described (21, 22). Briefly, amine-modified siRNA or polymers, respectively, were mixed with p-Bn-SCN-DTPA at pH 8.5 and reacted for 45 minutes. Polymers were easily purified using centricon YM-10 spin columns (Millipore, Schwalbach, Germany), siRNA was precipitated in absolute ethanol and purified using RNeasy Mini columns (Qiagen, Hilden, Germany). DTPA-coupled polymers or siRNA were then incubated for 30 minutes with $^{111}\text{InCl}_3$ (Covidien Deutschland GmbH, Neustadt a.d. Donau, Germany) in 0.1 M sodium acetate buffer, pH 5.4 for radiolabeling before siRNA was purified from free $^{111}\text{InCl}_3$ by size exclusion chromatography (SEC) on PD-10 Sephadex G25 (GE Healthcare, Freiburg, Germany) and RNeasy spin column purification, and polymers were purified by SEC only.

Four to six week old BALB/c mice were anaesthetized with Xylacin/Ketamin and fixed in a supine position on a 60° incline board by holding their upper incisor teeth. The tongue was gently extended using coated tweezers as previously described (23). Mice were intubated through mouth and trachea using the flexible tube of a 24-gauge catheter (BD Insyte™, Becton Dickinson GmbH, Heidelberg, Germany). Polyplexes prepared in PBS containing 35 µg siRNA and the corresponding amount of polymer for N/P 6 were formed with either radiolabeled siRNA or radiolabeled polymers in order to differentiate between the biodistribution of vector and payload. Polyplexes were incubated for 10 minutes and instilled into the murine lungs through the BD Insyte™ tubus. Blood samples were withdrawn retroorbitally 1, 3, 5, 15, 30, 60, and 120 minutes after instillation. Three-dimensional SPECT and planar gamma camera images were recorded 2, 24, and 48 hours after instillation using a Siemens e.cam gamma camera (Siemens AG, Erlangen, Germany) on which a custom built multiplexing multipinhole collimator was mounted. Planar images were analyzed for radioactivity in regions of interest (ROIs) by Syngo software (Syngo, Siemens Medical Solutions, Erlangen, Germany). Dual-isotope SPECT images were recorded 15 minutes after an additional tail vein injection of 4 MBq $^{99\text{m}}\text{Tc}$ -labeled macro-

agglomerated albumin (MAA, Mallinkrodt, Hennef/Sieg, Germany). SPECT images were recorded for each isotope separately and later superimposed by the software (Syngo, Siemens Medical Solutions, Erlangen, Germany). After 48 hours, animals treated with ^{111}In -labeled polyplexes only were sacrificed and biodistribution of radiolabeled material in dissected organs was measured using a Gamma Counter Packard 5005 (Packard Instruments, Meriden, CT, USA). Radioactive decay of the isotope was factored in to the calculations and results are given as mean percentage of the injected dose (% ID). Control animals were either instilled with PBS only (PBS control) or were anaesthetized but not instilled (anaesthesia control) in order to assess stress levels caused by bolus instillation or anaesthesia, respectively.

Broncho-Alveolar Lavage (BAL):

Animals were sacrificed 48 hours after treatment. BAL was performed as previously described (24). Briefly, tracheae were cannulated using a BD Insite™ catheter, lungs were rinsed ten times with 1 ml fresh PBS supplemented with cOmplete Protease Inhibitor Cocktail (Roche Diagnostics, Mannheim, Germany). BAL fluids of each animal were pooled, and the total number of leukocytes captured by lavage was determined using a Casy TT cell counter (Schaerfe Systems, Reutlingen, Germany). Aliquots of 100.000 cells were spun down on glass slides (100 x g, 5 min) to prepare cytopspins, and BAL cells were stained for differentiation with Diff-Quick (DADE Diagnostics, Unterschleissheim, Germany). 100 cells were counted and classified concerning morphology and staining. Secretion of 22 pro- and anti-inflammatory cytokines was measured in cell-free BAL fluids by Luminex technology (Luminex System, Bio-Rad Laboratories, Germany) as previously described (25).

Lung Histology:

The influence of exposure of lung tissue to nanomaterials was also examined histologically. Therefore, lungs were inflated via the trachea with and after dissection fixed in a 4 % paraformaldehyde solution before they were paraffin-embedded. Paraffin sections (8 μm) were deparaffinized and stained with hematoxylin and eosin (H&E).

In vivo Knock Down:

Four to six week old C57BL/6-Tg(CAG-EGFP)10sb/J mice were anaesthetized with Xylacin/Ketamine and fixed in a supine position and intubated as described above.

Polyplexes containing 50 µg siRNA and the corresponding amount of polymer PEI25k-PEG(2k)₁₀ for N/P 6 were formed in 5 % glucose solution (total volume per mouse: 50 µl), and instilled into murine lungs using the tubus. Control mice were treated with 5 % glucose only. Animals were sacrificed 5 days after instillation and lungs were inflated with 4 % paraformaldehyde, dissected and stored in 4 % paraformaldehyde in the dark, before they were embedded in paraffin. The deparaffinized slices (3 µm) were counterstained with 1 µg/ml 4'6-diamidino-2-phenylindole (DAPI) (Molecular Probes, Invitrogen, Karlsruhe, Germany) solution in PBS for 30 minutes under light exclusion, and embedded with FluorSave (Calbiochem, Merck Biosciences, Darmstadt, Germany) to protect the fluorophores.

Confocal Laser Scanning Microscopy (CLSM):

A Zeiss Axiovert 100 M microscope coupled to a Zeiss LSM 510 scanning device (Zeiss, Oberkochen, Germany) was used for confocal microscopy. For excitation of EGFP fluorescence, an argon laser with an excitation wavelength of 488 nm was used. Fluorescence emission was detected using a 505 nm long-pass filter. Transmission images were obtained in the same scan. In a second scan of the multi-track image, DAPI was detected using a Coherent Enterprise II 653 laser (Coherent, Inc., Santa Clara, CA) with an excitation wavelength of 351 nm and a 385-470 nm bandpass emission filter. All confocal images were acquired with the same settings with respect to laser intensity, filter block, and detector gain.

Flow Cytometric Quantification of Knock Down:

C57BL/6-Tg(CAG-EGFP)10sb/J mice were instilled as described above with 50 µg siRNA (either siEGFP targeting EGFP or siLuc targeting firefly luciferase as negative control) complexed with PEI25k-PEG(2k)₁₀ at N/P 6. As blanks, C57BL/6 mice not expressing EGFP were treated the same way. Animals were sacrificed 5 days after instillation, exsanguinated and perfused with PBS via the left ventricle. BAL was performed as described above before lungs were excised. Lung homogenates were obtained by incubating the excised lungs in 2 ml of a 1 mg/ml Collagenase D solution (Roche, Mannheim, Germany) at 37 °C for 20 minutes before processing the tissue through a nylon Cell Strainer 100 µm (BD Falcon, Heidelberg, Germany). Cells were then suspended in 10 ml PBS, centrifuged at 350 g for 10 minutes. The supernatant was decanted, the cells were resuspended, once again centrifuged and resuspended in 500 µl CellFIX (BD Biosciences,

Heidelberg, Germany) for flow cytometry. The residual EGFP expression in the fixed cells was quantified on a FACScan (BD Biosciences, Heidelberg, Germany) flowcytometer with an excitation laser of 488 nm and an bandpass filter of 530/30 nm by counting 10,000 events. Data acquisition and analysis was performed using CellQuest Pro (BD Biosciences, Heidelberg, Germany) and FCS Express V3.00 (DeNovo Software, Thornhill, Canada). Results are given as the average mean fluorescence intensity (MFI) \pm SD of the gated viable cells.

Statistics:

All analytical assays were conducted in quadruple, and all in vivo experiments included 5 animals per group. Results are given as mean values \pm standard deviation (SD). Two way ANOVA, statistical evaluation and calculation of the AUC was done using Graph Pad Prism 4.03 (Graph Pad Software, La Jolla, USA).

7.4 Results and Discussion

In our earlier study, we had shown that the polymers we used here were all able to condense siRNA into complexes of 150 nm hydrodynamic diameter (26). Zeta potentials were found to be positive (22 mV for PEI 25k) and slightly decreased for PEG-PEI complexes (15 and 16 mV for PEI(25k)-PEG(2k)10 and PEI(25k)-PEG(20k)1, respectively). Stability against RNase degradation and competition with other polyanions has also been described (26), and serum stability of these complexes has been investigated by Fluorescence Fluctuation Spectroscopy in a later study²¹. In this study, we mainly focused on stability in biological fluids present in the lung such as mucin and surfactants, and we also quantified condensation efficiency of siRNA by the polymers used as follows:

SYBR® Gold Dye Binding Assay:

Condensation efficiency of the polymers considered the complexation of nucleic acids which are not accessible to intercalating dyes can be quantified in indirect approaches such as the ethidium bromide quenching assay (27). Due to the costs of siRNA, SYBR® Gold staining, which is 25-100 times more sensitive than ethidium bromide, is much more suitable and gives rise to sufficiently high signals in the micromolar range. In the assays we performed with 1 μ g siRNA (59 pmol), we observed good condensation of siRNA even at low N/P ratios (Figure 1A). Unmodified branched 25 kDa PEI showed full condensation at

N/P 1 already, whereas the condensation profiles of the PEGylated PEIs varied depending on their PEGylation pattern. PEI25k-PEG(20k)₁ exhibited the worst condensation profile which corroborates our data obtained in polyacrylamide gel electrophoresis assays (data not shown). This polymer has also been reported to form polyplexes of low stability in the presence of serum (22). PEI25k-PEG(2k)₁₀, on the other hand, showed only slight differences at N/P 1 compared to PEI 25k. The long PEG chain in PEI25k-PEG(20k)₁ seems to be disadvantageous for complex formation whereas a higher PEG density of short PEG chains affects complex formation only at low N/P ratios. Unmodified 21mer siRNA was shown to be fully condensed at N/P 3 with all of the polymers used in a recent study (26). Since gel electrophoresis utilized in the latter report is a more qualitative method, we cannot rule out that slight differences observed in the condensation behavior of unmodified versus 2'-OMe modified siRNA are significant.

Fluorescence Quenching Assay:

Another approach for investigating condensation efficiency is the use of assays involving directly labeled nucleic acids that do not require a staining step. Thus, we condensed fluorescently labeled siRNA of the same sequence at the same N/P ratios and the same concentrations as described above. This assay revealed a peculiarity that has previously been described by Van Rompaey et al (28) for oligonucleotide containing poly- and dendriplexes. Interestingly, each curve had a minimum of fluorescence at N/P 1, before fluorescence increased again upon increasing the N/P ratio (Figure 1B). Van Rompaey et al. have described this phenomenon as a reorganization of the polyplexes. They explained that at the minimum of fluorescence a large number of fluorescently labeled molecules are entrapped in one polyplex, quenching each other due to their close spatial proximity. At higher N/P ratios, polyplexes apparently do not “layer up”, forming additional layers of polymer on top of the polyplexes, but a redistribution of the number of nucleic acid molecules per polyplex occurs. Therefore, at higher N/P ratios, the number of labeled molecules that are present in one polyplex and trapped in close proximity is decreased, leading to less self-quenching and thus higher intensity fluorescence signals. Van Rompaey et al. had not described this finding for complexation of oligodeoxynucleotides by PEG-PEI, but as previously reported by Glodde et al. (29), properties of complexes made of the same polymer but different types of nucleic acids may vary considerably. Our findings indicate that, independent of the polymer, at N/P 20 all polyplexes contained so little siRNA that almost no quenching could be observed, although the SYBR® Gold dye

binding assays proved that siRNA was entrapped and inaccessible for intercalation. Differences between the PEGylated polymers and unmodified PEI 25kDa were opposite to what has been described above concerning dye binding: PEI 25 kDa had the lowest quenching efficiency, whereas PEI25k-PEG(20k)₁ decreased the fluorescence the most. Comparison of both, the indirect and the direct approach, exhibited properties of a dynamic polyplex – polymer equilibrium that reorganizes according to concentration changes and proved that polyplex formation is not a trivial process. Also the direct approach does not allow for prediction of condensation at a certain N/P ratio. Additionally, we have to keep in mind that by fluorescent labeling, the siRNA duplex is certainly affected in its chemical properties and might behave differently concerning complexation, even though functionality of the duplex is maintained.

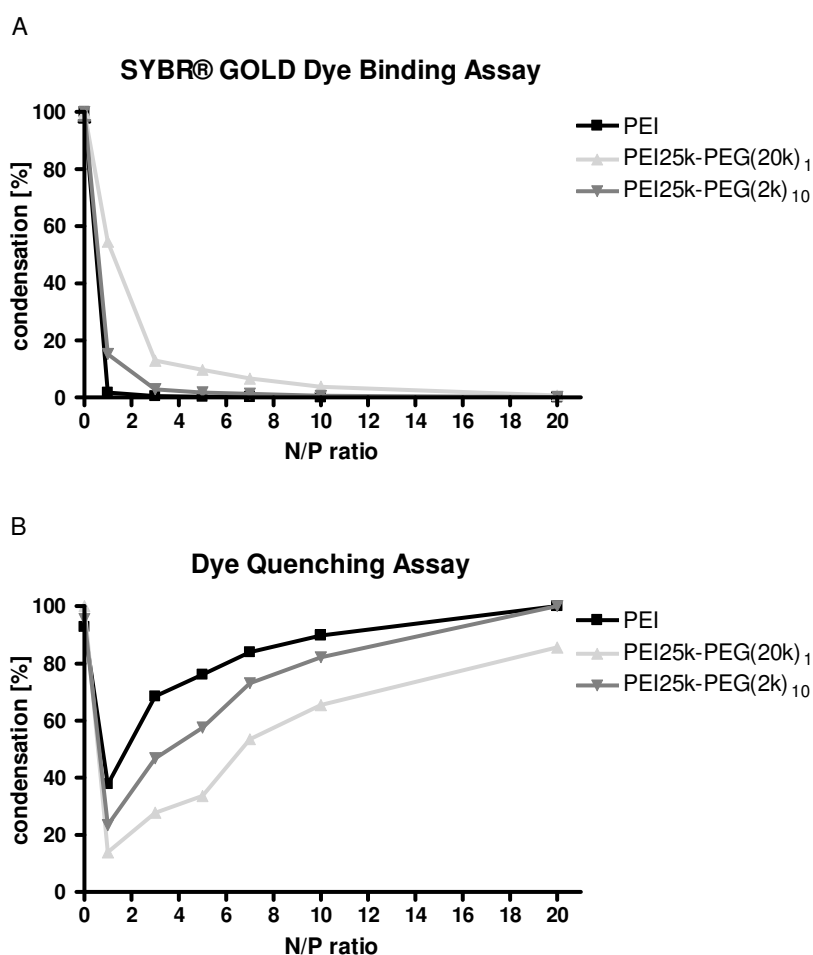


Figure 1A: The SYBR® Gold Dye Binding Assay revealed very effective encapsulation and protection from intercalation of 2'-OMe DsiRNA. PEI 25 kDa showed the highest efficiency, followed by PEI25k-PEG(2k)₁₀ and PEI25k-PEG(20k)₁. **1B:** The Dye

Quenching Assay using fluorescently labeled siRNA on the other hand demonstrated a phenomenon earlier described for oligodeoxyribonucleotides (28). Data obtained by this method therefore has to be interpreted critically.

Circular Dichroism (CD):

CD is traditionally used to investigate the tertiary structure of nucleic acids. Changes in the spectra can be caused by conformational changes, such as different base stacking which can be observed at the long-wavelength band (30), and changes at 210 nm which are attributed to backbone conformational transitions (31). Therefore, this method can also be utilized to investigate variations in the duplex structure caused by electrostatic interaction with polycations. In our study we observed different effects that varied for the three polymers investigated. In general, all spectra recorded had strong resemblance with the A-form of free double stranded RNA characterized by a C3'-endo conformation (32), which has also been confirmed for 2'-OMe RNA duplexes (33). One of the effects observed was that PEI 25 kDa, even at low N/P ratios (N/P 1 and 3), caused a slightly decreased Cotton effect (molar ellipticity) at 264 nm compared to that of free siRNA (Figure 2A). Upon increasing the amount of polymer used for complexation (N/P 5-10), the Cotton effect at 264 nm was further decreased, but all spectra for N/P 10, 15, 20, 30, and 40 (N/P 30 and 40 not shown) were very similar, exhibiting a decreased degree of polarization at 264 nm, a very flat curve between 240 and 225 nm and a less negative and slightly red shifted peak at 210 nm. PEI25k-PEG(20k)₁, on the other hand, showed a very strongly decreased Cotton effect at ~265 nm at N/P 1 which was increased at N/P 3, 5, and 7 (Figure 2B). Complexation at N/P 7 caused only a small decrease of polarization at 264 nm but an extremely flat curve between 240 and 225 nm and the strongest effects at 210 nm, where the slight minimum was red shifted. Upon increasing the N/P ratio, this effect was reversed. Curves at N/P 10, 15, and 20 were very similar, as observed with PEI 25k. This again could be a sign of a reorganization process depending on polymer concentration, as observed in the dye quenching assay, with the strongest effects on backbone conformation (210 nm) observed at N/P 7. As shown in Figure 2 C, PEI25k-PEG(2k)₁₀ caused a decreased Cotton effect at 264 nm at all N/P ratios, and curves were similar from N/P 1 up to N/P 20 being comparable to the curves observed with PEI 25k. These findings indicated that all of our polymers did interact with siRNA leading to changes in backbone conformation and base stacking. The disappearance of the negative peak at 210 nm has, on the other hand, previously been attributed to high concentrations of PEG, due to an overlapping, positive CD band at shorter

wavelengths (34). But if PEG was the reason, the phenomenon would be accompanied by an up to 12.5 fold increase of the maximum at 264 nm shifted to 270 nm. Since this was not observed, but the negative peak also disappeared upon complexation with PEG-free PEI 25 kDa, we hypothesize that it was caused by complexation dependent changes in the backbone conformation. In contrast to spermine, a tetravalent polycation which was reported to stabilize the A-form of dsRNA by increasing the intensity of the positive band at 264 nm in a concentration range between N/P 1 and 10 (35), all of our polycations destabilized the base stacking of the siRNA. While the same report also described an increase of intensity of the negative band at 210 nm, Steely et al. explained that a decrease of intensity at 210 nm is related to condensation of dsRNA (36). In our study, we showed that while concentration dependent effects were different for each polymer, siRNA nucleobase stacking and backbone conformation were influenced upon complexation with each polymer at every single N/P ratio corroborating the results from the SYBR® Gold assay.

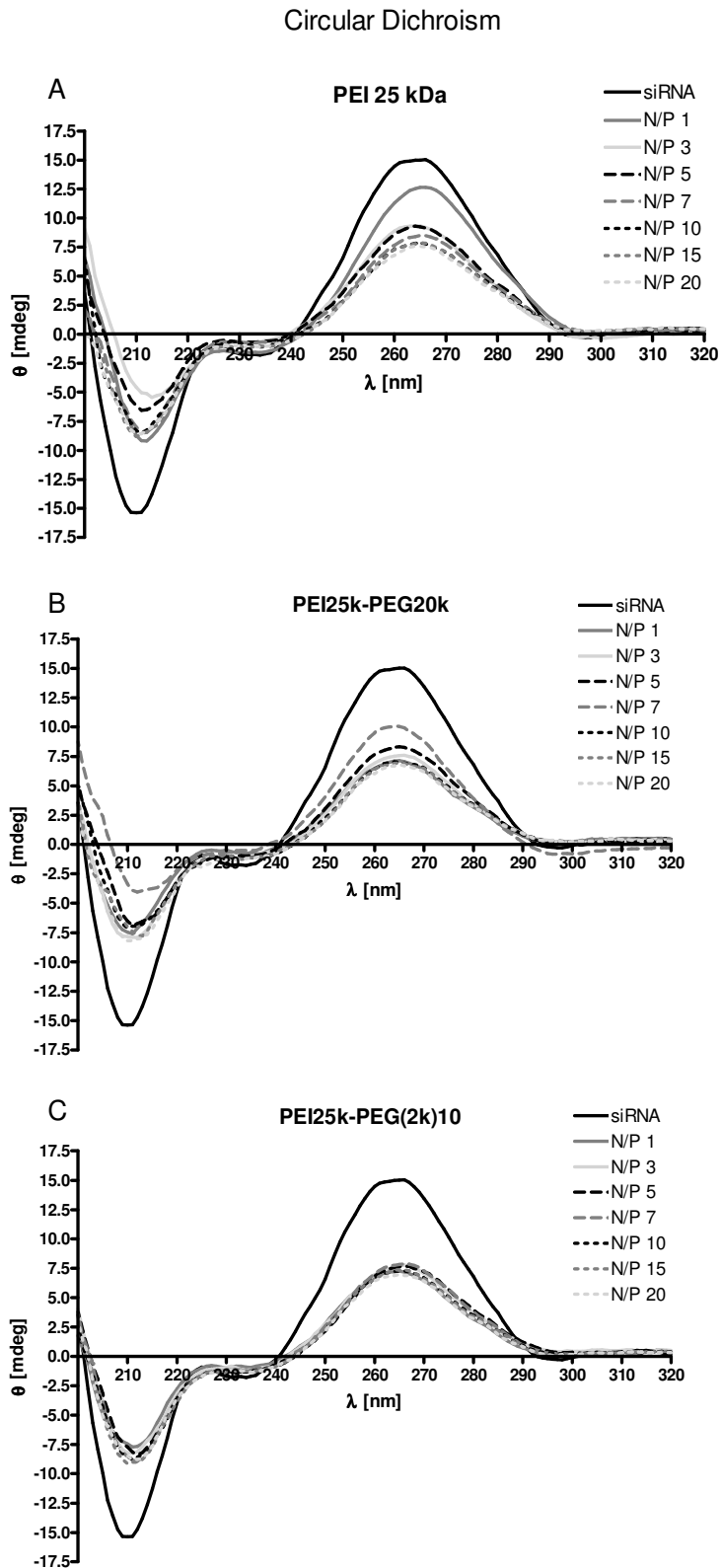


Figure 2: Circular dichroism (CD) spectroscopy emphasized differences in the condensation behavior of the various polymers. While PEI 25 kDa (**A**) showed increasing condensation with increasing polymer concentration, PEI25k-PEG(20k)1 (**B**) caused a

minimum of condensation at N/P 7, and PEI25k-PEG(2k)10 (C) had almost the same effect on siRNA at every N/P tested.

Stability Assay in Presence of Mucin and Lung Surfactants:

Stability of nanocarriers in biological fluids is a major limitation for systemic application and was found to be insufficient for PEI or PEG-PEI polyplexes (22). Due to decreased nuclease activity in the lung, even naked siRNA yielded successful knock down of gene expression (14, 37), but formulations of siRNA were expected to overcome several barriers present in the lung allowing reduction of the applied dose by increasing the active concentration in the cytosol, thus limiting adverse side effects. Before contact with the airway cell membranes occurs, however, nanocarriers need to penetrate the mucus layer, the surfactant layer, and the periciliary fluid layer covering the airway cells (38), all of which pose considerable biomechanical hurdles in pulmonary siRNA delivery. To investigate whether polyplexes could penetrate the airway lining fluids as intact nanocarriers, we performed SYBR® Gold staining assays in the presence of Alveofact® or mucin, respectively, to quantify the release of siRNA from polyplexes. Reduced stability of pDNA/PEI complexes compared to pDNA/TAT-PEG-PEI complexes were observed in presence of surfactant or BAL fluid ³⁸, yet siRNA complexes showed different stability profiles. After an incubation period of 20 minutes, PEI complexes were more stable in the presence of surfactant or mucin than PEG-PEI complexes, as shown in Figure 3. Whilst PEI complexes released only 2.5 % of their payload in 0.33 mg/ml mucin and 1.0 % in 0.33 mg/ml surfactant, PEI25k-PEG(20k)1 complexes were less stable and released 34.1 % and 15.8 % in 0.33 mg/ml mucin and surfactant respectively. The PEI25k-PEG(2k)10 complexes exhibited intermediate stability with release of 18.9 % and 5.0 % of their payload in 0.33 mg/ml mucin and surfactant respectively. The same trend had been shown earlier concerning stability in the presence of serum (22). Unmodified PEI formed the strongest complexes in terms of electrostatic interactions, while this interaction is decreased in PEGylated PEIs, where non-charged PEG chains are present which are hypothesized to hinder complex formation. In vivo, on the other hand, these electrostatically formed complexes can dissociate when high concentrations of competing polyanions are present. Further, it has to be noted that electrolyte complexes which are stable in vitro are not necessarily resistant to interaction with other charged components (39), while this is a property of sterically shielding complexes (29).

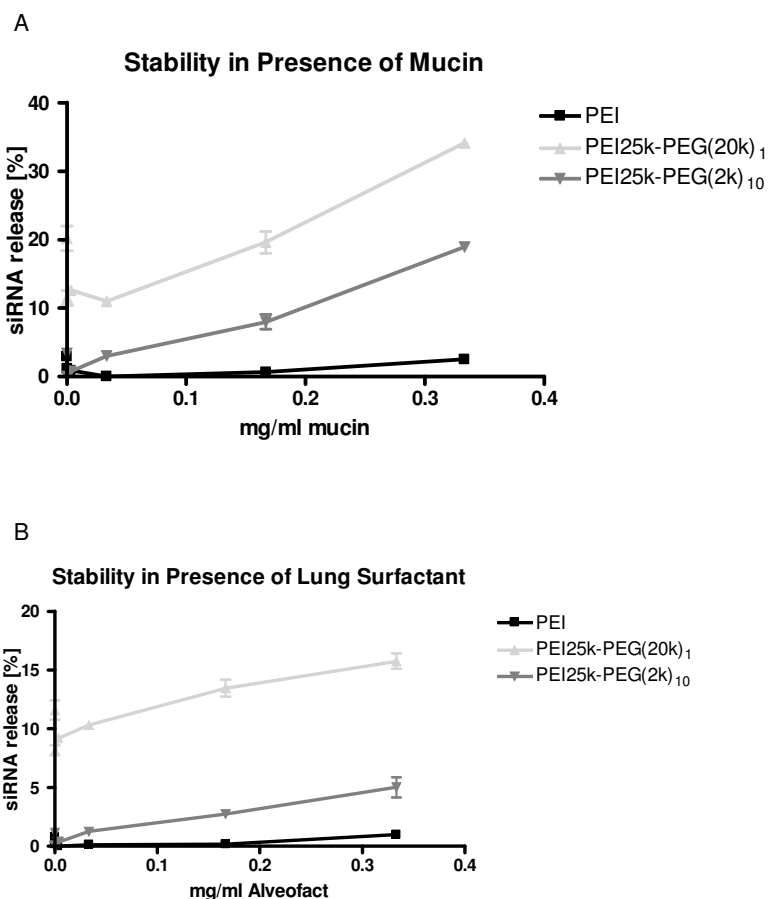


Figure 3: Stability of polyplexes in the presence of **A:** Mucin and **B:** Lung surfactant was the highest for unmodified PEI, followed by PEI25k-PEG(2k)₁ and PEI25k-PEG(20k)₁. This trend corroborates observations made in the presence of serum (22) but does not solely determine suitability for pulmonary application.

In vivo Biodistribution and Kinetics after Intratracheal Application:

As previously described (21, 40), radiolabeling nanocarriers with γ -emitters such as ^{111}In enables non-invasive three-dimensional imaging. Dual-isotope SPECT imaging was applied to non-invasively prove instillation into the lungs in living animals by co-localization of ^{111}In -labeled nanocarriers and $^{99\text{m}}\text{Tc}$ -labeled macro-agglomerated albumin (MAA), which is routinely used in the clinics for lung perfusion imaging due to accumulation in airway capillaries (41). Since the SYBR® Gold assays had revealed good condensation and the dye quenching assay had proven sufficient loading in terms of molecules of siRNA per polyplex, an N/P 6 was chosen for in vivo application which had been well tolerated in studies where polyplexes were applied intravenously (21, 40). Dual-isotope SPECT, shown in Figure 4A, proved non-invasively by co-localization of the $^{99\text{m}}\text{Tc}$ signal (greyscale) and

the ^{111}In signal (color) that the radiolabeled polyplexes were applied to the lungs. Interestingly, in some animals, a larger part of the dose was directed to the left lobe, which is also shown in Figure 4A, and depends on the position of the tubus during instillation and on the anatomy of the murine lung (42). Variations in airway branching patterns in mammals are known to contribute to differences in regional deposition in the lungs (43, 44). Three-dimensional (3D) SPECT images of mice that were only treated with ^{111}In -labeled polyplexes (but not with MAA) were taken 2, 24, and 48 hours after instillation to monitor biodistribution and clearance of the applied polyplexes. As demonstrated in Figure 4B, which shows a 6-week old balb/c mouse treated with siRNA/ ^{111}In -DTPA-PEI25k-PEG(2k)₁₀ polyplexes, radioactive signal could still be observed in the mouth and the upper trachea 24 hours post treatment, and excretion via the kidneys was slightly visible. Another 24 hours later (Figure 4C), radiolabeled material was obviously excreted via the kidneys, and liver deposition became slightly visible (See Supporting Information for 3D images). But the strongest signal was still observed in the lung; and only in the lower trachea radioactive material was still present. Labeled siRNA did not show accumulation in the kidneys but higher signals in the bladder and urine, as shown in Figure 5A. For more precise quantification, animals were sacrificed 48 hours post treatment, and organs were dissected for scintillation counting. Figure 5A only shows organs that demonstrated significant uptake. As already discussed for the 3D SPECT images, radioactive substance was still measurable in the trachea 48 hours after instillation. Interestingly, the residence time in the trachea decreased with PEGylation and was only detectable for polymers, not for siRNA. This can be explained by the interaction of the polymer with both mucus and cell surfaces, while siRNA was possibly released from the complex and was then most probably degraded and cleared from the trachea. As already discussed above, the deposition of instilled material depends strongly on the position of the tubus, the murine lung anatomy, and aerosolization would yield a more even distribution throughout the whole organ (42). Due to handling of radioactive materials, we decided to use instillation, which is a commonly used technique as well (2, 23, 37, 45). The disadvantages of liquid instillation are clearly local irritations evoked by intubation, the stress that the liquid bolus causes, of which an unknown amount may be coughed up or swallowed, and the non-uniform distribution due to the position of the application device in the trachea during delivery affecting the percentage of material deposited in the different lung lobes (46).

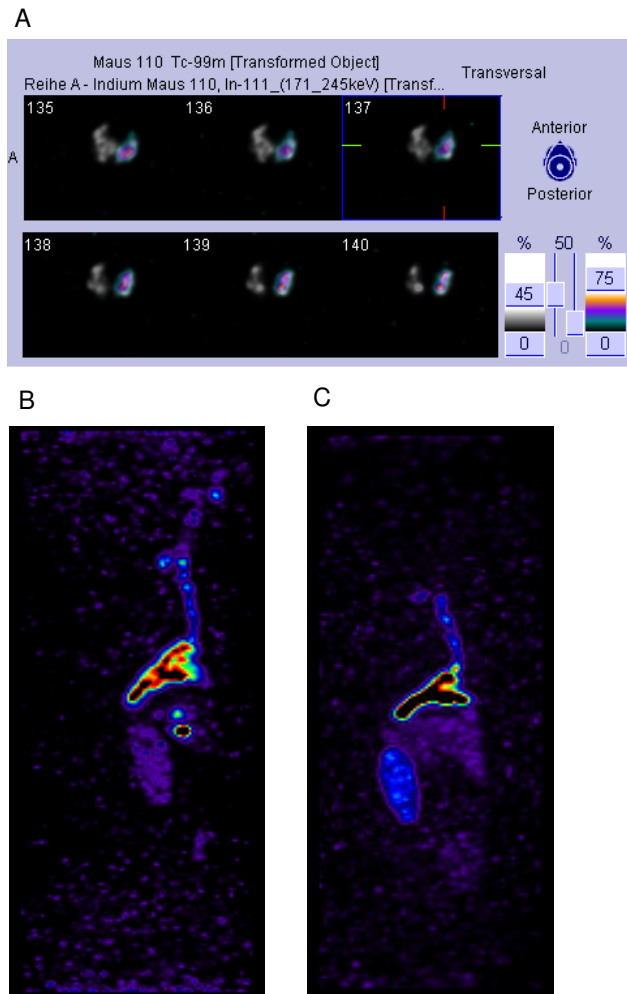


Figure 4A: Dual-Isotope SPECT Imaging of mice treated with ^{111}In -labeled PEI25k-PEG(2k)10/siRNA polyplexes and $^{99\text{m}}\text{Tc}$ -labeled MAA allowed for control of intratracheal application in the living animal. **4B:** 3D-SPECT after 24 and 48 (Figure 4C) hours post instillation showed slow elimination of radiolabeled polymer via the kidneys and circumvention of the first pass effect.

Especially in the group of mice treated with ^{111}In -DTPA-PEI25k /siRNA, a strong discrepancy between deposition to the left and right lobes was observed, which was only minor in all other groups. Interestingly, unmodified PEI 25 kDa remained in the lung to the greatest extent of all compounds labeled (total left + right lobe: 25.7 % ID, compare Figure 6B), while the two PEGylated polymers showed only about half the dose left after 48 hours. This again can be explained by stronger interaction of unmodified PEI with mucus and especially cell membranes which might cause sticking of the polymer. Another indication which corroborates this assumption is the fact that PEI25k-complexed siRNA did not remain in the lung to a greater extent than free siRNA. Apparently, 48 hours after

application, all siRNA complexed with PEI 25kDa was released from the polymer that possibly, after penetration of mucus, interacted strongly with cells and did not behave any differently from free siRNA. PEG-PEI/siRNA complexes, on the other hand, showed lower total retention but equivalent percentages of polymer and siRNA left after 48 hours. This let us hypothesize that PEG-PEI complexes were more stable after intratracheal application than PEI complexes, and this hypothesis will further be discussed below in the context of lung kinetics. Additionally to stability in vivo, another point that was crucial in our study was the circumvention of the first-pass effect, which is known to be fairly high for cationic carriers, due to rapid uptake by the reticulo-endothelial system (RES) (47). Here we showed that liver uptake, which was very prominent after i.v. injection of the same polyplexes (22), was strongly decreased to about 5 % ID of polymers and negligible amounts of siRNA. Interestingly, kidney accumulation of polymers increased with PEGylation, which was the other way round after systemic application (22). This surprising effect can be explained, though, by the large amount of unmodified PEI which remained in the lung and the lower systemic availability and renal excretion. Labeled siRNA, on the other hand did not accumulate in the kidneys but was found in the urine. This trend is fully in line with our earlier report that showed that (PEG)-PEI/siRNA polyplexes that reach the circulation dissociate, with the polymer accumulating in liver and kidneys and the siRNA being excreted into the urine (22). Systemic availability of all labeled compounds was measured in blood samples collected over 2 hours post application. While earlier systemic availability of pulmonary applied nanoparticles was only attributed to phagocytosis by macrophages in the deep lung (48), translocation of inhaled particles is now being studied by several groups who have demonstrated transcytosis (49) or transport of systemically available particles into the brain via olfactory nerves after pulmonary application (50). One concern we thoroughly addressed in order to avoid misleading pharmacokinetic data, is purification of the labeled material. With our optimized 2-step purification procedure (21), we are able to ensure that no free radiometal ions are present in the complex solution. Free indium or DTPA-indium would not accumulate in the liver or kidneys either, so we are rather sure that the systemically available radioactivity was not free label. Systemically available free siRNA is known to be excreted faster than degraded (1), although it is possible that part of the signal in the urine was caused by degradation of nucleic acids. Full length siRNA can be re-extracted from tissue, blood or urine samples and quantified, e.g. by autoradiography (51), which will be subject to a more thorough investigation which is currently underway. Although uptake of labeled siRNA into the circulation seemed to be very similar, no matter

which polymer was used for complexation (Figure 5B), calculation of the area under the curve (AUC) (Figure 5D) revealed following differences: Whilst PEI 25kDa complexed siRNA was available to the lowest extent in the first 20 minutes, which corroborates our data from the stability assay, the release of siRNA seemed to be delayed, and systemic availability surpassed that of free siRNA 1 hour after administration. PEG-PEI complexed siRNA, on the other hand, exhibited higher initial blood concentrations, according to their stability profiles shown in Figure 3, which did not further increase but even decreased in the case of PEI25k-PEG(2k)10 complexed siRNA. The decrease in systemic availability can easily be explained by extensive excretion into the urine, as shown in Figure 5A. Polymers that were endocytosed or transcytosed from the lung were deposited in the liver and kidneys to a greater extent than their payload, as demonstrated in Figure 5A. This also revealed shorter circulation and lower AUC values. PEI 25kDa, which was strongly retained in the lung, was only to a low extent taken up into circulation. The decrease in blood levels after 1 hour post application can be attributed to liver and kidney accumulation. PEI25k-PEG(20k)1 showed increasing systemic availability over 20 minutes post instillation followed by a steady state concentration. This polymer, equipped with one long PEG chain, is possibly least prone to recognition by liver macrophages or interaction with the cationic basal membrane in the kidneys. The systemic concentration of PEI25k-PEG(2k)10 increased more slowly but was also followed by a steady state concentration after 1 hour post application. The lower AUC and the slower increase of blood levels can be explained by stronger liver and kidney accumulation shown in Figure 5A and Figures 4B and 4C. Overall, AUC values of polymers were significantly lower than those of siRNA (** $p < 0.01$, Figure 5D). No differences were observed amongst the different polymers, but differences were more striking concerning siRNA. Due to the strong increase in blood levels of PEI 25kDa complexed siRNA after 20 minutes post application, AUC of free and PEI 25 kDa complexed siRNA were not significantly different. The AUC of PEI25k-PEG(20k)1 complexed siRNA was not significantly lower, whereas the decreased AUC of the PEI25k-PEG(2k)10 complexed siRNA was significant (* $p < 0.05$, Figure 5D), which was certainly an effect of excretion and stronger initial stability of the complexes, as also demonstrated in Figure 1B.

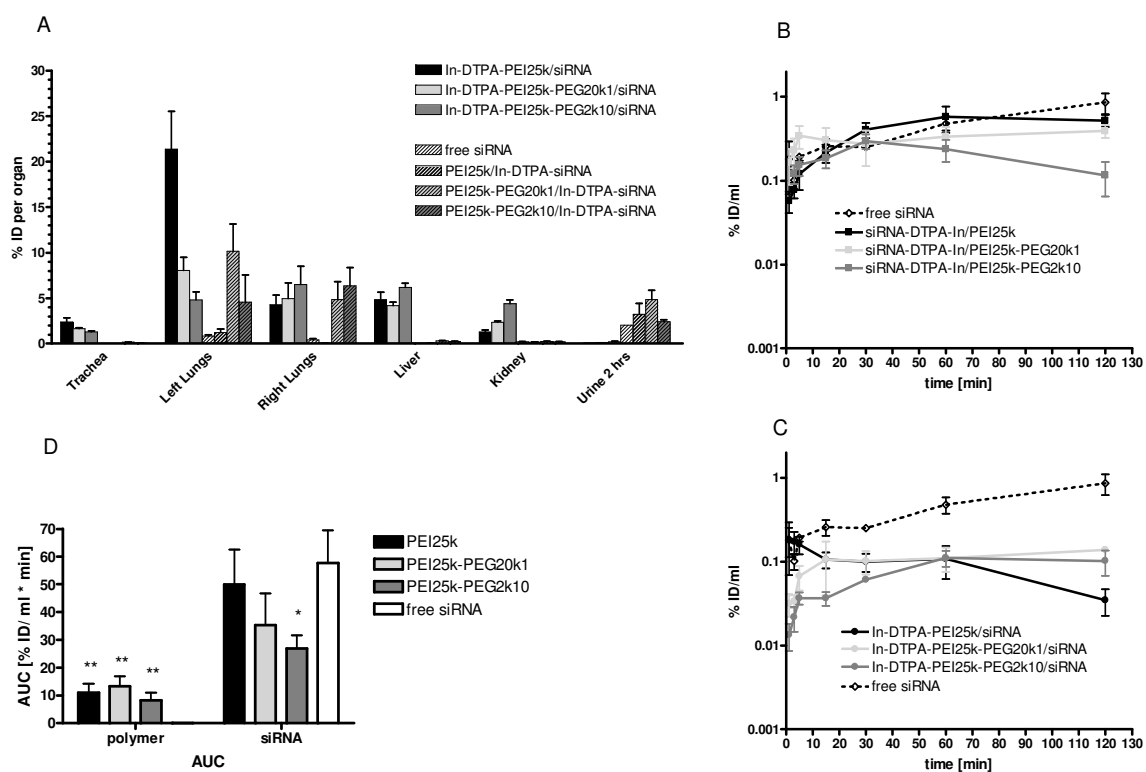
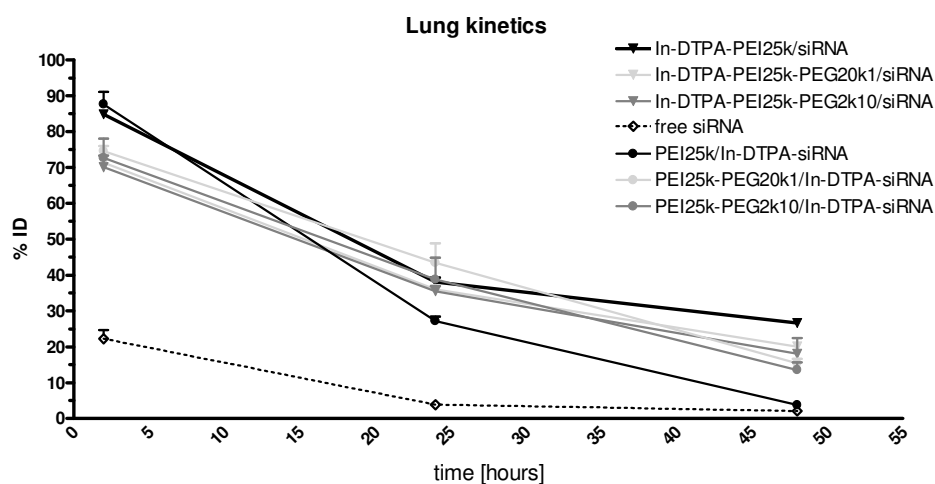


Figure 5A: Biodistribution of radiolabeled polymeric vectors and their payload measured in dissected organs 48 hours post instillation revealed that the highest signals were still found in the lungs, whereas liver deposition of polymers was about 5 % ID and siRNA was rather excreted than accumulated. **5B:** Systemic bioavailability of labeled siRNA complexed with PEI 25 kDa increased strongly 30 minutes post instillation, while PEG-PEI complexed siRNA showed higher blood levels immediately after application and did not further increase or even decreased over time. **5C:** Radiolabeled polymers were retained stronger in the lung (PEI 25 kDa) or accumulated slightly in the kidneys (PEG-PEIs) and showed lower blood levels than siRNA. **5D:** AUC values of labeled polymers were accordingly significantly (**p<0.01) lower than those of labeled siRNA. PEI25k-PEG(2k)10 complexed siRNA also exhibited a lower AUC value, caused by excretion to the urine.

While endpoint scintillation counting of dissected lungs only revealed residual concentration after sacrifice of the animals (Figure 5A), SPECT and planar gamma camera imaging enabled non-invasive imaging and quantification of the retention of radiolabeled material in the same animal over time. Scintillation counting analysis suggested that complexation of siRNA with PEI 25kDa did not provide any benefit over application of

free siRNA. If considering the kinetics of residual radioactivity in the lung over time, the picture looks a bit different: Although in the stability assay PEI complexes seemed to be most stable, it certainly has to be acknowledged that stability over time, and especially in high ionic strength solutions, might be lower than in the *in vitro* assay. We already discussed increasing blood levels of PEI 25 kDa complexed siRNA after 20 minutes post instillation, letting us assume that the polyplexes were stable in the presence of mucus and surfactant, but the release of siRNA obviously occurred to a later time point – possibly when polyplexes reached the cells and strongly interacted with cell surfaces. The analysis of radioactivity signals in the lungs taken by planar gamma camera imaging and analysis of ROIs, very well corroborated this assumption (Figure 6A). Whereas the amount of radioactively labeled PEI 25 kDa decreased slowly over 48 hours, that of PEI 25 kDa complexed siRNA decreased more rapidly than PEG-PEI complexed siRNA. The curves for PEG-PEI polymer and the corresponding payload showed very similar behavior. The analysis of three time points certainly can not be considered a pharmacokinetic study, but as shown in Figure 6B, data acquired in the imaging approach coincides well enough with that obtained from dissected organs to make a non-invasive prediction of the retention of labeled material in the lung. Most importantly, we were able to prove our assumption that PEG-PEI/siRNA complexes are more suitable for lung application than PEI/siRNA complexes concerning protection of siRNA and residing times in the lung.

A



B

	free siRNA		PEI 25 kDa		PEI25k-PEG(20k)1		PEI25k-PEG(2k)10	
	scintillation	imaging	scintillation	imaging	scintillation	imaging	scintillation	imaging
polymer			25.7% ± 4.8	26.7% ± 2.4	12.9% ± 2.1	20.1% ± 0.6	11.3% ± 2.7	18.0% ± 9.9
siRNA	1.2% ± 0.2	2.1% ± 1.2	1.3% ± 1.4	3.8% ± 0.7	14.9% ± 3.6	15.4% ± 2.9	11.0% ± 3.2	13.6% ± 4.7

Figure 6A: Kinetic profiles of radioactively labeled compounds in the lungs over 48 hours acquired by planar gamma camera imaging. **6B:** Comparison of data obtained by non-invasive imaging and scintillation counting of residual radioactivity in the lungs 48 hours post instillation.

Broncho-Alveolar Lavage:

Since there are various reports in the literature stating that cationic lipids used for pulmonary gene delivery result in immune and cytokine responses in mice (52-55), whereas aerosol delivery of PEI/DNA complexes did not induce high levels of cytokines (56), we investigated the effect of our siRNA loaded nanocarriers. Interestingly, as shown in Figure 7, our PEI/siRNA complexes had the lowest proinflammatory effect, whereas PEI25k-PEG(20k)1 complexes caused a 13-fold increase of CXCL1 (53.2pg/ml±53.3 vs. 4.1 pg/ml±2.6), 2-fold elevated levels of IL-6 (4.9pg/ml 2.2 vs. 2.3pg/ml±0.8) and a 2.5-fold increase of TNF- α (4.5pg/ml±2.5 vs. 2.1pg/ml±0.2) in the BALF. PEI(25)-PEG(2k)10 complexes caused a 1.5-fold increase of CXCL1 (21.4pg/ml±13.8 vs. 4.1 pg/ml±2.6), a 3-fold increase of IL-6 (7.5pg/ml±3.8 vs. 2.3pg/ml±0.8) and a 2.5-fold increase of TNF-

α levels (5.2pg/ml \pm 5.5 vs. 2.1pg/ml \pm 0.2). In addition to the acute phase cytokines response, the release of granulocyte-colony stimulating factor (G-CSF) and the interferon- γ inducible protein 10 (CXCL10) was more than ten times elevated for PEI(25)-PEG(2)10 compared to control (1x PBS treated mice), G-CSF (46.3pg/ml \pm 54.0 vs. 3.1pg/ml \pm 0.7) and CXCL10 (16.2pg/ml \pm 16.7 vs. 2.8pg/ml \pm 1.6). The PEGylated nanocarriers were therefore considered to have a moderate proinflammatory effect which was more prominent for PEI(25)-PEG(2)10. Concerning differential analysis of BAL cells, the two PEG-modified PEI nanocarriers caused more than 20 % recruitment of polymorphonuclear neutrophilic granulocytes (PMN), which is regarded as a hallmark of lung inflammation especially for the 48h response (data not shown). While BAL cells of mice treated with PEI 25kDa/siRNA polyplexes were exclusively macrophages, in accordance to our cytokine profile, where we could not detect elevated levels of acute phase cytokines could. It has to be remarked, though, that BAL was performed 48 hours post instillation, but cytokine levels in the BALF were reported to peak at 24 h after PEI/DNA aerosol exposure (56). A kinetic analysis as performed in the latter report will be part of our kinetic study concerning gene silencing.

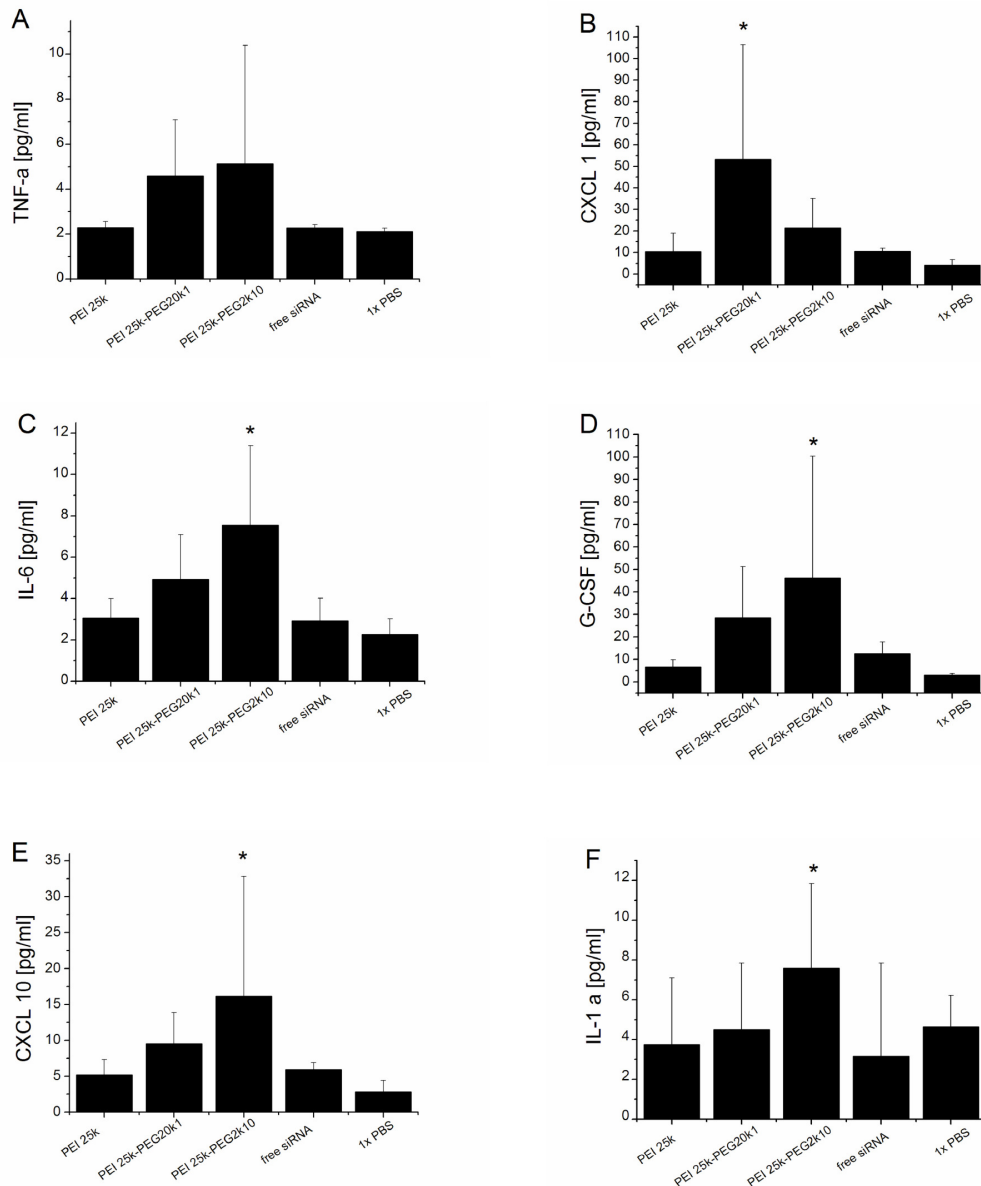


Figure 7 A-F: Cytokine release in BALF 48h after intratracheal instillation of siRNA polyplexes. Data represent mean \pm SD (n=8 for treatment with PEI polyplexes, n= 4 for controls (free siRNA and 1xPBS); significantly increased cytokine levels compared to control (1xPBS) were marked with an asterisk (*p<0.05).

Lung Histology:

Whilst nanomedicine is an emerging and promising field, possible health risks need to be considered as well. Application of nanomaterials to the lung often evokes an allusion to the effects of asbestos fibers on lung tissue. Indeed, also carbon black nanoparticles have been shown to bear health risks by interfering with cell signaling (57). The airways are a relatively robust barrier, being protected by a viscous layer of mucus and equipped with an

effective clearance mechanism, but alveoli are presumably more prone to damage. In the alveolar region, macrophage phagocytosis is the main mechanism of clearance, but nano-sized particles are designed not to be recognized by alveolar macrophages, which possibly might increase their irritating or toxic effects. In the case of positively charged particles, interaction with and toxic effects on cell membranes are well known and studied (58). Concerning lung toxicity, it has been shown that the three-dimensional structure and flexibility of the macromolecules has a strong impact on accessibility of charges and thus on their cytotoxic profiles (59). In order to study the impact of our nanocarriers, which have already been characterized for *in vitro* toxicity (Beyerle et al, in preparation), on lung tissue *in vivo*, we fixed dissected lungs in paraformaldehyde and analyzed paraffin sections after H&E staining. As demonstrated in Figure 8, we did not observe indications of inflammation in any of the lungs investigated at the light microscopic level. It has to be acknowledged though, that chronic effects cannot be precluded based on a single application and observation for just 48 hours.

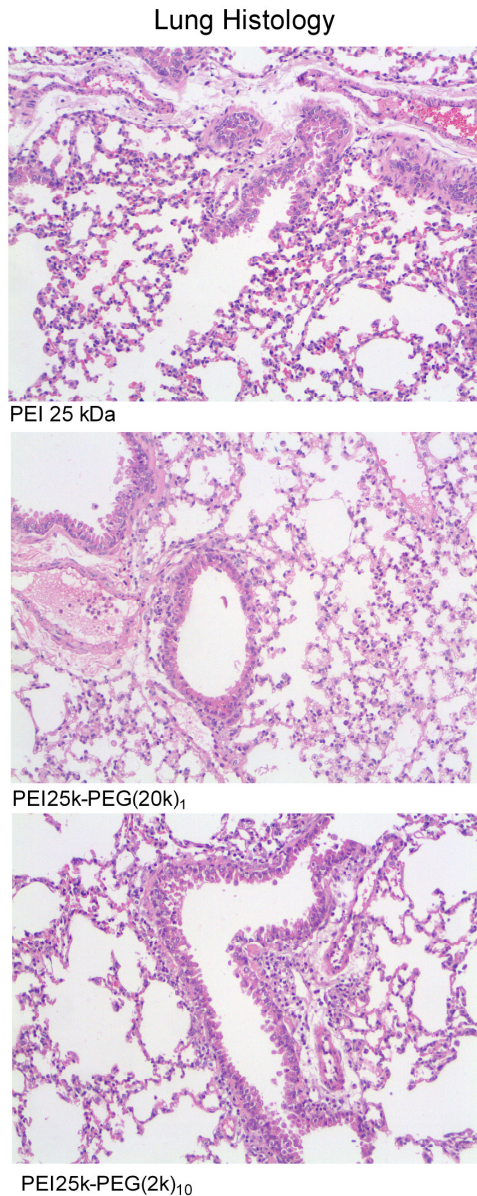


Figure 8: Light microscopy disclosed normal lung tissue. The bronchiolar and alveolar epithelium appeared normal and the interstitium and alveolar lumina showed no inflammation.

In vivo Knock Down:

In order to confirm that intratracheal siRNA delivery leads to effective intracellular siRNA concentration and functional activity, we treated actin-EGFP expressing mice with polyplexes containing 50 μg of anti-EGFP siRNA. This dose has been reported to be efficient in down regulation of EGFP in the same mouse strain after high pressure tail vein (HPTV) injection (60), and is below the dose that has been reported to be effective after intratracheal instillation (45). Due to the sustained retention of the polyplexes in the lung,

mice were sacrificed 5 days after instillation, and lungs were paraffin embedded after fixation in paraformaldehyde. In a preliminary study (data not shown) we compared fluorescence of paraffin sections to cryo sections in order to check on any adverse effects of paraformaldehyde or paraffin on fluorescence intensity. Neither revealed disadvantages, but cells in paraffin sections retained their morphology much better than those in cryo sections which encouraged us to embed all lungs for this study in paraffin. CLSM allowed us to qualitatively investigate the effects of anti-EGFP siRNA on the expression of EGFP. Figure 9A shows a bronchiolus of an untreated actin-EGFP mouse, where especially type II pneumocytes, but also all surrounding cells exhibit high fluorescence intensity. In the siRNA-treated mouse, fluorescence intensity in the bronchial cells seemed to be decreased (Figure 9B), and the effect becomes more apparent in the alveolar cells of non-treated (Figure 9C) versus treated animals (Figure 9D). Although we are well aware that this microscopic indication needs to be quantified in order to test the hypothesis, at this point we can safely assume that polyplexes reached the alveoli after instillation and are taken up into alveolar tissue where they are released into the cytosol in sufficient concentration for functional activity. In a first approach to quantify the knock down of EGFP expression, we have treated EGFP-expressing mice with PEG-PEI complexed specific (siEGFP) and non-specific (siFLuc) siRNA and measured EGFP in total lung homogenates. EGFP expression was found to be 42 % knocked down compared to siFLuc-treated animals and thereby significantly ($*p < 0.05$) reduced, and not significantly different from animals that do not express EGFP at all but only show autofluorescence of macrophages ($p > 0.05$). A thorough follow-up study investigating the time-course and dose-dependency of polyplexes made of the different polymers and the fractionation of lung homogenates into different populations of cells will provide more details.

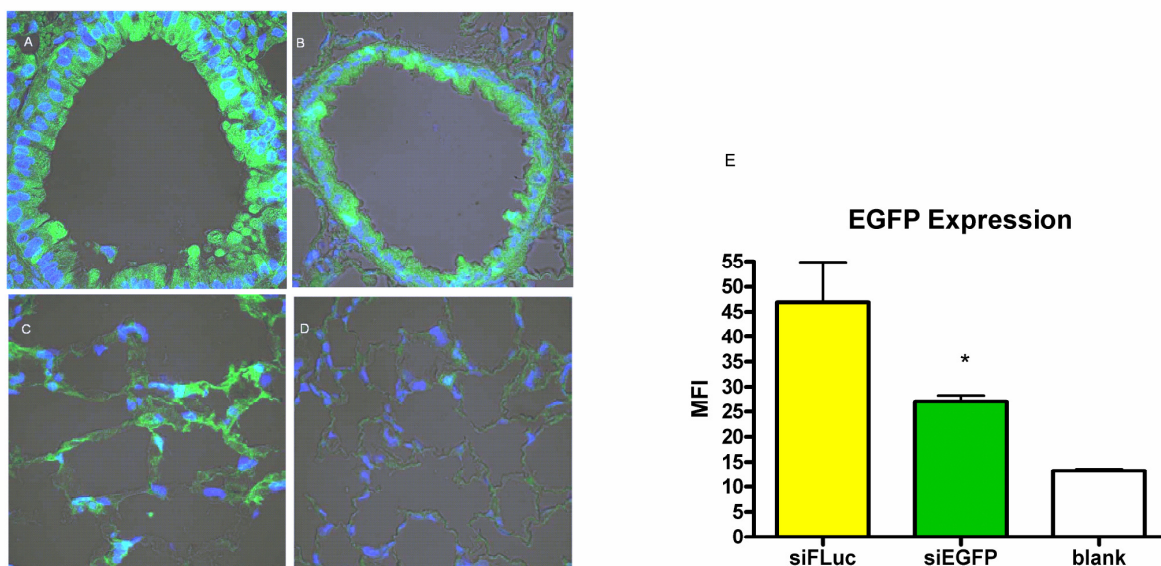


Figure 9: Knock down in actin-EGFP mice. **9A:** Bronchiolus of a control EGFP-mouse displaying high fluorescence intensity. **9B:** Bronchiolus of a PEI25k-PEG(2k)10/siRNA treated EGFP-mouse displaying lower fluorescence intensity. **9C:** Alveolar epithelium of a control EGFP-mouse displaying high fluorescence intensity. **9D:** Alveolar epithelium of a PEI25k-PEG(2k)10/siRNA treated EGFP-mouse displaying almost complete loss of fluorescence signal. **9E:** Knock down in actin-EGFP mice compared to non-EGFP-expressing mice (blank). EGFP-expression in lungs of siEGFP/PEI(25k)-PEG(2k)10 treated mice was down regulated by 42 % and is significantly ($p < 0.05$) lower than in mice treated with siFLuc/PEI(25k)-PEG(2k)10.

7.5 Conclusion

In conclusion, we have shown that 25/27mer partial 2'-OMe modified DsiRNA can be efficiently condensed with PEI and PEG-PEI. From our direct condensation assay we have learned that this type of experiment reveals data that has to be critically interpreted. We have disclosed that PEI/siRNA polyplexes are more stable than PEG-PEI/siRNA polyplexes over 20 minutes in the presence of mucin or surfactant under in vitro conditions. By comparison of planar imaging with conventional scintillation counting techniques, we showed that for the understanding of the behavior of nanocarriers in vivo, simple endpoint measurements are insufficient. While data obtained by both methods coincided well, 3D and planar imaging enabled tracking the biodistribution over time. Although PEI/siRNA complexes seemed to be most stable in the in vitro stability assays, their in vivo performance was poor with PEI being left in the lungs and the siRNA payload released and

excreted. Despite of their slightly higher proinflammatory potential, we favored PEG-PEI/siRNA complexes for investigation of functional gene silencing activity in vivo for sustained release reasons and were able to report indications of success with no histological abnormality detected. These results are very encouraging for further investigation and quantification of in vivo gene silencing in the lung after intratracheal instillation of PEG-PEI/siRNA complexes.

7.6 Acknowledgements

We are grateful to Prof. Renz and Dr. Garn (Department of Clinical Chemistry, Philipps-Universität Marburg) for the generous use of equipment and facilities, to Viktoria Morokina (Department of Pathology, University Hospital Giessen-Marburg) and Klaus Keim (Department of Pharmaceutics and Biopharmacy, Philipps Universität Marburg) for excellent technical support and to Thomas Carlsson (Department of Experimental Neurology, Philipps Universität Marburg) for supplying us with Actin-GFP expressing mice. Deutsche Forschungsgemeinschaft (DFG Forschergruppe 627), MEDITRANS, an Integrated Project funded by the European Commission under the Sixth Framework (NMP4-CT-2006-026668), and the German Lung Foundation (Deutsche Lungenstiftung e.V.) are gratefully acknowledged.

7.7 References

- (1) Dykxhoorn, D. M., Palliser, D., and Lieberman, J. (2006) The silent treatment: siRNAs as small molecule drugs. *Gene Ther* 13, 541-52.
- (2) Garbuzenko, O. B., Saad, M., Betigeri, S., Zhang, M., Vetcher, A. A., Soldatenkov, V. A., Reimer, D. C., Pozharov, V. P., and Minko, T. (2009) Intratracheal versus intravenous liposomal delivery of siRNA, antisense oligonucleotides and anticancer drug. *Pharm Res* 26, 382-94.
- (3) Chandy, D., Maguire, G., and Aronow, W. S. (2009) Lung cancer: the importance of early intervention. *Compr Ther* 35, 18-23.
- (4) Centre, W. M. (2008) in *Fact Sheet N°310*, World Health Organization, Geneva.
- (5) Zhang, W., and Tripp, R. A. (2008) RNA interference inhibits respiratory syncytial virus replication and disease pathogenesis without inhibiting priming of the memory immune response. *J Virol* 82, 12221-31.

- (6) Bitko, V., Musiyenko, A., Shulyayeva, O., and Barik, S. (2005) Inhibition of respiratory viruses by nasally administered siRNA. *Nat Med* 11, 50-5.
- (7) Kwok, T., Helfer, H., Alam, M. I., Heinrich, J., Pavlovic, J., and Moelling, K. (2009) Inhibition of influenza A virus replication by short double-stranded oligodeoxynucleotides. *Arch Virol* 154, 109-14.
- (8) Hammond, S. M., Boettcher, S., Caudy, A. A., Kobayashi, R., and Hannon, G. J. (2001) Argonaute2, a link between genetic and biochemical analyses of RNAi. *Science* 293, 1146-50.
- (9) Kim, D. H., Behlke, M. A., Rose, S. D., Chang, M. S., Choi, S., and Rossi, J. J. (2005) Synthetic dsRNA Dicer substrates enhance RNAi potency and efficacy. *Nat Biotechnol* 23, 222-6.
- (10) Manoharan, M. (2004) RNA interference and chemically modified small interfering RNAs. *Curr Opin Chem Biol* 8, 570-9.
- (11) Geary, R. S., Watanabe, T. A., Truong, L., Freier, S., Lesnik, E. A., Sioufi, N. B., Sasmor, H., Manoharan, M., and Levin, A. A. (2001) Pharmacokinetic properties of 2'-O-(2-methoxyethyl)-modified oligonucleotide analogs in rats. *J Pharmacol Exp Ther* 296, 890-7.
- (12) Judge, A. D., Robbins, M., Tavakoli, I., Levi, J., Hu, L., Fronda, A., Ambegia, E., McClintock, K., and MacLachlan, I. (2009) Confirming the RNAi-mediated mechanism of action of siRNA-based cancer therapeutics in mice. *J Clin Invest* 119, 661-73.
- (13) Sioud, M., Furset, G., and Cekaite, L. (2007) Suppression of immunostimulatory siRNA-driven innate immune activation by 2'-modified RNAs. *Biochem Biophys Res Commun* 361, 122-6.
- (14) Zhang, X., Shan, P., Jiang, D., Noble, P. W., Abraham, N. G., Kappas, A., and Lee, P. J. (2004) Small interfering RNA targeting heme oxygenase-1 enhances ischemia-reperfusion-induced lung apoptosis. *J Biol Chem* 279, 10677-84.
- (15) Massaro, D., and Massaro, G. D. (2004) Critical period for alveologenesis and early determinants of adult pulmonary disease. *Am J Physiol Lung Cell Mol Physiol* 287, L715-7.
- (16) Kong, X., Zhang, W., Lockey, R. F., Auais, A., Piedimonte, G., and Mohapatra, S. S. (2007) Respiratory syncytial virus infection in Fischer 344 rats is attenuated by short interfering RNA against the RSV-NS1 gene. *Genet Vaccines Ther* 5, 4.

-
- (17) Tompkins, S. M., Lo, C. Y., Tumpey, T. M., and Epstein, S. L. (2004) Protection against lethal influenza virus challenge by RNA interference in vivo. *Proc Natl Acad Sci U S A* 101, 8682-6.
- (18) Petersen, H., Fechner, P. M., Fischer, D., and Kissel, T. (2002) Synthesis, Characterization, and Biocompatibility of Polyethylenimine-graft-poly(ethylene glycol) Block Copolymers. *Macromolecules* 35, 6867-6874.
- (19) Rose, S. D., Kim, D. H., Amarzguioui, M., Heidel, J. D., Collingwood, M. A., Davis, M. E., Rossi, J. J., and Behlke, M. A. (2005) Functional polarity is introduced by Dicer processing of short substrate RNAs. *Nucleic Acids Res* 33, 4140-56.
- (20) Breunig, M., Hozsa, C., Lungwitz, U., Watanabe, K., Umeda, I., Kato, H., and Goepferich, A. (2008) Mechanistic investigation of poly(ethylene imine)-based siRNA delivery: disulfide bonds boost intracellular release of the cargo. *J Control Release* 130, 57-63.
- (21) Merkel, O. M., Librizzi, D., Pfestroff, A., Schurrat, T., Behe, M., and Kissel, T. (2009) In vivo SPECT and real-time gamma camera imaging of biodistribution and pharmacokinetics of siRNA delivery using an optimized radiolabeling and purification procedure. *Bioconjug Chem* 20, 174-82.
- (22) Merkel, O. M., Librizzi, D., Pfestroff, A., Schurrat, T., Buyens, K., Sanders, N. N., De Smedt, S. C., Behe, M., and Kissel, T. (2009) Stability of siRNA polyplexes from poly(ethylenimine) and poly(ethylenimine)-g-poly(ethylene glycol) under in vivo conditions: Effects on pharmacokinetics and biodistribution measured by Fluorescence Fluctuation Spectroscopy and Single Photon Emission Computed Tomography (SPECT) imaging. *J Control Release*.
- (23) Yu, H., Buff, S. M., Baatz, J. E., and Virella-Lowell, I. (2008) Oral instillation with surfactant phospholipid: a reliable alternative to intratracheal injection in mouse studies. *Lab Anim* 42, 294-304.
- (24) Herz, U., Braun, A., Ruckert, R., and Renz, H. (1998) Various immunological phenotypes are associated with increased airway responsiveness. *Clin Exp Allergy* 28, 625-34.
- (25) Prabhakar, U., Eirikis, E., Reddy, M., Silvestro, E., Spitz, S., Pendley, C., 2nd, Davis, H. M., and Miller, B. E. (2004) Validation and comparative analysis of a multiplexed assay for the simultaneous quantitative measurement of Th1/Th2

- cytokines in human serum and human peripheral blood mononuclear cell culture supernatants. *J Immunol Methods* 291, 27-38.
- (26) Mao, S., Neu, M., Germershaus, O., Merkel, O., Sitterberg, J., Bakowsky, U., and Kissel, T. (2006) Influence of Polyethylene Glycol Chain Length on the Physicochemical and Biological Properties of Poly(ethylene imine)-graft-Poly(ethylene glycol) Block Copolymer/SiRNA Polyplexes. *Bioconjug Chem* 17, 1209-18.
- (27) Germershaus, O., Mao, S., Sitterberg, J., Bakowsky, U., and Kissel, T. (2008) Gene delivery using chitosan, trimethyl chitosan or polyethylenglycol-graft-trimethyl chitosan block copolymers: establishment of structure-activity relationships in vitro. *J Control Release* 125, 145-54.
- (28) Van Rompaey, E., Engelborghs, Y., Sanders, N., De Smedt, S. C., and Demeester, J. (2001) Interactions between oligonucleotides and cationic polymers investigated by fluorescence correlation spectroscopy. *Pharm Res* 18, 928-36.
- (29) Glodde, M., Sirsi, S. R., and Lutz, G. J. (2006) Physicochemical properties of low and high molecular weight poly(ethylene glycol)-grafted poly(ethylene imine) copolymers and their complexes with oligonucleotides. *Biomacromolecules* 7, 347-56.
- (30) Gray, D. (1996) Circular Dichroism of Protein - Nucleic Acid Interactions, in *Circular Dichroism and the Conformational Analysis of Biomolecules (The Language of Science)* (Fasman, G., Ed.) pp 469-500, Plenum Press, New York.
- (31) Woody, R. W. (1995) Circular dichroism. *Methods Enzymol* 246, 34-71.
- (32) Saenger, W. (1984) *Principles of Nucleic Acid Structure*, Springer-Verlag, Berlin.
- (33) Inoue, H., Hayase, Y., Imura, A., Iwai, S., Miura, K., and Ohtsuka, E. (1987) Synthesis and hybridization studies on two complementary nona(2'-O-methyl)ribonucleotides. *Nucleic Acids Res* 15, 6131-48.
- (34) Evdokimov, Y. M., Pyatigorskaya, T. L., Polyvtsev, O. F., Akimenko, N. M., Kadykov, V. A., Tsvankin, D. Y., and Varshavsky, Y. M. (1976) A comparative X-ray diffraction and circular dichroism study of DNA compact particles formed in water-salt solutions, containing poly(ethylene glycol). *Nucleic Acids Res* 3, 2353-66.
- (35) Minyat, E. E., Ivanov, V. I., Kritzyn, A. M., Minchenkova, L. E., and Schyolkina, A. K. (1979) Spermine and spermidine-induced B to A transition of DNA in solution. *J Mol Biol* 128, 397-409.

-
- (36) Steely, H. T., Jr., Gray, D. M., and Lang, D. (1986) Study of the circular dichroism of bacteriophage phi 6 and phi 6 nucleocapsid. *Biopolymers* 25, 171-88.
- (37) Li, B. J., Tang, Q., Cheng, D., Qin, C., Xie, F. Y., Wei, Q., Xu, J., Liu, Y., Zheng, B. J., Woodle, M. C., Zhong, N., and Lu, P. Y. (2005) Using siRNA in prophylactic and therapeutic regimens against SARS coronavirus in Rhesus macaque. *Nat Med* 11, 944-51.
- (38) Rubin, B. K. (2002) Physiology of airway mucus clearance. *Respir Care* 47, 761-8.
- (39) Burke, R. S., and Pun, S. H. (2008) Extracellular barriers to in Vivo PEI and PEGylated PEI polyplex-mediated gene delivery to the liver. *Bioconjug Chem* 19, 693-704.
- (40) Merkel, O., Librizzi, D., Pfestroff, A., Schurrat, T., Buyens, K., Sanders, N., De Smedt, S. C., Behe, M., and Kissel, T. (2009) Stability of siRNA polyplexes from poly(ethylenimine) and poly(ethylenimine)-g-poly(ethylene glycol) under in vivo conditions: Effects on pharmacokinetics and biodistribution measured by Fluorescence Fluctuation Spectroscopy and Single Photon Emission Computed Tomography (SPECT) imaging. *Journal of Controlled Release*.
- (41) Shih, W. J., Robinson, M. C., Huber, C., and Pulmano, C. (1995) Tc-99m MAA lung perfusion scintigraphy performed before and after pulmonary embolectomy for saddle-type pulmonary embolism. *Clin Nucl Med* 20, 128-31.
- (42) Cryan, S. A., Sivadas, N., and Garcia-Contreras, L. (2007) In vivo animal models for drug delivery across the lung mucosal barrier. *Adv Drug Deliv Rev* 59, 1133-51.
- (43) Esch, J. L., Spektor, D. M., and Lippmann, M. (1988) Effect of lung airway branching pattern and gas composition on particle deposition. II. Experimental studies in human and canine lungs. *Exp Lung Res* 14, 321-48.
- (44) Spektor, D. M., Hunt, P. R., Rosenthal, F., and Lippmann, M. (1985) Influence of airway and airspace sizes on particle deposition in excised donkey lungs. *Exp Lung Res* 9, 363-87.
- (45) Lomas-Neira, J. L., Chung, C. S., Wesche, D. E., Perl, M., and Ayala, A. (2005) In vivo gene silencing (with siRNA) of pulmonary expression of MIP-2 versus KC results in divergent effects on hemorrhage-induced, neutrophil-mediated septic acute lung injury. *J Leukoc Biol* 77, 846-53.
- (46) Burnell, P. K. P., Kidger, J., Gascoigne, M., and Kotzer, C. (2006) Powder deposition in rats assessed in vivo and in silico, in *Respiratory Drug Delivery X*

- (Dalby, R. N., Byron, P. R., Peart, J., Suman, J., and Farr, S., Eds.) pp 625–627, Davis Healthcare International Publishing, LCC, River Grove, IL.
- (47) Fenske, D. B., MacLachlan, I., and Cullis, P. R. (2001) Long-circulating vectors for the systemic delivery of genes. *Curr Opin Mol Ther* 3, 153-8.
- (48) Nemmar, A., Vanbilloen, H., Hoylaerts, M. F., Hoet, P. H., Verbruggen, A., and Nemery, B. (2001) Passage of intratracheally instilled ultrafine particles from the lung into the systemic circulation in hamster. *Am J Respir Crit Care Med* 164, 1665-8.
- (49) Kato, T., Yashiro, T., Murata, Y., Herbert, D. C., Oshikawa, K., Bando, M., Ohno, S., and Sugiyama, Y. (2003) Evidence that exogenous substances can be phagocytized by alveolar epithelial cells and transported into blood capillaries. *Cell Tissue Res* 311, 47-51.
- (50) Oberdorster, G., Sharp, Z., Atudorei, V., Elder, A., Gelein, R., Lunts, A., Kreyling, W., and Cox, C. (2002) Extrapulmonary translocation of ultrafine carbon particles following whole-body inhalation exposure of rats. *J Toxicol Environ Health A* 65, 1531-43.
- (51) Malek, A., Merkel, O., Fink, L., Czubayko, F., Kissel, T., and Aigner, A. (2009) In vivo pharmacokinetics, tissue distribution and underlying mechanisms of various PEI(-PEG)/siRNA complexes. *Toxicol Appl Pharmacol* 236, 97-108.
- (52) Li, S., Wu, S. P., Whitmore, M., Loeffert, E. J., Wang, L., Watkins, S. C., Pitt, B. R., and Huang, L. (1999) Effect of immune response on gene transfer to the lung via systemic administration of cationic lipidic vectors. *Am J Physiol* 276, L796-804.
- (53) Freimark, B. D., Blezinger, H. P., Florack, V. J., Nordstrom, J. L., Long, S. D., Deshpande, D. S., Nochumson, S., and Petrak, K. L. (1998) Cationic lipids enhance cytokine and cell influx levels in the lung following administration of plasmid: cationic lipid complexes. *J Immunol* 160, 4580-6.
- (54) Freimark, B. D., Blezinger, H. P., Florack, V. J., Nordstrom, J. L., Long, S. D., Deshpande, D. S., Nochumson, S., and Petrak, K. L. (1998) Cationic Lipids Enhance Cytokine and Cell Influx Levels in the Lung Following Administration of Plasmid: Cationic Lipid Complexes. *J Immunol* 160, 4580-4586.
- (55) Li, S., Wu, S.-P., Whitmore, M., Loeffert, E. J., Wang, L., Watkins, S. C., Pitt, B. R., and Huang, L. (1999) Effect of immune response on gene transfer to the lung via systemic administration of cationic lipidic vectors. *Am J Physiol Lung Cell Mol Physiol* 276, L796-804.

- (56) Gautam, A., Densmore, C. L., and Waldrep, J. C. (2001) Pulmonary cytokine responses associated with PEI-DNA aerosol gene therapy. *Gene Ther* 8, 254-7.
- (57) Brown, D. M., Donaldson, K., Borm, P. J., Schins, R. P., Dehnhardt, M., Gilmour, P., Jimenez, L. A., and Stone, V. (2004) Calcium and ROS-mediated activation of transcription factors and TNF-alpha cytokine gene expression in macrophages exposed to ultrafine particles. *Am J Physiol Lung Cell Mol Physiol* 286, L344-53.
- (58) Hong, S., Leroueil, P. R., Janus, E. K., Peters, J. L., Kober, M. M., Islam, M. T., Orr, B. G., Baker, J. R., Jr., and Banaszak Holl, M. M. (2006) Interaction of polycationic polymers with supported lipid bilayers and cells: nanoscale hole formation and enhanced membrane permeability. *Bioconjug Chem* 17, 728-34.
- (59) Singh, A. K., Kasinath, B. S., and Lewis, E. J. (1992) Interaction of polycations with cell-surface negative charges of epithelial cells. *Biochim Biophys Acta* 1120, 337-42.
- (60) Wesche-Soldato, D. E., Chung, C. S., Lomas-Neira, J., Doughty, L. A., Gregory, S. H., and Ayala, A. (2005) In vivo delivery of caspase-8 or Fas siRNA improves the survival of septic mice. *Blood* 106, 2295-301.

8 Off-target effects in non-viral siRNA delivery – A study on the effect of polymer genomics on in vitro cell culture models

In Preparation for the Journal of Controlled Release

8.1 Abstract

Since off-target effects in non-viral siRNA delivery are common but not well understood, in this study we thoroughly investigated single sources of unexpected events and their interplay.

A variety of stably luciferase expressing cell lines was compared concerning toxic effects after transfection with polyplexes of siRNA and polyethylene imine (PEI) or polyethylene glycol-grafted PEI (PEG-PEI). Cell viability, LDH release, genetic profiles of molecular mechanisms of toxicity and activation of the driving promoter were investigated. Eventually, two cell lines which only differed in the driving promoter were established.

We were able to confirm that PEG-PEI is generally better tolerated than PEI, but also showed that in a cell line and concentration dependent manner, PEG-PEIs can activate apoptosis pathways. While both polymers caused sigmoidal dose-response curves of cell viability in L929 cells ($IC_{50}(\text{PEI}) = 6 \mu\text{g/ml}$, $IC_{50}(\text{PEG-PEI}) = 11 \mu\text{g/ml}$), H1299/Luc cells exhibited only sigmoidal dose-response for PEI but strongly increased cell viability between 0.002 and 0.25 mg/ml PEG-PEI. Gene expression profiling revealed that these cells appeared to undergo apoptosis via thousand-fold activation of TNF receptor-associated factors. Additional to the influence of cell type, the role of the promoter driving the gene of interest in artificial cell culture models was elucidated, and it was shown that NF κ B mediated activation of CMV promoter interferes with knockdown experiments.

Polymeric vectors cannot be considered as inert substances. Their effects in vitro and in vivo depend on a number of parameters which have to be investigated before a vector and model can be used together. While ruling out off-target effects is highly important in screening models, these effects can therapeutically be exploited for synergism.

8.2 Introduction

Due to safety issues of viral vectors, non-viral systems for siRNA delivery enjoy great popularity. Several cationic lipids, polymers or dendrimers are sold as handy transfection reagents. But in the last years, reports about “polymer genomics” (1) or “toxicogenomics” (2) are increasing, proving that many drug delivery systems are not inert components. Polyethyleneimine (PEI), the most commonly used polymer in gene transfection, poloxamers, poly amidoamine (PAMAM) and diaminobutane (DAB) have been reported to

cause up- and down-regulation of hundreds of genes in treated cells (2). One has to differentiate between the effects the pure transfection reagents cause and those generated by lipo-, poly- or dendriplexes.

Another issue in vitro screening of bioactivity of transfection reagents or siRNA sequences is the cell model used. Reporter genes like GFP, luciferase, β -galactosidase are commonly utilized in cell culture models since their expression can easily and relatively inexpensively be quantified. In case of siRNA delivery studies, reporter gene assays can only be employed if either the plasmid encoding the reporter gene is co-delivered (3-5), or if stably transfected cell lines are used (6-8). Both approaches display major drawbacks: “Co-transfection” of plasmid and siRNA requires plasmid and siRNA to be complexed with the same transfection reagent, since it can not be maintained that there will not be interchange between the two sorts of nucleic acids complexed by different transfection reagents. And as reported earlier, transfection reagents that work well for plasmid delivery are not necessarily good for siRNA transfection and vice versa (6, 9, 10). By transfecting cells with a certain transfection reagent, uniform protein expression can not be ensured. Therefore, co-transfection bears a second source of uncertainty concerning the results of protein downregulation. Hence, stably transfected cells that “pseudo-endogenously” express reporter genes are widely used. After stable transfection, cells are selected by treatment with antibiotics against which the successfully transfected cells are resistant. Single clones are picked and propagated, and the expression of the gene of interest in a certain population is widely uniform (11). The catch of this system is that a rather artificial cell system is generated in which the reporter gene expression is driven by a certain promoter. If this promoter is down- or up-regulated, the expression of the target gene is affected as well.

Due to several observations of effects of polymeric vectors (1, 2) and influences on the driving promoter (12), in this study we investigated both phenomena separately as well as the interconnection between both of them in order to interpret off-target effects in non-viral siRNA delivery and to optimize further polymer and cell culture design.

8.3 Materials and Methods

Materials:

Branched polyethylene imine with a molecular weight of 25 kDa (PEI 25 kDa, Polymin™, 25 kDa) was a gift from BASF (Ludwigshafen, Germany). The block copolymers poly(ethylene glycol)-poly(ethylene imine) PEI(25k)-PEG(30k)1, PEI(25k)-PEG(20k)1,

and PEI(25k)-PEG(550)30 were synthesized as described earlier (13). Two different siRNA duplexes, siLuc (Anti-Luciferase specific sequence) and siCONTROL (non-specific control sequence IX), were bought from Dharmacon (Lafayette, CO, USA). The luciferase encoding plasmid pTRE2hyg-Luc and the cell lines CHO/Luc and HeLa/TetOff were purchased from Clontech (Saint-Germain-en-Laye, France). Luciferase Assay Reagent (LAR) and Cell Culture Lysis Reagent (CCLR) were bought from Promega (Mannheim, Germany), LipofectamineTM2000 from Invitrogen (Karlsruhe, Germany), *E. coli* K12 DH5 α (laboratory stock), the restriction enzymes BamHI and NotI from Fermentas (St. Leon-Rot, Germany), Qiagen Plasmid Giga Kit and RNeasy Mini columns from Qiagen (Hilden, Germany), and the PCR-Array RT²-ProfilerTM, the cDNA synthesis assay kit First Strand Kit (C-02), and the mastermix Super Array PCR master mix were bought from SuperArray Bioscience Corporation (Frederick, MD, USA).

Cell Culture:

L929 murine fibroblasts were purchased from LG Promochem, (Wesel, Germany) and maintained in DMEM low glucose (PAA Laboratories, Cölbe, Germany), supplemented with 10% fetal calf serum (Cytogen, Sinn, Germany), in humidified atmosphere with 5% CO₂ at 37°C.

NCI-H1299 cells were purchased from LG Promochem (Wesel, Germany), and transfected with a StimulightTM Reporter Vector pHTS-CRE (Biomyx, San Diego, USA) containing the luciferase reporter gene and a hygromycin resistance gene formulated with Lipofectamine and PLUS reagent (Invitrogen, Karlsruhe, Germany) as recommended by the manufacturer. Stably transfected cells were selected in cell culture medium containing 200 μ g/ml hygromycin B (Invitrogen, Karlsruhe, Germany) in a previously described procedure (14). Briefly, clones were propagated and characterized concerning luciferase expression and proliferation rate, and only one of the clones was picked for the further propagation. Cells were maintained in RPMI 1640 (PAA Laboratories, Cölbe, Germany), supplemented with 10 mM HEPES, 1.0 mM sodium pyruvate, and 10 % fetal bovine serum (Cytogen, Sinn, Germany), in humidified atmosphere with 8 % CO₂ at 37°C.

HeLa/TetOff and CHO/Luc cells were purchased from Clontech (Saint-Germain-en-Laye, France) and maintained in DMEM high glucose (PAA Laboratories, Cölbe, Germany), supplemented with 10 % fetal bovine serum (Cytogen, Sinn, Germany), in humidified atmosphere with 5 % CO₂ at 37°C.

Transfection Experiments:

Transfections were performed as previously described (14). Briefly, cells were seeded in 96 well plates (Thermo Fisher Scientific (Nunc GmbH & Co. KG), Langenselbold, Germany) with a density of 8,000 cells per well. Transfection efficiencies of the polymers were compared to PEI 25kDa and Lipofectamine2000 (Invitrogen, Karlsruhe, Germany) (LF) as a positive control by treating the cells with polyplexes of 10 pmol siLuc or non-specific control siCONTROL and polymers at N/P 10 in a total volume of 200 μ l (50nM). In mock transfections, cells were treated with polymer or lipid only. Medium was changed 4 hours post transfection and cells were incubated for another 44 hours before they were washed with PBS buffer, lysed with CCLR (Promega, Mannheim, Germany) and assayed for luciferase expression with a 10 mM luciferin containing solution (Promega, Mannheim, Germany) on a BMG LUMIstar OPTIMA luminometer plate reader (BMG Labtech, Offenburg, Germany). Results are given as mean values of a replicate of four \pm SD.

MTT-Assays:

Cytotoxicity of the polymers was investigated by MTT assay as reported earlier (15). 24 hours before they were treated with polymer solutions of increasing concentrations in the range of 0.0005 to 0.4 mg/ml, murine L929 fibroblasts or human non-small cell lung cancer cells H1299/Luc were seeded on 96-well plates at a density of 8000 cells per well. Another 24 hrs later, medium was changed; MTT solution was added into fresh serum-free medium and incubated with the cells for 4 hrs. Remaining mitochondrial enzyme activity compared to untreated cells was determined photometrically after cell lysis in 200 μ l DMSO by measuring absorbance of enzymatically formed formazane at 580 nm with 690 nm background corrections. Results are gives as mean values of a replicate of four \pm SD.

LDH-Assays:

Membrane toxicity of the polymers was investigated by LDH assay (CytoTox-OneTM, Promega, Mannheim, Germany) according to the manufacturer's protocol. H1299/Luc cells were seeded in puruvate-free medium on white FluoroNuncTM 96 well plates (Nunc, Thermo Fisher Scientific, Langenselbold, Germany) at a density of 8000 cells per well 24 hours before they were treated with polymer solutions of increasing concentrations in the range of 0.004 to 0.2 mg/ml. Another 24 hrs later, 100 μ l of a mixture of substrate mix and

assay buffer were added into the polymer containing medium and incubated with the cells and used medium for 10 minutes at 22 °C before 50 µl of stop solution were added. LDH release of leaky cells compared to no-cell control (0 %) and Triton-X 100 lysed (100 %) cells was determined fluorometrically by measuring emission of the NADH caused oxidation product of resazurine, namely resofurin, at 560 nm excitation and 590 nm emission wavelengths. Results are given as mean values of a replicate of four ± SD.

PCR-Array:

In a PCR-based multiarray, 84 apoptosis-related genes were investigated concerning up- or downregulation compared to control cells after treatment with polymer solutions. H1299/Luc cells were seeded with 500,000 cells per well in 6-well-plates 24 hours prior to treatment with two different concentrations (2 µg/ml and 20 µg/ml) of either PEI 25kDa or PEI25k-PEG(30k)1. RNA was isolated 6 or 24 hours after treatment. Control cells were untreated, and RNA was isolated at the same time points as from treated cells. RNA quality was checked with an Agilent BioAnalyzer 2100, and RNA from replicates of three was pooled for cDNA synthesis which was performed according to the manufacturer's protocol. After mixing with the specific Super Array PCR master mix, aliquots of 25 µl were pipetted into the wells of the primer-containing plate and a qRT-PCR was run on an ABI 7500 RT PCR System. A gene map is to be found in the Supporting Informations.

Establishment of two stably luciferase expressing cell lines:

In order to establish two different cell lines HeLa/Luc in which the luciferase expression would be driven either by the CMV promoter or an endogenous promoter, HeLa/TetOff cells were stably transfected with different restriction products. First of all, chemically competent *E. coli* DH5α were transformed by heat shock with the Luciferase Reporter Vector pTRE2hyg-Luc (Clontech, Saint-Germain-en-Laye, France) containing the luciferase reporter gene and a hygromycin resistance gene, and an ampicillin resistance gene. Bacteria were cultured on ampicillin containing LB plates over night at 37 °C before 3 colonies were picked. Selected colonies were used to inoculate 500 ml cultures of LB medium. After 24 hours of incubation, cultures were centrifuged and plasmid was prepared with a Qiagen Plasmid Giga Kit (Qiagen, Hilden, Germany) before it was linearized with either BamH1 or NotI according to the manufacturer's protocol. For a 95 % confluent 10 cm Petri dish of HeLa/TetOff cells, 20 µg linearized plasmid were mixed with Lipofectamine and PLUS reagent (Invitrogen, Karlsruhe, Germany) as recommended by

the manufacturer and added to cells in serum- and antibiotics-free medium. Four hours later, medium was changed and cells were treated with hygromycin-containing medium for two weeks before single clones were selected and propagated as described above. After the selection process, cells were maintained in DMEM high glucose (PAA Laboratories, Cölbe, Germany), supplemented with 10 % fetal bovine serum (Cytogen, Sinn, Germany), in humidified atmosphere with 5 % CO₂ at 37°C.

Titration of Concentration-Dependent Off-Target-Effects:

After establishment of the two cell lines in which the luciferase expression is either driven by a CMV promoter or not, the effect of polymer addition at different concentrations was compared. Cells were seeded 24 hours prior to treatment. Medium was changed and polymer dilutions analogous to the concentrations used for transfections at certain N/P ratios were added. Medium was again changed 4 hours after mock transfection, and cells were incubated for another 44 hours before luciferase expression was assessed as described above.

8.4 Results and Discussion

Observation of Off-Target Effects in Transfection Experiments:

A couple of years ago, it was reported that by grafting poly (ethylene glycol) (PEG) on to PEI, shortly PEGylating PEI, biocompatibility could be increased (13). But in the first transfection experiments with the stably transfected cell line H1299/Luc, morphologic changes to the cells transfected with PEG-PEI/siRNA complexes were observed which had never been described before (Figure 1A and 1B). The transfected cells were swollen and their growth was strongly impaired which had caused low cell density in the wells of transfected cells. The reproducibility of this effect was given every time the experiment was repeated ($n > 10$), and the same morphologic effects as after transfection were also caused with free polymer solutions at 2 µg/ml final solution (Figure 1C), but not at a final concentration of 20 µg/ml. Interestingly, cells transfected with PEI25kDa/siRNA complexes or free PEI 25kDa did not reveal these strong morphologic effects (data not shown). Since exactly the PEG-PEIs used for the latter experiments (16, 17) as well as other PEG-PEI conjugates (18, 19) have been described to be less toxic than PEI 25 kDa in various cell lines and in vivo, it seemed to be interesting to find out why the H1299/Luc cells were so susceptible to PEG-PEI in this particular concentration-dependent manner.

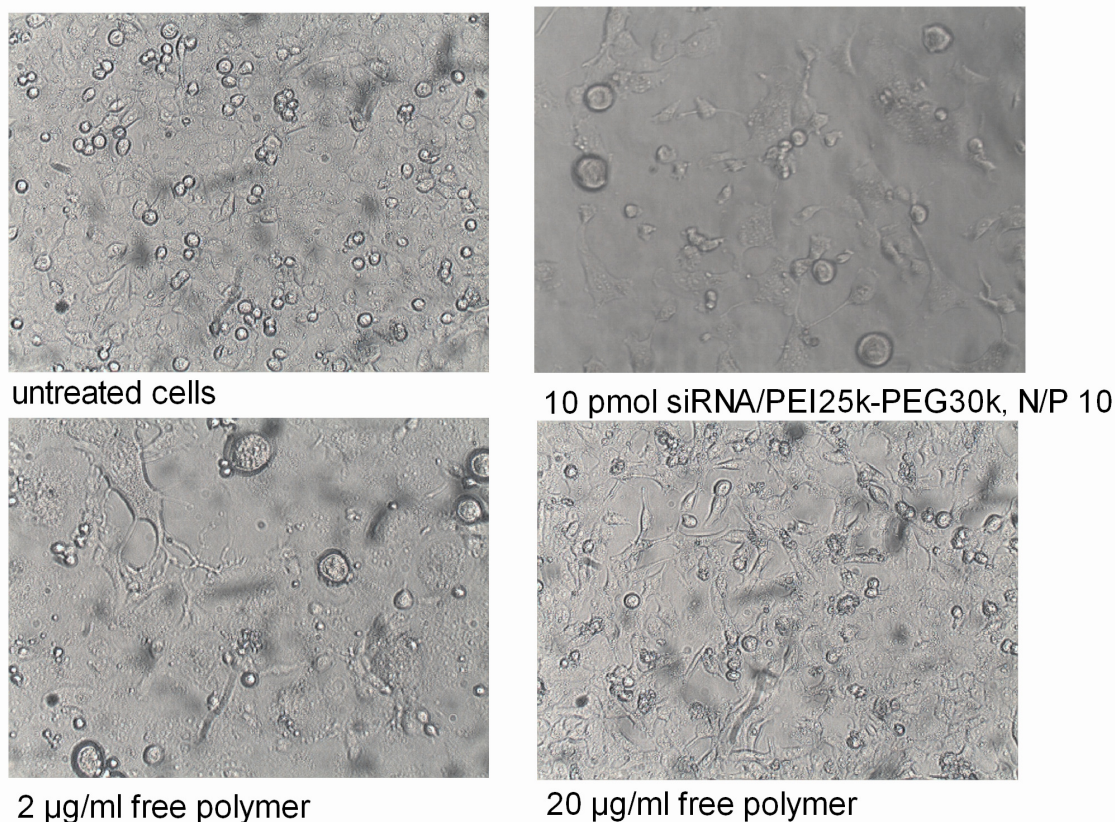


Figure 1: Effects of polymer treatment on cell morphology. 1A: H1299/Luc untreated control cells, 1D: H1299/Luc cells 24 hours after transfection with 10 pmol siRNA (50 nM) complexed with PEI(25k)-PEG(30k)1 at an N/P ratio of 10 exhibit the same morphologic changes as cells treated with 2 µg/ml free polymer. 1C: H1299/Luc cells treated with 2 µg/ml PEI(25k)-PEG(30k)1 reveal strong changes in morphology towards swollen vacuolized cells. 1D: Treatment with higher concentrations of PEG-PEI (20 µg/ml) did not cause such effects.

Various mechanisms of toxicity related with non-viral delivery systems for nucleic acids (20) and caused by siRNA itself have been described (21-23). Recently, a report by Robbins et al. revealed that some of the siRNA-based success was caused by activation of Toll-like receptors and not by RNAi (21). The Toll-like receptors 7 and 8, which are present in endosomes (24), can be activated upon endocytosis of complexed siRNA and cause release of inflammatory cytokines. Polymers, which are used as non-viral vectors, are known to be intrinsically toxic as well. While membrane activity, that leads to nano-hole formation, is reported for several cationic polymers and dendrimers such as poly-L-lysine (PLL), polyethylenimine (PEI), diethylaminoethyl-dextran (DEAE-DEX) and sphere-like poly(amidoamine) (PAMAM) (25), some of these polycations can also exhibit immune-

stimulatory effects (*1*). Additionally, charge dependent activation of the complement system has been reported for PLL, PAMAM, PEI and dioctadecylamidoglycylspermine (DOGS) (*26*).

In order to systematically find out the exact reason for the interesting behavior of the H1299/Luc cells used in the transfection assays, we investigated the following points:

- 1) Is the effect caused by siRNA, the polymer, or the polyplex?
- 2) How is cell viability decreased by the different polymers?
- 3) Is the effect observed cell line-specific?
- 4) Is membrane toxicity involved?
- 5) Are caspases or death receptor activated?

To answer these questions, a number of experiments were performed:

Cell Viability:

Since the effects observed did not increase but disappeared with increasing concentration of PEI25k-PEG(30k)₁ and were not observed after transfection with PEI 25k, it was suspected that they were either caused by polymer or polyplex. To test this and effects on cell viability, cells were treated with a broad range of concentrations of the two polymers and investigated for remaining viability in MTT-assays as described above. In order to compare the data with previously collected and published results (*16*), MTT assays were performed in both H1299/Luc cells and L929 fibroblasts, which are routinely used for the determination of IC₅₀ values, according to the US Pharmacopoeia. This also allowed for investigation of cell line-specificity of the observed toxic effects. While PEI 25kDa showed a clear concentration-dependent sigmoidal dose-response in both cell lines (Figure 2A and 2B), PEG-PEI data could only be well fitted for results from L929 cells (Figure 2B) ($R^2 = 0.71$ in H1299/Luc cells, Figure 2A). In H1299/Luc cells, a relative minimum in cell viability was observed at 0.004 mg/ml polymer, which is slightly lower than the concentration at which the transfections were performed (dashed vertical line, Figure 2A). IC₅₀ values were higher for PEG-PEI than for PEI in both cell lines, although the value for PEG-PEI in H1299/Luc cells cannot be trusted, as it is derived from the non-linear fit. Still, it has to be admitted that low concentrations of PEG-PEI are better tolerated in H1299/Luc

cells than low concentrations of PEI. The more interesting part of the curve, however, is the concentration range between 0.002 and 0.25 mg/ml.

With this assay we were able to determine that 1) the effects are caused by the polymer, 2) cell viability is affected in an unexpected way by PEG-PEI treatment, and 3) the effects are only observed in H1299/Luc cells, but not in L929 cells.

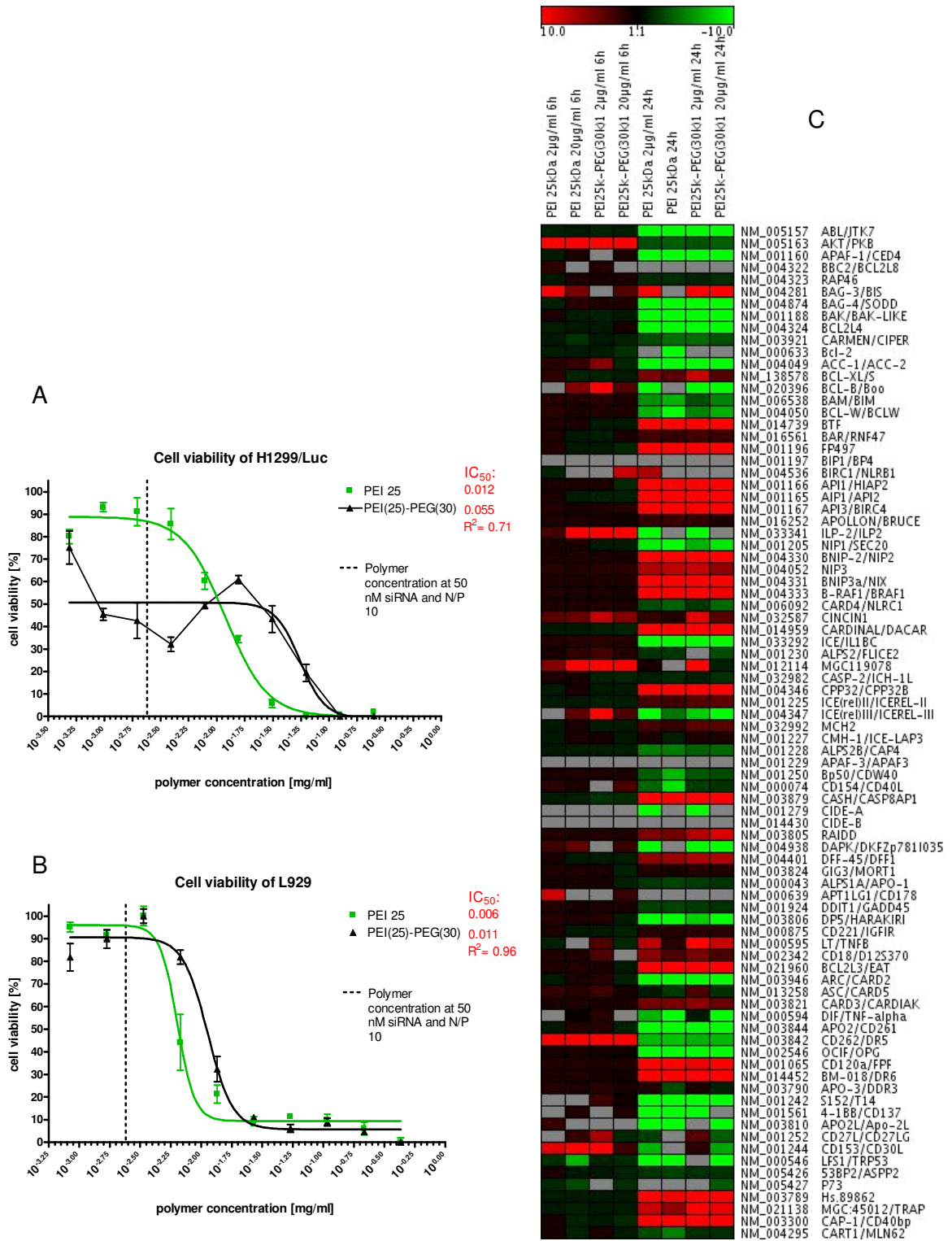


Figure 2: Cell viability of A: H1299/Luc and B: L929 cells treated with various concentrations of PEI 25k and PEI(25k)-PEG(30k)1. While L929 cells show sigmoidal dose-response, H1299/Luc cells exhibit a minimum at 0.004 mg/ml PEG-PEI. C: Heat map of the gene expression profile of H1299/Luc cells treated with 2 μ g/ml or 20 μ g/ml PEI

25kDa or PEI25k-PEG30k after 6 or 24 hours. The color scale above the expression profile shows that positive fold change is expressed by red color, while negative fold change is shown in green.

Membrane Toxicity:

As polycations like PEI are known to create or expand defects in the lipid bilayers of cells (25, 27), it could be assumed that the low cell viability at 0.004 mg/ml PEG-PEI in H1299/Luc cells was caused by membrane interaction. In that case, lactate dehydrogenase (LDH) would be released from the cytosol into cell culture medium. LDH assays were performed as described above but revealed a rather more favorable profile for PEG-PEI than for PEI over a broad concentration range and confirmed, what has been reported earlier (13, 16, 28) for specific concentrations. No minima or peculiar deviations from the sigmoidal dose-response were observed. Simple membrane toxicity was therefore ruled out as main cause of the interesting behavior of H1299/Luc cells if treated with PEG-PEI.

Since in this assay we were able to prove that PEG-PEI even causes lower LDH release than PEI, issue number 4), namely membrane toxicity, could be ruled out as a relevant factor.

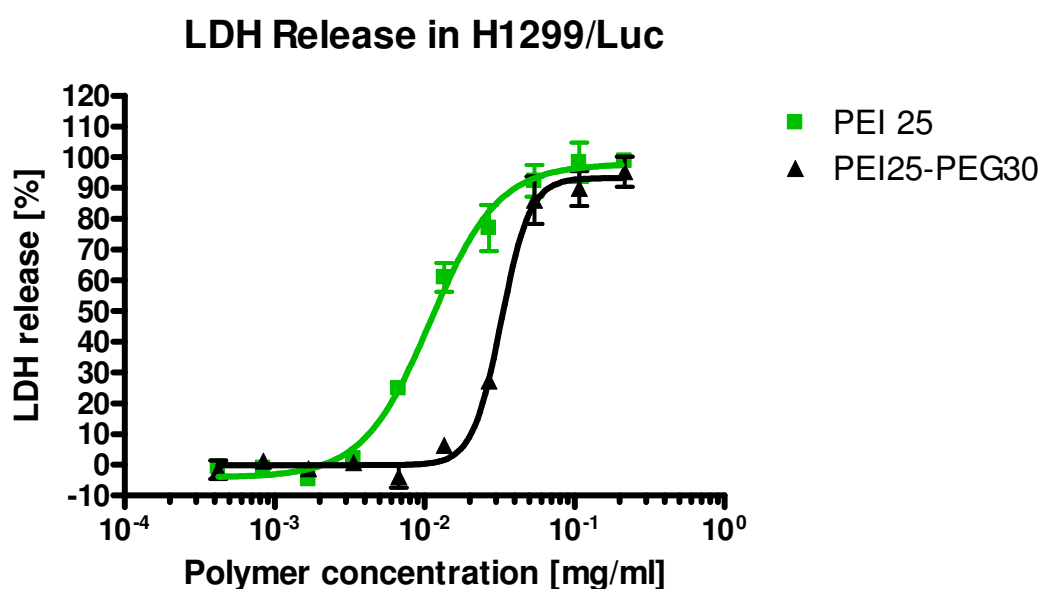


Figure 3: LDH release of H1299/Luc cells treated with various concentrations of PEI 25k and PEI(25k)-PEG(30k)1. Both polymers cause a sigmoidal dose-response while PEI 25 kDa has a stronger effect than PEG-PEI.

Regulation of Gene Expression:

PEI is known to cause apoptosis by interaction with mitochondrial membranes which leads to loss of mitochondrial membrane potential, a decrease in ATP, and decreased cell viability, as well as activation of caspases and cytochrome c release (29). As reduced cell viability was observed, but not linked to membrane toxicity, we further investigated the genetic profiles of apoptosis-related pathways in PEG-PEI and PEI treated cells in a PCR-based array. The PCR array allowed for investigation of up- and down-regulation of 84 genes that are related to apoptosis, but also anti-apoptotic genes, TNF ligand and receptor genes, caspases, the Bcl-family, death domain, death effector domain family and p53 as well as DNA damage response genes, such as many others.

From the heat map, it is obvious that 6 hours after treatment, only a few genes were up-regulated, whereas after 24 hours, a number of genes were up- and a comparably number of genes were down-regulated. This can be understood as a response to early effects that activated further pathways. While genes in between a family of genes were not only up- or only down-regulated, just a few patterns were perceptible. Genes of the caspase recruitment domain (CARD) family, for example BIRC2, BIRC3, CARD6, and CARD8 were rather up-regulated. Genes that also belong to the inhibitor of apoptosis (IAP) family, like BIRC2, BIRC3, BIRC4, BIRC6, and BIRC8 were down-regulated 6 hours after treatment, but strongly up-regulated 18 hours later (for description of genes, see Supplementary Information). Genes of the B-cell lymphoma 2 (Bcl-2) family which can either be pro- or antiapoptotic, depending on the protein they homo- or heterodimerize with (30), were partially up- and partially down-regulated. The same was true for genes related with p53 and DNA damage response, while it has to be mentioned that the cell line is homozygous partially p53-depleted. The caspases were rather up-regulated, especially at the later timepoint, whereas interestingly caspase 2 and caspase 8 were down-regulated at either timepoint. This is an indication that rather mitochondrial death was involved in the effects observed, but no or little death receptor-mediated apoptosis. This question, on the other hand, cannot be answered with on the mRNA level but caspase activity must be measured. While we were not able to observe strong differences between the two different polymers or the two different concentrations, respectively, we focused on striking red spots in the left half of the heat map demonstrating the 6-hour values. It is not surprising that polycations can activate and abrogate hundreds of genes, but the effects that were observed with 2 μg PEG-PEI could be retrieved in the heat map: One red spot at 2 $\mu\text{g}/\text{ml}$ PEG-PEI can be

found for Bcl-B/Boo (BCL2L10), one for CINCIN1 (CARD6, a caspase recruitment domain protein), one for ICE(rel)III (caspase 5), and one for CD27L (CD70). The strongly increased expression of BCL2L10, which is able to block the mitochondria death pathway but not TNF- α induced apoptosis (31), might be a result of activation of this pathway. Other strongly increased values that are less striking in the heat map but functionally interesting were found for CD153/CD30L (TNFSF8), IAP-1/CD40 (TRAF3) and LT/TNFB (LTA). It has been reported that TNFSF8 (CD30) stimulation can cause apoptosis of anaplastic large cell lymphoma cells (32), with TRAFs downstream of CD30 involved in apoptosis induction (33) by NF κ B activation. The pathway must be understood as crosstalk with TRADD (Hs.89862) after activation by FADD (CASH/CASP8AP1), two genes that were also activated in our assay and related to death receptor mediated apoptosis. Since CD30 activation was also reported to enhance production of lymphotoxin α (LT/TNFB) (34), which was up-regulated with PEG-PEI as well, there are a number of indications that CD30 activation triggered a lot of the effects observed, that must be seen in context of p53-depletion in H1299 cells.

When combined into a therapeutic delivery system, activation of molecular mechanisms by biologic response modifiers can be exploited for synergistic effects, as described for pluronic block copolymers (35), which have been shown to effectively sensitize multi-drug resistant cancer cells (36, 37).

These results, of course, raised further questions, especially concerning the suitability of other cell lines as screening model for non-viral vectors. If our hypothesis proved true, p53-sufficient cells would not react in the same way p53-deficient cells do.

Influence of Cell Line:

Since we confirmed that PEG-PEIs are generally less toxic than PEI 25 kDa and found that the highly interesting effects caused in H1299/Luc cells were cell line specific, we investigated knockdown efficiency and biocompatibility of PEG-PEI/siRNA complexes in the cell line CHO/Luc. In this cell line, we did not observe any microscopically visible morphologic effects, but when the cells were lysed and assayed for luciferase expression, or rather knockdown efficiency, again, puzzling results were obtained: While Lipofectamine had mediated specific knockdown without unspecific effects of siCONTROL lipoplexes or free Lipofectamine, PEI25k did neither cause specific nor unspecific events. Cells transfected with the A-B-block copolymers PEI(25k)-PEG(30k)₁ and PEI(25k)-PEG(20k)₁,

which contain one PEI and one PEG domain, on the other hand, exhibited highly increased luciferase expression. It has to be emphasized that cells that underwent “mock transfection” and were therefore treated with polymer only, showed lower up-regulation of pseudo-endogenous luciferase expression, as reported earlier (12). As already described by Akhtar et al., polymers and polyplexes have to be considered totally different systems when it comes to toxicogenomics (2). While polymer dilutions are molecular solutions, self-assembled polyplexes have particulate properties. Another striking observation we were able to make in this assay was the fact that highly PEGylated polymers, that have earlier been described to be less active than derivatives with lower grafting degree (28), did not increase the luciferase expression in CHO/Luc cells. Knockdown of the target gene expression was not observed either. Keeping in mind that the luciferase expression in those cells is driven by a CMV promoter, the effects caused by A-B-block polyplexes can be understood as results of activation of the CMV promoter. If NF- κ B is released by phosphorylation and degradation of inactivated I κ B α (38), it can bind to the CMV promoter and activate it, since the transcription factor binding site of NF- κ B is unique for the CMV promoter (39). While this effect is desirable in pDNA transfections, as it leads to higher transgene expressions, it strongly complicates data interpretation in siRNA transfection experiments.

This experiment clearly proved that p53-sufficient cells are not susceptible to PEG-PEI. But as a new kind of off-target effects was observed on the other hand, the hypothesis of promoter activation had to be challenged as well

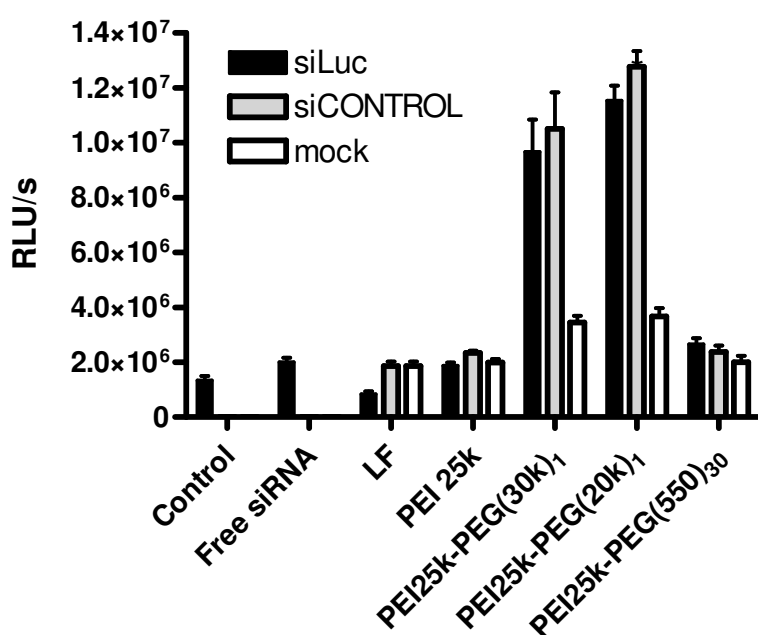


Figure 4: Transfection in CHO/Luc, Activation of CMV-promoter after treatment with AB-diblock-like copolymer complexed siRNA, stronger effects than with free polymer.

Influence of Promoter:

After cell line specific effects on signal transduction pathways and most probably activation of the driving promoter were observed, two cell lines that only differed in the driving promoter were established for direct comparison. Since the restriction enzyme BamHI cuts the plasmid pTRE2hyg-Luc between the CMV promoter and the luciferase gene, the luciferase expression in those cells that were transfected with the BamHI-linearized vector (HeLa/Luc BamHI) was no longer driven by the CMV promoter and therefore independent of excretion of TNF α (12). The restriction enzyme NotI, on the other hands, cuts the vector after the sequence that encodes the luciferase gene. Therefore, luciferase expression in cells transfected with NotI-linearized vector (HeLa/Luc NotI) was still depending on activation of the CMV promoter.

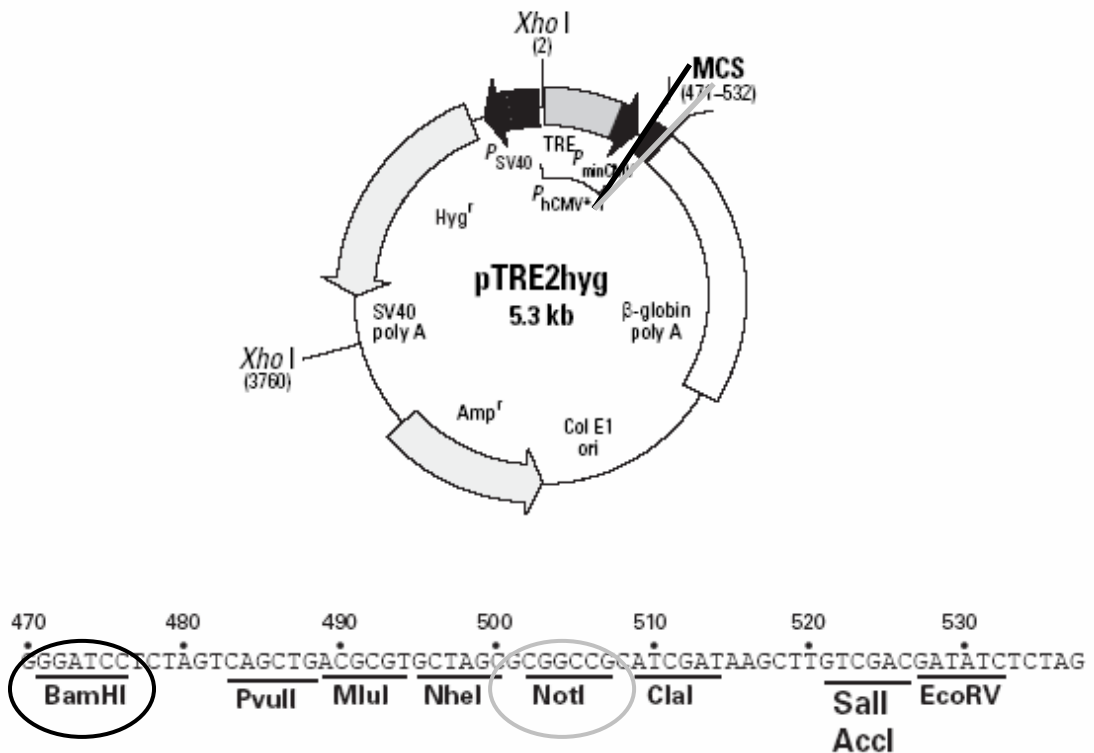


Figure 5: Establishment of two stably luciferase expressing cell lines, Amplification of plasmid pTRE2hygLuc, Linearization with 2 different restriction enzymes

After selection of single clones (clone A6 of HeLa/Luc NotI cells and clone B1 of HeLa/Luc BamHI cells) that expressed the luciferase gene well and also grew without complications, master and working cell banks were created. Cells were seeded in 96-well plates as described above and subjected to mock transfections for proof of principle. HeLa/NotI cells exhibited higher basal luciferase expression, of course, since the gene encoding the sequence for luciferase was right downstream to the CMV promoter. In HeLa/BamHI cells, luciferase expression was independent of the CMV promoter, and therefore in general lower than in HeLa/NotI cells (Figure 6A). When treated with polymer solutions of PEI(25k)-PEG(20k) of increasing concentrations, HeLa/NotI cells expressed significantly higher levels of luciferase than untreated cells (**p < 0.01, ***p < 0.001). Luciferase expression in HeLa/BamHI cells, on the other hand, was not significantly affected by PEG-PEI treatment (Figure 6A). It was therefore concluded to finally have established a cell line which would be not adversely affected by PEG-PEI in siRNA transfection experiments. To prove the assumption, HeLa/Luc BamHI cells were transfected with polyplexes of PEI 25 kDa or PEI(25k)-PEG(20k) and lipoplexes of Lipofectamine as positive control. Mock transfections were performed as well, and this setup finally revealed data similar to our previously reported results (40). While Lipofectamine caused specific and significant (***p < 0.001) knockdown accompanied by little toxicity of free cationic lipid, PEI 25 kDa was not able to mediate significant down regulation of luciferase expression. PEI(25k)-PEG(20k), on the other hand, caused specific and significant (**p < 0.01) knockdown of 45 % without apparent toxicity or promoter activation.

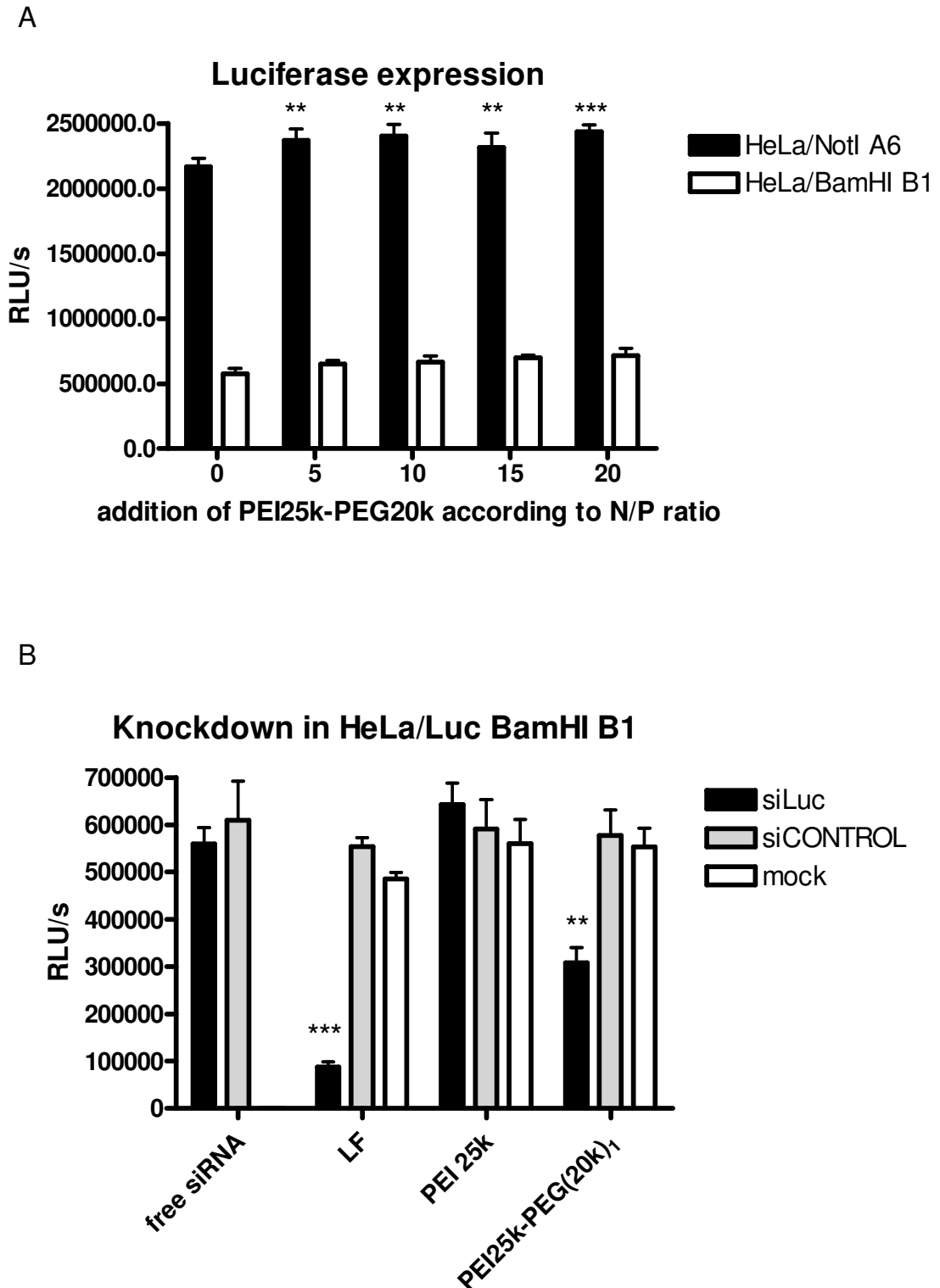


Figure 6A: Influence of promoter: Luciferase expression in HeLa/Luc NotI, driven by CMV-promoter, is significantly increased by treatment with PEI(25k)-PEG(20k)₁ (** $p < 0.01$ at N/P 5-15, and *** $p < 0.001$ at N/P 20) compared to untreated cells, whereas no significant differences are observed in HeLa/Luc BamHI. 6B: Specific and significant

knockdown of luciferase expression without significant off-target effects can be achieved in HeLa/Luc BamHI cells.

8.5 Conclusion

Off-target effects in *in vitro* and *in vivo* siRNA delivery are common and often not well understood. As we systematically built up in this study, various parameters may have an influence on unwanted effects and were therefore investigated. First of all, certain siRNA duplexes can induce the innate immune system, which can be avoided with validated sequences. Second, the delivery vehicle, or the formulation can have severe influence in a number of pathways that may alter signal transduction. Third, effects can be cell line specific, and especially stably transfected cells are genetically altered organisms, that have to be handled with care. Fourth, if reporter genes are utilized, the driving promoter is crucially important, or rather its transcription factor binding sites. We observed that every single parameter can induce further reactions which may differ from cell line to cell line. While activation of TNF-related pathways that finally leads to activation of NF κ B can cause apoptosis in p53-deficient cells, it leads to up-regulation of CMV-promoter driven genes in other cell lines. Additionally, the diblock-like PEGylated PEI that is designed to be less toxic can stimulate other pathways than PEI and lead to more striking off-target effects in a cell line and promoter dependent manner. In a cell culture screening model, all of these determining factors have to be kept in mind and essential control experiments have to be performed in order to obtain valid data. While in cell culture models off-target effects are troublesome, the investigation of their mechanisms may even lead to synergistic therapeutic effects.

8.6 Acknowledgements

We are thankful to Eva Mohr, Sandra Engel (DPB), Dominik Helmecke (DPC) and Birgit Frankenberger (ILB) for excellent technical support. Financial support by Deutsche Forschungsgemeinschaft (DFG Forschergruppe 627) is gratefully acknowledged.

8.7 References

- (1) Kabanov, A. V., Batrakova, E. V., Sridibhatla, S., Yang, Z., Kelly, D. L., and Alakov, V. Y. (2005) Polymer genomics: shifting the gene and drug delivery paradigms. *J Control Release* 101, 259-71.
- (2) Akhtar, S., and Benter, I. (2007) Toxicogenomics of non-viral drug delivery systems for RNAi: potential impact on siRNA-mediated gene silencing activity and specificity. *Adv Drug Deliv Rev* 59, 164-82.
- (3) Schiffelers, R. M., Ansari, A., Xu, J., Zhou, Q., Tang, Q., Storm, G., Molema, G., Lu, P. Y., Scaria, P. V., and Woodle, M. C. (2004) Cancer siRNA therapy by tumor selective delivery with ligand-targeted sterically stabilized nanoparticle. *Nucleic Acids Res* 32, e149.
- (4) Sun, T. M., Du, J. Z., Yan, L. F., Mao, H. Q., and Wang, J. (2008) Self-assembled biodegradable micellar nanoparticles of amphiphilic and cationic block copolymer for siRNA delivery. *Biomaterials* 29, 4348-55.
- (5) Thomas, M., Lu, J. J., Ge, Q., Zhang, C., Chen, J., and Klibanov, A. M. (2005) Full deacylation of polyethylenimine dramatically boosts its gene delivery efficiency and specificity to mouse lung. *Proc Natl Acad Sci U S A* 102, 5679-84.
- (6) Grayson, A. C., Ma, J., and Putnam, D. (2006) Kinetic and efficacy analysis of RNA interference in stably and transiently expressing cell lines. *Mol Pharm* 3, 601-13.
- (7) Leng, Q., Scaria, P., Zhu, J., Ambulos, N., Campbell, P., and Mixson, A. J. (2005) Highly branched HK peptides are effective carriers of siRNA. *J Gene Med* 7, 977-86.
- (8) Nguyen, J., Steele, T. W., Merkel, O., Reul, R., and Kissel, T. (2008) Fast degrading polyesters as siRNA nano-carriers for pulmonary gene therapy. *J Control Release*.
- (9) Gary, D. J., Puri, N., and Won, Y. Y. (2007) Polymer-based siRNA delivery: perspectives on the fundamental and phenomenological distinctions from polymer-based DNA delivery. *J Control Release* 121, 64-73.
- (10) Tseng, S.-j., and Tang, S.-C. (2007) Development of Poly(amino ester glycol urethane)/siRNA Polyplexes for Gene Silencing. *Bioconjugate Chem.* 18, 1383-1390.

-
- (11) Merkel, O., Librizzi, D., Pfestroff, A., Schurrat, T., Buyens, K., Sanders, N., De Smedt, S. C., Behe, M., and Kissel, T. (2009) Stability of siRNA polyplexes from poly(ethylenimine) and poly(ethylenimine)-g-poly(ethylene glycol) under in vivo conditions: Effects on pharmacokinetics and biodistribution measured by Fluorescence Fluctuation Spectroscopy and Single Photon Emission Computed Tomography (SPECT) imaging. *Journal of Controlled Release*.
 - (12) Lai, C., Jiang, X., and Li, X. (2006) Development of luciferase reporter-based cell assays. *Assay Drug Dev Technol* 4, 307-15.
 - (13) Petersen, H., Fechner, P. M., Fischer, D., and Kissel, T. (2002) Synthesis, Characterization, and Biocompatibility of Polyethylenimine-graft-poly(ethylene glycol) Block Copolymers. *Macromolecules* 35, 6867-6874.
 - (14) Merkel, O. M., Librizzi, D., Pfestroff, A., Schurrat, T., Buyens, K., Sanders, N. N., De Smedt, S. C., Behe, M., and Kissel, T. (2009) Stability of siRNA polyplexes from poly(ethylenimine) and poly(ethylenimine)-g-poly(ethylene glycol) under in vivo conditions: Effects on pharmacokinetics and biodistribution measured by Fluorescence Fluctuation Spectroscopy and Single Photon Emission Computed Tomography (SPECT) imaging. *J Control Release*.
 - (15) Germershaus, O., Mao, S., Sitterberg, J., Bakowsky, U., and Kissel, T. (2008) Gene delivery using chitosan, trimethyl chitosan or polyethyleneglycol-graft-trimethyl chitosan block copolymers: establishment of structure-activity relationships in vitro. *J Control Release* 125, 145-54.
 - (16) Malek, A., Czubayko, F., and Aigner, A. (2008) PEG grafting of polyethylenimine (PEI) exerts different effects on DNA transfection and siRNA-induced gene targeting efficacy. *J Drug Target* 16, 124-39.
 - (17) Merdan, T., Kunath, K., Petersen, H., Bakowsky, U., Voigt, K. H., Kopecek, J., and Kissel, T. (2005) PEGylation of poly(ethylene imine) affects stability of complexes with plasmid DNA under in vivo conditions in a dose-dependent manner after intravenous injection into mice. *Bioconjug Chem* 16, 785-92.
 - (18) Kleemann, E., Neu, M., Jekel, N., Fink, L., Schmehl, T., Gessler, T., Seeger, W., and Kissel, T. (2005) Nano-carriers for DNA delivery to the lung based upon a TAT-derived peptide covalently coupled to PEG-PEI. *J Control Release* 109, 299-316.
 - (19) Liang, B., He, M. L., Xiao, Z. P., Li, Y., Chan, C. Y., Kung, H. F., Shuai, X. T., and Peng, Y. (2008) Synthesis and characterization of folate-PEG-grafted-

- hyperbranched-PEI for tumor-targeted gene delivery. *Biochem Biophys Res Commun* 367, 874-80.
- (20) Hunter, A. C. (2006) Molecular hurdles in polyfectin design and mechanistic background to polycation induced cytotoxicity. *Adv Drug Deliv Rev* 58, 1523-31.
- (21) Robbins, M., Judge, A., Ambegia, E., Choi, C., Yaworski, E., Palmer, L., McClintock, K., and MacLachlan, I. (2008) Misinterpreting the therapeutic effects of small interfering RNA caused by immune stimulation. *Hum Gene Ther* 19, 991-9.
- (22) Agrawal, S., and Kandimalla, E. R. (2004) Antisense and siRNA as agonists of Toll-like receptors. *Nat Biotechnol* 22, 1533-7.
- (23) Marques, J. T., and Williams, B. R. (2005) Activation of the mammalian immune system by siRNAs. *Nat Biotechnol* 23, 1399-405.
- (24) Sioud, M. (2005) Induction of inflammatory cytokines and interferon responses by double-stranded and single-stranded siRNAs is sequence-dependent and requires endosomal localization. *J Mol Biol* 348, 1079-90.
- (25) Hong, S., Leroueil, P. R., Janus, E. K., Peters, J. L., Kober, M. M., Islam, M. T., Orr, B. G., Baker, J. R., Jr., and Banaszak Holl, M. M. (2006) Interaction of polycationic polymers with supported lipid bilayers and cells: nanoscale hole formation and enhanced membrane permeability. *Bioconjug Chem* 17, 728-34.
- (26) Plank, C., Mechtler, K., Szoka, F. C., Jr., and Wagner, E. (1996) Activation of the complement system by synthetic DNA complexes: a potential barrier for intravenous gene delivery. *Hum Gene Ther* 7, 1437-46.
- (27) Leroueil, P. R., Hong, S., Mecke, A., Baker, J. R., Jr., Orr, B. G., and Banaszak Holl, M. M. (2007) Nanoparticle interaction with biological membranes: does nanotechnology present a Janus face? *Acc Chem Res* 40, 335-42.
- (28) Petersen, H., Fechner, P. M., Martin, A. L., Kunath, K., Stolnik, S., Roberts, C. J., Fischer, D., Davies, M. C., and Kissel, T. (2002) Polyethylenimine-graft-poly(ethylene glycol) copolymers: influence of copolymer block structure on DNA complexation and biological activities as gene delivery system. *Bioconjug Chem* 13, 845-54.
- (29) Moghimi, S. M., Symonds, P., Murray, J. C., Hunter, A. C., Debska, G., and Szcwzyk, A. (2005) A two-stage poly(ethylenimine)-mediated cytotoxicity: implications for gene transfer/therapy. *Mol Ther* 11, 990-5.

-
- (30) Ke, N., Godzik, A., and Reed, J. C. (2001) Bcl-B, a novel Bcl-2 family member that differentially binds and regulates Bax and Bak. *J Biol Chem* 276, 12481-4.
- (31) Zhang, H., Holzgreve, W., and De Geyter, C. (2001) Bcl2-L-10, a novel anti-apoptotic member of the Bcl-2 family, blocks apoptosis in the mitochondria death pathway but not in the death receptor pathway. *Hum Mol Genet* 10, 2329-39.
- (32) Gruss, H. J., Boiani, N., Williams, D. E., Armitage, R. J., Smith, C. A., and Goodwin, R. G. (1994) Pleiotropic effects of the CD30 ligand on CD30-expressing cells and lymphoma cell lines. *Blood* 83, 2045-56.
- (33) Hsu, H., Shu, H. B., Pan, M. G., and Goeddel, D. V. (1996) TRADD-TRAF2 and TRADD-FADD interactions define two distinct TNF receptor 1 signal transduction pathways. *Cell* 84, 299-308.
- (34) Gruss, H. J., Ulrich, D., Braddy, S., Armitage, R. J., and Dower, S. K. (1995) Recombinant CD30 ligand and CD40 ligand share common biological activities on Hodgkin and Reed-Sternberg cells. *Eur J Immunol* 25, 2083-9.
- (35) Batrakova, E. V., and Kabanov, A. V. (2008) Pluronic block copolymers: evolution of drug delivery concept from inert nanocarriers to biological response modifiers. *J Control Release* 130, 98-106.
- (36) Kabanov, A. V., Batrakova, E. V., and Alakhov, V. Y. (2002) Pluronic block copolymers for overcoming drug resistance in cancer. *Adv Drug Deliv Rev* 54, 759-79.
- (37) Kabanov, A. V., Batrakova, E. V., and Alakhov, V. Y. (2002) Pluronic block copolymers as novel polymer therapeutics for drug and gene delivery. *J Control Release* 82, 189-212.
- (38) Bergmann, M., Hart, L., Lindsay, M., Barnes, P. J., and Newton, R. (1998) IkappaBalpha degradation and nuclear factor-kappaB DNA binding are insufficient for interleukin-1beta and tumor necrosis factor-alpha-induced kappaB-dependent transcription. Requirement for an additional activation pathway. *J Biol Chem* 273, 6607-10.
- (39) Yang, Z., Zhu, J., Sriadibhatla, S., Gebhart, C., Alakhov, V., and Kabanov, A. (2005) Promoter- and strain-selective enhancement of gene expression in a mouse skeletal muscle by a polymer excipient Pluronic P85. *J Control Release* 108, 496-512.
- (40) Mao, S., Neu, M., Germershaus, O., Merkel, O., Sitterberg, J., Bakowsky, U., and Kissel, T. (2006) Influence of Polyethylene Glycol Chain Length on the

Physicochemical and Biological Properties of Poly(ethylene imine)-graft-Poly(ethylene glycol) Block Copolymer/SiRNA Polyplexes. *Bioconjug Chem* 17, 1209-18.

Supporting Information:

Chapter 8

GeneBank	Symbol	Description	Gene Name	GeneBank	Symbol	Description	Gene Name
NM_005157	ABL1	C-abl oncogene 1, receptor tyrosine kinase	ABL/JTK7	NM_001167	XIAP	X-linked inhibitor of apoptosis	API3/BIRC4
NM_005163	AKT1	V-akt murine thymoma viral oncogene homolog 1	AKT/PKB	NM_016252	BIRC6	Baculoviral IAP repeat-containing 6	APOLLON/B RUCÉ
NM_001160	APAF1	Apoptotic peptidase activating factor 1	APAF-1/CEd4	NM_033341	BIRC8	Baculoviral IAP repeat-containing 8	ILP-2/ILP2
NM_004322	BAD	BCL2-associated agonist of cell death	BBC2/BCL2 L8	NM_001205	BNIP1	BCL2/adenovirus E1B 19kDa interacting protein 1	NIP1/SEC20
NM_004323	BAG1	BCL2-associated athanogene	RAP46	NM_004330	BNIP2	BCL2/adenovirus E1B 19kDa interacting protein 2	BNIP-2/NIP2
NM_004281	BAG3	BCL2-associated athanogene 3	BAG-3/BIS	NM_004052	BNIP3	BCL2/adenovirus E1B 19kDa interacting protein 3	NIP3
NM_004874	BAG4	BCL2-associated athanogene 4	BAG-4/SODD	NM_004331	BNIP3L	BCL2/adenovirus E1B 19kDa interacting protein 3-like	BNIP3a/NIX
NM_001188	BAK1	BCL2-antagonist/killer 1	BAK/BAK-LIKE	NM_004333	BRAF	V-raf murine sarcoma viral oncogene homolog B1	B- RAF1/BRAF 1
NM_004324	BAX	BCL2-associated X protein	BCL2L4	NM_006092	NOD1	Nucleotide-binding oligomerization domain containing 1	CARD4/NLR C1
NM_003921	BCL10	B-cell CLL/lymphoma 10	CARMEN/CIPER	NM_032587	CARD6	Caspase recruitment domain family, member 6	CINCIN1
NM_000633	BCL2	B-cell CLL/lymphoma 2	Bcl-2	NM_014959	CARD8	Caspase recruitment domain family, member 8	CARDINAL/ DACAR
NM_004049	BCL2A1	BCL2-related protein A1	ACC-1/ACC-2	NM_033292	CASP1	Caspase 1, apoptosis-related cysteine peptidase (interleukin 1, beta, convertase)	ICE/L1BC
NM_138578	BCL2L1	BCL2-like 1	BCL-XL/S	NM_001230	CASP10	Caspase 10, apoptosis-related cysteine peptidase	ALPS2/FLIC E2
NM_020396	BCL2L10	BCL2-like 10 (apoptosis facilitator)	BCL-B/Boo	NM_012114	CASP14	Caspase 14, apoptosis-related cysteine peptidase	MGC119078
NM_006538	BCL2L11	BCL2-like 11 (apoptosis facilitator)	BAM/BIM	NM_032982	CASP2	Caspase 2, apoptosis-related cysteine peptidase	CASP-2/ICH- 1L
NM_004050	BCL2L2	BCL2-like 2	BCL-W/BCLW	NM_004346	CASP3	Caspase 3, apoptosis-related cysteine peptidase	CPP32/CPP 32B
NM_014739	BCLAF1	BCL2-associated transcription factor 1	BTF	NM_001225	CASP4	Caspase 4, apoptosis-related cysteine peptidase	ICE(reI)/ICE REL-II
NM_016561	BFAR	Bifunctional apoptosis regulator	BAR/RNF47	NM_004347	CASP5	Caspase 5, apoptosis-related cysteine peptidase	ICE(reI)/ICE EREL-III
NM_001196	BID	BH3 interacting domain death agonist	FP497	NM_032992	CASP6	Caspase 6, apoptosis-related cysteine peptidase	MCH2
NM_001197	BIK	BCL2-interacting killer (apoptosis-inducing)	BIP1/BP4	NM_001227	CASP7	Caspase 7, apoptosis-related cysteine peptidase	CMH-1/ICE- LAP3
NM_004536	NAIP	NLR family, apoptosis inhibitory protein	BIRC1/NLRB1	NM_001228	CASP8	Caspase 8, apoptosis-related cysteine peptidase	ALPS2B/CA P4
NM_001166	BIRC2	Baculoviral IAP repeat-containing 2	API1/HIAP2	NM_001229	CASP9	Caspase 9, apoptosis-related cysteine peptidase	APAF- 3/APAF3
NM_001165	BIRC3	Baculoviral IAP repeat-containing 3	AIP1/API2	NM_001250	CD40	CD40 molecule, TNF receptor superfamily member 5	Bp50/CDW4 0
NM_000074	CD40LG	CD40 ligand	CD154/CD40L	NM_001065	TNFRSF1A	Tumor necrosis factor receptor superfamily, member 1A	CD120a/FPF
NM_003879	CFLAR	CASP8 and FADD-like apoptosis regulator	CASH/CASP8AP1	NM_014452	TNFRSF21	Tumor necrosis factor receptor superfamily, member 21	BM-018/DR6
NM_001279	CIDEA	Cell death-inducing DFFA-like effector a	CIDE-A	NM_003790	TNFRSF25	Tumor necrosis factor receptor superfamily, member 25	APO- 3/DDR3
NM_014430	CIDEB	Cell death-inducing DFFA-like effector b	CIDE-B	NM_001242	CD27	CD27 molecule	S152/T14
NM_003805	CRADD	CASP2 and RIPK1 domain containing adaptor with death domain	RAIDD	NM_001561	TNFRSF9	Tumor necrosis factor receptor superfamily, member 9	4- 1Bb/CD137
NM_004938	DAPK1	Death-associated protein kinase 1	DAPK/DKFZ p781k035	NM_003810	TNFSF10	Tumor necrosis factor (ligand) superfamily, member 10	AP02L/Apo- 2L
NM_004401	DFFA	DNA fragmentation factor, 45kDa, alpha polypeptide	DFF-45/DFF1	NM_001252	CD70	CD70 molecule	CD27/CD27 LG
NM_003824	FADD	Fas (TNFRSF6)-associated via death domain	GIG3/MORT1	NM_001244	TNFSF8	Tumor necrosis factor (ligand) superfamily, member 8	CD153/CD30 L
NM_000043	FAS	Fas (TNF receptor superfamily, member 6)	ALPS1A/APO-1	NM_000546	TP53	Tumor protein p53	LFS1/TRP53
NM_000639	FASLG	Fas ligand (TNF superfamily, member 6)	APT1LG1/C D178	NM_005426	TP53BP2	Tumor protein p53 binding protein, 2	53BP2/ASP P2
NM_001924	GADD45A	Growth arrest and DNA-damage-inducible, alpha	DDIT1/GADD45	NM_005427	TP73	Tumor protein p73	P73
NM_003806	HRK	Harakini, BCL2 interacting protein (contains only BH3 domain)	DP5/HARAKIRI	NM_003789	TRADD	TNFRSF1A-associated via death domain	Hs.89862
NM_000875	IGF1R	Insulin-like growth factor 1 receptor	CD221/IGF1R	NM_021138	TRAF2	TNF receptor-associated factor 2	MGC:45012/ TRAP
NM_000595	LTA	Lymphotoxin alpha (TNF superfamily, member 1)	LT/TNFB	NM_003300	TRAF3	TNF receptor-associated factor 3	CAP- 1/CD40bp
NM_002342	LTBR	Lymphotoxin beta receptor (TNFR superfamily, member 3)	CD18/D12S370	NM_004295	TRAF4	TNF receptor-associated factor 4	CART1/MLN 62
NM_021960	MCL1	Myeloid cell leukemia sequence 1 (BCL2-related)	BCL2L3/EAT	NM_004048	B2M	Beta-2-microglobulin	B2M
NM_003946	NOL3	Nucleolar protein 3 (apoptosis repressor with CARD domain)	ARC/CARD2	NM_000194	HPRT1	Hypoxanthine phosphoribosyltransferase 1	HGPRT/HPRT
NM_013258	PYCARD	PYD and CARD domain containing	ASC/CARD5	NM_012423	RPL13A	Ribosomal protein L13a	RPL13A
NM_003821	RIPK2	Receptor-interacting serine-threonine kinase 2	CARD3/CARDIAK	NM_002046	GAPDH	Glyceraldehyde-3-phosphate dehydrogenase	G3PD/GAP D
NM_000594	TNF	Tumor necrosis factor (TNF superfamily, member 2)	DIF/TNF-alpha	NM_001101	ACTB	Actin, beta	PS1TP5BP1
NM_003844	TNFRSF10A	Tumor necrosis factor receptor superfamily, member 10a	APO2/CD261	SA_00105	HGDC	Human Genomic DNA Contamination	HIGX1A
NM_003842	TNFRSF10B	Tumor necrosis factor receptor superfamily, member 10b	CD262/DR5	SA_00104	RTC	Reverse Transcription Control	RTC
NM_002546	TNFRSF11B	Tumor necrosis factor receptor superfamily, member 11b	OCIF/OPG	SA_00104	RTC	Reverse Transcription Control	RTC

SI Table 1: Gene Map of 84 apoptosis-related genes investigated in a PCR array. For clarity, gene bank numbers, symbols, descriptions, and gene names are given.

9 Summary and Perspectives

9.1 Summary

In this thesis, new and multifunctional non-viral vectors for delivery of nucleic acids were synthesized and characterized concerning biophysicochemical parameters. The first part of this work deals with *in vitro* studies of gene delivery which was accomplished by synthesis of PEI-based targeted vectors and a new class of triazine-based dendritic vectors. In the second part, *in vitro* and *in vivo* delivery of siRNA with PEI-based polymers is addressed by different routes of application and non-invasive imaging.

Chapter 1 introduces into the field of nanomedicine which advanced drug delivery systems can be numbered among. The questions which this work was based on, such as specificity of non-viral vectors, use of dendrimers as gene delivery vectors, pharmacokinetic issues of *in vivo* administered siRNA, *in vivo* stability of polyelectrolyte complexes, suitability of application routes, *in vivo* RNAi, and nanotoxicology are elucidated.

Chapter 2 describes the synthesis of 5 different PEI-based integrin $\alpha_v\beta_3$ -targeting conjugates by attaching a novel small molecule in two different coupling routes. Increasing the multimodality of these conjugates by fluorescent and radioactive labeling allowed for further characterization concerning their ability to condense pDNA into nano-sized complexes, concerning their surface charge, biocompatibility, transfection efficiency, and finally specificity. Highly specific and efficient transgene expression was observed in integrin-overexpressing MeWo cells, where the most efficient conjugate lead to 26-fold higher luciferase expression than the PEG-PEI the conjugate was based on. Interestingly, the conjugates with lower coupling degree of the targeting moiety were more efficient *in vitro*, which can be explained by the adverse effect strong blocking of integrin receptors can have.

In *Chapter 3*, a novel family of dendrimers for gene delivery is presented. The synthesis of 8 new modifications in the periphery of generation 2 rigid piperazine-connected triazine dendrimers is described as well as the periphery-induced impact on biophysicochemical parameters of self-assembled “dendriplexes” from pDNA and dendrimer. Eventually, transfection efficiencies of the differently substituted triazine dendrimers was assessed leading to the result that a certain amount of primary amines or guanidinium groups among the end groups is most important to maintain good transfection efficiency, while alkylation

also enhanced transgene expression. Since the toxicity of all triazine dendrimers, except for the alkylated dendrimer, was at least an order of magnitude lower than that of PEI, triazine dendrimers were considered promising vectors.

Chapter 4 is the direct continuation of *Chapter 3*, involving further synthetic progress concerning the structure of triazine dendrimers. Design criteria for this two-dimensional study were to investigate both the influence of generation and of core structure on in vitro parameters. Therefore, generation 1, 2 and 3 of the rigid triazine-piperazine structures were compared with each other. But also more flexible generation 2 cores involving piperazine- and ethylene glycol-connection between the triazines in a “bow-tie” structure, and mostly ethylene glycol chains in a flexible structure were synthesized and compared with the rigid core dendrimers. While toxicity increased with generation and increasing numbers of peripheral primary amines, the change of core flexibility had the most striking and promising effect: At comparably low toxicity, the highly flexible generation 2 dendrimer achieved higher transfection efficiencies than both PEI and SuperFect®, which is a commercially available generation 4 fractured PAMAM dendrimer.

Chapter 5, already belonging to the second part of this thesis, deals with siRNA delivery in vivo. It describes the problem that non-invasive detection of pharmacokinetic parameters of in vivo siRNA administration is most desirable but has not extensively been described in the literature. Nuclear imaging techniques are suitable for longitudinal measurements in the same animal, while the main issue is probe design. This chapter therefore describes a fast and efficient method to radiolabel and purify siRNA, and also shows results of in vivo application and SPECT imaging. Invasively and non-invasively acquired pharmacokinetic parameters and distributional data are compared for free siRNA and PEI-complexed siRNA which showed well known accumulation in the liver.

In *Chapter 6*, the method optimized in the chapter before was applied to radiolabel siRNA for an extensive comparative study on in vivo stability, pharmacokinetics and biodistribution of differently PEGylated PEI/siRNA complexes. In order to investigate stability of these complexes and to distinguish between possibly different distribution profiles of vector and load, each component was separately labeled and pharmacokinetic and distributional profiles were assessed for each vector and load invasively and by SPECT imaging. Additionally, Fluorescence Fluctuation Spectroscopy was applied to quantify stability under in vivo conditions. In this chapter, a great contingent of the toolbox of

multifunctionality was made use of: PEI, known to pH-sensitively buffer endosomal acidification, grafted with PEG to shield the positive charges of siRNA/PEI complexes in vivo was further functionalized with a chelating moiety for nuclear imaging. Fluorescently or radioactively labeled siRNA was complexed to allow for investigation of in vivo stability and biopharmaceutical parameters. This multidisciplinary approach yielded in the awareness, that the modified siRNA which was used in vivo apparently bound to serum albumins and, possibly as partially degraded albumin complex, circulated longer than any other component. It was also observed, that PEG-PEI/siRNA complexes were less stable than PEI/siRNA complexes, which all seemed to disassemble in the liver, although at the concentration applied, the complexes seemed to be stable in circulation.

Due to the rather poor pharmacokinetic profiles of intravenously administered (PEG-)PEI/siRNA polyplexes, *Chapter 7* investigates suitability of the same complexes for intratracheal application. Therefore, in stability of the complexes, in vivo residence time in the lung, biocompatibility and knock down efficiency in transgenic mice was tested. While PEI/siRNA complexes seemed to be more stable in vitro, even in presence of mucin or lung surfactant, the in vivo conditions were the opposite. PEI-complexed siRNA did not experience any benefit compared with free siRNA concerning lung residence time or washout. PEG-PEI/siRNA complexes, on the other hand seemed to be stable after intratracheal application and to exhibit sustained release of siRNA which allowed for significant down-regulation of EGFP in the lung five days after treatment of Actin-EGFP-expressing mice. Biocompatibility was tested, and only six of 22 chemo- and cytokines were found to be increased in the BALF.

Chapter 8 deals with an unpopular but very important issue in non-viral siRNA delivery, namely off-target effects. After unaccountable toxic effects of PEG-PEI were observed in a stably luciferase-expressing cell line, which was supposed to serve as a screening model, the reasons for these effects were systematically investigated. Reproducibility of the effects was maintained, and cell viability was strongly impaired at a certain concentration of PEG-PEI. Membrane toxicity was investigated but found not to be the cause. An array experiment for investigation of gene up- and down-regulation allowed presuming that not mitochondrial death but activation of CD30 regulated certain pro-apoptotic pathways involving NF κ B in this p53-deficient cell line. In other cell lines, NF κ B did not cause severe cell death but activation of CMV-promoter driven luciferase expression. Only the

establishment of a luciferase expressing cell line where the reporter gene was independent of a CMV-promoter allowed for specific RNAi without major off-target effects.

9.2 Perspectives

In continuation of the projects described, a number of further developments are possible. The targeted vectors described in Chapter 2 are certainly worth investigating *in vivo*. Integrin targeting has been described for tumor therapy and diagnostics. Since we have been able to radiolabel the conjugates with a gamma emitter, they could be used for nuclear imaging as well as for gene delivery into a tumor. Additionally, suitability as delivery vehicles for siRNA should be tested.

Since triazine dendrimers seem to be well tolerated *in vivo*, these vectors could be applied as *in vivo* gene delivery systems, but could of course also be tested for siRNA delivery. Further generations or attachment of different peripheral groups can be synthetically achieved, as well as modification with imaging or targeting moieties.

The method described in Chapter 5 for radiolabeling siRNA will certainly be further employed in the future for the investigation of biopharmaceutical parameters of siRNA delivery systems.

Since polyplexes of pre-PEGylated PEI with siRNA did not show superiority over PEI complexes in Chapter 6, post-PEGylation, which has successfully enhanced circulation times of DNA complexes, needs to be investigated.

In vivo bioactivity and knock down of EGFP in the lung of Actin-EGFP expressing mice in Chapter 7 is the most impressive result of this work, but it has to be further characterized concerning time-course and dose response. Additionally, it has to be investigated which cells in the lung are preferentially transfected.

Little is known about the differences of pathways that are activated or inactivated in different cells transfected with polycations. The study on off-target effects in Chapter 8 is evocative that not all effects measured are RNAi and that screening systems have to be carefully characterized before valid data can be acquired.

9.3 Zusammenfassung

In der vorliegenden Arbeit wurden neue und multifunktionelle nicht-virale Vektoren für den Transport von Nukleinsäuren synthetisiert und charakterisiert bezüglich ihrer biophysikochemischen Eigenschaften. Der erste Teil der Arbeit handelt von in vitro Untersuchungen zum Gentransfer, welcher mit PEI-basierten zielgerichteten Vektoren und einer neuen Substanzgruppe von Gentransfer-Vektoren basiert auf Triazin-Dendrimeren erreicht wurde. Im zweiten Teil wird in vitro und in vivo Transfer von siRNA mit PEI-basierten Polymeren in unterschiedlichen Applikationsrouten und mit radioaktiver Bildgebung untersucht.

Kapitel 1 leitet ein ins Feld sogenannter "Nanomedizin", wozu hochentwickelte Arzneiformen gezählt werden können. Die Fragen, auf denen diese Arbeit beruhte, wie Spezifität nicht-viraler Vektoren, die Verwendung von Dendrimeren als Genvektoren, pharmakokinetische Fragestellungen in vivo applizierter siRNA, Stabilität von Polyelektrolytkomplexen unter in vivo Bedingungen, Eignung verschiedener Applikationsrouten, in vivo RNAi und Nanotoxikologie werden erläutert.

Kapitel 2 beschreibt die Synthese 5 verschiedener $\alpha_v\beta_3$ -Integrin gerichteter Konjugate durch die Kopplung eines neuartigen kleinen Moleküls in zwei verschiedenen Kopplungsstrategien. Die Steigerung der Multimodalität dieser Konjugate durch Fluoreszenz- und Radioaktiv-Markierung erlaubten die weitere Charakterisierung ihrer Fähigkeit, pDNA in nanoskalige Komplexe zu kondensieren, die Charakterisierung ihrer Oberflächenladung, Bioverträglichkeit, Transfektionseffizienz und schließlich Spezifität. Hoch spezifische Expression des Transgens wurde in Integrin-überexprimierenden MeWo-Zellen beobachtet, wo das effizienteste Konjugat zu einer 26-fach höheren Luciferase-Expression führte als das PEG-PEI, auf dem das Konjugat basiert. Interessanterweise waren die Konjugate mit niedrigerem Kopplungsgrad in vitro effizienter, was durch die nachteiligen Effekte, die starke Integrin-Blockade haben kann, erklärt werden kann.

In *Kapitel 3* wird eine neue Familie von Dendrimeren zum Gentransfer präsentiert. Die Synthese von 8 neuen Modifikationen in der Peripherie von starren Generation 2 Piperazin-verknüpften Triazin-Dendrimerem wird beschrieben, sowie der Peripherie-bedingte Einfluss auf biophysikochemische Eigenschaften selbst-angeordneter „Dendriplexe“ aus pDNA und Dendrimer. Schließlich wurde die Transfektionseffizienz der unterschiedlich

substituierten Dendrimere untersucht, was zum Ergebnis führte, dass eine gewisse Menge primärer Amine oder Guanidinium-Gruppen als Endgruppen am wichtigsten für gute Transfektionseffizienz ist, während Alkylierung auch die Transfektionseffizienz erhöhte. Da die Toxizität der Triazin-Dendrimere, abgesehen vom alkylierten Dendrimer, mindestens eine Zehnerpotenz niedriger als die von PEI was, wurden die Triazin-Dendrimere als chancenreiche Transfektions-Vektoren erachtet.

Kapitel 4 ist die direkte Fortsetzung *Kapitel 3* und beinhaltet weiteren Fortschritt in der Synthese bezüglich der Struktur von Triazin-Dendrimeren. Entwicklungskriterien dieser zweidimensionalen Studie waren, den Einfluss der Generation und der Kernstruktur auf in vitro Eigenschaften zu untersuchen.

Deshalb wurden die Generationen 1, 2 und 3 der starren Triazin-Dendrimere miteinander verglichen. Aber auch flexiblere Kernstrukturen der Generation 2, die Piperazin- und Ethylenglykol-Verknüpfung zwischen den Triazinen einer „Fliegen-Struktur“ oder hauptsächlich Ethylenglykol-Verknüpfungen in einer flexiblen Struktur beinhalteten, wurden synthetisiert und mit den starren Dendrimeren verglichen. Während die Toxizität der Dendrimere mit der Generation und der zunehmenden Anzahl primärer Amine in der Peripherie anstieg, hatte die Änderung der Kern-Flexibilität den auffälligsten und aussichtsvollsten Effekt: Bei vergleichsweise niedriger Toxizität erreichte das flexibelste Dendrimer der Generation 2 höhere Transfektionseffizienzen als PEI und SuperFect®, was ein käuflich erwerbliches abgebautes PAMAM-Dendrimer der Generation 4 ist .

Kapitel 5, was bereits zum zweiten Teil dieser Arbeit gehört, beschäftigt sich mit in vivo Transfer von siRNA. Es beschreibt das Problem, dass nicht-invasive Beobachtung pharmakokinetischer Parameter höchst erstrebenswert ist, für siRNA aber in der Literatur nicht ausführlich beschrieben wurde. Radioaktive Bildgebungstechniken sind gut geeignet für längslaufende Messungen im selben Tier, während das größte Problem die Entwicklung von Sonden ist. Dieses Kapitel beschreibt deshalb ein schnelles und effizientes Verfahren zum Radiomarkieren und Aufreinigen von siRNA und zeigt Resultate von in vivo Anwendung und SPECT-Bildgebung. Invasiv und nicht-invasiv erhobene pharmakokinetische Parameter und Verteilungsdaten freier und PEI-komplexierter siRNA werden verglichen, was bereits bekannte Akkumulation PEI-komplexierter siRNA in der Leber zeigte.

In *Kapitel 6* wurde die Methode, die im vorhergegangenen Kapitel optimiert wurde, verwendet, um siRNA für eine ausgiebige Vergleichsstudie zur in vivo Stabilität, Pharmakokinetik und Bioverteilung unterschiedlich PEGylierter PEI/siRNA Komplexe. Um die Stabilität dieser Komplexe zu untersuchen und um zwischen etwaig unterschiedlicher Verteilungsprofile von Vektor und Ladung unterscheiden zu können, wurde jede Komponente einzeln markiert, und pharmakokinetische und Verteilungsprofile wurden für jeden Vektoren und dessen Beladung invasiv und nicht-invasiv mittels SPECT erfasst. Zusätzlich wurde Fluoreszenz-Fluktuations Spektroskopie angewendet, um die Stabilität unter in vivo Bedingungen zu quantifizieren. In diesem Kapitel wurde ein großer Anteil der Multifunktionalitäts-Werkzeugkiste gebraucht: PEI, was bekanntlich die endosomale Azidifizierung puffert, gepfropft mit PEG, um die positive Ladung von siRNA/PEI-Komplexen in vivo abzuschirmen, wurde weiterhin mit einem Chelator für radioaktive Bildgebung funktionalisiert. Fluoreszenz- oder radioaktiv-markierte siRNA wurde für die Untersuchung biopharmazeutischer Parameter und der Stabilität in vivo komplexiert. Diese multidisziplinäre Herangehensweise brachte die Erkenntnis hervor, dass die modifizierte siRNA, die in vivo verwendet worden war, anscheinend an Serumalbumin band und, möglicherweise teilweise abgebaut, als Albumin-Komplex länger zirkulierte als alle anderen Komponenten. Es wurde auch beobachtet, dass PEG-PEI/siRNA-Komplexe weniger stabil waren als PEI/siRNA-Komplexe, welche alle in der Leber zu zerfallen schienen obwohl sie bei der applizierten Konzentration in der Zirkulation stabil zu sein schienen.

Aufgrund der eher dürftigen pharmakokinetischen Profile intravenös verabreichter (PEG-)PEI/siRNA-Polyplexe untersucht *Kapitel 7* die Eignung der gleichen Komplexe für die intratracheale Anwendung. Dafür wurde in vitro Stabilität der Komplexe, in vivo Verweildauer in der Lunge, Biokompatibilität und Herunterregulierung in transgenen Mäusen getestet. Während PEI/siRNA-Komplexe in vitro, sogar in Anwesenheit von Mucin und Lungensurfactant, stabiler zu sein schienen, waren die in vivo Gegebenheiten entgegengesetzt. PEI-komplexierte siRNA erfuhr keinerlei Vorteil gegenüber freier siRNA bezüglich Verweildauer in der Lunge oder Ausscheidung. PEG-PEI/siRNA-Komplexe hingegen schienen nach intratrachealer Applikation stabil zu sein und fortwährende Freisetzung von siRNA aufzuweisen, was signifikante Reduktion von EGFP-Expression in der Lunge fünf Tage nach Behandlung Actin-EGFP exprimierender Mäuse ermöglichte. Bioverträglichkeit wurde untersucht, und es wurde nur für 6 von 22 Chemo- und Zytokinen

erhöhte Werte in der BALF gefunden.

Kapitel 8 behandelt ein wenig beliebtes aber sehr wichtiges Thema im Bereich nicht-viralen Transfers von siRNA, und zwar unerwünschte Effekte. Nachdem unerklärliche toxische Effekte in einer stabil Luciferase-exprimierenden Zelllinie beobachtet worden waren, welche gedacht war, als Selektions-Modell zu dienen, wurden die Gründe dieser Effekte systematisch untersucht. Reproduzierbarkeit war gegeben, und Zell-Lebendigkeit war stark eingeschränkt bei einer gewissen Konzentration von PEG-PEI. Membrantoxizität wurde untersucht aber nicht als Ursache festgestellt. Ein Matrix-Versuch zur Bestimmung der Hoch- und Runterregulierung von Genen ermöglichte anzunehmen, dass nicht Mitochondrientod sondern Aktivierung von CD30 bestimmte pro-apoptotische Signalwege in der p53-defizienten Zelllinie regulierte, die NFκB-Aktivierung einschlossen. In anderen Zelllinien verursachte NFκB zwar keinen Zelltod aber Aktivierung des CMV-Promotors, der die Luciferase-Expression reguliert. Nur die Etablierung einer Luciferase-exprimierenden Zelllinie, in der die Luciferase-Expression CMV-unabhängig ist, ermöglichte spezifische RNAi ohne größere Nebeneffekte.

9.4 Ausblick

Als Weiterführung der beschriebenen Projekte ist eine Menge von Weiterentwicklungen denkbar. Die zielgerichteten Vektoren in Kapitel 2 sind es sicherlich wert, in vivo untersucht zu werden. Integrin-Targeting ist bereits zur Tumor-Therapie und –Diagnostik beschrieben worden. Da es bereits möglich war, die Konjugate mit Gammastrahlern zu markieren, könnten sie für radioaktive Bildgebung, aber ebenso für Gentransfer in einen Tumor verwendet werden. Zusätzlich sollte die Eignung als siRNA-Vektoren getestet werden.

Da Triazin-Dendrimere in vivo gut vertragen werden, könnten diese Vektoren als in vivo Gentransfer-Vektoren angewendet werden, aber könnten natürlich ebenso für den Transfer von siRNA ausprobiert werden. Weitere Generationen oder Anhängen anderer Endgruppen kann synthetisch erreicht werden, ebenso wie Modifikationen mit Bildgebungs- oder Targeting-Liganden.

Die Methode, die zur radioaktiven Markierung von siRNA in Kapitel 5 beschrieben wurde, wird sicherlich in Zukunft weiter Anwendung finden, um biopharmazeutische Parameter von siRNA-Vektoren zu untersuchen.

Da Polyplexe aus pre-PEGyliertem PEI und siRNA in Kapitel 6 keine Verbesserung gegenüber PEI zeigten, muss post-PEGylierung untersucht werden, was bereits erfolgreich die Zirkulationsdauer von DNA-Komplexen erhöht hat.

Biologische in vivo Aktivität und Reduktion von EGFP-Expression in der Lunge von Actin-EGFP exprimierenden Mäusen in Kapitel 7 ist das eindrucklichste Ergebnis dieser Arbeit, aber muss weiter bezüglich zeitlichen Verlaufs und Dosis-Optimierung charakterisiert werden. Zusätzlich muss untersucht werden, welche Lungenzellen bevorzugt transfiziert werden.

Es ist wenig darüber bekannt über die Unterschiede von Signalwegen, die in unterschiedlichen Zellen, nach polykationischer Transfektion aktiviert oder inaktiviert werden. Die Studie zu Nebeneffekten in Kapitel 8 erinnert daran, dass nicht alle gemessenen Effekte RNAi sind, und dass Selektions-Systeme sorgfältig charakterisiert werden müssen, bevor valide Daten erhoben werden können.

10 Appendices

10.1 Abbreviations

2'OMe	2'O-Methoxy-
AFM	Atomic Force Microscopy
ANOVA	Analysis of Variance
AUC	Area under the Curve
BAL	Bronchio-Alveolar Lavage
BALF	Bronchio-Alveolar Lavage Fluid
CD	Circular Dichroism
CLSM	Confocal Laser Scanning Microscopy
CT	Computed Tomography
DLS	Dynamic Light Scattering
DDS	Drug Delivery System
DTPA	Diethylenetriaminepentaacetic Acid
dsRNA	Double-Stranded RNA
EGFP	Enhanced Green Fluorescent Protein
EPR	Enhanced Permeability and Retention
FACS	Fluorescence Assisted Cell Sorting
FFS	Fluorescence Fluctuation Spectroscopy
FITC	Fluorescein-Isothiocyanate
HEPES	2-[4-(2-Hydroxyethyl)-1-piperazinyl]ethanesulfonic Acid
HIV	Human Immunodeficiency Virus
IC50	Half-Inhibitory Concentration
LDA	Laser Doppler Anemometry
LMW	Low Molecular Weight
MCT	Monochlorotriazine
MRI	Magnetic Resonance Imaging
MTT	3-(4,5-Dimethylthiazol-2-yl)-2,5-diphenyltetrazolium Bromide
N/P	Nitrogen to Phosphate Ratio
PBS	Phosphate Buffered Saline
PCR	Polymerase Chain Reaction
pDNA	Plasmid DNA
PAMAM	Polyamidoamine

PEG	Polyethylenglycol
PEI	Polyethylenimine
PET	Positron Emission Tomography
PDI	Polydispersity Index
PLL	Poly-L-Lysine
PM	Particulate Matter
QD	Quantum Dot
RES	Reticuloendothelial System
RGD	Arginine-Glycine-Aspartic Acid
RGD-M	RGD-Mimetic
RISC	RNA Induced Silencing Complex
RNAi	RNA Interference
ROI	Region of Interest
siRNA	Short Interfering RNA
SPDP	N-succinimidyl 3-(2-pyridyldithio)propionate
SPECT	Single Photon Emission Computed Tomography
TLR	Toll-Like Receptor

10.2 List of Publications

10.2.1 Articles

Olivia M. Merkel, Andrea Beyerle, Benedikt Beckmann, Roland Hartmann, Tobias Stoeger, Thomas Kissel: **Off-target effects in non-viral siRNA delivery – A study on the effect of polymer genomics on in vitro cell culture models**

In Preparation for the Journal of Controlled Release

Olivia M. Merkel*, Meredith Mintzer*, Eric Simanek, Thomas Kissel: **Triazine dendrimers: Structure-Function relationships of a new class of non-viral gene delivery systems**

Bioconjugate Chemistry, 2009, doi: 10.1021/bc900243r

Andrea Beyerle, Olivia Merkel, Tobias Stoeger, Thomas Kissel: **PEGylation affects cytotoxicity and biocompatibility of poly(ethylene imine) for lung application : structure-function relationships**

Submitted to Toxicology and applied pharmacology (TAAP-D-09-00493)

Olivia M. Merkel, Andrea Beyerle, Damiano Librizzi, Andreas Pfestroff, Thomas M. Behr, Brian Sproat, Peter J. Barth, Thomas Kissel: **Biodistribution and pharmacokinetics of intratracheally instilled siRNA polyplexes**

Molecular Pharmaceutics, 2009, 6 (4), 1246-1260

Yu Liu, Juliane Nguyen, Terry Steele, Olivia Merkel, Thomas Kissel: **A new synthesis method and degradation of hyper-branched polyethylenimine grafted polycaprolactone block mono-methoxyl poly (ethylene glycol) copolymers (hy-PEI-g-PCL-b-mPEG) as potential DNA delivery vectors**

Polymer, 2009, 50 (16), 3895-3904

Meredith A. Mintzer*, Olivia M. Merkel*, Thomas Kissel, Eric Simanek: **Polycationic triazine-based dendrimers: Effect of peripheral groups on transfection efficiency**

New Journal of Chemistry, 2009, doi: 10.1039/b908735d.

*Both authors contributed equally to this work with synthesis (MAM) and biological and physicochemical characterization (OMM).

Olivia M. Merkel, Oliver Germershaus, Carol K. Wada, Peter J. Tarcha, Thomas Merdan and Thomas Kissel: **Integrin alpha-v-beta-3 targeted gene delivery using RGD peptidomimetic conjugates with copolymers of PEGylated poly(ethylene imine)**
Bioconjugate Chemistry 2009, 20 (6), 1270-1280

Olivia M. Merkel, Damiano Librizzi, Andreas Pfestroff, Tino Schurrat, Kevin Buyens, Niek N. Sanders, Stefaan DeSmedt, Martin Béhé and Thomas Kissel: **Influence of in vivo stability of various PEI/siRNA complexes on pharmacokinetics and biodistribution – Correlation of FFS and SPECT data**
Journal of Controlled Release, 138 (2), 148-159

Anastasia Malek, Olivia Merkel, Ludger Fink, Frank Czubyko, Thomas Kissel and Achim Aigner: **In vivo pharmacokinetics, tissue distribution and underlying mechanisms of various PEI(-PEG)/siRNA complexes.**
Toxicology and applied pharmacology, 2009, 236 (1), 97-108

Olivia M. Merkel, Damiano Librizzi, Andreas Pfestroff, Tino Schurrat, Martin Béhé and Thomas Kissel: **In vivo SPECT and real-time gamma camera imaging of biodistribution and pharmacokinetics of siRNA delivery after novel radio labeling and purification**
Bioconjugate Chemistry, 2009, 20 (1), 174-182

Juliane Nguyen*, Terry W.J. Steele*, Olivia Merkel, Regina Reul and Thomas Kissel: **Fast degrading polyesters as siRNA nano-carriers for pulmonary gene therapy**
Journal of Controlled Release, 2008, 132, 243–251

Shirui Mao, Michael Neu, Oliver Germershaus, Olivia Merkel, Johannes Sitterberg, Udo Bakowsky, Thomas Kissel: **Influence of polyethylene glycol chain length on the physicochemical and biological properties of poly (ethylene imine)-graft-poly (ethylene glycol) block copolymer/ siRNA polyplexes**
Bioconjugate Chemistry, 2006, 17 (5), 1209-1218

10.2.2 Patents

Olivia M. Merkel, Oliver Germershaus, Carol K. Wada, Peter J. Tarcha, Thomas Merdan and Thomas Kissel: **Particulate delivery systems containing substituted polycations**, Provisional Application US 61/048,449

Eric Simanek, Meredith A. Mintzer, Olivia M. Merkel, Thomas Kissel: **Melamine-based dendrimers for DNA transfection**, Provisional Application US 61/092,249.

10.2.3 Poster Presentations

Anastasia Malek, Olivia Merkel, Frank Czubayko, Thomas Kissel, and Achim Aigner: **Polyethylenimines (PEIs) and PEG-PEIs for the therapeutic application of siRNA in vivo**

36th Annual Meeting and Exposition of the Controlled Release Society, Copenhagen, Denmark, July 18-22, 2009

Olivia M. Merkel, Andrea Beyerle, Damiano Librizzi, Thomas Kissel: **Nuclear imaging of intratracheal siRNA delivery with PEG-PEI copolymers**

4th European Molecular Imaging Meeting, Barcelona, Spain, May 27-30, 2009

Olivia M. Merkel, Andrea Beyerle, Damiano Librizzi, Thomas Kissel: **Nuclear imaging of intratracheal siRNA delivery with PEG-PEI copolymers**

17th International Congress of the International Society for Aerosols in Medicine, Monterey, CA, USA, May 10-14, 2009

Andrea Beyerle, Olivia M. Merkel, Thomas Kissel, Holger Schulz, Tobias Stöger: **Safety Profiling of Non-Viral Vector Systems for Pulmonary Gene and siRNA Delivery**

14th International Symposium on Recent Advances in Drug Delivery Systems, Salt Lake City, UT, USA, January 15-18, 2009

Olivia M. Merkel, Damiano Librizzi, Andreas Pfestroff, Tino Schurrat, Martin Béhé, Thomas Kissel: **SPECT imaging for quantification of the in vivo biodistribution of siRNA polyplexes**

GRC On Drug Carriers In Medicine & Biology, Big Sky, MT, USA, August 24-29, 2008

Meredith A. Mintzer, Olivia M. Merkel, Thomas Kissel, Erik E. Simanek: **Synthesis and Biological Evaluation of Triazine-based Dendrimers for In Vitro Gene Transfection**
236th ACS National Meeting & Exposition, Philadelphia, PA, USA, August 17-21, 2008

Olivia M. Merkel, Meredith A. Mintzer, Erik E. Simanek, Thomas Kissel: **Physico chemical characterization of triazine dendrimers as vectors for siRNA: Investigation of structure-function relationships**

4. Materialforschungstag Mittelhessen, Marburg, Germany, June 20, 2008

Meredith Mintzer, Olivia Merkel, Thomas Kissel, Eric E. Simanek: **Evaluation of Triazine Dendrimers for Gene Transfection**

5th International Dendrimer Symposium, Toulouse, France, August 28 - September 01, 2007

Anastasia Malek, Olivia Merkel, Frank Czubayko, Thomas Kissel and Achim Aigner: **PEG-PEI/siRNA and PEI/siRNA Complexes for siRNA Delivery to Induce RNA Interference (RNAi)**

48. Frühjahrstagung der Deutschen Gesellschaft für Pharmakologie und Toxikologie, Mainz, Germany, March 13-15, 2007

Olivia Merkel, Thomas Kissel: **Suitability of Homologues and Derivatives of PEI for in vitro siRNA Delivery**

Thirteenth International Symposium on Recent Advances in Drug Delivery Systems, Salt Lake City, UT, USA, February 26-28, 2007

Olivia Merkel, Michael Neu, Oliver Germershaus, Thomas Kissel: **PEGylated PEI for siRNA delivery: Structure-function relationships of poly (ethylene imine)-graft-poly (ethylene glycol) block copolymer/ siRNA polyplexes**

GRC On Drug Carriers In Medicine & Biology, Big Sky, MT, USA, August 20-25, 2006

Shirui Mao, Olivia Merkel, Oliver Germershaus, Michael Neu, Thomas Kissel:

Physicochemical characterization of polyethyleneimine-graft-poly(ethylene glycol) block copolymers as carriers of siRNA: Influence of polyethylene glycol chain length.

CRS, Vienna, July 22-26, 2006

Olivia Merkel, Shirui Mao, Oliver Germershaus, Michael Neu, Thomas Kissel:

Physicochemical characterization of polyethyleneimine-graft-poly(ethylene glycol) block copolymers as carriers of siRNA: Influence of polyethylene glycol chain length.

2. Materialforschungstag Mittelhessen, Rauischholzhausen, June 30, 2006

10.2.4 Lectures

Olivia M. Merkel and Thomas Kissel: **Imaging Pulmonary siRNA Delivery**

Lecture, Center of Excellence for RNA Therapeutics, Roche Kulmbach GmbH, Kulmbach, Germany, June 23, 2009

Olivia M. Merkel and Thomas Kissel: **Nuclear Imaging of Pulmonary siRNA Delivery**

Lecture, Desai Lab, University of California San Francisco, San Francisco, CA, USA, May 16, 2009

Olivia M. Merkel, Andrea Beyerle, Damiano Librizzi, Thomas Kissel: **Nuclear imaging of intratracheal siRNA delivery with PEG-PEI copolymers**

Oral Presentation, Meditrans Second Annual Meeting, Weizmann Institute of Science, Rehovot, Israel, March 26-29, 2009

Olivia M. Merkel, Meredith A. Mintzer, Erik E. Simanek, Thomas Kissel: **Physicochemical characterization of triazine dendrimers as vectors for siRNA: Investigation of structure-function relationships**

Oral Presentation, Globalization of Pharmaceuticals Education Network, Leuven, Belgium, September 9-12, 2008

Olivia Merkel, Meredith Mintzer, Eric E. Simanek, Thomas Kissel: **Triazine dendrimers: Structure-Function relationships of a new class of non-viral gene delivery systems**

Oral Presentation, 7th International Symposium on Polymer Therapeutics, Valencia, Spain, May 26-28, 2008

Olivia Merkel, Meredith Mintzer, Eric E. Simanek, Thomas Kissel: **Triazine dendrimers: Structure-Function relationships of a new class of non-viral gene delivery systems**

Oral Presentation, CRS German Chapter Annual Meeting 2008, Braunschweig, Germany, March 04-05, 2008

Olivia Merkel, Meredith Mintzer, Eric E. Simanek, Thomas Kissel: **Triazine dendrimers: Structure-Function relationships of a new class of non-viral gene delivery systems**

Lecture, Texas A&M, College Station, Texas, USA, January 24, 2008

Olivia Merkel, Thomas Kissel: **Influence of buffer systems and sequence of siRNA on size and stability of polyplexes**

Oral Presentation, GTRV Summer School 2007, La Grande-Motte, France, September 06-08, 2007

Olivia Merkel, Shirui Mao, Thomas Kissel: **SiRNA-Transfer mittels Biokonjugaten**

Lecture, Molekulares Targeting in der Tumorthapie: Neue Strategien und Entwicklungen, 26.-27. Juli 2007, Rauischholzhausen; Veranstalter: Prof. Dr. Roland Kontermann, Institut für Zellbiologie und Immunologie, Uni Stuttgart

Olivia Merkel, Thomas Kissel: **Suitability of homologues and derivatives of PEI for siRNA delivery to the lung**

Oral Presentation, Controlled Release Society German Chapter Annual Meeting 2007, Freiburg, Germany, March 22-23, 2007

10.2.5 Abstracts

Thomas Kissel, Juliane Nguyen, Olivia Merkel and Terry Steele: **Nano-carriers for pulmonary drug and gene delivery**

36th Annual Meeting and Exposition of the Controlled Release Society, Copenhagen, Denmark, July 18-22, 2009

Erik E. Simanek, Meredith A. Mintzer, Olivia M. Merkel, Vincent Venditto, Jong Doo Lim, Anil Patri, Thomas Kissel: **Triazine dendrimers for drug and gene delivery**

IDS6, Stockholm, Sweden, June 14-18, 2009

Anastasia Malek, Olivia Merkel, Frank Czubayko, Thomas Kissel, Achim Aigner: **RNA interference (RNAi) in vitro and in vivo: PEGylated and non-PEGylated polyethylenimines for siRNA delivery**

Controlled Release Society German Chapter Annual Meeting 2007, Freiburg, Germany, March 22-23, 2007

10.2.6 Awards and Prizes

Nachwuchsförderung der Deutschen Lungenstiftung, e.V., 17th International Congress of the International Society for Aerosols in Medicine, Monterey, CA, USA, May 10-14, 2009

GSK Travel Grant, 17th International Congress of the International Society for Aerosols in Medicine, Monterey, CA, USA, May 10-14, 2009

ISAM Student Award, 17th International Congress of the International Society for Aerosols in Medicine, Monterey, CA, USA, May 10-14, 2009

Poster Prize, Flash Oral Presentation, GRC On Drug Carriers In Medicine & Biology, Big Sky, MT, USA, August 24-29, 2008

Travel Grant Award, 7th International Symposium on Polymer Therapeutics, Valencia, Spain, May 26-28, 2008

Best Nanomedicine Poster, 5th International Dendrimer Symposium, Toulouse, France, August 28 - September 01, 2007

10.3 Curriculum Vitae

Personalien:

Merkel, Olivia Monika

geboren am 25.03.1981 in Villingen-Schwenningen

Staatsangehörigkeit : deutsch

Ausbildung und Berufspraxis:

Juni 2000	Abitur, Gymnasium am Romäusring, Villingen
Oktober 2000 – September 2004	Studium der Pharmazie, Philipps-Universität Marburg
Oktober 2004 – März 2006	Studium der Humanmedizin, Philipps-Universität Marburg
November 2004 – April 2005	1. praktisches Halbjahr : Institut für Pharmazeutische Technologie und Biopharmazie, Philipps-Universität Marburg Anfertigung einer Diplomarbeit
Mai 2005 – Oktober 2005	2. praktisches Halbjahr : Sonnenapotheke Marburg
Dezember 2005	Approbation zur Apothekerin
Juli 2006	Diplomverteidigung
Seit Februar 2006	Wissenschaftliche Mitarbeiterin im Institut für Pharmazeutische Technologie und Biopharmazie, Philipps-Universität Marburg Anfertigung der vorliegenden Dissertation

10.4 Danksagung

Mein ganz besonderer Dank gilt meinem Doktorvater Herrn Prof. Dr. Thomas Kissel, der mir seit meinen ersten Schritten im Arbeitskreis und besonders bei der Anfertigung dieser Arbeit mit vielen interessanten Diskussionen und Ideen zur Seite stand und den ich zu jeder Zeit als gerechten Chef erleben durfte. Vor allem möchte ich mich für die großartige Unterstützung und das mir entgegengebrachte Vertrauen bedanken, wodurch ich mich selbst weiterentwickeln konnte. Ich möchte mich für all die Freiheiten bedanken, die ich genießen durfte, für Großzügigkeit, Offenheit, Lob und für Ermutigungen, die auch notwendig waren. Ihre immer wieder überraschenden Ideen sowie Ihr großer Erfahrungsschatz haben bewirkt, dass mir nie langweilig wurde, und haben maßgeblich zum Gelingen dieser Arbeit beigetragen.

Herrn Prof. Dr. Carsten Culmsee möchte ich einerseits für die Erstellung des Zweitgutachtens, andererseits aber auch für die wissenschaftlichen Diskussionen bezüglich siRNA Delivery sowie für unsere offene Unterhaltung bezüglich weiterer Karriereplanung bedanken.

Herrn Prof. Dr. Udo Bakowsky möchte ich sowohl als Vorsitzenden der Prüfungskommission danken, aber auch für eine gute Zusammenarbeit in der Charakterisierung von Dendriplexen mittels Rasterkraftmikroskopie sowie für die Beantwortung von Fragen bezüglich Isothermischer Titrationskalorimetrie.

Außerdem möchte ich mich ganz besonders herzlich bei Herrn Prof. Dr. Eric Simanek und Frau Meredith Mintzer vom Institut für Chemie an der Texas A&M Universität in College Station, bedanken, ohne die diese Arbeit nicht in diesem Umfang möglich gewesen wäre. Bei Frau Mintzer möchte ich mich herzlich für die Synthese einer Bibliothek von Triazin-Dendrimeren bedanken und bei der gesamten Gruppe für die äußerst gastfreundliche Aufnahme am Institut.

Mein besonderer Dank gilt außerdem Herrn Dr. Thomas Merdan, Frau Dr. Carol Wada und Herrn Dr. Peter Tarcha von Abbott Laboratories für die Zusammenarbeit bezüglich Integrin-Targeting und für die Bereitstellung des Targeting-Liganden. Herrn Dr. Thomas Merdan danke ich für viele Gespräche und vor allem dafür, mir den Weg in die Forschung gebahnt und den Kontakt zu Herrn Prof. Kissel hergestellt zu haben.

Herzlich danken möchte ich auch Herrn Dr. Tobias Stöger und Frau Andrea Beyerle sowie der gesamten Gruppe von Herrn Dr. Stöger am Helmholtz-Zentrum München für die freundliche Aufnahme im Institut und für die lehrreiche und interessante Zusammenarbeit.

Ohne die vielen etablierten Untersuchungsmethoden, auf die zurückgreifen durfte, wäre die Durchführung der Experimente zu Off-Target Effekten sowie die Evaluierung der Proben aus den in vivo Versuchen nicht möglich gewesen. Ganz besonders möchte ich mich bei Frau Beyerle bedanken, die Tage und Nächte, Feiertage und Wochenenden mit mir am Stück durchgearbeitet hat, um die in vivo Versuche möglich zu machen.

Herrn Dr. Martin Béhé sowie Herrn Prof. Dr. Thomas Behr, Herrn Dr. Andreas Pfestroff und Herrn Damiano Librizzi, Frau Ulla Cramer und Frau Gudrun Höhn vom Institut für Nuklearmedizin danke ich herzlich für die Möglichkeit zur unkomplizierten Verwirklichung der in vivo Pharmakokinetik- und Biodistributionsversuche. Die Arbeit in der Nuklearmedizin war immer sehr angenehm und äußerst produktiv. Ebenso möchte ich mich für die vielen Diskussionen mit Herrn Dr. Béhé bedanken, die mir oftmals neue Perspektiven eröffnet haben. Herrn Librizzi und Herrn Dr. Pfestroff danke ich für viele lustige Stunden im Labor und an der Kamera sowie außerhalb der Klinik. Bei Herrn Librizzi möchte ich mich ganz besonders herzlich für eine Unmenge an Überstunden unter Einsatz seines Lebens bedanken.

Herrn Prof. Dr. Stefaan De Smedt, Frau Dr. Katrien Remaut, Herrn Kevin Buyens und Herrn Broes Naeye möchte ich für die freundliche Aufnahme im Arbeitskreis von Herrn Prof. De Smedt an der Fakultät für Pharmazeutische Wissenschaften an der Universität Ghent danken. Mein Dank gilt besonders Herrn Buyens für die Zusammenarbeit bezüglich Messung von Komplex-Stabilität mittels Fluoreszenz-Fluktuations-Spektroskopie.

Bei Herrn Prof. Dr. Roland Hartmann, Herrn Dr. Arnold Grünweller, Herrn Benedikt Beckmann und Herrn Robert Prinz in der Pharmazeutischen Chemie möchte ich mich für die gute Zusammenarbeit, die Nutzung von Geräten und die Unterstützung in molekularbiologischen Fragen bedanken.

Außerdem möchte ich mich bei Herrn Prof. Dr. Harald Renz, Herrn Dr. Holger Garn, Frau Tanja Dicke, Frau Anja Spieß und allen anderen Mitgliedern der Arbeitsgruppe von Herrn Prof. Renz in der Klinischen Chemie für die unkomplizierte Zusammenarbeit und die Möglichkeit, Labor und Geräte zu allen Tages- und Nachtzeiten nutzen zu dürfen, bedanken.

Herrn Prof. Dr. Peter Barth und Frau Viktoria Morokina vom Institut für Pathologie danke ich herzlich für die entspannte Zusammenarbeit und für Aufarbeitung einer Vielzahl von Organproben sowie das Anfertigen mikroskopischer Präparate.

Herrn PD Dr. Günter Höglinger und Herrn Dr. Thomas Carlsson aus dem Institut für Experimentelle Neurologie möchte ich für die Bereitstellung gentechnisch veränderter

Mäuse bedanken, bei Herrn Dr. Andreas Matusch für die Herstellung des Kontakts und bei Herrn Dr. Ondrej Fiala für die interessanten Versuche intrastriataler Applikation von siRNA.

Allen Mitgliedern der DFG-Forschergruppe „Nanohale“ möchte ich für die vielen Diskussionen und die Zusammenarbeit über die letzten Jahre hinweg danken.

Bei allen Mitgliedern des EU-Projekts „Meditrans“ möchte ich für die schönen gemeinsamen Kongresse, die vielfach vernetzte Zusammenarbeit und die Offenheit gegenüber so vieler neuer Ideen bedanken. Ganz besonders möchte ich mich bei Herrn Dr. Brian Sproat von Integrated DNA Technologies in Leuven für die Hilfe in allen Fragen bezüglich siRNA- und Peptid-Synthese sowie für die großzügige Versorgung mit siRNA und Peptiden bedanken. Außerdem danke ich Frau Dr. Shellie Singelton und Herrn Dr. Matt Bunker sowie der ganzen AFM- und TEM-Gruppe bei Molecular Profiles in Nottingham für viele schöne Aufnahmen, die hoffentlich bald veröffentlicht werden. Auch bei Frau Prof. Dr. Michal Neeman und Herrn Sefi Addadi vom Weizman Institut Rehovot möchte ich mich für die Kooperationsbereitschaft und vor allem für die Gastfreundlichkeit und Einladung bedanken.

Allen Mitgliedern des Instituts für pharmazeutische Technologie und Biopharmazie bin ich zu größtem Dank verpflichtet.

Besonders hervorheben möchte ich die ehemaligen Kollegen Frau Dr. Elke Kleemann und Herrn Dr. Oliver Germershaus, die mich noch zu Studienzeiten eingearbeitet haben, und von denen ich eine Vielzahl an Methoden gelernt habe. Für die hilfreiche Unterstützung vom ersten bis zum letzten Tag möchte ich mich ganz besonders herzlich bei Herrn Dr. Germershaus bedanken. Bei ihm sowie meinen ehemaligen Kollegen Frau Dr. Elke Kleemann, Frau Jutta Fuchs, Frau Dr. Juliane Nguyen, Herrn Dr. Florian Unger, Herrn Dr. Terry Steele und Herrn Daniel Siebert möchte ich mich für die lustigen Stunden in der Behring-Villa bedanken. Herrn Lehardt danke ich für die Zeit, in der wir das Büro geteilt haben, aber auch für die hervorragende und unkomplizierte gemeinsame Organisation des Praktikums.

Ich danke Frau Eva Mohr und Frau Sandra Engel für ihre ausgezeichnete Arbeit in der Zellkultur und Herrn Klaus Keim für die Organisation der Bestellungen und für die stete Unterstützung in allen grafischen Fragen.

Weiterhin möchte ich meinen Kollegen Nadja Bege, Moritz Beck-Broichsitter, Markus Benfer, Dr. Cuifang Cai, Eyas Dayyoub, Heiko Debus, Thomas Endres, Nico Harbach, Dr.

Peter Hölig, Anchalee Jintapattanakit, Dr. Elke Kleemann, Tobias Lehardt, Vincent Lima, Dr. Yu Liu, Dr. Sascha Maretschek, Elena Marxer, Frank Morell, Aybike Özçetin, Dr. Claudia Packhäuser, Christian Pfeiffer, Thomas Renette, Regina Reul, Susanne Rösler, Jens Schäfer, Dr. Julia Schnieders, Christoph Schweiger, Nina Seidel, Anett Sommerwerk und Nan Zhao für die vielen gemeinsamen Stunden in der Uni und für die gemeinsamen Freizeitaktivitäten ganz herzlich danken.

In größter Verbundenheit möchte ich mich bei meinem allerbesten Freund Michael Dutescu für viel seelische und moralisch Unterstützung, ein immer offenes Ohr, stundenlange Telefonate, die lustigsten Emails und besten Skype-Gespräche, für Aufmunterung und für großartige Wochenenden und Urlaube bedanken, die mir den nötigen Abstand und die nötige Erholung erlauben.

Von tiefstem Herzen möchte ich mich bei meiner Familie für die immerwährende Unterstützung, ihren Glauben an mich und ihre Liebe bedanken, ohne die ich nicht der Mensch wäre, der ich bin.